Master of Science in Viticulture & Enology

Joint diploma " Vinifera EuroMaster Degree Program " awarded by:

L'INSTITUT NATIONAL D'ENSEIGNEMENT SUPERIEUR POUR L'AGRICULTURE, L'ALIMENTATION ET L'ENVIRONNEMENT
AND
HOCHSCHULE GEISENHEIM UNIVERSITY

Master Thesis

Impact of Water Deficit on the Functioning of LowSugarBerry Wine Varieties

Raimundo Prieto Nixon

2023-2025 (P17)

Supervisor 1
Prof. Dr. Manfred Stoll
Hochschule Geisenheim University, Germany

Supervisor 2
Prof. Dr. Anne Pellegrino
L' Institut Agro-Montpellier, France

Supervisor 3
Prof. Dr. Laurent Torregrosa
L' Institut Agro-Montpellier, France

Montpellier, 3rd of November 2025

Statement of Academic Honesty

I herewith declare in lieu of oath that the submitted master's thesis with the title “Impact of water deficit on the functioning of LowSugarBerry wine varieties” has been composed by myself without any inadmissible help and without the use of sources other than those given due reference in the text and listed in the list of references.

I further declare that all persons and institutions that have directly or indirectly helped me with the preparation of the thesis have been acknowledged and that this thesis has not been submitted, wholly or substantially, as an examination document at any other institution.

I hereby confirm that I am familiar with the standards of Scientific Integrity and with the guidelines of Good Scientific Practice, and that this work fully complies with these standards and guidelines.

Montpellier, 3rd of November 2025 Raimundo Prieto Nixon

Acknowledgements

This thesis would not have been possible without the guidance, support, and encouragement of many individuals and institutions.

First and foremost, I extend my deepest gratitude to my supervisors, Professor Dr. Anne Pellegrino, Professor Dr. Laurent Torregrosa, and Professor Dr. Manfred Stoll, for their invaluable expertise, patience, and dedication throughout this research. Your insightful feedback and unwavering support have been instrumental in shaping both this work and my development as a researcher.

I am profoundly grateful to the Chaire d'Entreprises Vigne et Vin for financing my internship and thesis, making this research possible. I also wish to thank the LEPSE research center for providing exceptional facilities and a stimulating intellectual environment.

I am indebted to numerous colleagues who contributed to this work through technical assistance, scientific discussions, and moral support. In particular, I thank Luciana, Die, Maëlle, Javier, Romain, and Gaëlle, as well as many others at LEPSE who made this research experience enriching and enjoyable.

To my family, thank you for your unconditional love and support throughout this journey. Your belief in me has been a constant source of strength.

I am deeply grateful to God for the opportunity, wisdom, and perseverance to complete this work.

Finally, and most especially, I thank my partner Estefanía. Your unwavering support, patience, and encouragement have been a cornerstone of this experience. This accomplishment is as much yours as it is mine.

Abstract

Climate change threatens Mediterranean viticulture through rising temperatures and water scarcity, driving excessive sugar accumulation and reducing wine quality, while Low Sugar Berry (LSB) genotypes, characterized by 20-30% lower berry hexose concentration, offer potential for climate adaptation. This study investigated whether reduced berry sugar demand in LSB genotypes (G5, G14) compared to non-LSB genotypes (3159, 3176) derived from Muscadinia rotundifolia × Vitis vinifera crosses confers drought advantages through improved carbon allocation and water use efficiency. Short-term experiments imposing acute water deficit at green and ripening stages, combined with long-term experiments maintaining moderate deficit throughout ripening, revealed no LSB advantages at berry or leaf scales, with developmental stage determining stress sensitivity and all genotypes exhibiting similar stomatal and photosynthetic responses. However, a carbon-normalization treatment increasing LSB berry numbers by 35% to equalize total fruit carbon demand revealed that carbon-normalized LSB genotypes under water deficit demonstrated superior resource allocation, maintaining fruit carbon while investing substantially more in roots, enabling exceptional whole-plant water use efficiency, whereas standard LSB genotypes showed no advantages. Carbon isotope analysis confirmed uniform leaf-level efficiency but weak correlation with whole-plant performance, indicating that LSB advantages arise from allocation flexibility manifesting only when high carbon sink demand, sustained moderate deficit, and sufficient duration align. These findings demonstrate that LSB operates as a system-level trait enabling adaptive resource allocation rather than constitutive drought tolerance, with implications for breeding strategies targeting allocation flexibility through carbon-normalized screening under prolonged stress to develop climate-resilient grapevines maintaining productivity and moderate alcohol wines under Mediterranean conditions.

Keywords: Low Sugar Berry, water deficit, water use efficiency, carbon allocation, source-sink relationships, grapevine, climate adaptation, *Vitis vinifera*

Table of Contents

List of Abbreviations

An	Net photosynthesis rate (µmol CO_2 m^{-2} s^{-1})
ANOVA	Analysis of Variance
DAF	Days After Flowering
DAV	Days After Veraison
DOY	Day Of Year
DW	Dry Weight (g)
E	Transpiration rate (mmol H_2O m^{-2} s^{-1})
Fm	Maximum fluorescence (dark-adapted)
Fm'	Maximum fluorescence (light-adapted)
Fo	Minimum fluorescence (dark-adapted)
Fo'	Minimum fluorescence (light-adapted)
FTSW	Fraction of Transpirable Soil Water
Ft	Steady-state fluorescence
FW	Fresh Weight (g)
FFW	Fresh Fruit Weight (g)
gm	Mesophyll conductance
gs	Stomatal conductance (mol H_2O m^{-2} s^{-1})
H_2M	Malic acid
H_2T	Tartaric acid
HPLC	High-Performance Liquid Chromatography
HSD	Honestly Significant Difference (Tukey's test)
INRAE	Institut National de Recherche pour l'Agriculture, l'alimentation et l'Environnement
IRGA	Infrared Gas Analyzer
iWUE	Intrinsic Water Use Efficiency (An/gs, µmol CO_2 mol^{-1} H_2O)
Jmax	Maximum rate of electron transport (µmol m^{-2} s^{-1})
LA	Leaf Area (m^2)
LEPSE	Laboratoire d'Écophysiologie des Plantes sous Stress Environnementaux
LSB	Low Sugar Berry
LTS	Long-Term Stress (Experiment 2)

M. rotundifolia	*Muscadinia rotundifolia*
n	Sample size
p	Probability value
PAR	Photosynthetically Active Radiation (µmol photons m^{-2} s^{-1})
PPFD	Photosynthetic Photon Flux Density (µmol photons m^{-2} s^{-1})
PSII	Photosystem II
qN	Non-photochemical quenching coefficient
qP	Photochemical quenching coefficient
QTL	Quantitative Trait Locus/Loci
R^2	Coefficient of determination
Rd	Dark respiration
RGR	Relative Growth Rate (day^{-1})
SD	Standard Deviation
SE	Standard Error
SMC	Soil Moisture Capacity
SPAD	Soil Plant Analysis Development (chlorophyll meter reading)
SS	Soluble Sugars
STS	Short-Term Stress (Experiment 1)
STS-G	Short-Term Stress - Green stage
STS-R	Short-Term Stress - Ripening stage
TPU	Triose-phosphate utilization
TR	Total plant transpiration (L)
UE	Unité Expérimentale
V. vinifera	*Vitis vinifera*
varC	Variation in fruit carbon content (g C)
Vcmax	Maximum rate of carboxylation (µmol m^{-2} s^{-1})
VPD	Vapor Pressure Deficit (kPa)
WD	Water Deficit (treatment)
WD-C	Water Deficit Carbon-normalized (treatment)
WUE	Water Use Efficiency (general)
WUEi	Instantaneous Water Use Efficiency (An/E, µmol CO_2 mol^{-1} H_2O)
WUEpl	Whole-Plant Water Use Efficiency (varC/TR, g C L^{-1})
WUEpl_n	Normalized Whole-Plant Water Use Efficiency (g C L^{-1})
WW	Well-Watered (treatment)
WW-C	Well-Watered Carbon-normalized (treatment)
°Brix	Degrees Brix (soluble solids concentration)
$\delta^{13}C$	Carbon isotope discrimination (%)
ΦCO_2	Apparent quantum yield for CO_2 assimilation
Ψmd	Midday leaf water potential (MPa)
Ψpd	Predawn leaf water potential (MPa)
Ψstem	Stem water potential (MPa)

List of Figures

List of Tables

Overview of Tools Used

Context of use	Digital tool	Version
Writing, editing and formatting text	Microsoft Word	2019
Formatting Text	Chat GPT	Free-5
R script development	Chat GPT	Free-5
Data management	Microsoft Excel	2019
Illustration creation	Canva	1.117.1.0
Statistical analysis	R Studio	4.3.0
Reference management	Scribbr	-

1 Literature Review

1.1 Introduction

Climate change poses an unprecedented threat to viticulture, with rising temperatures fundamentally altering the delicate balance between sugar accumulation and acidity that defines wine quality. This challenge is particularly acute in the grapevine (*Vitis vinifera* L. subsp. vinifera), which represents one of the world's most economically and culturally significant fruit crops, with viticulture serving as both an economic pillar and cultural cornerstone across many regions (Alston & Sambucci, 2019; Baltazar et al., 2025; Keller, 2020). Global wine exports, valued at 35.8 billion EUR in 2024, continue to grow despite shifting consumption patterns (OIV, 2025; Sheppard, 2025). The European Mediterranean Basin—particularly France, Italy, and Spain—dominates global production, with 7.1 million hectares of vineyards producing approximately 225.8 million hectoliters annually (OIV, 2025). These regions share Mediterranean climatic conditions characterized by warm, dry summers and wet winters (Köppen-Geiger Csa/Csb classification), which have historically favored viticulture (Baltazar et al., 2025; Rubel & Kottek, 2010). However, recent climate records show that in both northeastern Spain and southern France, winter rainfall has become increasingly irregular and total annual precipitation has trended downward over the last decade, with the period 2022–2024 marked by severe deficits in Languedoc-Roussillon and Catalonia (AEMET, 2024; Météo-France, 2025).

Grapevines evolved in semi-arid environments, developing sophisticated mechanisms to cope with water scarcity and nutrient-poor soils (Baltazar et al., 2025; Khadatkar et al., 2025). This evolutionary adaptation proved advantageous for wine quality, as moderate water deficit can enhance fruit composition by restricting vegetative growth and concentrating metabolites essential for wine quality (Jackson, 2008; Keller, 2020). Wine quality depends on achieving optimal balance between primary metabolites (sugars and organic acids) and secondary metabolites (phenolic and aromatic compounds), with water availability playing a crucial role in this equilibrium (Cosme et al., 2016; Reynolds, 2021). However, climate change increasingly challenges this delicate balance. Rising temperatures, altered precipitation patterns, and more frequent extreme weather events threaten traditional viticulture regions (Baltazar et al., 2025). Mean growing season temperatures in major wine regions have increased by 1.5-2°C since the 1980s, with projections suggesting further warming of 2-4°C by 2050, fundamentally challenging the thermal suitability of traditional varieties in their historic regions (Hannah et al., 2013; Morales-Castilla et al., 2020). These shifts necessitate adaptive strategies, including the development of new varieties that maintain quality under changing environmental conditions. This context underscores the importance of understanding water deficit impacts on carbon and water functioning in emerging fungi-

resistant varieties, particularly those bred for lower sugar accumulation to address climate-induced challenges in traditional wine regions.

1.2 Challenges of Grapevine Production Under Climate Change

1.2.1 Environmental Constraints Facing Mediterranean Vineyards

Climate change is now one of the most pressing threats to viticulture globally. Rising temperatures, prolonged droughts, and altered precipitation patterns are increasingly compromising vine physiology and berry development (Droulia & Charalampopoulos, 2021; IPCC, 2023). The Intergovernmental Panel on Climate Change (IPCC) has reported that the Earth's average surface temperature has increased significantly over the past century due to greenhouse gas emissions (IPCC, 2023), with notable implications for agricultural systems—including viticulture. In particular, elevated temperatures during ripening accelerate sugar accumulation while reducing organic acid content, leading to wines with higher alcohol levels and diminished freshness (Bigard et al., 2022; Sweetman et al., 2014). This phenomenon threatens the typicity and market appeal of wines from traditional regions. The region of southern France exemplifies the implications that climate change has for agriculture and viticulture. Fernandez-Mena et al. (2023) identified environmental limitations on grapevine yield in the Languedoc-Roussillon region of France (Figure 1), well known for being the most important French region in terms of volume of wine produced and in terms of the significance of viticulture to the region's economy (Harding et al., 2023), where they classified that the region is considered dry to very dry by the climatic Dryness Index (Tonietto & Carbonneau, 2004). This situation will become more severe as climate change progresses.

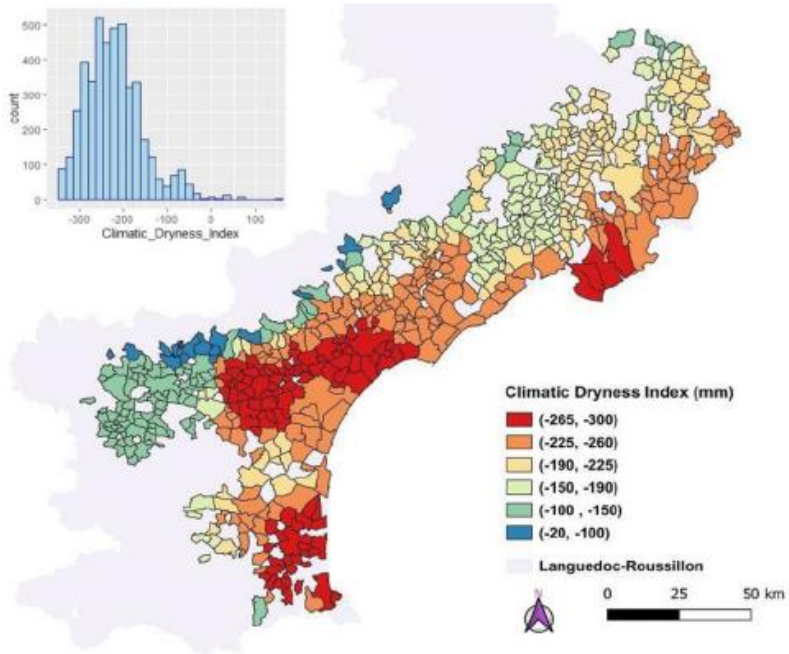

Figure 1. Average Climatic Dryness Index (CDI) of each municipality in Languedoc-Roussillon between 2010 and 2018 (Fernandez-Mena et al., 2023).

Moreover, changes in rainfall distribution and frequency are increasing the occurrence of extreme weather events such as heatwaves and heavy rainfalls, both of which can damage vines and reduce yield stability (Stratonovitch & Semenov, 2015; Yang et al., 2023). Prolonged summer droughts limit water availability, affecting photosynthesis, transpiration, and carbon allocation (Keller, 2020). While the Mediterranean climate's characteristic dry summers naturally limit fungal disease pressure—enabling the Occitanie region to produce approximately half of France's organic wine—climate change is creating new disease dynamics. Warmer temperatures combined with increasingly erratic precipitation patterns, particularly unseasonal rainfall events during sensitive phenological stages, can create sporadic but intense disease pressure from pathogens like *Plasmopara viticola* (downy mildew) and *Botrytis cinerea* (Juroszek & Von Tiedemann, 2015; Reineke & Thiéry, 2016). These episodic outbreaks, though less frequent than in humid regions, can be particularly damaging as growers in traditionally dry areas may be less prepared for rapid disease management responses. These environmental shifts are not merely altering yields or harvest dates; they are disrupting the delicate biochemical balance of berries. Studies have shown that rising temperatures during ripening cause premature degradation of malic acid and alter secondary metabolite profiles, including anthocyanins and aroma compounds, ultimately changing wine flavor and structure (Rienth et al., 2021; Sweetman et al., 2014; Van Leeuwen & Destrac-Irvine, 2017). Such changes challenge the very notion of "terroir", where wine character is intrinsically linked to the specific climate and soil of a region. A specific study done by Bécart et al. (2022) gathered and analyzed 50 years' worth of data of primary components of Grenache grapes in the southern Rhone Valley (Rhône meridional), another highly relevant viticultural mediterranean area with high production (Harding et al., 2023), revealing that potential alcohol increased year by year, while berry acidity and yield are decreasing yearly (Figure 2).

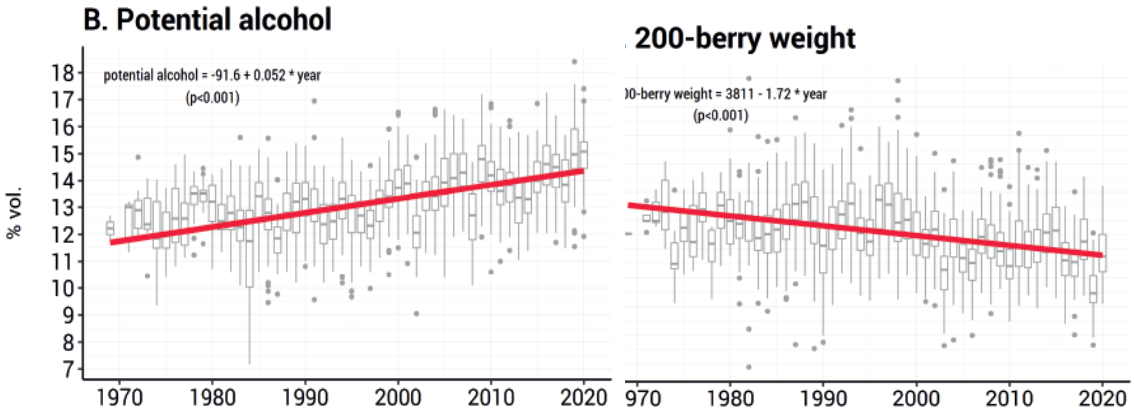

Figure 2. Overview of Grenache maturity at harvest in the southern Rhône valley from 1969 to 2020 (Bécart et al., 2022).

1.2.2 Eco-Friendly Production and Evolving Consumer Trends

The evolving landscape of wine consumption and production is increasingly shaped by consumer preferences for sustainability and health-conscious choices, particularly in response to climate change and environmental awareness. One of the most significant shifts in demand has been the growing preference for lower-alcohol wines, driven by health considerations, lifestyle changes, and a broader trend toward moderation and wellness (Fortune Business Insights, 2025). This shift is especially pronounced among younger consumers, who not only seek lighter wines but also prioritize environmentally responsible production practices. As a result, the wine industry is under pressure to adapt its viticultural and enological methods to align with these expectations while navigating the challenges posed by a warming climate.

Climate change has intensified the tension between traditional wine styles and modern consumer preferences. While historically, moderate stress conditions were seen as beneficial to wine quality, today's extreme and prolonged heat events push vineyards beyond their optimal physiological thresholds, producing wines that do not meet either sensory or market expectations (Keller, 2020; Rienth et al., 2021). This misalignment between climate-driven berry composition and consumer taste profiles has created a critical need for adaptive strategies in viticulture, including varietal selection, canopy management, and precision irrigation (van Leeuwen & Destrac-Irvine, 2017; Fraga et al., 2018).

In parallel, there is increasing regulatory and societal pressure to adopt sustainable agricultural practices, especially within the European Union and other wine-producing regions committed to global climate goals. The EU Green Deal, launched in 2019, sets ambitious targets for reducing chemical inputs, lowering carbon emissions, and promoting biodiversity across agriculture sectors, including viticulture (European Commission, 2020). Specifically, the Farm to Fork Strategy, part of the Green Deal, calls for a 30% reduction in pesticide use by 2030 and an increase in organic farming practices, directly impacting how vineyards manage pests, fertilizers, and water resources (European Commission, 2020). These policies reflect broader international efforts, such as those promoted by the United Nations Sustainable Development Goals (SDGs) and organizations like the World Health Organization (WHO), which advocate for healthier diets and reduced alcohol consumption (UN, 2023; WHO, 2024). In this context, winemakers are encouraged to reduce reliance on synthetic chemicals and produce wines that are both sustainably made and lower in alcohol, responding to both regulatory frameworks and shifting consumer values.

Consumer interest in eco-friendly products is no longer limited to niche markets. A 2023 report from the International Organisation of Vine and Wine (OIV) highlighted that certified sustainable wines are gaining traction globally, with many producers adopting organic, biodynamic, or low-intervention practices to meet market demands (OIV, 2025). This shift is supported by research showing that environmentally conscious consumers are willing to pay premiums for wines produced with minimal ecological impact (CNBC, 2025). However, despite advancements, the wine sector still faces significant hurdles in reconciling climate-induced changes in berry composition with consumer expectations for balance, typicity, and moderate alcohol levels. Traditional varieties selected for high sugar accumulation may no longer be suitable under future climatic scenarios, calling for a reevaluation of cultivar suitability and breeding priorities (Delrot et al., 2020; van Leeuwen et al., 2019). In this context, innovative approaches such as the development of new genotypes are becoming essential for sustaining wine production in line with both environmental and consumer trends.

1.3 Grapevine Responses to Water Deficit and Elevated Temperatures

1.3.1 Water Loss and Regulation at Plant and Organ Levels

Water is a fundamental component of grapevine physiology, playing a central role in cell turgor maintenance, nutrient transport, and berry development. In *Vitis vinifera*, water is primarily absorbed through the root system and transported via the xylem to the canopy and fruit. The efficiency of this process depends on the vine's hydraulic architecture, including root distribution, xylem vessel connectivity, and stomatal regulation (Keller, 2020).

The movement of water through the plant can be conceptualized using the soil-plant-atmosphere continuum (SPAC) framework, where water flows along a series of hydraulic resistances driven by water potential gradients (Figure 3). Water potential decreases progressively from the soil (approximately -0.05 MPa under well-watered conditions) through the root, stem, and leaf tissues, ultimately reaching highly negative values in the atmosphere (approximately -50 MPa at typical relative humidity). This water potential gradient drives transpiration and water uptake, with the overall rate of water transport determined by the hydraulic conductances of each pathway segment. According to Ohm's law analogy, the whole-plant hydraulic conductance represents the sum of individual resistances in the root (kroot), stem (kstem), and leaf (kleaf) systems, with additional vapor-phase resistances at the stomatal and boundary layer interfaces (Tyree and Ewers, 1991). Under well-watered conditions, xylem vessels ensure that leaves and berries receive adequate hydration to support growth and metabolic activity. However, under water deficit conditions, hydraulic conductivity decreases, affecting water distribution throughout the plant (Tyerman et al., 2009).

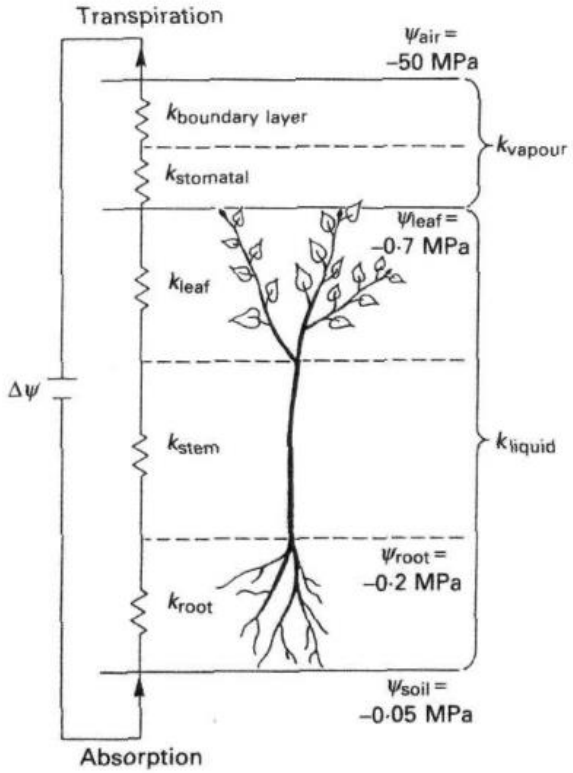

Figure 3. Conceptual model of hydraulic architecture in woody plants. Water transport through the soil-plant-atmosphere continuum can be conceptualized as a series of hydraulic resistances analogous to an electrical circuit. Water moves from the soil (Ψsoil = -0.05 MPa) through the root system, stem, leaves, and ultimately to the atmosphere (Ψair = -50 MPa), driven by water potential gradients (Δψ). Each segment of the pathway has an associated hydraulic conductance (k), with the root (kroot), stem (kstem), leaf (kleaf), stomatal (kstomatal), and boundary layer (kboundary layer) conductances determining the overall rate of water flow. The vapor phase conductances are typically orders of magnitude lower than liquid phase conductances, creating the steep water potential gradient between the leaf interior and atmosphere that drives transpiration. Under water deficit, reductions in hydraulic conductance at any point in the pathway can limit whole-plant water transport. Adapted from Tyree and Ewers (1991).

The regulation of water loss at the whole-plant level involves multiple integrated mechanisms, with leaf area adjustment being the most sensitive and earliest response to water deficit. Grapevines actively reduce their transpiring surface through several processes: inhibition of lateral shoot growth, reduced leaf expansion rates, and in severe cases, leaf abscission (Lebon et al., 2006; Pellegrino et al., 2005). This morphological plasticity serves as the first line of defense against water stress, as reducing total leaf area directly decreases whole-plant transpiration, hence water demand. Studies have shown that leaf expansion is more sensitive to water deficit than stomatal conductance, with growth cessation occurring at higher water potentials (-0.2 to -0.4 MPa) than stomatal closure (-0.8 to -1.2 MPa) (Schultz, 2003; Zufferey et al., 2011). The sensitivity of leaf area development to water deficit is mediated by changes in cell division and

expansion rates, with cell expansion being particularly vulnerable due to its dependence on turgor pressure (Tardieu et al., 2011).

The leaf stomata serve as regulators of transpiration, modulating water loss while allowing CO_2 entry for photosynthesis. Under water deficit, grapevines typically exhibit reduced transpiration rates and stomatal closure as mechanisms aimed at conserving water and maintaining turgor pressure (Baeza et al., 2019; Chaves et al., 2010; Prieto et al., 2010; Tarara & Peña, 2015). These responses are closely linked to abscisic acid (ABA) signaling, particularly from the roots, which plays a central role in coordinating whole-plant acclimation strategies under drought (Ojeda et al., 2002; Rossdeutsch et al., 2016). Stomatal behavior varies among cultivars, with some varieties exhibiting isohydric behavior (maintaining leaf water potential by closing stomata early under stress), while others behave anisohydrically (allowing leaf water potential to decline before initiating stomatal closure) (Chaves et al., 2010; Hochberg et al., 2018).

At the cellular level, water movement across membranes is facilitated by aquaporins, a family of membrane proteins that regulate cellular permeability and hydraulic conductivity. Aquaporin activity influences both root water uptake and water distribution within the plant, especially in tissues such as the petiole and pericarp (Tyerman et al., 2009). Under water deficit, aquaporin expression and activity are often downregulated, contributing to reduced hydraulic conductivity and water conservation strategies.

The anatomical organization of grapevine roots profoundly affects their hydraulic properties and capacity for water uptake. Grapevine fine roots exhibit dramatic structural changes along their developmental axis, from the unsuberized meristematic and elongation zones near the root tip to mature regions undergoing secondary growth (Figure 4). In young root tips, the undifferentiated tissues of the exodermis, cortex, and stele lack suberized barriers, facilitating high rates of radial water transport. As roots mature, primary xylem and phloem differentiate, and a suberized endodermis develops in the maturation zone, creating selective apoplastic barriers that regulate solute and water movement. The initiation of secondary growth marks a critical transition in root hydraulic properties, as the vascular cambium produces secondary xylem and phloem tissues, and a multilayer suberized periderm replaces the original cortex and epidermis. This periderm formation substantially reduces the hydraulic conductivity of mature root portions, with measurements indicating that root tips exhibit hydraulic conductivity approximately 10-fold greater than secondary growth zones (Gambetta et al., 2013). Despite lower conductivity, woody suberized roots constitute the vast majority of root surface area in mature vines and thus can contribute significantly to whole-plant water uptake, particularly during periods when unsuberized root tips are scarce or absent. The developmental progression of root anatomy and suberization represents a trade-off

between water uptake capacity and protection against water loss to dry soils, with important implications for drought adaptation strategies in grapevines.

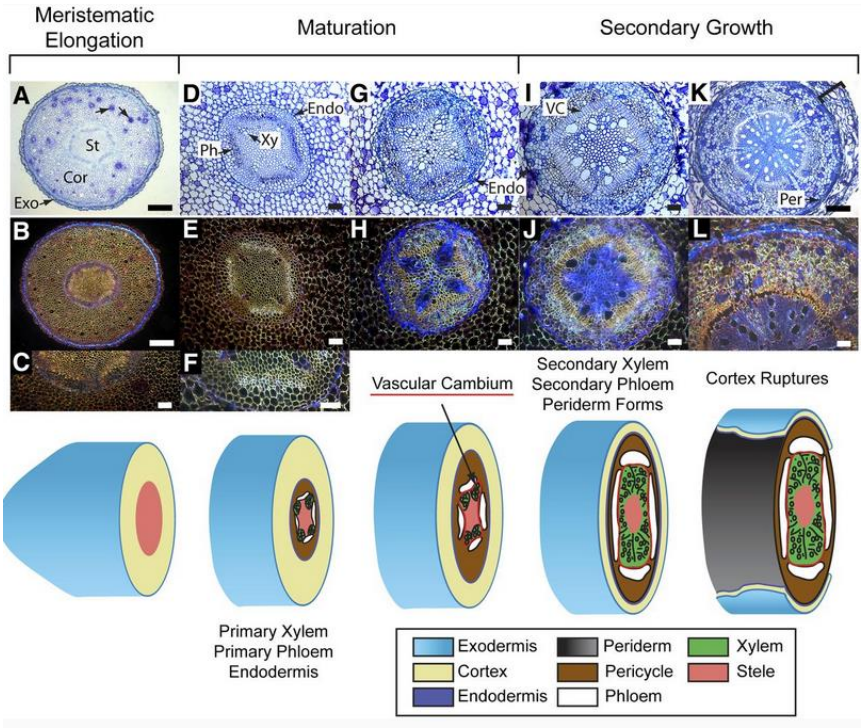

Figure 4. Developmental anatomy and hydraulic architecture of grapevine fine roots. Cross-sections showing progressive tissue differentiation along the root developmental axis. (A-C) Meristematic and elongation zones contain undifferentiated tissues with exodermis (Exo), cortex (Cor), and stele (St), lacking suberized barriers and exhibiting maximal hydraulic conductivity. (D-H) Maturation zone exhibits differentiation of primary xylem (Xy), primary phloem (Ph), and an identifiable endodermis (Endo), with development of selective apoplastic barriers. (I-L) Secondary growth zone shows vascular cambium (VC) activity producing secondary vascular tissues and formation of a multilayer periderm (Per). At advanced stages (K-L), the outer cell layers including exodermis, cortex, and endodermis rupture and are lost (bracketed in K), leaving the suberized periderm as the primary barrier to radial water transport. This anatomical progression results in approximately 10-fold reduction in root hydraulic conductivity from tip to woody portions, though suberized roots can still contribute substantially to water uptake due to their large surface area. Scale bars = 200 µm (A, B, K), 40 µm (F), and 80 µm (all others). Adapted from Gambetta et al. (2013).

1.3.2 Carbon Gain and Allocation to Plant Organs

Carbon assimilation in grapevines is primarily achieved through photosynthesis in the canopy, where atmospheric CO_2 is fixed into sugars via the Calvin cycle (Keller, 2020). Under optimal conditions, these carbohydrates are converted to sucrose and transported via the phloem to various sink organs, including developing berries, roots, and shoot tissues (Lecourieux et al., 2013; Walker et al., 2021). The balance between carbon gain and demand determines the vine's overall carbon status and its ability to

sustain fruit development and vegetative growth (Douthe et al., 2018; Keller, 2011; Salazar-Parra et al., 2015; Muller et al., 2011).

Under water deficit, photosynthetic activity is significantly reduced due to both stomatal and non-stomatal limitations. Initial responses involve stomatal closure to prevent water loss, which simultaneously restricts CO_2 entry and reduces net assimilation (An) (Flexas et al., 2002). As water stress intensifies, non-stomatal limitations become prominent, including enzyme deactivation, chlorophyll degradation, and photoinhibition (Cramer et al., 2013; Urban et al., 2017). This leads to a decline in carbon supply to sink organs, particularly berries during ripening (Alatzas et al., 2021; Pellegrino et al., 2006). During fruit development, the coordination between water and sugar transport becomes particularly critical. According to Savoi et al. (2021) (Figure 5), sugar transport in ripening berries follows an energetically optimized pathway where passive "SWEET" transporters facilitate sucrose export from the phloem, while energy-demanding H^+/sugar antiporters at the tonoplast drive sugar accumulation into the vacuole. Water movement occurs passively through aquaporins, following the solute gradient without additional energy cost (Zhang & Keller, 2017). Under water deficit, both sugar transporters and aquaporins are dramatically down-regulated when phloem unloading ceases at berry maturity (Savoi et al., 2021), affecting berry size and composition.

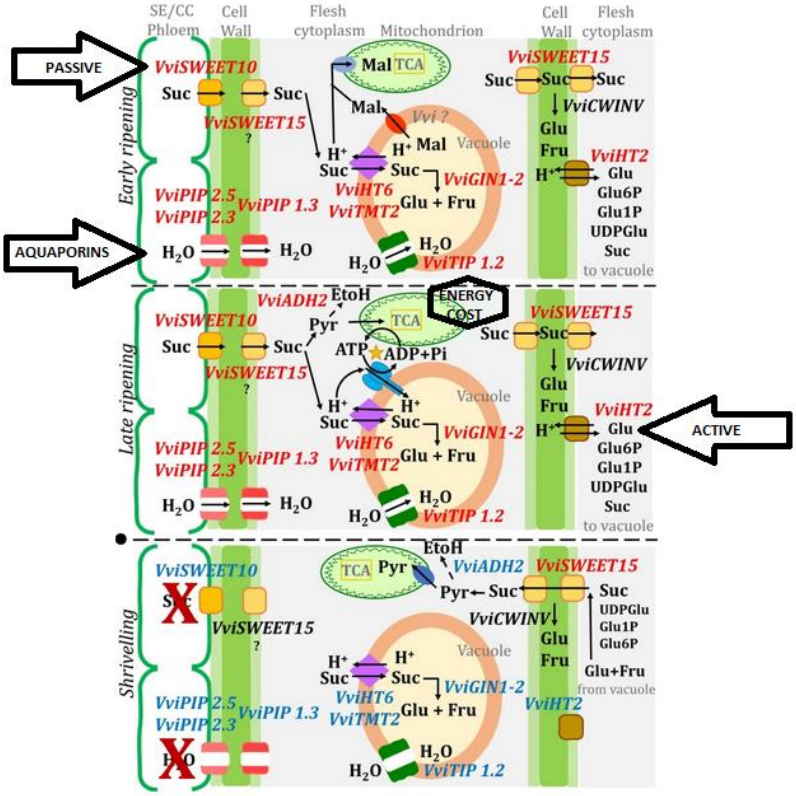

Figure 5. Cellular mechanisms of sugar and water transport during grape berry ripening (adapted from Savoi et al., 2021). The figure illustrates the hypothetical model of the energy-efficient apoplastic pathway across three ripening stages: early ripening (upper panel), late ripening (middle panel), and shriveling (lower panel, cessation of transport marked by red X). Passive transport (left, no ATP required) occurs via SWEET transporters (VvSWEET10, VvSWEET15) facilitating sucrose export from phloem sieve element/companion cell (SE/CC) complex into the apoplast, and aquaporins (VvPIP2.5, VvPIP2.3, VvPIP1.3) enabling water movement following osmotic gradients. Active transport (right, ATP-dependent) involves H^+/sugar antiporters (VvHT6, VvTMT2) and proton pumps (VvtGIN1-2) driving sugar accumulation into the vacuole, with energy supplied by mitochondrial ATP production (center) via the TCA cycle and oxidative phosphorylation. Gene names in red italics indicate upregulated expression; blue italics indicate downregulated expression at specific stages.

These water transport mechanisms determine how different grapevine genotypes manage internal water balance under both optimal and stress conditions. Water use efficiency (WUE) becomes a critical parameter under deficit conditions, measurable at multiple scales: leaf level (AN/E or AN/gs), whole-plant, and field scale (yield/water use) (Medrano et al., 2015; Tomás et al., 2012). The $\delta^{13}C$ method provides an integrated assessment of WUE over time, with less negative values indicating higher WUE and greater water stress during berry ripening (Gaudillère et al., 2002; Brillante et al., 2020).

The source-sink relationship undergoes significant changes under water deficit. Early in the season, water stress during flowering and fruit set can reduce inflorescence fertility and impair cell division, leading to smaller berries and reduced yield potential (Keller, 2020; Matthews & Anderson, 1989; Ojeda et al., 2001; Pellegrino et al., 2005; Zhu et al., 2020). These early impacts may persist even after stress relief, affecting bunch weight and cluster number (Guilpart et al., 2014).

The balance between source capacity (photosynthetic leaf area) and sink demand (primarily developing fruits) fundamentally regulates photosynthetic activity through feedback mechanisms (Figure 6). When sink demand is high relative to source capacity, photosynthesis (An) is typically upregulated through increased stomatal conductance and enhanced biochemical capacity, while low sink demand can lead to feedback inhibition of photosynthesis (Quereix et al., 2001; Paul & Foyer, 2001). This sink regulation of photosynthesis operates through multiple pathways, including sugar-sensing mechanisms that modulate gene expression and enzyme activities when photosynthates accumulate in source leaves (Iglesias et al., 2002; Paul & Pellny, 2003). Under optimal conditions, grapevines with higher fruit loads generally maintain higher photosynthetic rates throughout the season, as the strong sink demand prevents carbohydrate accumulation and associated feedback inhibition (Naor et al., 2002; Poni et al., 1993).

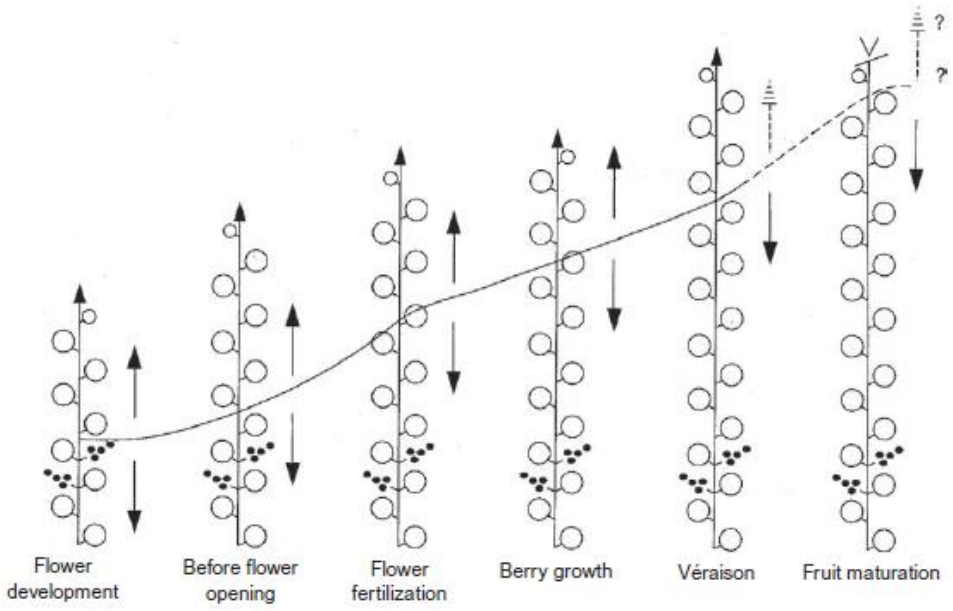

Figure 6. Source-sink relationships in grapevine shoots change throughout the growing season (adapted from Keller, 2020, originally from Koblet, 1969). Arrows indicate the direction of photoassimilate movement at six developmental stages from flower development to fruit maturation. Young leaves export assimilates toward the growing shoot tip, while older leaves export toward the shoot base and roots. As berries develop, they become increasingly strong sinks, attracting carbon from nearby source leaves. The changing patterns illustrate how assimilate transport adapts to the vine's developmental status and competing sink demands.

Water deficit fundamentally alters these source-sink dynamics. While stomatal limitations initially reduce An (net photosynthesis) under drought, the simultaneous reduction in vegetative growth often increases the fruit:leaf ratio, potentially intensifying sink strength per unit of leaf area (Medrano et al., 2003). This can create a compensatory effect where the remaining functional leaves maintain relatively high photosynthetic rates despite water stress, driven by strong sink demand (Escalona et al., 2003). However, this compensation has limits - severe water deficit can overwhelm sink-driven photosynthetic upregulation, particularly when non-stomatal limitations become dominant (Flexas et al., 2004). The interaction between water status and source:sink ratio thus becomes critical in determining overall carbon balance, with genotypes that maintain appropriate source:sink ratios under drought potentially showing better carbon economy and stress resilience (Keller, 2005; Sadras & Moran, 2012).

During berry ripening, water deficit alters carbon allocation priorities. While sugar concentrations in berries often remain stable or increase due to reduced dilution, the absolute amount of carbon allocated to fruit growth decreases (Ojeda et al., 2001; Sweetman et al., 2014). Vines shift their carbon allocation strategy under stress, favoring maintenance respiration over growth, especially in older leaves and woody tissues

(Keller, 2020; Vivin et al., 2002; Zufferey et al., 2012). This results in increased fruit load per unit leaf area, which can further reduce resource partitioning efficiency and delay maturity in some genotypes (Berhe, 2022; De Toda & Balda).

Carbon storage in perennial tissues becomes critically affected under prolonged water deficit. Reduced photosynthetic capacity limits starch accumulation in trunk and roots, compromising reserves essential for supporting budbreak and early shoot growth in subsequent seasons (Pellegrino et al., 2014; Zapata et al., 2004; Zufferey et al., 2012). This reduction in stored carbon can have lasting effects on vine performance, especially in regions experiencing repeated drought events (Rogiers et al., 2022; Santos et al., 2020; van Leeuwen & Destrac-Irvine, 2017). Furthermore, water deficit can induce premature leaf senescence or defoliation, further limiting the vine's ability to replenish carbohydrate reserves (Bennett et al., 2005; Li et al., 2024; Pellegrino et al., 2014). This creates a negative feedback loop where reduced carbon storage leads to weaker growth in following seasons, potentially resulting in interannual variability in crop load and quality.

The hierarchy of carbon allocation among different organs shifts dramatically under water deficit, with the severity of stress determining which sinks are prioritized or sacrificed. Under mild water deficit (Ψstem > -1.0 MPa), carbon allocation typically favors reproductive tissues and root growth at the expense of shoot elongation and lateral branch development, reflecting an adaptive strategy to ensure reproduction while exploring soil water resources (Lovisolo et al., 2010; Medrano et al., 2015). As water stress intensifies to moderate levels (Ψstem -1.0 to -1.4 MPa), berries continue to receive priority for carbon allocation, maintaining sugar accumulation despite reduced photosynthesis, while vegetative growth essentially ceases and root growth slows (Gambetta et al., 2020; Figure 7). This cascade of physiological responses follows a predictable sequence as stem water potential becomes more negative (Figure 7) with stomatal conductance and transpiration declining first, followed by reductions in photosynthesis, and ultimately affecting fruit yield when stress becomes severe (Gambetta et al., 2020). This preferential allocation to fruits is mediated by their strong sink strength during ripening and the maintenance of phloem functionality to reproductive organs even under stress (Castellarin et al., 2007; Keller et al., 2015).

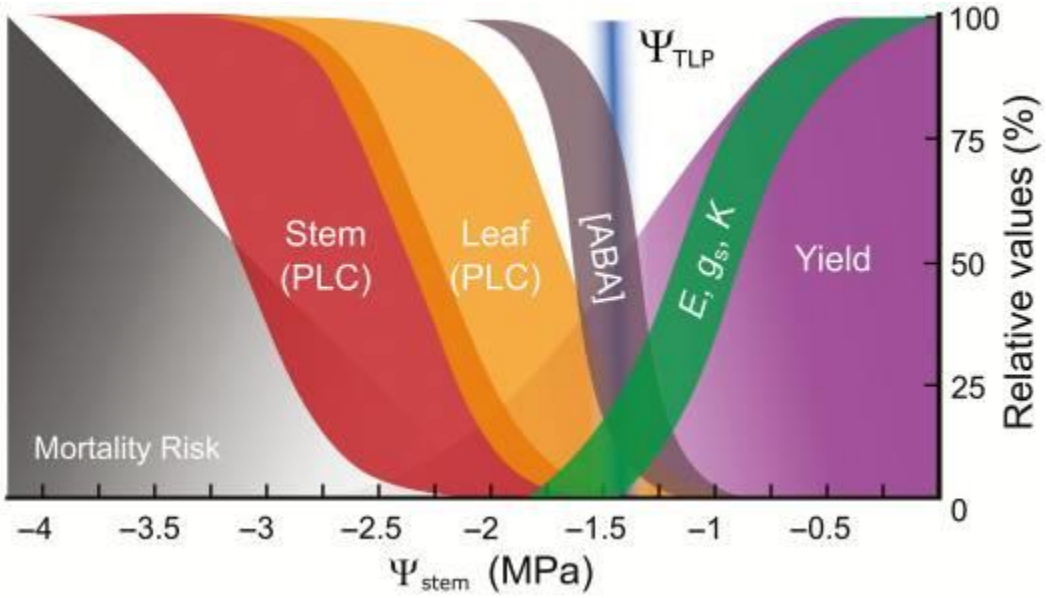

Figure 7. Sequence and thresholds of grapevine physiological responses to water deficit. The diagram shows the relative timing and severity of grapevine responses across a gradient of stem water potential (Ψstem). Irrigated vineyards typically function within a safe range (green zone, Ψstem > -1.5 MPa) where transpiration (E), stomatal conductance (gs), hydraulic conductance (K), photosynthesis, and fruit yield progressively decline (purple). As water deficit intensifies, vines acclimate through osmotic adjustment, with leaf turgor loss point (ΨTLP, blue) becoming more negative. Severe water deficit (Ψstem < -1.6 MPa) can cause embolism in xylem vessels, with leaves (orange) more vulnerable than perennial tissues (red stems), creating a "hydraulic fuse" that protects vital organs. Extensive embolism can lead to vine mortality (grey). ABA concentration increases only after substantial stomatal closure. Adapted from Gambetta et al. (2020).

Under severe water deficit (Ψstem < -1.4 MPa), the allocation hierarchy undergoes further reorganization. Carbon is redirected from growth processes to osmotic adjustment and protective mechanisms, with increased allocation to soluble sugars and compatible solutes in leaves and roots for maintaining cell turgor (Chaves et al., 2010). Perennial tissues (trunk and cordons) may experience net carbon loss as starch reserves are mobilized to support basic metabolism and osmotic adjustment, while fine root mortality increases, reducing the vine's absorptive capacity (Bauerle et al., 2008; Comas et al., 2010). Berry growth may be arrested despite continued sugar accumulation, leading to excessive fruit sugar concentrations through dehydration rather than active loading (Ojeda et al., 2001). The recovery of normal allocation patterns after drought relief depends on the duration and severity of stress, with prolonged severe deficit causing persistent alterations in source-sink relationships that can affect multiple growing seasons (Girona et al., 2006; Intrigliolo & Castel, 2010).

The efficiency of carbon allocation under water deficit is also influenced by nitrogen availability, which affects enzyme synthesis for sugar transport and utilization (Verdenal et al., 2021). Hormonal regulation, particularly through auxins and gibberellins,

modulates phloem loading and carbon delivery priorities under stress conditions (Keller, 2020; Kliewer & Dokoozlian, 2005; Moreno et al., 2011; Stoll et al., 2000).

1.3.3 Impact of Warming on Berry Development and Composition

Temperature fundamentally drives grapevine phenology and berry metabolism, with warming accelerating developmental rates while disrupting the coordination between technological and phenolic maturity. The decoupling of sugar accumulation from other ripening processes under elevated temperatures represents one of the most significant challenges for maintaining wine quality under climate change (Rienth et al., 2016; Sweetman et al., 2014).

During berry development, temperature affects multiple physiological processes with different thermal optima and sensitivities. Sugar accumulation accelerates with warming up to approximately 30°C, while organic acid degradation, particularly malic acid respiration, increases exponentially above 20°C (Sweetman et al., 2014). This differential temperature response creates an imbalance where berries reach high sugar concentrations while retaining insufficient acidity, resulting in wines with elevated alcohol content and compromised freshness (Rienth et al., 2016; Figure 8). The phenomenon is particularly pronounced in Mediterranean regions where ripening increasingly coincides with heat waves exceeding 35°C, temperatures that can arrest anthocyanin biosynthesis and accelerate their degradation (Mori et al., 2007).

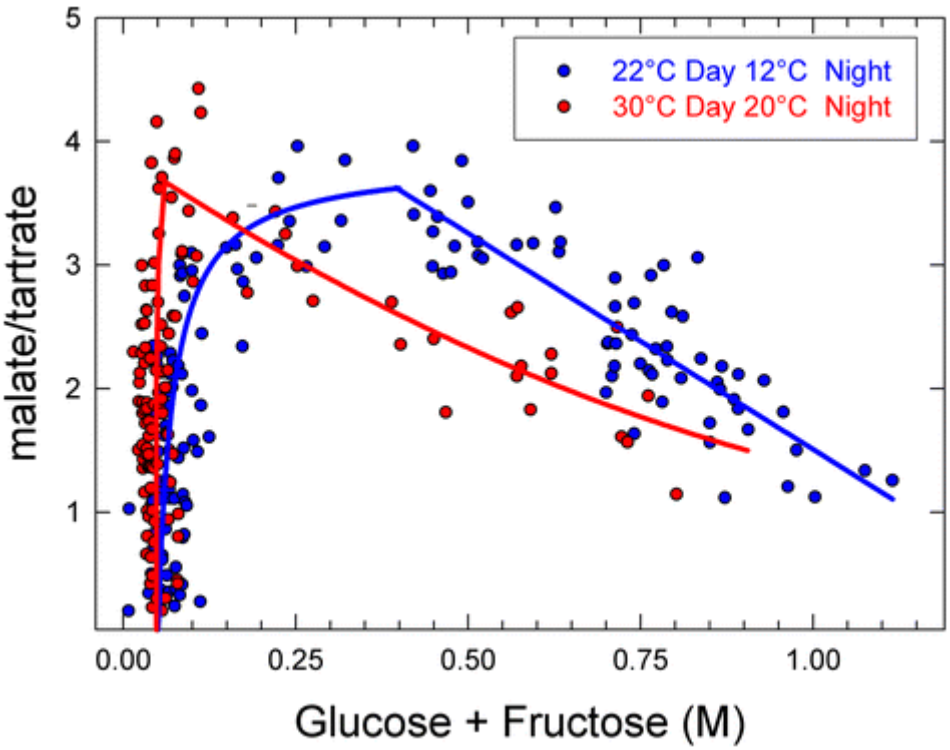

Figure 8. Temperature-induced imbalance between sugar and organic acid accumulation during grape berry ripening (adapted from Rienth et al., 2016). The malate/tartrate ratio is plotted against total hexose concentration (glucose + fructose in molarity) for berries developing under cool (22°C day/12°C night, blue circles) versus warm (30°C day/20°C night, red circles) conditions. Each data point represents one cluster of approximately 30 berries sampled during the ripening progression from veraison through harvest. Fitted curves demonstrate that elevated temperature accelerates malic acid degradation relative to sugar accumulation, creating a compositional imbalance where berries achieve high sugar levels with insufficient organic acid retention. Under warm conditions (red trajectory), the malate/tartrate ratio declines more steeply as hexoses accumulate, demonstrating the differential thermal sensitivities that lead to excessive alcohol potential and reduced wine freshness under climate warming.

The interaction between warming and water deficit amplifies these compositional imbalances through multiple mechanisms. Elevated temperatures increase vapor pressure deficit (VPD), driving higher transpiration rates even when soil water is adequate, effectively intensifying physiological drought stress (Rogiers et al., 2012). This warming-induced increase in evaporative demand can trigger stomatal closure at higher soil water potentials than would occur under cooler conditions, reducing photosynthesis and altering carbon allocation patterns (Greer & Weedon, 2012). Furthermore, the combination of high temperatures and water deficit during ripening concentrates sugars through both enhanced import (when water is adequate) and berry dehydration (under deficit), creating a compound effect that accelerates alcohol potential beyond either stress alone (Van Leeuwen & Destrac-Irvine, 2017).

At the biochemical level, warming affects the expression and activity of key enzymes involved in sugar metabolism and transport. Hexose transporters show increased expression under moderate warming, facilitating rapid sugar accumulation, while invertase activity remains elevated at temperatures that would normally trigger its decline (Lecourieux et al., 2017). This sustained enzymatic activity under warming conditions contributes to the problematic accumulation of fermentable sugars. Conversely, the biosynthesis of flavor and aroma compounds shows variable temperature responses, with many volatile compounds showing reduced accumulation above 30°C, fundamentally altering wine sensory profiles (Bonada et al., 2013).

The search for varieties that can maintain balanced composition under warming has led to renewed interest in genotypes with altered sugar accumulation patterns. Traditional approaches have focused on late-ripening varieties or high-acidity cultivars, but these strategies often merely delay harvest into equally warm periods or fail to address the fundamental sugar-acid imbalance (Duchêne et al., 2010). The identification of germplasm with intrinsically lower sugar accumulation potential, independent of ripening timing, represents a promising avenue for breeding programs targeting climate adaptation. Such varieties could theoretically achieve physiological and phenolic maturity at lower sugar concentrations, avoiding the current dilemma of choosing

between excessive alcohol potential or unripe flavors. This has motivated recent screening efforts across Vitis germplasm to identify genotypes with modified sugar-water import dynamics that could maintain quality parameters under warming scenarios (Duchêne, 2016; Van Leeuwen et al., 2019).

1.3.4 Strategies to Mitigate Water Deficit Effects

Grapevine growers have developed various strategies to mitigate the negative impacts of water deficit, ranging from short-term management practices to long-term adaptations. Deficit irrigation techniques represent the most widely adopted approach for managing water stress while optimizing fruit quality. Regulated deficit irrigation (RDI) and partial root zone drying (PRI) have been shown to improve water use efficiency while maintaining or even enhancing berry composition in semi-arid regions (Romero et al., 2022). The application of low annual water volumes (85-90 mm $year^{-1}$) combined with appropriate rootstock selection can maintain wine quality while significantly reducing water consumption (Romero et al., 2020). These techniques exploit the fact that moderate water stress at specific phenological stages can improve berry composition without severely impacting yield.

Canopy management practices also play a crucial role in drought mitigation. Modifying canopy architecture, such as implementing west-leaning systems under Mediterranean conditions, can maximize radiation interception during cooler morning hours while limiting exposure during high evaporative demand periods in the afternoon (Buesa et al., 2020). Additionally, soil management practices including mulching, cover crops, and organic matter amendments can improve soil water retention and reduce evapotranspiration losses (Medrano et al., 2015).

The use of drought-tolerant rootstocks represents a powerful tool for adapting to water-limited conditions without changing the scion variety. Rootstocks like 140Ru and 110R with effective root/water transport systems maintain high water uptake capacity and carbon gain under prolonged moderate/severe deficit irrigation, while others like 161-49C and 1103P show greater water stress sensitivity (Romero et al., 2025). Drought-tolerant rootstocks such as Ramsey maintain higher root hydraulic conductivity and faster recovery after re-watering compared to sensitive rootstocks like Riparia (Bonarota et al., 2024). Berlandieri-Rupestris crossings (110R, 99R, 1103P, 140Ru) reduce root growth less than Riparia-Berlandieri (5BB, SO4) or Riparia-Rupestris (3309C, 101-14MGT) rootstocks when water becomes limiting (Ollat et al., 2015; Yildirim et al., 2018). These drought-tolerant rootstocks typically exhibit deeper rooting patterns, enhanced root morphological plasticity, and improved hydraulic efficiency under stress conditions (Bauerle et al., 2008).

1.3.5 Breeding for Climate Adaptation: A Long-term Solution

While management practices and rootstock selection offer immediate to medium-term solutions, breeding new grapevine varieties represents the most promising long-term strategy for climate adaptation. Modern breeding programs increasingly focus on combining traditional goals like disease resistance with climate adaptation traits, particularly drought tolerance and modified phenology (Töpfer et al., 2011). Traditional breeding for drought tolerance has been limited by the complexity of drought-related traits and the long generation time of grapevines (20-25 years from cross to commercial release). Marker-Assisted Selection (MAS) programs have begun targeting specific quantitative trait loci (QTLs) related to transpiration rate, $\delta^{13}C$ values, transpiration efficiency, and water extraction capacity (Marguerit et al., 2012). However, current breeding programs remain more oriented towards disease tolerance than climate change adaptation (Duchêne, 2016).

Recent advances in genomic technologies offer new opportunities for accelerated breeding. Genomic prediction methods can reduce breeding cycles by predicting genotypic values using molecular markers, potentially accelerating the development of varieties adapted to specific environmental conditions (Brault et al., 2024). The development of high-density genetic maps and the identification of drought tolerance QTLs enable more targeted breeding approaches (Pirrello et al., 2023). The vast genetic diversity within Vitis species provides a rich resource for breeding climate-adapted varieties. The OIV recommends strengthening international collaboration to facilitate research on selection and breeding, including characterization of traditional varieties particularly adapted to climate change constraints (OIV, 2021). Wild relatives like *Vitis cinerea* var. helleri, which showed high tolerance to calcareous soils and drought, have been successfully used in rootstock breeding programs (Töpfer et al., 2011).

Intra-varietal variability also offers opportunities for selection, as different clones can exhibit significantly different sugar accumulation patterns and stress responses under elevated temperatures and CO_2 (Pastore et al., 2022). This clonal diversity can be exploited through polyclonal selection strategies to enhance vineyard resilience. Emerging technologies promise to revolutionize grapevine breeding for climate adaptation. CRISPR/Cas9 genome editing has been successfully used to develop grapevines with enhanced water stress tolerance through the inactivation of VvEPFL9-1 (Clemens et al., 2022). More recently, Shahbaz et al. (2025) demonstrated that knockout of VvEPFL9-2, which specifically regulates stomatal density during leaf expansion rather than in leaf primordia, resulted in up to 84% reduction in stomatal density with significant improvements in intrinsic water-use efficiency under both well-watered and water-stressed conditions. Remarkably, moderate reductions in stomatal density (around 60%) maintained photosynthetic rates comparable to wild-type plants while

enhancing drought survival, suggesting that targeted manipulation of specific EPFL9 paralogs could optimize the trade-off between water conservation and carbon assimilation (Shahbaz et al., 2025). New genomic technologies (NGTs), combined with pangenome development and high-throughput phenotyping, can identify structural variants and accelerate the breeding of drought-tolerant varieties (Schmidt et al., 2025).

Epigenome editing offers the possibility of heritable trait improvement without DNA sequence changes, while graft-transmissible gene editing via engineered rootstocks could allow trait modification without directly altering the scion genome (Veley et al., 2021; Yang et al., 2023). These approaches could overcome consumer resistance to genetically modified grapevines while providing rapid adaptation to climate challenges. Successful climate adaptation will require integrating breeding efforts with other mitigation strategies. While vineyard design adaptations may initially reduce yield, this can be compensated by appropriate irrigation management, and negative effects of irrigation on berry composition can be offset by adapted plant material such as drought-tolerant rootstocks (Naulleau et al., 2021). This systems approach recognizes that no single strategy will be sufficient for adaptation to complex climate challenges.

Moving forward, breeding programs must adopt multi-trait selection approaches that balance drought tolerance with other essential characteristics including disease resistance, phenological adaptation, and wine quality maintenance. Key research priorities include identifying genetic determinants of drought tolerance traits such as maximum transpiration rate, stomatal regulation, turgor loss point acclimation, and xylem plasticity (Gambetta et al., 2020). Understanding the genetic basis of these traits and their interconnections will be crucial for developing varieties that can thrive under future climate scenarios while maintaining the quality characteristics demanded by consumers and regional wine identities.

1.4 Low Sugar Berry (LSB) Genotypes: A Lever to Cope with Drought and Warming?

1.4.1 Physiological Characteristics of LSB Genotypes

From past research, a new class of grapevine genotypes has emerged that exhibits a unique physiological trait: the ability to achieve 20–30% lower hexose concentrations compared to traditional varieties, while maintaining similar berry growth, total acidity, and cation accumulation (Bigard et al., 2022). This trait is particularly noteworthy given the extensive diversity in water/solute balances documented across Vitis vinifera germplasm, where sugar concentrations can vary from 752 to 1353 mmol. L^{-1} and cation accumulation shows significant genotypic control independent of sugar loading (Bigard et al., 2018, 2020). These genotypes, collectively referred to as Low Sugar Berry (LSB) or "sugarless" types, represent a significant shift in our understanding of fruit development

physiology, particularly during the ripening phase, where the coupling between sugar loading and water uptake is traditionally tight (Bigard et al., 2025; Keller et al., 2015).

Importantly, these genotypes show comparable leaf-level photosynthesis rates to conventional varieties, despite their reduced fruit sugar requirements (Wilhelm De Almeida et al., 2024a). This implies that photosynthetic activity is not compromised in LSB varieties. Instead, the allocation of assimilates is redirected toward other metabolites, particularly organic acids, as evidenced by their higher malic acid/tartaric acid balance (Bigard et al., 2022) and maintained cation accumulation (Bigard et al., 2020). This metabolic flexibility, where similar carbon assimilation supports lower fruit sugar accumulation, suggests that LSB genotypes may maintain a lower source-to-sink ratio, potentially improving vine carbon status. Beyond their physiological novelty, this trait directly addresses the primary consequence of warming on berry composition—excessive sugar accumulation leading to high alcohol wines—positioning LSB genotypes as particularly relevant for maintaining wine style and quality under both current and projected temperature increases.

In conventional Vitis vinifera cultivars, berry development follows a double sigmoid growth curve with two distinct phases of cell expansion (Figure 9). The first phase occurs during the green stage and is driven primarily by the accumulation of organic acids (mainly tartaric and malic acids), which lower the osmotic potential and drive water uptake (Kliewer, 1965; Ojeda et al., 1999; Terrier & Romieu, 2001). Following a lag phase, the second expansion phase begins at veraison and is driven by the massive importation of sugars via the phloem and their subsequent hydrolysis from sucrose to hexoses (glucose and fructose) by invertases, which dramatically lowers osmotic potential ($\Psi\pi$) and drives further water uptake into the fruit (Figure 9) (Matthews et al., 1987; Davies & Robinson, 1996; Zhang et al., 2006).

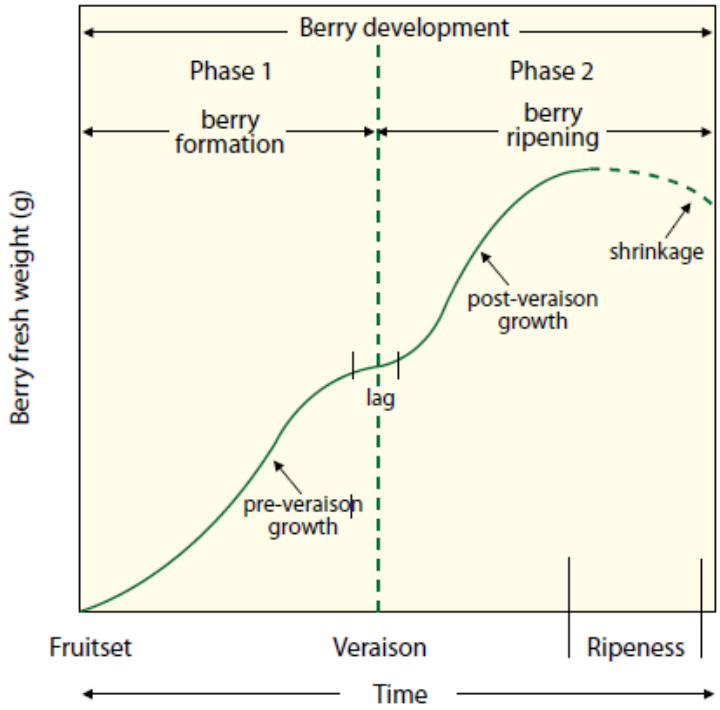

Figure 9. Double sigmoid growth curve of grape berry development (adapted from Iland et al., 2017). Berry fresh weight follows two growth phases separated by a lag phase. Phase 1 (berry formation) is driven by organic acid accumulation. Phase 2 (berry ripening, after veraison) is driven by sugar accumulation and water import. This pattern reflects the fundamental shift in berry metabolism that occurs at veraison, which is particularly relevant for understanding Low Sugar Berry genotypes that decouple sugar import from water uptake during Phase 2.

LSB genotypes such as G5 and G14, derived from interspecific hybrids involving Muscadinia rotundifolia, demonstrate a clear decoupling of sugar import from water uptake (Bigard et al., 2022; Figure 10). They can maintain comparable fruit size and volume with significantly reduced sugar levels, suggesting a more flexible pericarp cell wall structure and possibly alternative osmoregulatory mechanisms beyond glucose and fructose (Bigard et al., 2020 & 2022). As illustrated in Figure 10, this decoupling manifests in two ways: at equivalent fresh weight, LSB berries accumulate less sugar than traditional varieties, while at equivalent sugar content, LSB berries achieve greater expansion. This physiological flexibility represents a fundamental shift from the traditional coupling where osmotic potential driven by hexose accumulation is the primary determinant of berry water import during ripening.

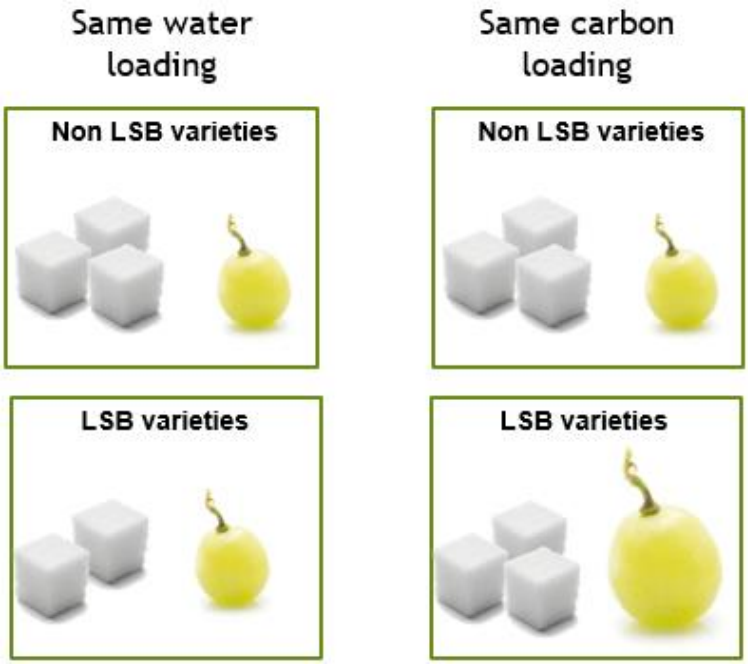

Figure 10. Conceptual comparison of carbon and water relationships in LSB versus non-LSB grapevine genotypes. The left panel illustrates that at equivalent water accumulation (berry fresh weight), LSB genotypes require less carbon input (represented by sugar cubes) compared to traditional non-LSB varieties, demonstrating the decoupling of sugar import from water uptake. The right panel shows that at equivalent carbon loading (total sugar content), LSB genotypes produce berries with higher fresh weight, indicating more efficient water import relative to sugar accumulation. This decoupling suggests alternative osmoregulatory mechanisms in LSB genotypes, likely involving enhanced cell wall extensibility and greater flexibility in the relationship between turgor and growth, allowing normal berry expansion with reduced osmotic drive from hexose accumulation. These alternative mechanisms position LSB genotypes as valuable germplasm for breeding climate-adapted varieties that maintain fruit development with reduced sugar concentrations.

The osmotic gradient model reveals key differences: in traditional varieties, the massive drop in $\Psi\pi$ during ripening creates a strong driving force for phloem unloading, resulting in rapid berry filling with sugars and water (Keller et al., 2015; Shahood et al., 2020). In contrast, LSB genotypes accumulate sugars at a lower rate, likely due to enhanced cell wall extensibility and greater flexibility in vascular transport, enabling normal expansion with reduced sugar input (Bigard et al., 2022).

Understanding these physiological mechanisms requires careful consideration of measurement scale. As Bigard et al. (2025) emphasize, "the asynchrony and heterogeneity of single berry development prevent data extrapolation from grape clusters to single fruits." This is particularly critical for understanding sugar demand dynamics, as individual berry analyses reveal the actual water and carbon flow patterns that are masked when averaging across asynchronous berry populations. Single-berry approaches allow identification of precise developmental stages and thresholds, while population-level measurements provide commercially relevant yield and quality

parameters. The integration of both approaches is essential for understanding how "the balance between water imported into the fruit... and tissue turgidity regulation... are crucial in determining the fruit final soluble solids' concentration" (Bigard et al., 2025).

1.4.2 LSB Responses to Water Deficit: Current Knowledge

Recent studies reveal that LSB genotypes exhibit distinct responses to water deficit compared to traditional varieties. The key difference lies in their sugar-water transport dynamics: conventional varieties show tight coupling between sugar accumulation and water import, meaning that under water deficit, reduced water availability directly limits berry expansion while concentrating sugars through dehydration. In contrast, LSB genotypes' already-decoupled sugar-water transport provides inherent protection against drought-induced sugar concentration, as their berry expansion is less dependent on sugar-driven osmotic gradients (Wilhelm de Almeida et al., 2023, 2024a).

Controlled phenotyping platform experiments demonstrate that G14 achieved superior whole-plant water use efficiency (WUEpl_n) under high water deficit, reaching 2.8 g C L^{-1} compared to 2.1 g C L^{-1} for conventional varieties (Wilhelm de Almeida et al., 2024a) (Figure 11). These platform studies showed enhanced photosynthetic rates and maintained carboxylation capacity in LSB genotypes under severe progressive drought conditions (Ψpd to -1.2 MPa). However, comparison with multi-year field observations (Wilhelm de Almeida et al., 2023) revealed important genotype × environment interactions, where field conditions produced more complex responses as factors such as rootstock interactions, soil heterogeneity, and variable environmental conditions modulated the advantages observed under controlled platform conditions. This highlights the importance of testing across both controlled and field environments to understand true drought adaptation potential.

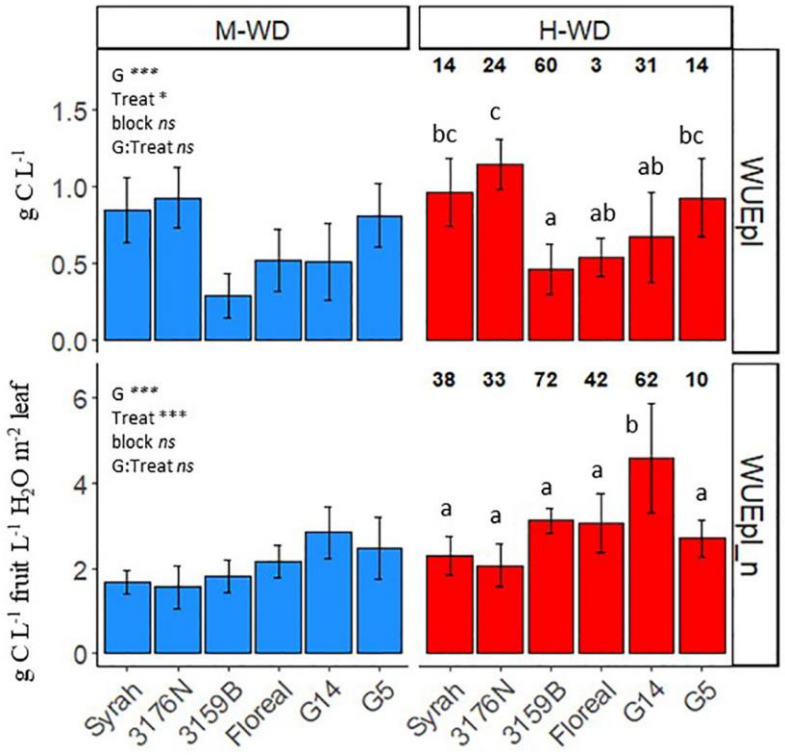

Figure 11. Multi-scale water use efficiency in fungus-tolerant grapevine genotypes under contrasting water deficit levels (adapted from Wilhelm de Almeida et al., 2024a). Upper panel: Leaf-level intrinsic water use efficiency (WUEi = An/gs). Lower panel: Normalized whole-plant water use efficiency (WUEpl_n) accounting for plant architectural differences (fruit-to-leaf ratio). Blue bars represent moderate water deficit (M-WD, SMC ~0.6) and red bars represent high water deficit (H-WD, SMC ~0.3) imposed during berry ripening. Numbers above bars indicate relative percentage increase from M-WD to H-WD. Error bars represent standard deviations. Different letters indicate significant differences among genotypes within each water treatment ($p < 0.05$). LSB genotype G14 exhibited the highest WUEpl_n under H-WD with the greatest relative increase (62%) compared to M-WD, demonstrating superior drought adaptation at the whole-plant level. At the leaf level, both G14 and 3176N showed elevated WUEi under H-WD. This multi-scale comparison demonstrates that LSB genotypes possess physiological advantages in water use efficiency that manifest from leaf-level processes to whole-plant performance under water-limited conditions. Statistical significance: Genotype effect (), Treatment effect () for both WUEi and WUEpl_n. Adapted from Wilhelm de Almeida et al. (2024a).

Long-term field observations (2019-2022) revealed genotype-specific drought strategies. G14 reduced vegetative growth more than reproductive development while maintaining carbon reserves, whereas G5 showed high sensitivity across all parameters (Wilhelm de Almeida et al., 2023). Despite different strategies, both LSB genotypes maintained similar total sugar content per berry due to larger fruit size, indicating that reduced carbon demand in fruits allows alternative allocation patterns during drought.

The carbon partitioning under water deficit shows that while sugar concentrations remain stable, organic acid metabolism varies significantly among genotypes. LSB varieties maintain lower tartaric but higher malic acid levels, with G14 showing minimal

sugar reduction (-7%) but substantial malate consumption (-20%) under severe deficit, suggesting active osmotic adjustment (Wilhelm de Almeida et al., 2024b).

The main finding from current research is that LSB genotypes' decoupled sugar-water transport provides a buffering mechanism against drought-induced compositional imbalances. However, the expression of this advantage depends on both stress severity and environmental complexity. Controlled phenotyping platforms reveal underlying physiological mechanisms and allow precise quantification of water use efficiency under standardized conditions (Wilhelm de Almeida et al., 2024a), while field observations demonstrate how these mechanisms perform under realistic growing conditions with multiple interacting stresses (Wilhelm de Almeida et al., 2023). This underscores the need for integrated controlled-environment and field approaches to validate the true adaptive value of the LSB trait for climate-resilient viticulture.

Critical gaps remain in understanding the genetic and molecular basis of LSB drought responses, particularly the regulation of sugar transporters and phloem machinery under stress. The fate of carbon not allocated to fruit sugars and its partitioning to other organs under drought remains unquantified. Root system responses and belowground signaling in LSB genotypes are completely unexplored. These knowledge gaps limit our ability to predict LSB performance across diverse environments and to effectively incorporate this trait into breeding programs for climate adaptation.

1.5 Scientific Questions, Hypothesis and Approaches of the Present Study

The primary objective of this study is to investigate how Low Sugar Berry (LSB) genotypes respond to water deficit compared to traditional grapevine varieties, particularly in terms of their carbon assimilation and allocation and physiological acclimation strategies under varying water regimes. The research addresses the hypothesis that at equivalent fruit water budget (fresh fruit yield), the lower berry sugar demand in LSB genotypes favors a more comfortable carbon status of the vine under water deficit, which is the main limiting factor of carbon assimilation during summer in the Mediterranean area. Two key research questions guide this investigation: first, whether individual berries of LSB and non-LSB genotypes display similar growth and primary net responses to short-term water deficit treatments applied at the green versus ripening stage, and second, what is the impact of long-term moderate water deficit over the ripening period on the carbon balance terms in LSB versus non-LSB genotypes.

To answer these questions, two complementary experiments were designed that simulate both short-term and long-term water stress scenarios, reflecting the dynamic nature of drought in viticultural environments. These experiments are grounded in the understanding that climate change is altering precipitation patterns and increasing the

frequency and severity and the timing of drought events, making it imperative to evaluate how different grapevine genotypes adapt to fluctuating water availability.

The first experiment focuses on short-term water deficit applied at two critical developmental landmarks: green stage and ripening stage. These stages were specifically selected due to their fundamentally different osmotic potentials and water transport mechanisms. During the green stage, berries maintain low osmotic potential (high water potential) with organic acids as the primary osmolytes, and water transport occurs predominantly through the xylem following a favorable water potential gradient from soil to fruit. In contrast, during ripening, berries import massive amounts of sugar up to high concentrations (>1 $mol.l^{-1}$ in conventional varieties), creating very low osmotic potential that drives water import despite the shift from xylem to phloem transport pathway (Zhang et al., 2006; Keller et al., 2015) and the decrease in stem water potential. This dramatic change in osmotic gradient between soil-vessel-fruit systems makes these two stages ideal for examining water flow dynamics under drought stress, as the driving forces for water movement differ fundamentally. Given the short duration of this experiment, the focus is on immediate hydraulic responses rather than long-term carbon accumulation patterns, allowing us to isolate how water deficit affects water transport under contrasting osmotic conditions.

This experiment was conducted under semi- controlled greenhouse conditions to isolate the effects of early and late water deficit on berry development and physiology. For the early water deficit treatment, six well-watered plants were compared with six unirrigated plants, with one of the three genotypes being an LSB variety (G5). Similarly, for the late water deficit treatment, the experiment was conducted in the Phenodyn phenotyping platform, where a fraction of transpirable soil water content of 0.26 was established, again including one LSB genotype (G5) alongside non-LSB varieties such as 3159 and Luminan. Phenodyn is an automated greenhouse equipped with a set of climatic sensors that measure light intensity, relative humidity, air temperature and VPD every minute (https://www6.montpellier.inrae.fr/lepse/Plateformes-de-phenotypage-M3P). By comparing these treatments, the study aims to determine whether berry growth and primary metabolic responses differ between LSB and non-LSB genotypes under acute water stress, particularly during critical phases of berry development.

The second experiment addresses long-term water deficit starting at the softening stage and continuing through ripening. Unlike the short-term experiment that focused solely on water flow dynamics, this long-term experiment investigates the interactive effects of carbon demand and water availability on berry development through a comprehensive multi-scale approach. During the softening-to-ripening transition, berries become strong carbon sinks requiring substantial sugar import for accumulation. As Holzapfel et al. (2012) demonstrated, carbohydrate reserves show distinct seasonal

dynamics, with root and trunk reserves being depleted from budbreak until around anthesis, then gradually restored, but the presence of developing fruit creates competitive demand for photoassimilates that can delay reserve replenishment until after harvest. Indeed, Greer and Sicard (2009) found that in Semillon vines, bunches alone sequestered 28% of total fixed carbon while accounting for 54% of shoot biomass at harvest, demonstrating the magnitude of carbon demand during ripening. This competition intensifies under water deficit, which simultaneously restricts both carbon assimilation (through reduced photosynthesis) and sugar transport to fruits (through limiting phloem sap flow or energetic supply) (Holzapfel et al., 2012; Savoi et al., 2021). This creates a complex interplay where water deficit not only affects water relations but also carbon availability and allocation patterns - a critical consideration for LSB genotypes that inherently have lower carbon requirements in fruits.

Conducted in the Phenodyn platform, this experiment includes four genotypes: G5 (LSB), G14 (LSB), and two non-LSB varieties (3159 and 3179). Water status is continuously monitored through soil moisture measurements and predawn water potential (Ψp) assessments. The experimental design captures drought responses at three hierarchical levels: (i) at the whole-plant level, measuring vegetative development, yield components, whole-plant transpiration, and carbohydrate (CHO) storage in perennial organs; (ii) at the organ level, tracking growth dynamics via imaging and primary metabolite accumulation through HPLC analysis; and (iii) at the leaf level, assessing gas exchange parameters (gs, A, E, A:gs), photosynthesis biochemistry, fluorescence parameters, and CHO storage. This multi-scale approach allows for a mechanistic understanding of how water deficit affects carbon-water interactions from cellular to whole-plant processes.

To specifically test how carbon demand modulates drought responses, some plants were adjusted to achieve comparable carbon sink strength by manipulating fruit load. LSB plants received a 50% increase in berry number compared to non-LSB genotypes, effectively normalizing the total carbon demand at the whole-plant level despite their lower per-berry sugar accumulation. This experimental design allows us to decouple the effects of inherent carbon demand differences from water deficit responses, revealing whether the LSB trait confers drought advantages through reduced carbon requirements or through other physiological mechanisms.

This adjustment ensures that carbon allocation dynamics can be accurately compared across genotypes, given that LSB varieties naturally produce higher yields at similar sugar content levels. By simulating prolonged moderate water deficit, the study aims to assess how LSB genotypes maintain their carbon balance and fruit quality under sustained water stress, relative to traditional cultivars. The integration of measurements across plant, berry, and leaf levels provides a holistic view of how reduced fruit carbon demand

in LSB genotypes cascades through different organizational scales, potentially affecting water use efficiency, carbon reserve management, and overall drought resilience. The long-term nature of this experiment captures the cumulative effects of reduced carbon assimilation under drought, altered source-sink relationships, and the potential benefits of lower fruit carbon demand in maintaining vine carbon reserves and overall plant fitness.

These experiments are highly relevant in the context of climate change, as rising temperatures and irregular rainfall patterns are increasingly challenging traditional grapevine management practices. The ability of LSB genotypes to decouple sugar accumulation from water import during ripening suggests a novel adaptation strategy that could mitigate the negative impacts of drought on fruit composition and yield stability. Moreover, LSB genotypes achieve similar fresh yields at lower fruit sugar concentrations, addressing the problematic trend of increasing alcohol content in wines caused by warming temperatures. This positions the LSB trait as a dual adaptation mechanism to the two primary constraints of climate change: water scarcity and excessive heat accumulation. Furthermore, the carbon savings achieved by LSB genotypes through reduced sugar allocation to fruits could enhance homeostasis of the plant's carbohydrate reserves in perennial organs, potentially improving resilience to other abiotic stresses and biotic constraints such as wood diseases. By evaluating their performance under controlled water deficit scenarios, the research seeks to identify whether LSB traits offer breeding opportunities for developing climate-resilient grapevines capable of maintaining balanced fruit composition and sustainable productivity under future climatic conditions.

Based on preliminary observations and existing literature, it is anticipated that LSB genotypes may exhibit greater flexibility in resource allocation under water deficit, potentially leading to reduced sensitivity to water stress due to flexible pericarp cell walls and alternative osmoregulatory mechanisms, improved carbon efficiency during ripening allowing them to maintain fruit size and quality with less reliance on high sugar loading, and enhanced drought tolerance compared to non-LSB varieties, particularly when normalized for fruit water budget or carbon demand. By addressing these hypotheses and questions, this study aims to provide empirical evidence for the physiological basis of the LSB trait and its implications for viticultural adaptation strategies. The results will inform breeding programs and management practices aimed at sustaining wine production in a changing climate, highlighting the potential benefits of LSB genotypes in balancing yield, quality, and environmental resilience.

2 Materials & Methods

2.1 Plant Material and Growth Conditions

Two experiments ("Short Term Stress (STS)" & "Long Term Stress (LTS)") were conducted from April 2025 to August 2025 using five fungus disease-tolerant grapevine genotypes comprising two Low Sugar Berry (LSB) varieties, G5 and G14, and three non-LSB varieties, 3159, 3179 and Luminan, all derived from *Muscadinia rotundifolia* × *Vitis vinifera* crosses (Wilhelm de Almeida et al., 2023). STS experiment divided in two developmental stages: green stage (STS-G) and ripening stage (STS-R). All plants (STS-G with 12 plants; STS-R with 12 plants; LTS with 56 plants) were growth from the year 2023 from hardwood cuttings, then grafted into SO4 rootstocks (with the exception of four 3159 vines that were grafted into RSB1 rootstock and two G14 vines that were grafted into 5C) and grown in 7L pots filled with a mixture of peat:perlite:sand (2:1:1, v/v/v). Plants were trained in order to maintain a structure that allowed breaking the apical dominance and allowing to have 4 fruitfull shoots along the cane (Keller, 2020). This was achieved by making a loop with the cane as seen in Figure 12. Information on plant material and experimental design are shown in Table 1. Plants were three years old at the beginning of the experiments and were pruned to maintain four shoots with comparable vigor.

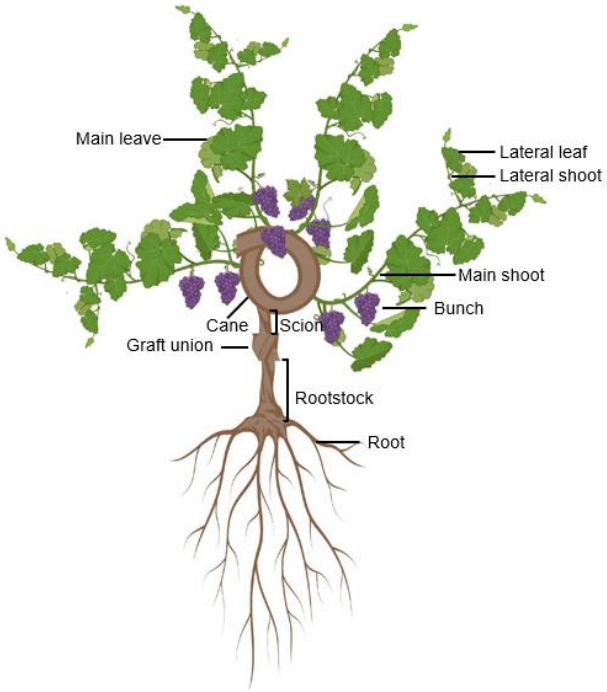

Figure 12. Scheme of pruning and training system implemented in the plants used in the experiments.

Table 1. Plant material and experimental design.

Experiment	Genotype	Treatment	Plant Age (years)	n (plants)	Rootstock	Duration (days)
STS-G	G5	WW	3	2	SO4	14
STS-G	G5	NI	3	2	SO4	14
STS-G	3159	WW	3	2	SO4	14
STS-G	3159	NI	3	2	SO4	14
STS-G	Luminan	WW	3	2	SO4	14
STS-G	Luminan	NI	3	2	SO4	14
STS-R	G5	WW	3	2	SO4	14
STS-R	G5	WD	3	2	SO4	14
STS-R	3159	WW	3	2	SO4	14
STS-R	3159	WD	3	2	SO4	14
STS-R	Luminan	WW	3	2	SO4	14
STS-R	Luminan	WD	3	2	SO4	14
LTS	3159	WW	3	5	SO4/RSB1*	49
LTS	3159	WD	3	5	SO4	49
LTS	3176	WW	3	6	SO4	44
LTS	3176	WD	3	3	SO4	44
LTS	G14	WW	3	4	SO4	41
LTS	G14	WD	3	4	SO4	41
LTS	G14	WD-C	3	3	SO4	41
LTS	G5	WW	3	3	SO4	47
LTS	G5	WD	3	4	SO4	47
LTS	G5	WW-C	3	3	SO4	47
LTS	G5	WD-C	3	4	SO4	47

WW = well-watered, NI = no irrigation (Exp1 Lot1 only), WD = water deficit, WW-C/WD-C = carbon-normalized treatments with increased berry load (LSB genotypes only). All plants grafted on SO4 rootstock except four 3159 plants grafted on RSB1 (*). Duration represents treatment period: 14 days for STS (short-term water deficit), and veraison to physiological ripeness for LTS (mean ± SD across individual plants within each genotype; see Table 4 for phenological details).

Plants initial growth took place in one of the Institut Agro Montpellier's greenhouses (43°61'N, 3°85'E). Right before the treatments started, the leaf number was adjusted similarly for all genotypes. A total of 60 main leaves were evenly distributed for Exp1 plants and 40 main leaves for LTS were retained to standardize the transpiring surface.

STS-G, that started at green stage between mid-green course and plateau (4 weeks post-flowering, 2 weeks after pea-size berries), was conducted in the same greenhouse, while for STS-R, that started at ripening at mid growth course (2 weeks post-softening) and LTS, that started from veraison to physiological maturity, plants were moved to another greenhouse of the site equipped with the Phenodyn automated phenotyping platform

(https://www6.montpellier.inrae.fr/lepse/Plateformes-de-phenotypage-M3P). In this platform, individual plant water consumption is continuously monitored through automated weighing systems providing precise irrigation control. The automated weighing and irrigation system utilized load cells with 0.01 kg precision to record pot weight every 5 minutes.

From budburst until flowering (STS-G) and two weeks prior of veraison (STS-R and LTS), plants were irrigated to meet climatic demand and maintain a well-watered condition with 500 mL of water supply 2-3 times per week. Fertilization included Osmocote and iron applied 1 week after budburst; when fruitset was occurring, another iron application was made. Finally, when STS-R and LTS were active during the ripening phase, 3 additions of nitrogen were made, one every week for 3 weeks in order to evidence any impact on the leaf SPAD values.

2.2 Environmental Monitoring

During the growing season prior to treatment initiation (STS-G), plants were maintained in the Institut Agro greenhouse where climatic conditions of 28°C day temperature and 23°C night temperature were targeted. A cooling system was activated whenever day temperatures exceeded the target, while a heating system maintained temperatures above 23°C at night.

During STS-R and LTS, environmental conditions including air temperature, vapor pressure deficit (VPD), and photosynthetic photon flux density (PPFD) were continuously monitored using the integrated sensor network of the Phenodyn phenotyping platform. Day and night periods were defined as 6:00-19:00h and 19:00-6:00h, respectively. Target environmental conditions were set at 28°C during the day and 20°C at night, with automated climate control systems maintaining these set points throughout the experimental period. Air temperature and relative humidity measurements were recorded every 10 minutes, from which VPD was calculated for day and night periods. Daily cumulative PPFD was measured by 6 sensors positioned above the plant canopy and integrated over 24-hour periods to provide mol m^{-2} d^{-1} values.

Soil temperature was continuously monitored at three depths (10, 20, and 30 cm) in six representative plants throughout LTS. Three plants were maintained under well-watered conditions (pots 2098, 2081, 2004) and three under water deficit conditions (pots 2099, 2089, 2075). Temperature measurements were recorded using thermocouples connected to a data logger, providing continuous monitoring of root zone thermal conditions throughout the experimental period from DOY 153 to 196 (June 2 to July 15, 2025; 44 days).

2.3 Leaf Area and Crop Load Normalization

To ensure comparable water and/or carbon demands between LSB and non-LSB genotypes, leaf to fruit ratio was adjusted before the beginning of the experiments.

At flowering stage, before the beginning of the experiments, 40 main leaves (10 leaves per shoot) and 8 bunches (2 per shoot) were retained on all plants (STS and LTS) to standardize the transpiring surface and C demand.

For STS, only plant water demand was normalized through leaf area adjustment. STS-G maintained 40 main leaves per plant (10 leaves per shoot) in all individuals. However, for STS-R, plants were adjusted to 60 main leaves per plant (15 leaves per shoot) to support the increased transpirational demand associated with berry expansion during ripening, when berry volume typically doubles from veraison to harvest.

At the beginning of LTS, crop load was more precisely adjusted based on approximate berry number per plant, determined through non-destructive visual classification of cluster size into three categories (small, medium, large) corresponding to estimated berry counts of 50-70, 70-90, and 90-110 berries per cluster, and the projected average berry weight and sugar concentration at harvest estimated from previous experiments conducted under identical growing conditions in the same phenotyping platform using the same genotypes (Wilhelm de Almeida et al., 2024a). The adjustment protocol involved increasing berry number by 50% in LSB genotypes through selective cluster thinning, retaining 210 berries per plant, while non-LSB genotypes were trimmed to 140 berries per plant. The different projections of water and carbon demand and their associated berry numbers are shown in Table 2.

Table 2. Experimental design and carbon demand normalization for LSB and Non-LSB genotypes.

Genotype	Treatment	Berry nb	Berry Weight (g)	Total Berry FW (g)	°Brix	Total C Demand (g)*
3159	WW/WD	140	3.94	552	21	46.3
3176	WW/WD	140	4.19	586	21	49.3
G14	WW/WD	140	4.00	560	15.75	35.3
G14	WD-C	210	4.00	840	15.75	52.9
G5	WW/WD	140	4.00	560	15.75	35.3
G5	WW-C/WD-C	210	4.00	840	15.75	52.9

*Total carbon demand = berry number × berry weight × °Brix × 0.4. WW = well-watered, WD = water deficit, and -C = carbon-normalized treatments (increased berry load in LSB genotypes to equalize total carbon demand with non-LSB genotypes). Estimated values based on previous experiments under similar conditions (Wilhelm de Almeida et al., 2024a). Carbon-normalized treatments (-C) received +50% berry number to compensate for LSB genotypes' 20-30% reduction in sugar concentration, resulting in approximately 10-15% higher projected carbon demand than non-LSB genotypes. Actual berry numbers at harvest (Table 6, Supplementary Table S4) were higher than these initial targets (mean 230 berries for

standard treatments, 285 berries for carbon-normalized treatments) due to the practical limitations of visual estimation during cluster thinning at fruit set. However, the relative increase in fruit load for carbon-normalized treatments (+22-36%) was maintained, preserving the intended experimental contrast between LSB and non-LSB genotypes' sink strengths under water deficit.

2.4 Water Management and Monitoring

2.4.1 Water Management Strategies Across Experiments

The two experiments employed different water management strategies based on their environmental conditions and objectives. STS-G, conducted in greenhouse conditions during the green berry stage, utilized a progressive drying approach where plants transitioned from well-watered to non-irrigated conditions. This design aimed to characterize immediate hydraulic responses to severe short-term water stress and subsequent recovery dynamics. During the green stage, berries maintain relatively high water potential with organic acids as primary osmolytes, and water transport occurs predominantly through the xylem following favorable water potential gradients from soil to fruit (Zhang et al., 2006; Keller et al., 2015). Under this non-irrigated (NI) treatment, plants experienced progressive soil drying until berry shriveling was observed (defined as 10% of berries displaying wrinkled skin surface), at which point recovery irrigation was applied to return plants to well-watered conditions. Predawn water potential (Ψpd), reported to two decimal places (±0.01 MPa precision), was monitored daily for NI plants and every other day for WW plants to track stress progression and recovery dynamics (see Section 2.6.3 for detailed measurement protocols). The short duration of this treatment (14 days) allowed isolation of acute water transport responses without the confounding effects of long-term carbon depletion.

In contrast, STS-R and LTS, conducted in the Phenodyn platform, required precise water status control through continuous pot weighing and automated irrigation systems to maintain stable, moderate water deficit conditions over extended periods. For STS-R (ripening stage short-term stress), a more gradual water deficit approach was employed, with berry shriveling triggering recovery irrigation. Daily monitoring of WD plants and every-other-day monitoring of WW plants allowed precise tracking of stress development and identification of the shriveling threshold (see Section 2.6.3). Once transferred to the Phenodyn platform (May 5, DOY 125), plants underwent a priming phase starting May 8 (DOY 128) at FTSW 0.6 to promote synchronized veraison across genotypes (Ojeda et al., 2002). This mild water deficit was maintained for 9-16 days (genotype-dependent) until 50% of berries within each genotype showed softening, which occurred between DOY 137-144. At veraison, differentiated water treatments were imposed: well-watered (WW) at FTSW 0.8 and water deficit (WD) at FTSW 0.28. For LTS (long-term stress treatment), stable FTSW levels were maintained through

automated irrigation, with weekly Ψpd monitoring providing validation of target water status thresholds (see Section 2.6.3).

For ripening stage experiments, berry growth compensation was incorporated into irrigation management, as berry volume typically doubles from veraison to harvest (Coombe & McCarthy, 2000; Ollat et al., 2002). Initial plant vegetative biomass at the start of STS-R and LTS was estimated based on destructive measurements of 14 plants (including plants from STS-G plus additional border plants) sampled at the green stage. These plants, representing all five genotypes (G5, G14, 3159, 3176, and Luminan), were destructively harvested to determine shoot, leaf, and trunk fresh and dry weights (Supplementary Tables S1 and S2). Shoot weight showed substantial genotypic variation, ranging from 145.66 g (G14, plant 2036) to 228.40 g (3159, plant 2040), with mean values by genotype used to estimate initial vegetative biomass for FTSW calculations at the beginning of controlled treatments. A daily weight correction factor of 2.2% was applied throughout LTS experiment to account for the estimated 100% berry mass increase over the 45-day treatment period, ensuring accurate maintenance of target FTSW levels despite ongoing fruit growth.

2.4.2 FTSW-Ψpd Calibration

To establish target FTSW values for controlled environment experiments (STS-R and LTS), the relationship between fraction of transpirable soil water (FTSW) and predawn leaf water potential (Ψpd) was determined by integrating data from two sources. FTSW reference values were obtained from previous experiments conducted under similar environmental conditions in the Phenodyn phenotyping platform, using identical substrate composition and pot dimensions. These FTSW values were related to Ψpd measurements obtained during the green stage progressive water deficit treatment (STS-G), where predawn water potential was monitored daily as plants experienced soil drying.

A four-parameter logistic model was fitted to the combined dataset (n = 39) using nonlinear least squares regression, yielding an R^2 of 0.911. This calibration revealed that FTSW values of 0.8, 0.6, and 0.28 corresponded to Ψpd of approximately -0.08, -0.09, and -0.31 MPa, respectively (Supplementary Figure S1). The logistic model appropriately captured the sigmoid relationship between soil and plant water status, including the plateau in Ψpd at high FTSW values characteristic of well-watered conditions. These empirically determined relationships guided the selection of FTSW target values to achieve desired plant water status thresholds in subsequent experiments.

2.4.3 FTSW Calculation and Threshold Definition

Following the methodology of Wilhelm de Almeida et al. (2024a), water deficit thresholds were established using the fraction of transpirable soil water (FTSW) approach, calculated as:

$$\text{FTSW} = \frac{(\text{SWactual} - \text{SWmin})}{(\text{SWmax} - \text{SWmin})} (Equation\ 1)$$

where SWactual represents daily total pot weight obtained from the automated balance system, SWmax represents total pot weight at field capacity, and SWmin represents total pot weight at permanent wilting point.

At planting, all pot components were weighed individually: empty pot weight, dry substrate weight, and initial plant fresh weight. SWmax was determined after substrate saturation and 24-hour drainage, calculated as the sum of pot tare weight, substrate weight at field capacity, and estimated plant weight for the corresponding growth stage. SWmin was determined through preliminary drying curves when relative transpiration fell below 0.1, calculated as pot tare weight plus substrate weight at permanent wilting point plus plant weight. Plant weight evolution was measured at key phenological stages (flowering, veraison, and harvest) through destructive sampling of border plants to determine actual FTSW values a posteriori, accounting for plant biomass accumulation throughout the experiment.

For practical irrigation management, target pot weights were calculated by applying the water content corresponding to 0.8 FTSW (well-watered) and 0.28 FTSW (water deficit) thresholds to the respective tare weights (pot + dry substrate + plant biomass), determining irrigation triggers for the automated system.

The threshold FTSW of 0.28 was validated through preliminary experiments showing stomatal conductance declining to 40% of well-watered controls (Lebon et al., 2006) while maintaining positive net photosynthesis rates above 5 µmol CO_2 m^{-2} s^{-1} and avoiding irreversible leaf damage indicators such as chlorophyll degradation or membrane leakage. This threshold corresponded to predawn leaf water potentials between -0.8 and -1.0 MPa across genotypes, providing a physiologically meaningful stress level for comparing genotypic responses.

2.5 Experiments

2.5.1 *Experiment 1: Short-Term Water Deficit (STS)*

The first experiment employed a factorial design examining three genotypes (G5, 3159, Luminan) under two water treatments during distinct developmental stages. As mentioned, experiment 1 was divided into two sequential phases using different plant

cohorts: green stage (STS-G) (Figure 13) and ripening stage (STS-R) (Figure 14), each consisting of 12 plants (4 plants × 3 genotypes) and conducted over 14 days each (Table 1).

For the green stage phase (STS-G), two treatments were imposed: Well-Watered (WW) plants maintained at 0.8 FTSW through daily irrigation of 0.8-1.0 L day^{-1}, and No-Irrigation (NI) plants experiencing progressive soil drying without irrigation. Plant water status was monitored through predawn water potential (Ψpd) measurements until berry shriveling (defined as 10% of berries displaying wrinkled skin surface) was observed, triggering recovery irrigation to return plants to well-watered conditions (see Section 2.6.3 for detailed measurement protocols).

The ripening stage phase (STS-R) utilized a modified approach based on STS-G results, where abrupt water stress in NI plants caused excessive Ψpd decline. Plants were adjusted to 60 main leaves (15 leaves per shoot) to support increased berry volume during ripening. Following a priming phase at 0.6 FTSW initiated at veraison, the Water Deficit (WD) treatment involved gradual FTSW reduction from 0.6 to 0.24, while control plants remained well-watered at 0.8 FTSW. **T**he WD treatment was maintained until berry shriveling occurred, triggering recovery irrigation. Water status monitoring protocols were identical to STS-G (see Section 2.6.3). This gradual approach provided a clearer physiological response to water deficit compared to the abrupt stress observed in STS-G.

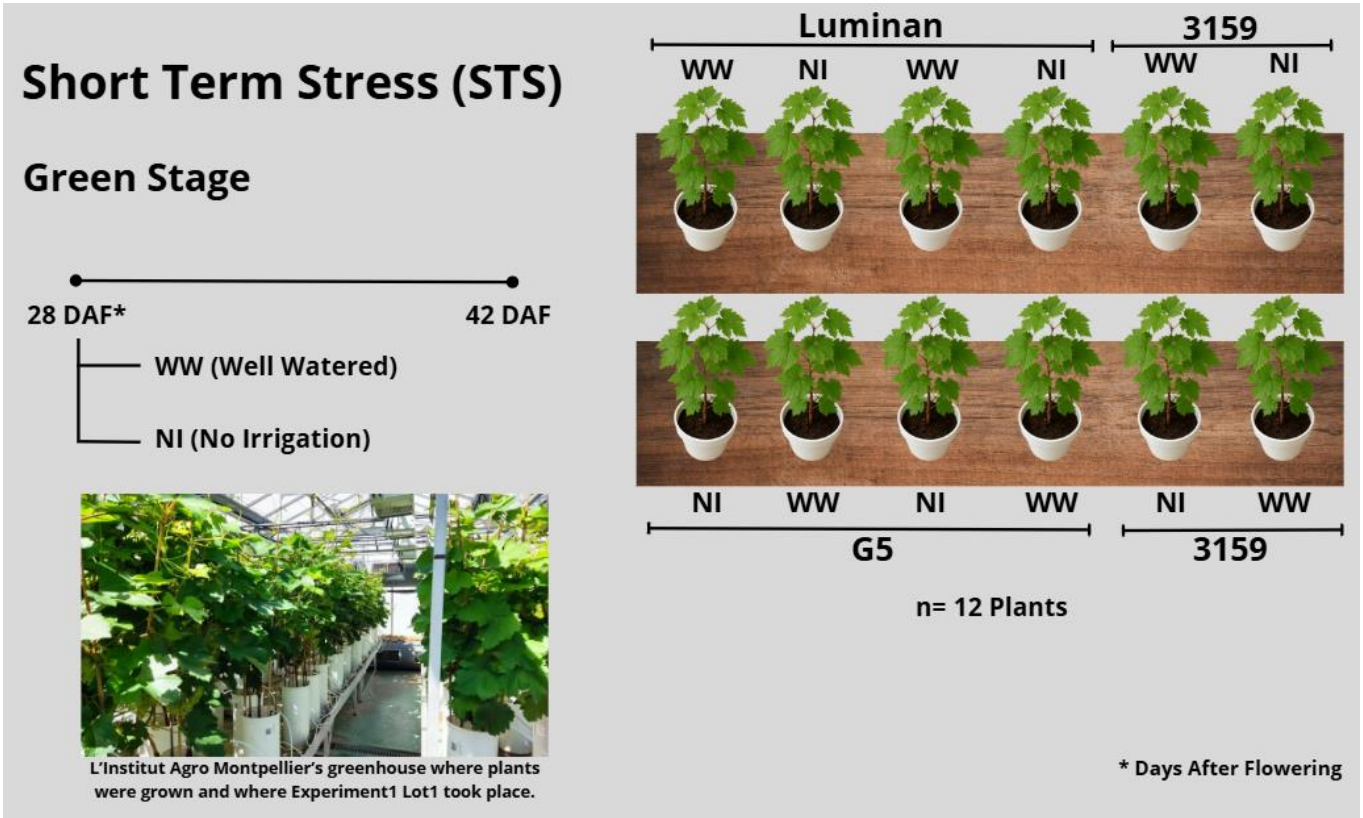

L'Institut Agro Montpellier's greenhouse where plants were grown and where Experiment1 Lot1 took place.

Figure 13. Illustration of experimental design of STS (Short-Term Stress) -G (Green Stage).

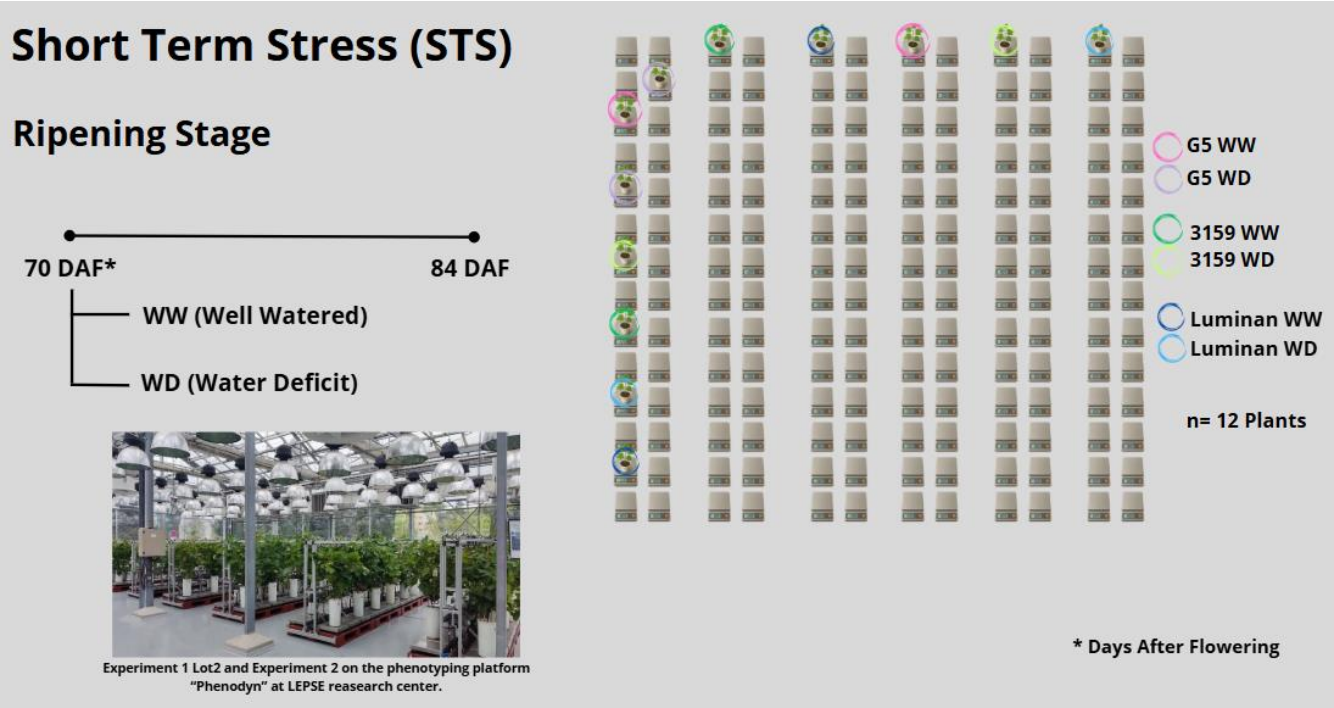

Figure 14. Illustration of experimental design of STS (Short-Term Stress) -R (Ripening Stage).

2.5.2 *Experiment 2: Long-Term Water Deficit (LTS)*

The second experiment followed a split-plot design with water treatment as the main plot factor (well-watered vs. water deficit) and genotype as the subplot factor (G5, G14, 3159, 3176) (Figure 15). An additional subplot factor was included for the Low Sugar Berry (LSB) genotypes G5 and G14 to account for crop load adjustment, comparing standard crop load with carbon-normalized crop load. The carbon normalization treatment involved increasing berry number by 50% to compensate for the approximately 25% reduction in sugar concentration characteristic of LSB genotypes, thereby equalizing total carbon demand relative to non-LSB genotypes. This treatment was designated with a "C" suffix (G5 WW-C, G5 WD-C, G14 WD-C). The interaction between water treatment and crop load adjustment allowed examination of whether carbon demand normalization in LSB genotypes would alter their physiological responses to water deficit compared to both standard LSB plants and non-LSB genotypes. This factorial design enabled separation of the effects of reduced sugar accumulation trait from the compensatory crop load adjustment on water use efficiency at both leaf and whole-plant scales. The experimental layout consisted of 56 plants total, with six plants per genotype per treatment combination for most treatments, except

G14 well-watered carbon-normalized conditions which included four plants, and five plants for each of the remaining G14 treatments (Table 1). Plants were randomly assigned within each main plot to minimize positional effects, with one empty balance position between each experimental unit to prevent competition and overlapping shade effects. Edge positions were excluded to avoid border effects from differential light exposure and temperature variations. On Figure 4 an illustration of the experimental design is shown alongside treatments and populations information.

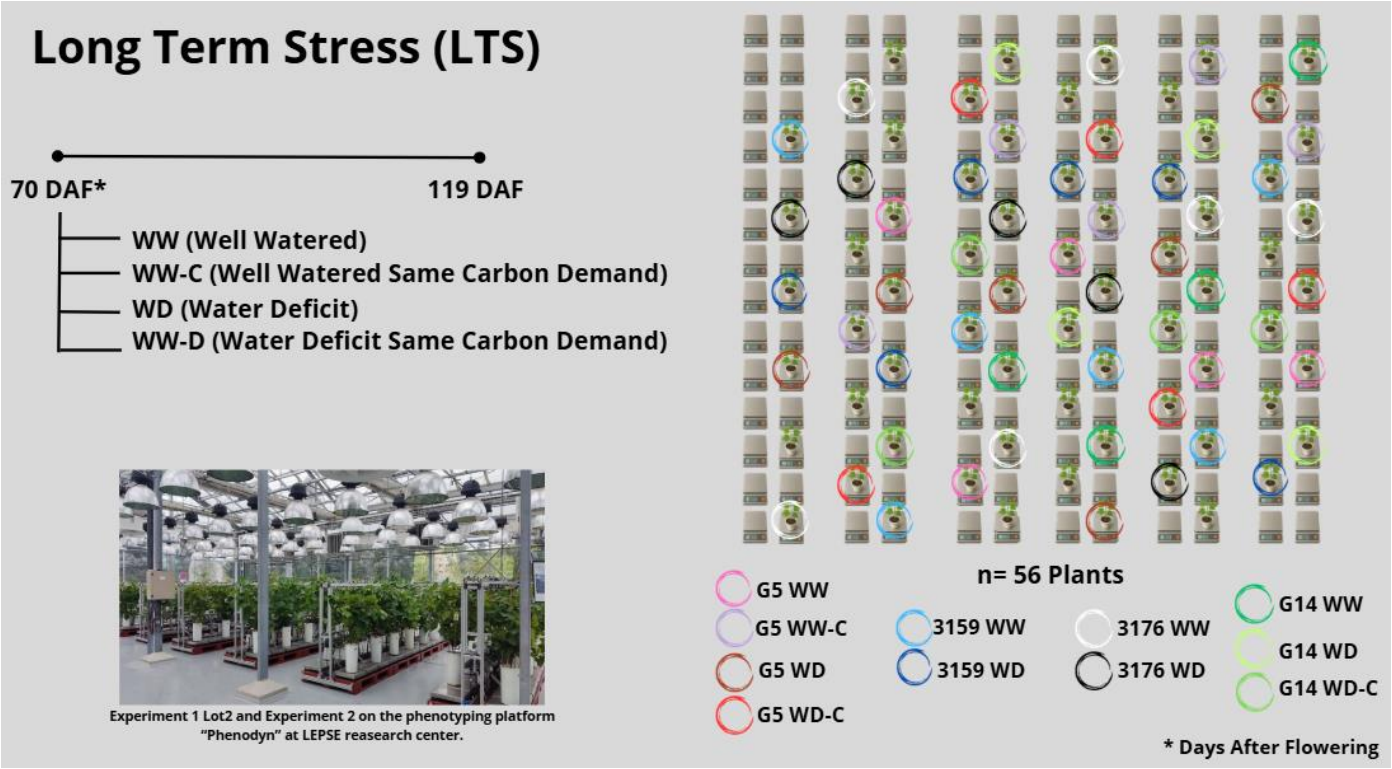

Figure 15. Illustration of experimental design of LTS (Long-Term Stress).

The well-watered (WW) treatment maintained soil water content at 80% of pot capacity through daily automated irrigation, replacing transpired water to maintain a fraction of transpirable soil water (FTSW) of 0.8 and targeting a predawn leaf water potential (Ψpd) greater than -0.2 MPa. The water deficit (WD) treatment involved withholding irrigation until reaching an FTSW of 0.28 ± 0.05, maintaining a target Ψpd between -0.8 and -1.0 MPa. The relationship between FTSW and Ψpd was established by combining FTSW reference values from previous experiments conducted under similar conditions in the Phenodyn platform with Ψpd measurements from the green stage water deficit treatment (STS-G). A logistic regression model fitted to these combined data ($R^2 = 0.911$) indicated that FTSW values of 0.8, 0.6, and 0.28 corresponded to Ψpd of approximately -0.08, -0.09, and -0.31 MPa, respectively (Supplementary Figure S1). These conditions were associated with stomatal conductance declining to 40% of well-watered controls (Lebon et al., 2006). During the treatment period, automated irrigation provided variable

amounts depending on treatment, with WW plants receiving approximately 1.0-1.5 L day^{-1} to maintain target FTSW, while WD plants received restricted irrigation of 0.2-0.4 L day^{-1} to maintain the stress level.

2.6 Measurements

The following tables correspond to a summary of all measurements done for STS and LTS (Table 3) and all of the calculated integrated values that were analyzed upon the results (Table 4).

Table 3. Summary of experimental measurements by organ level and timeline for STS and LTS.

Plant-Level Measurements						
Parameter	**Method**	**Instrument**	**Frequency**	**Exp 1**	**Exp 2**	**Purpose**
Water Relations						
Whole-plant transpiration	Gravimetric (pot weighing)	Balance/Scale	Daily	-	✓	Calculate WUEpl
Predawn water potential (Ψpd)	Pressure chamber	Scholander chamber	2x/week	✓	✓	Plant water status
Soil moisture content	Weight-based calculation	Balance	Daily	✓	✓	Maintain water treatments
Soil temperature at 3 depths (10, 20 and 30 cm)	Direct measurment	Thermocouple/ Data logger	Continuous	-	✓	Root zone conditions
Growth & Development						
Total leaf area	Image analysis	RGB camera	T0, Veraison, Harvest	-	✓	Normalize carbon demand
Vegetative biomass	Fresh/Dry weight	Balance	Harvest	-	✓	Carbon allocation
Yield components	Direct counting and weighing	Manual	Harvest	-	✓	Fruit-to-leaf ratio

Berry-Level Measurements

Parameter	Method	Instrument	Frequency	Exp 1	Exp 2	Purpose
Berry number/bunch	Manual counting	-	Weekly	✓	✓	Track fruit set
Berry volume	Image analysis (diameter measurements)	Canon EOS600D + ImageJ	Daily	✓	-	Harvest timing determination
Bunch area	Image analysis (2D projection)	Canon EOS600D + ImageJ	Weekly	-	✓	Harvest timing determination
Berry weight	Direct weighing	Precision balance	Veraison, Harvest	-	✓	Carbon accumulation
Berry dry weight	Oven drying with seed moisture correction	Drying oven + Precision balance	Harvest	-	✓	Total carbon investment
Sugar content (°Brix)	Refractometry	Digital refractometer	Weekly from veraison	-	✓	Primary metabolites
Organic acids (tartaric, malic)	HPLC	HPLC system	Harvest	-	✓	Carbon balance
Total soluble solids	HPLC analysis	HPLC system	Harvest	-	✓	Calculate varC

Leaf-Level Measurements

Parameter	Method	Instrument	Frequency	Exp 1	Exp 2	Purpose
Gas Exchange						
Net photosynthesis (An)	IRGA	LI-6800	5, 10, 25, 40 DAV	-	✓	Carbon assimilation
Stomatal conductance (gs)	IRGA	LI-6800	5, 10, 25, 40 DAV	-	✓	Water loss regulation
Transpiration rate (E)	IRGA	LI-6800	5, 10, 25, 40 DAV	-	✓	Leaf water loss
WUEi (An/gs)	Calculated	-	5, 10, 25, 40 DAV	-	✓	Instantaneous WUE
Photosynthetic Parameters						

Vcmax, Jmax	A-Ci curves	LI-6800	10 DAV	-	✓	Biochemical limitations
ΦCO2 (quantum yield)	Light curves	LI-6800	25 DAV	-	✓	Light use efficiency
qP, qN	Chlorophyll fluorescence	LI-6800 fluorometer	25 DAV	-	✓	Photoprotection
Dark respiration (Rd)	Gas exchange	LI-6800	25 DAV	-	✓	Carbon losses
Other Leaf Parameters						
Chlorophyll content	SPAD readings	SPAD meter	Weekly	-	✓	N status proxy

DAV= Days After Veraison. Measurements were conducted at plant, berry, and leaf scales throughout the experimental period. Checkmarks indicate which experiment included each measurement. Frequency indicates measurement timing relative to key phenological stages. WUEi was calculated from gas exchange parameters (see Table 4).

Table 4. Calculated integrated variables derived from primary measurements.

Variable	Formula	Scale	Data Integration
Berry volume	$0.89 \times \pi \times (D1 \times D2 \times D3) / 6$	Berry	Berry growth dynamics from imaging
Relative Growth Rate (RGR)	$\ln(V_2/V_1) / (t_2 - t_1)$	Berry	Berry growth dynamics from imaging
Mean berry weight	Total FFW / Berry number	Berry/Plant	Individual berry size
WUEpl	varC / TR	Plant	Berry C gain / Total transpiration
WUEpl_n	WUEpl × (Fruit/Leaf ratio)	Plant	Normalized to 1 kg fruit/m^2 leaf
WUEi	An/gs	Leaf	Intrinsic water use efficiency
varC	Δ(Berry mass × °Brix × 0.4)	Plant	Carbon accumulation in fruits

FTSW	(SWactual - SWmin) / (SWmax - SWmin)	Plant	Soil water status
Total transpiration (TR)	Σ(Daily water loss)	Plant	Veraison to harvest
Daily TR	Total TR / Duration (days)	Plant	Mean daily transpiration rate
Leaf area-normalized TR	Daily TR / Total leaf area	Plant	Transpiration per unit leaf area (L m^{-2} day^{-1})
Total leaf area	239.94 × LeafDW - 4674.56	Plant	Transpiring surface (from calibration)
Fruit-to-leaf ratio	Fresh fruit weight / Leaf area	Plant	Sink-source balance
δ13C	[(Rsample/Rstandard) - 1] × 1000	Leaf	Integrated WUE over ripening

Variables were computed from data collected during Exp1 and Exp2 to assess water use efficiency at multiple scales (leaf, berry, plant), carbon accumulation dynamics, and plant balance parameters. WUEpl = plant-level water use efficiency; WUEpl_n = normalized WUEpl accounting for fruit-to-leaf ratio; WUEi = intrinsic water use efficiency; FTSW = fraction of transpirable soil water; varC = variation in fruit carbon content; TR = total transpiration; δ13C = carbon isotope discrimination as integrated WUE proxy; FFW = fresh fruit weight; LeafDW = leaf dry weight.

2.6.1 Evapotranspiration Measurements

Daily evapotranspiration (ET) was calculated post-experiment from the collected weight data, using the water balance equation:

$$ET = \Delta W + I - E \ (Equation\ 2)$$

where ΔW represents the daily weight change (kg) measured from 00:00 (or 00:30) to 24:00 of each day, I represents total irrigation input (L) summed across all irrigation events, and E represents substrate evaporation standardized at 0.035 L day^{-1}. The substrate evaporation rate was determined from previous experiments with bare substrate pots under identical Phenodyn platform conditions and remained relatively constant due to controlled environmental conditions. Total evapotranspiration was calculated as the sum of daily values from treatment initiation to harvest, excluding 3-4

days when plants were transferred to dark chambers for predawn water potential and dark respiration measurements.

Irrigation was applied through five daily cycles distributed throughout the day. Within each cycle, drip irrigation pulses were activated every 20-30 minutes until the target pot weight was achieved, ensuring precise maintenance of predetermined FTSW levels (0.8 for well-watered, 0.28 for water deficit treatments). Daily plant transpiration was calculated as ET, providing genotype-specific water use data throughout the experimental period. This correction for substrate evaporation was particularly important under water deficit conditions where it could represent 10-20% of total water loss.

2.6.2 Leaf Area Measurement

Leaf area estimation followed the Phenodyn imaging protocol ("PhenoArch"), with RGB cameras capturing whole-plant images (Figure 16) at the beginning, at the middle of the experiment and finally, at the end of the experiment when plants were harvested and destroyed.

Figure 16. Plant ID 2012 in PhenoArch imaging platform for automated phenotyping.

The images of all plants were acquired within the PhenoArch platform (Cabrera-Bosquet et al., 2016), hosted at M3P (Montpellier Plant Phenotyping Platforms, https://www6.montpellier.inrae.fr/lepse/Plateformes-de-phenotypage-M3P). Images were captured for each plant from 13 different angles, which included 12 side views with a 30° rotational difference, as well as one top view.

For vegetative biomass and total leaf area estimations at veraison, plant pixels were separated from the background using a combination of thresholding and random forest algorithms (Figure 17), following the methodology described by (Brichet et al., 2017) and converted into mm2 by calibrating camera positions using reference objects. Then, total plant leaf area and shoot fresh weight were determined from calibration curves established with multiple linear regression models (Equation 3). These models were constructed based on processed images taken in the 13 directions (grapevine database) against ground truth measurements of leaf area and fresh canopy biomass (excluding biomass of clusters) at different stages. The latter measurements (total leaf area and fresh canopy biomass) were taken at the conclusion of the experiment on plants subjected to the experiments treatments.

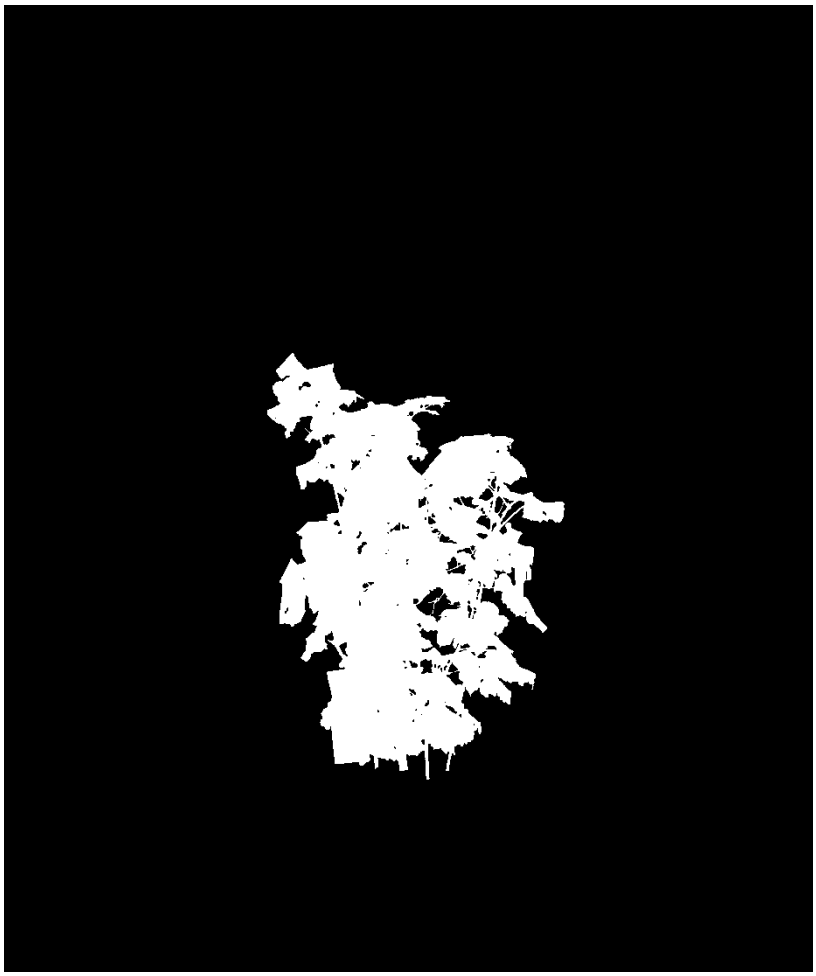

Figure 17. Plant pixel extraction through thresholding and machine learning classification.

In order to calibrate the data obtained from the Phenodyn leaf area measurements, destructive leaf area was evidenced by using a planimeter device (LI-3100C Area Meter, LiCor Biosciences GmbH, Bad Homburg, Germany). Image segmentation was performed using PlantCV software, and a calibration equation was developed from destructive measurements as shown in Equation 3 and in Figure 18.

$$LA\ (m2) = 0.95 \times Projected\_area - 0.02 (R^2 = 0.87,\ n = 56) (Equation\ 3)$$

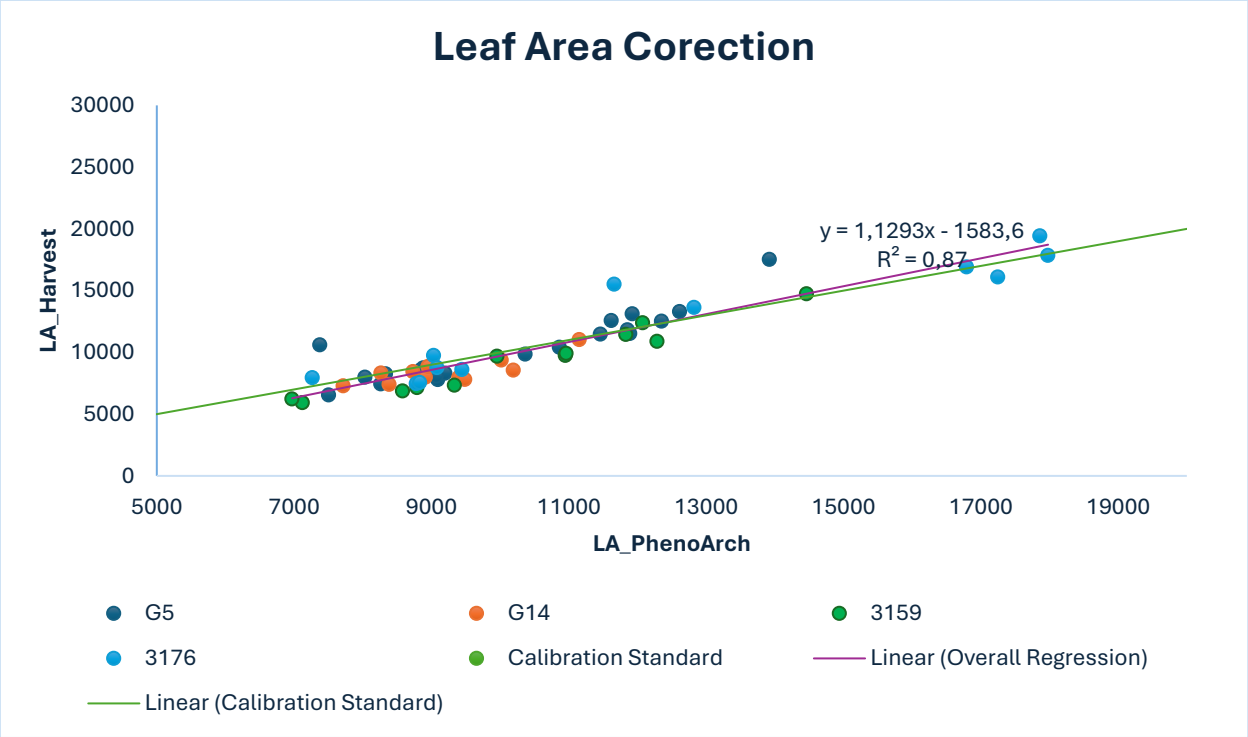

Figure 18. Leaf area calibration linear regression. Relationship between automated PhenoArch leaf area estimates (LA_PhenoArch) and destructive planimeter measurements (LA_Measured) for 56 harvested plants across genotypes. Points represent individual plants: G5 (blue), G14 (orange), 3159 (green), 3176 (cyan). Linear regression: y = 1.1283x - 1583.6, R^2 = 0.84 (pink line). Calibration Standard (green line) spans the full measurement range (0-25,000 mm^2) for calibration validation. Strong correlation (R^2 = 0.84) confirms the accuracy of non-destructive leaf area estimation throughout the experiment. Destructive measurements performed using LI-3100C Area Meter (LiCor Biosciences).

2.6.3 Water Status Measurements

Plant water status was assessed through predawn leaf water potential (Ψpd) measurements using a pressure chamber (PMS 1505D, PMS Instrument Company, Albany, OR, USA). Measurements were conducted on mature, fully expanded leaves from

the middle canopy position. The frequency and timing of measurements varied by experiment and treatment:

For STS-G (short-term stress at green stage), Ψpd was measured daily for NI plants between 04:00 and 06:00 hours under natural outdoor conditions to closely monitor stress progression until berry shriveling occurred, at which point recovery irrigation was applied. WW plants were measured every other day throughout the 14-day treatment period. Following recovery, NI plants continued to be measured every other day until the end of the treatment period.

For STS-R (short-term stress at ripening stage), plants were kept in a dark chamber overnight and Ψpd measurements were conducted between 09:00 and 11:00 hours. WD plants were measured daily to monitor stress progression until berry shriveling triggered recovery irrigation, while WW plants were measured every other day throughout the 14-day treatment period. Following recovery, WD plants continued to be measured every other day for the remainder of the treatment period.

For LTS (long-term stress treatment from veraison to harvest), plants were maintained in the dark chamber overnight with Ψpd measurements conducted weekly between 09:00 and 11:00 hours for all treatments throughout the treatment period.

For analysis of relationships between berry growth rate and plant water status, predawn water potential measured on the second day of each RGR calculation interval was used to characterize plant water status during the growth period. This approach associates each RGR value (calculated between consecutive days t_1 and t_2) with the water potential measured at time t_2, representing the water deficit severity at the end of the growth interval. This method captures the cumulative effect of water stress on berry expansion during each measurement period.

2.6.4 Gas Exchange Measurements

All gas exchange measurements were performed on one mature, fully expanded leaf per plant located in a well-exposed position in the middle canopy using a LI-6800 Portable Photosynthesis System equipped with the Multiphase Flash Fluorometer and Chamber (LI-COR Inc., Lincoln, NE, USA). Measurements were conducted approximately at 5, 10, 25, and 40 days after veraison (DAV), corresponding to DOY 154, 169, and 181 for most genotypes, with 5-6 plants measured per treatment on each date.

2.6.4.1 Standard Gas Exchange Under Saturating Light

For standard gas exchange measurements under saturating light conditions, chamber environmental parameters were set to flow rate of 600 mmol s^{-1}, photosynthetically active radiation (PAR) of 1500 µmol photons m^{-2} s^{-1}, CO_2 concentration of 400 µmol mol^{-1}, vapor pressure deficit (VPD) of 1.8 kPa, and leaf temperature of 28°C. Leaves were

systematically acclimated to chamber conditions for 5 minutes prior to measurement recording. Parameters measured included net photosynthesis (An), stomatal conductance (gs), and transpiration rate (E), from which instantaneous water use efficiency (WUE = An/E) and intrinsic water use efficiency (WUEi = An/gs) were calculated.

2.6.4.2 Dark-Adapted Gas Exchange Measurements

Dark-adapted measurements were conducted following 12-hour dark acclimation achieved by covering leaves with foil paper overnight. Chamber conditions were modified to flow rate of 400 mmol s^{-1} and PAR of 0 µmol photons m^{-2} s^{-1}. Dark respiration (Rd) and base An, gs, and E values were recorded under these conditions to assess metabolic activity and stomatal regulation independent of active photosynthesis.

2.6.4.3 Photosynthetic Capacity and Biochemical Parameters

Maximum rates of carboxylation (Vcmax) and electron transport (Jmax) were determined from photosynthesis response curves to varying intercellular CO_2 concentrations (A-Ci curves) assessed at 10 DAV on 5 plants per genotype. Response curves were measured using the dynamic assimilation technique with a continuous CO_2 ramp rate of 160 µmol mol^{-1} min^{-1}, consisting of a ramp down from 400 to 10 µmol mol^{-1} followed by a ramp up from 10 to 1100 µmol mol^{-1} (Saathoff and Welles, 2021). Vcmax and Jmax parameters were estimated from A-Ci fits using the 'plantecophys' R package (Duursma, 2015).

2.6.4.4 Light Response Curves and Chlorophyll Fluorescence

Light response curves (An-PAR) and chlorophyll fluorescence parameters were assessed at 25 DAV on 4 plants per treatment. Following dark adaptation and initial dark respiration measurements, leaves were acclimated at 1800 µmol photons m^{-2} s^{-1} and gas exchange measurements were recorded at 3-5 minute intervals at decreasing PAR levels of 1800, 1500, 1200, 900, 700, 600, 500, 400, 300, 200, 100, 50, and 0 µmol photons m^{-2} s^{-1}. Chlorophyll fluorescence measurements (Fm', Fo', Ft) were collected simultaneously to calculate photochemical quenching (qP) and non-photochemical quenching (qN). Apparent quantum yield (ΦCO_2) was estimated from light response curves fitted with the non-rectangular hyperbola model (Villalobos-González et al., 2022). Additionally, stomatal conductance was monitored twice weekly throughout the experimental period using a LI-600 Porometer (LI-COR Inc., Lincoln, NE, USA) to provide higher temporal resolution between comprehensive gas exchange measurement campaigns.

2.6.5 Leaf Chlorophyll Content (SPAD)

Leaf chlorophyll content was assessed weekly throughout LTS using a SPAD-502 Plus chlorophyll meter (Konica Minolta, Tokyo, Japan) as a proxy for nitrogen status and to monitor potential stress-induced chlorophyll degradation. Measurements were conducted on one mature, fully expanded leaf per plant located in a well-lit position in the middle canopy. Five SPAD readings were taken at different positions along each leaf and averaged to obtain a representative chlorophyll content value per plant per measurement date. Measurements were conducted weekly from veraison (approximately DOY 147) through harvest (DOY 181-196, depending on genotype), providing temporal assessment of leaf chlorophyll status throughout the ripening period.

2.6.6 Berry Image Analysis and Leaf:Fruit Ratios

Non-destructive monitoring of berry and bunch development was conducted through longitudinal imaging analysis. At the beginning of LTS, three representative clusters per plant were selected based on cluster size, berry density, and accessibility for consistent imaging, ensuring adequate berry number for longitudinal tracking throughout ripening. Selected clusters were tagged and imaged weekly from veraison through harvest.

2.6.6.1 Image Acquisition and Analysis

Images were captured using a professional digital camera (Canon EOS600D, Canon Inc., Tokyo, Japan) positioned approximately 1.5 meters from clusters under natural greenhouse lighting conditions. Images were transferred using EOS Utility2 software (Canon Inc.) and analyzed using ImageJ software (version 1.53, NIH, Bethesda, MD, USA) (Figure 19).

For STS (short-term stress experiments), 2-5 individual berries per plant within reference clusters were tagged and imaged daily to monitor rapid volume changes during acute water deficit, resulting in 7-9 tracked berries per genotype × treatment combination for analysis:

$$\text{Volume} = 0.89 \times \pi \times (\text{D1} \times \text{D2} \times \text{D3}) / 6 \quad (Equation\ 4)$$

where the coefficient 0.89 accounts for the deviation of grape berry shape from a perfect ellipsoid.

For temporal analysis of volume dynamics during STS experiments, absolute berry volumes were normalized to relative volume at treatment initiation. The initial volume measurement (V_o) taken at the start of each experiment (DOY 108 for STS-G, DOY 157 for STS-R) was set as the reference value (relative volume = 1.0). Subsequent volume measurements were expressed as:

$$\text{Relative Volume} = \text{V(t)} / \text{V}_0 \quad (\text{Equation } 5)$$

where V(t) represents berry volume at time t and V_0 represents initial berry volume. This normalization enabled direct comparison of volume change patterns across berries of different initial sizes and between genotypes."

For LTS (long-term treatment from veraison to harvest), bunch area (cm^2) was measured weekly from the three tagged clusters per plant using ImageJ polygon selection and area measurement tools. Bunch area dynamics were used to determine physiological ripeness, defined as maximum area followed by stable or declining measurements over consecutive monitoring dates, indicating completion of berry cell expansion. This criterion allowed genotype-specific harvest timing while ensuring all plants reached equivalent physiological maturity.

The analyzed images were used to determine treatment timing for NI and WD treatments for STS-G and STS-R, respectively, by indicating when berry shriveling occurred (defined as 10% of berries displaying wrinkled skin surface). Also, for LTS, berry imaging analysis was used to determine physiological ripeness (Wilhelm de Almeida et al. 2024a), thus terminating the ongoing treatment.

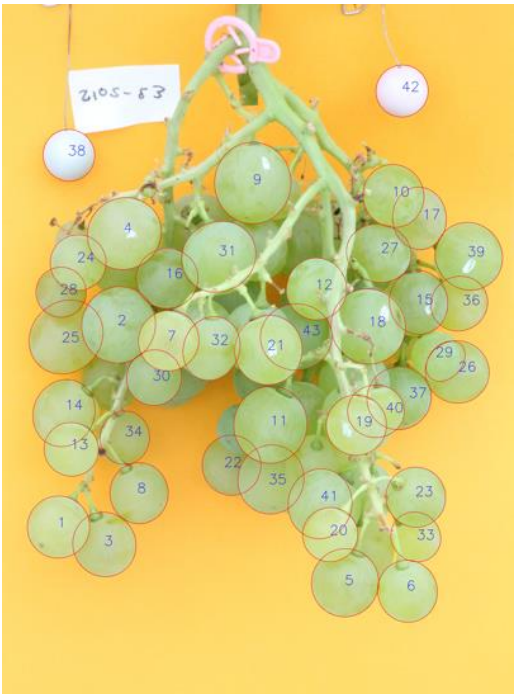

Figure 19. STS-G single berry image analyzed through software (EOS Utility2, ImageJ).

Destructive sampling was conducted at the end of experiments using 50-berry samples per plant to determine fresh weight. Dynamic leaf:fruit ratios were calculated as leaf area to berry ratio (total leaf area in cm^2 divided by total berry number), leaf area to yield ratio (total leaf area in m^2 divided by fresh fruit weight in kg), and source:sink index calculated as (An × LA) divided by (berry number × sugar accumulation rate).

2.6.6.2 Berry Growth Rate Analysis

Relative growth rate (RGR) was calculated to quantify instantaneous berry expansion rates between consecutive measurement points. RGR represents the fractional change in berry volume per unit time and was calculated as:

$$\mathrm{RGR} = [\ln(V_2) - \ln(V_1)] / (t_2 - t_1) \text{ (Equation 6)}$$

where V_1 and V_2 represent berry volumes at consecutive time points t_1 and t_2, and (t_2 - t_1) represents the time interval in days. RGR is expressed in units of day^{-1}, with positive values indicating volume increase (expansion) and negative values indicating volume decrease (shrinkage). This logarithmic transformation provides a growth rate metric that is independent of absolute berry size and accounts for compound growth dynamics.

For each tracked berry, RGR values were calculated between all consecutive measurement pairs throughout the experimental period. Berry growth data were subsequently classified into distinct response phases: stress phase (treatment initiation to shriveling point) and recovery phase (post-rewatering to experiment termination). Mean RGR values and their variability (standard deviation) were calculated separately for each phase, genotype, and treatment combination to characterize temporal growth dynamics under varying water status conditions.

2.6.7 Fruit Carbon Accumulation (varC)

Variation in fruit carbon content (varC) from veraison to harvest was calculated to quantify total carbon accumulation in berries during ripening. varC represents the change in carbon equivalents of major soluble metabolites (glucose, fructose, tartaric acid, and malic acid) measured at both veraison and harvest.

At both developmental stages, 50-berry samples were collected for HPLC analysis (see Section 2.6.8). Carbon content was derived from the molecular composition and carbon stoichiometry of each metabolite. Total plant fruit carbon content was calculated as:

$$\mathrm{varC} = \Delta(\text{Berry number} \times \text{Berry mass} \times {}^{\circ}\mathrm{Brix} \times 0.4) \ (Equation\ 7)$$

where Berry number is the total number of berries per plant at harvest, Berry mass is the average berry fresh weight (g), °Brix is the soluble solids concentration measured by refractometry, and 0.4 is the conversion factor from sugar content to carbon equivalents. The Δ symbol represents the change from veraison to harvest. This calculation provides a whole-plant measure of carbon investment in fruit development during ripening and was used to calculate plant-level water use efficiency (WUEpl = varC / TR).

2.6.8 Metabolite Analysis

2.6.8.1 Berry Sampling and Juice Preparation

At harvest (physiological ripeness), 50-berry samples were collected from each plant. Fresh berry juice was extracted by crushing the berries. For metabolite preservation and analysis, juice samples were prepared by adding 1 mL of fresh juice to 1 mL of HCl in microcentrifuge tubes. These acidified juice samples were then transported for external HPLC analysis.

2.6.8.2 Berry Dry Weight and Seed Moisture Correction

Berry dry weight was determined to assess total carbon investment per berry, including both structural components (pericarp and seed tissues) and accumulated non-structural carbohydrates. At harvest (physiological ripeness), 50-berry samples were collected from each plant and fresh berry weight was determined. Berries were then manually opened, and seeds were carefully extracted and weighed to determine seed fresh weight. Following seed removal, juice was extracted from the remaining pericarp tissue by crushing for metabolite analysis. The crushed pericarp tissue was then oven-dried at 60°C for 72 hours until constant weight was achieved, and dry pericarp weight was measured using a precision balance.

Total berry dry weight was calculated accounting for differential moisture retention between seed and pericarp tissues at physiological maturity. While pericarp tissue dries completely during oven drying, grape seeds retain residual moisture even at harvest maturity. Seed dry weight was calculated assuming 20% residual moisture content at harvest maturity. This value is supported by multiple studies documenting seed water content during late ripening in *Vitis vinifera*, which report seed moisture declining from approximately 35-40% at veraison to 19-26% at harvest maturity depending on cultivar, environmental conditions, and harvest timing (Ristic and Iland, 2005; Greer and Weston, 2010; Bonada et al., 2013). The 20% moisture content represents a conservative estimate within the reported range for harvest-mature seeds.

Total berry dry weight was calculated as:

$$\text{Berry DW} = \text{Pericarp DW} + (\text{Seed FW} \times 0.80) \quad (Equation\ 8)$$

where Berry DW represents total berry dry weight, Pericarp DW is the measured pericarp dry weight after oven drying, Seed FW is the measured seed fresh weight per berry, and 0.80 represents the seed dry matter fraction (100% - 20% moisture content). This calculation accounts for seeds retaining approximately 20% moisture at physiological maturity, ensuring accurate representation of total carbon investment in berry tissues including both structural and non-structural components.

2.6.8.3 Sugar Measurements

Sugar concentration was measured at harvest using two methods. Soluble solids concentration (°Brix) was determined by digital refractometry on fresh juice at physiological ripeness. Individual glucose and fructose concentrations were quantified by HPLC analysis following the methodology described in Bigard et al. (2022). Total hexose concentration was calculated as the sum of glucose and fructose concentrations and expressed in $mmol \cdot L^{-1}$. The glucose:fructose ratio was calculated to assess sugar balance in berries.

2.6.8.4 Organic Acid Analysis

Malic acid and tartaric acid concentrations were determined at harvest by HPLC analysis on the acidified juice samples. Concentrations were expressed in $mmol \cdot L^{-1}$ for both diprotic organic acids. The malic:tartaric acid ratio was calculated from these measurements to characterize the organic acid balance. Total organic acidity was calculated as the sum of malic and tartaric acid concentrations.

2.6.9 Carbon Isotope Discrimination (δ13C) Analysis

For LTS, at harvest, 50-berry samples were collected from each plant and crushed to extract fresh juice. For HPLC analysis, 1 mL of juice was mixed with 1 mL of HCl in microcentrifuge tubes. These samples were sent for external HPLC analysis to quantify glucose, fructose, malic acid, and tartaric acid concentrations following the methodology described in Bigard et al. (2022). Total hexose concentration was calculated as the sum of glucose and fructose. Soluble solids concentration (°Brix) was measured at harvest on fresh juice using a digital refractometer.

Carbon isotope discrimination (δ13C) was measured to assess integrated water use efficiency over the experimental period. Leaf samples were collected at harvest from the same leaves used for gas exchange measurements. Samples were oven-dried at 60°C for 72 hours, ground to fine powder using a ball mill, and weighed into tin capsules (0.8-1.0 mg). Carbon isotope composition was determined using an isotope ratio mass spectrometer (IRMS) coupled to an elemental analyzer. The δ13C values were calculated relative to the Vienna Pee Dee Belemnite (VPDB) standard as: $\delta^{13}C\ (‰) = [(R_{sample}/R_{standard}) - 1] \times 1000$, where R is the 13C/12C ratio. Carbon isotope discrimination (Δ13C) was calculated from δ13C values assuming an atmospheric δ13C of -8‰. Higher (less negative) δ13C values indicate greater water use efficiency, as stomatal closure under water deficit reduces discrimination against the heavier 13C isotope. Measurements were performed at the Stable Isotope Facility (Montpellier, France).

2.7 Statistical Analysis

Data were analyzed in R Studio version 4.3.0 using linear mixed-effects models with repeated measures, incorporating genotype, water treatment, time, and their interactions as fixed effects, with plant nested within treatment as a random effect. ANOVA for the split-plot design was performed using the car and lmerTest packages in R. Post-hoc comparisons were conducted using emmeans with Tukey adjustment for multiple comparisons. Pearson correlation analysis was performed to assess relationships between berry relative growth rate (RGR) and predawn water potential (Ψpd) in STS experiments, with correlations calculated separately for each genotype, developmental stage, and treatment combination. For each RGR value calculated between consecutive days, the corresponding Ψpd measured at the end of the growth interval was used in the correlation analysis. Statistical significance for all tests was assessed at $\alpha = 0.05$.

3 Results

3.1 *Experiment 1: Short-term Water Deficit Response (STS)*

3.1.1 Water Status Response to Short-term Stress

3.1.1.1 Green Stage Water Deficit (STS-G)

Under well-watered conditions, all three genotypes maintained stable predawn water potential (Ψpd) throughout the 14-day treatment period, with values ranging from -0.04 to -0.22 MPa (Figure 20). In contrast, no irrigation (NI) plants exhibited rapid and progressive decline in Ψpd beginning immediately after treatment initiation at DOY 108, demonstrating the sensitivity of green-stage berries to soil water depletion.

Genotypic differences in stress sensitivity were evident both in the rate of Ψpd decline and the minimum values reached before berry shriveling occurred. G5 displayed the highest susceptibility to water stress, with berries shriveling at relatively mild stress levels (Ψpd of -0.73 and -0.82 MPa, mean: -0.78 MPa, n=2 at DOY 113-116). Genotype 3159 showed intermediate stress tolerance, reaching minimum Ψpd values of -1.01 and -1.23 MPa (mean: -1.12 MPa) at DOY 112-116 before shriveling occurred. Luminan demonstrated the highest water stress tolerance among the three genotypes, withstanding the most severe water deficit before berry shriveling was observed, with minimum Ψpd values of -1.05 and -1.50 MPa (mean: -1.28 MPa) at DOY 113-114.

Following recovery irrigation, all genotypes exhibited rapid restoration of water status. Luminan, despite experiencing the most severe stress, showed the fastest recovery rate, returning to Ψpd values above -0.15 MPa within 3 days of re-watering. By DOY 117, Luminan plants recovered to Ψpd values of -0.15 MPa, while 3159 reached -0.08 MPa by DOY 117. G5 plants, which experienced milder stress, maintained stable Ψpd values around -0.15 MPa throughout the recovery period. Similarly, 3159 recovered to near well-watered status (-0.08 MPa) by DOY 117. G5 plants, having experienced less severe stress, maintained relatively stable Ψpd values throughout both the stress and recovery periods. By the conclusion of the 14-day treatment period (DOY 121), all NI plants had fully recovered, displaying Ψpd values comparable to their well-watered counterparts (-0.04 to -0.15 MPa).

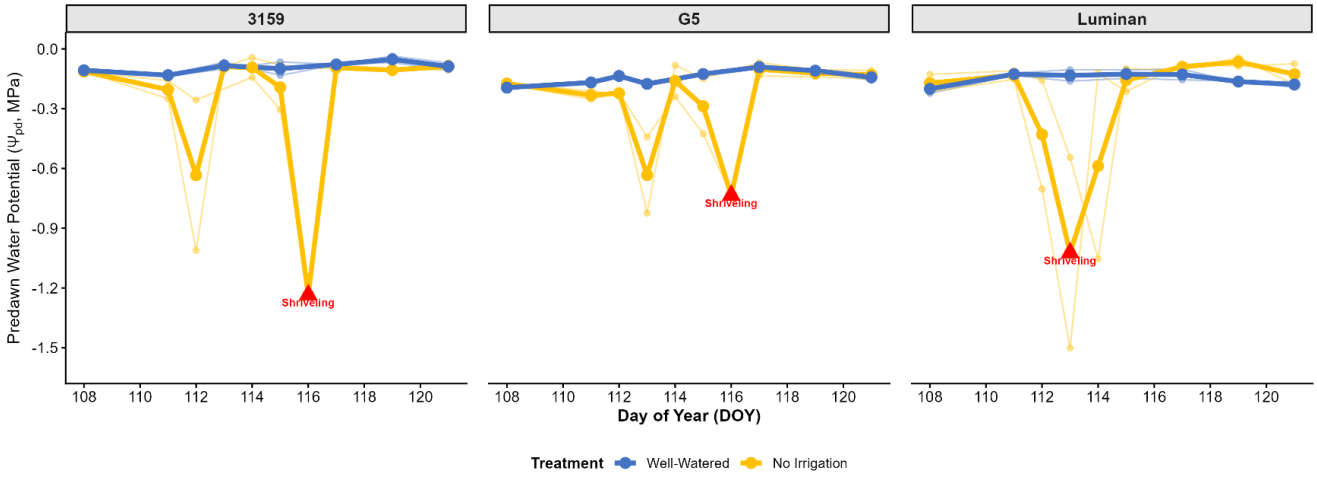

Figure 20. Predawn water potential response to water deficit at green stage (STS-G). Temporal dynamics of predawn water potential (Ψpd) in three grapevine genotypes (3159, G5, Luminan) subjected to well-watered (WW, blue) or no irrigation (NI, yellow) treatments during the green stage over a 14-day period (DOY 108-121). Thin lines represent individual plant trajectories (n=2 per genotype × treatment), while thick lines and large symbols represent treatment means. Red triangles mark the timing of berry shriveling observation (lowest mean Ψpd), which triggered recovery irrigation in NI plants. NI plants were measured daily to closely monitor stress progression, while WW plants were measured every other day. Lines connect data points across measurement dates to show temporal trends.

3.1.1.2 Ripening Stage Water Deficit (STS-R)

The ripening stage water deficit treatment (STS-R) (Figure 21) revealed markedly different stress dynamics compared to the green stage. The more gradual irrigation reduction, measured as Fraction of Transpirable Soil Water (FTSW) declining from 0.6 to 0.24 (Supplementary Figure S1), resulted in a slower Ψpd decline but ultimately reached lower minimum Ψpd values (mean: -1.51 MPa across genotypes) compared to the green stage (mean: -1.06 MPa). Well-watered plants maintained consistently high Ψpd values throughout the treatment period, ranging from -0.04 to -0.16 MPa, with minimal temporal variation.

Water deficit plants exhibited genotype-specific patterns of stress development and severity, with all genotypes reaching substantially lower minimum Ψpd values at shriveling during ripening (mean: -1.51 MPa) compared to the green stage (mean: -1.06 MPa). Genotype 3159 demonstrated the most pronounced stress tolerance, declining to minimum Ψpd values of -1.60 and -1.80 MPa (mean: -1.70 MPa) at DOY 162-163 (5-6 days after treatment initiation), representing the most severe water deficit tolerated before shriveling among all genotypes at the ripening stage. G5 plants exhibited intermediate stress severity, with berry shriveling occurring at minimum Ψpd values of -1.44 and -1.60 MPa (mean: -1.52 MPa) at DOY 162. Luminan showed the lowest tolerance, with shriveling observed at minimum Ψpd values of -1.06 and -1.56 MPa

(mean: -1.31 MPa) at DOY 162-163. These shriveling thresholds during ripening (Ψpd: -1.31 to -1.70 MPa) were substantially lower than those observed during the green stage (Ψpd: -0.78 to -1.28 MPa).

The ranking of genotypic tolerance to berry shriveling reversed between developmental stages. During the green stage, G5 showed the highest susceptibility (shriveling at Ψpd -0.78 MPa), while Luminan showed the lowest susceptibility (shriveling at -1.28 MPa), and 3159 was intermediate (shriveling at -1.12 MPa). During ripening, this pattern reversed: 3159 became the most tolerant (withstanding -1.70 MPa before shriveling), G5 showed intermediate tolerance (withstanding -1.52 MPa), and Luminan showed the lowest tolerance (shriveling at -1.31 MPa). Shriveling thresholds observed at the ripening stage showed genotype-specific shifts relative to the green stage. Luminan exhibited minimal change (0.03 MPa difference: -1.28 to -1.31 MPa), while G5 showed the largest shift (0.74 MPa difference: -0.78 to -1.52 MPa), and 3159 displayed an intermediate shift (0.58 MPa difference: -1.12 to -1.70 MPa).

Recovery dynamics following re-watering at ripening were more gradual than observed at the green stage. All genotypes required 4-6 days to return to Ψpd values above -0.20 MPa. By DOY 169 (end of the treatment period), all WD plants had recovered to stable Ψpd values ranging from -0.08 to -0.18 MPa, comparable to well-watered controls.

Genotypic ranking of stress tolerance at berry shriveling showed a developmental stage dependency. At the green stage, shriveling occurred at Ψpd values ranging from -0.78 to -1.28 MPa, while at the ripening stage, shriveling thresholds were lower, ranging from -1.31 to -1.70 MPa across genotypes. The order of genotypic susceptibility also differed between stages, with 3159 showing the highest tolerance during ripening (shriveling at -1.70 MPa) compared to its intermediate position during the green stage (shriveling at -1.12 MPa).

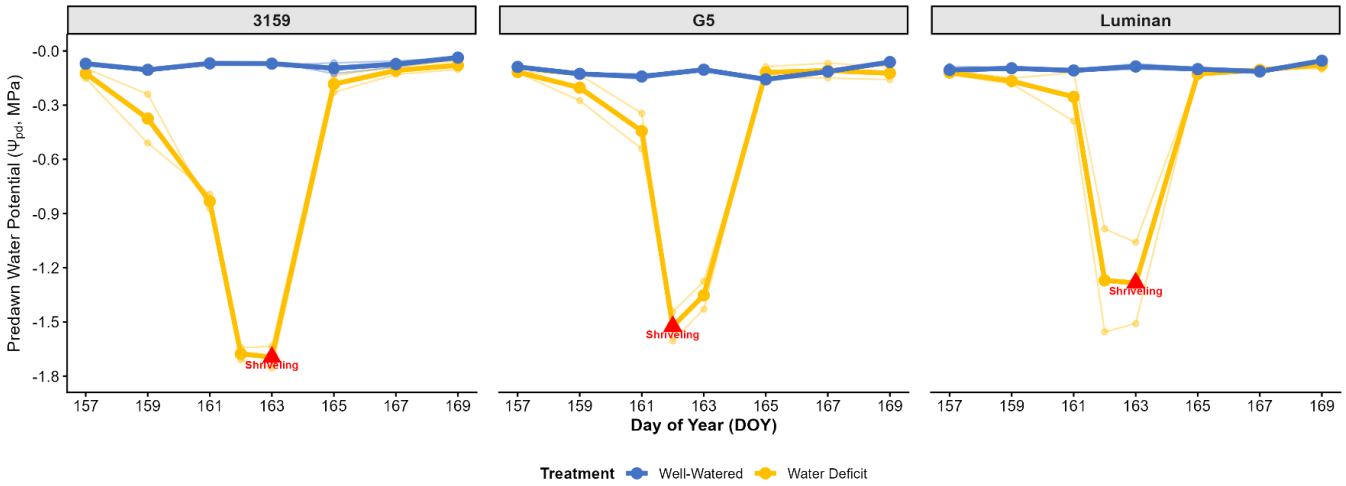

Figure 21. Predawn water potential response to water deficit at ripening stage (STS-R). Temporal dynamics of predawn water potential (Ψpd) in three grapevine genotypes (3159, G5, Luminan) subjected to well-watered (WW, blue) or water deficit (WD, yellow) treatments during the ripening stage over a 13-day period (DOY 157-169). Thin lines represent individual plant trajectories (n=2 per genotype × treatment), while thick lines and large symbols represent treatment means. Red triangles mark the timing of berry shriveling observation (lowest mean Ψpd), which triggered recovery irrigation in WD plants. WD plants were measured daily to closely monitor stress progression, while WW plants were measured every other day. Lines connect data points across measurement dates to show temporal trends.

3.1.2 Berry Growth Response to Water Deficit

3.1.2.1 Green Stage Berry Volume Response to Water Deficit

Berry volume responses to water deficit during the green stage were monitored through daily imaging analysis of individual tagged berries from DOY 108 to 123. Volume measurements were normalized to initial berry size at treatment initiation (relative volume = 1.0).

Under no irrigation (NI) conditions, berry volume trajectories diverged from well-watered (WW) controls beginning at DOY 110-112, corresponding to the period when plant predawn water potential declined below -0.4 MPa (Figure 22). At the point of berry shriveling (DOY 112-116, when 10% of berries displayed wrinkled skin surface), mean relative volume was 0.99 ± 0.21 for 3159, 1.26 ± 0.48 for G5, and 0.97 ± 0.15 for Luminan (Table 5). These values indicate minimal net volume loss, with G5 showing a mean volume increase of 26% at the shriveling point. Individual berry responses varied substantially within genotypes, as reflected in large standard deviations. For 3159, volume loss at shriveling ranged from -10.4% to +26.6% across individual berries. G5 exhibited the greatest variability, with individual berry volumes ranging from -44.3% to -0.2% (all showing net volume loss despite some berries maintaining nearly constant size) at the shriveling point. Luminan showed intermediate variability, with volume changes ranging from -28.0% to +16.6%.

Following recovery irrigation at DOY 113-116, berry volume increased rapidly across all genotypes (Figure 23). By DOY 117 (1-3 days post-rewatering), mean relative volumes reached 1.35 ± 0.25 for 3159, 1.68 ± 0.48 for G5, and 1.20 ± 0.18 for Luminan. Recovery to at least 95% of initial volume occurred within 1.0 to 1.38 days after rewatering across all genotypes. By the end of the experimental period (DOY 123), stressed berries had exceeded their initial volumes by 68 ± 72% (3159), 122 ± 125% (G5), and 46 ± 50% (Luminan). Final relative volumes were 1.68 ± 0.72, 2.22 ± 1.25, and 1.46 ± 0.50 for 3159, G5, and Luminan respectively.

Well-watered berries exhibited continuous growth throughout the 15-day period, with no plateau or decline phase observed (Figure 23). By DOY 123, WW berries reached relative volumes of 4.83 ± 1.18 (3159), 2.68 ± 0.52 (G5), and 2.02 ± 0.31 (Luminan). The

growth trajectory of 3159 WW berries showed marked acceleration after DOY 118, reaching approximately 5-fold initial volume by DOY 123, while G5 and Luminan WW berries displayed more gradual exponential expansion patterns.

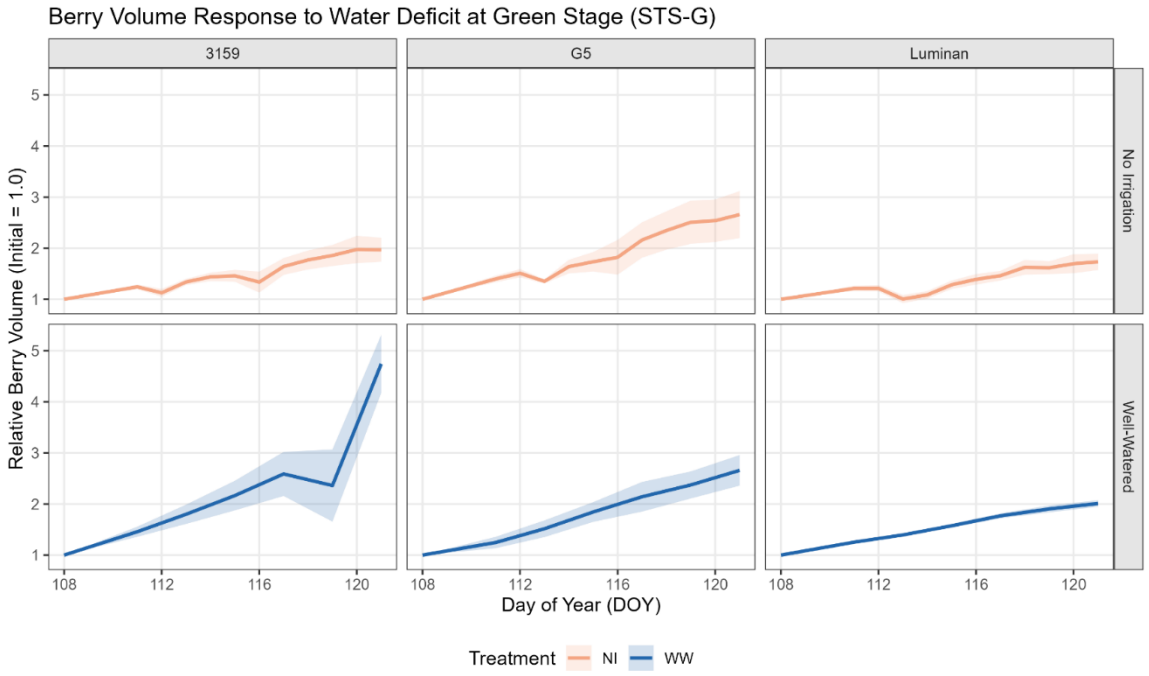

Figure 22. Berry volume response to water deficit at green stage (STS-G). Temporal dynamics of relative berry volume (normalized to initial volume = 1.0) in three grapevine genotypes (3159, G5, Luminan) subjected to well-watered (WW, blue) or no irrigation (NI, orange) treatments during the green stage over a 15-day period (DOY 108-123). Lines represent treatment means with shaded areas indicating standard error (n = 4 plants per genotype × treatment, 1-5 berries tracked per plant). Berry shriveling (10% of berries with wrinkled skin) occurred at DOY 112-116 for NI plants, triggering recovery irrigation. NI plants show minimal volume loss during stress followed by rapid recovery and continued growth after rewatering. WW plants display continuous exponential growth, particularly pronounced in genotype 3159 after DOY 118.

3.1.2.2 Ripening Stage Berry Volume Response to Water Deficit

Berry volume dynamics during the ripening stage were monitored from DOY 157 to 169 following treatments imposed after a priming period at veraison. Volume measurements were again normalized to initial size at the start of differentiated treatments (relative volume = 1.0).

Water deficit (WD) berries maintained relatively stable volumes throughout the stress period, despite plants reaching predawn water potential values of -1.44 to -1.75 MPa (Figure 24). At the point of berry shriveling (DOY 162-163), mean relative volumes were 0.97 ± 0.04 for 3159, 1.10 ± 0.06 for G5, and 1.15 ± 0.14 for Luminan (Table 5). Volume loss at shriveling was minimal: -2.57 ± 3.71% for 3159, +9.90 ± 6.08% for G5, and +14.5 ± 14.2% for Luminan. Individual berry variability during ripening was substantially

reduced compared to green stage, with volume changes at shriveling ranging from -0.7% to +4.8% (3159), -10.7% to -6.1% (G5), and -19.2% to -2.9% (Luminan). Notably, while mean relative volumes at shriveling suggested volume stability or slight gains for G5 and Luminan (1.10 and 1.15 respectively), individual berry trajectories showed that some berries within these populations experienced modest volume losses.

The time course of volume change showed minimal fluctuation in WD berries between DOY 157 and 162, with relative volumes remaining between 0.97 and 1.03 for 3159, 1.00 and 1.09 for G5, and 1.00 and 1.13 for Luminan (Figure 23). Following recovery irrigation at DOY 162-163, berry volumes increased modestly, reaching mean relative volumes of 1.02 ± 0.05 (3159), 1.18 ± 0.03 (G5), and 1.13 ± 0.06 (Luminan) by DOY 165. Recovery to at least 95% of initial volume occurred within 1.0 to 2.43 days after rewatering, with 3159 showing the slowest recovery response (2.43 ± 0.98 days) compared to G5 (1.0 ± 0 days) and Luminan (1.75 ± 1.04 days).

Final berry volumes at DOY 169 were 1.02 ± 0.19 for 3159, 1.21 ± 0.08 for G5, and 1.20 ± 0.18 for Luminan under WD conditions. This represented volume gains of 2%, 21%, and 20% respectively over the 13-day experimental period. Well-watered berries during ripening showed continued moderate expansion, reaching final relative volumes of 1.16 ± 0.06 (3159), 1.30 ± 0.18 (G5), and 1.17 ± 0.05 (Luminan) by DOY 169 (Figure 24). The growth rate of WW berries was substantially reduced compared to green stage, with volumes increasing by only 16-30% over the 13-day period compared to 102-383% over 15 days during green stage.

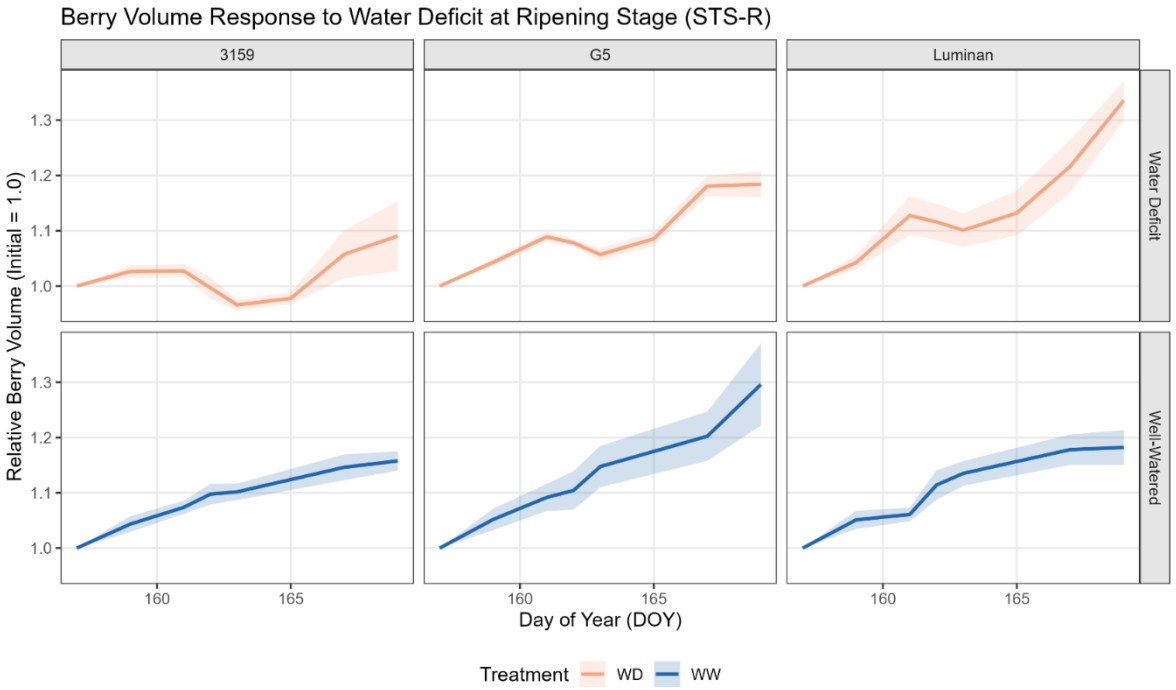

Figure 23. Berry volume response to water deficit at ripening stage (STS-R). Temporal

dynamics of relative berry volume (normalized to initial volume = 1.0) in three grapevine genotypes (3159, G5, Luminan) subjected to well-watered (WW, blue) or water deficit (WD, orange) treatments during the ripening stage over a 13-day period (DOY 157-169). Lines represent treatment means with shaded areas indicating standard error (n = 4 plants per genotype × treatment, 2-4 berries tracked per plant). Berry shriveling (10% of berries with wrinkled skin) occurred at DOY 162-163 for WD plants, triggering recovery irrigation. WD berries show remarkable volume stability during stress, with minimal shrinkage despite severe plant water deficit (Ψpd = -1.44 to -1.75 MPa). WW berries display modest continued growth throughout the ripening period, substantially reduced compared to green stage expansion rates.

Table 5. Berry volume responses at shriveling and recovery.

Genotype	Experiment	Treatment	Volume Loss (%)	Min / Max	Time to Shriveling (days)	Recovery Time (days)	Final Recovery (%)	N berries
3159	STS-G	NI	4.48 ± 12.93	-10.4 / 26.6	6.00 ± 2.83	1.00 ± 0.00	197 ± 57.1	6
G5	STS-G	NI	-25.66 ± 18.90	-44.3 / -0.2	6.50 ± 2.12	1.00 ± 0.00	266 ± 112.1	6
Luminan	STS-G	NI	3.06 ± 16.90	-28.0 / 16.6	4.67 ± 1.53	1.17 ± 0.41	168 ± 34.6	6
3159	STS-R	WD	3.00 ± 2.02	-0.7 / 4.8	5.50 ± 0.71	2.00 ± 0.71	109 ± 15.4	6
G5	STS-R	WD	-7.81 ± 1.56	-10.7 / -6.1	5.00 ± 0.00	1.00 ± 0.00	118 ± 6.2	7
Luminan	STS-R	WD	-11.12 ± 6.32	-19.2 / -2.9	5.50 ± 0.71	1.50 ± 0.55	121 ± 10.5	6

Values shown are mean ± standard deviation for stressed treatments only. Volume loss represents percentage change at shriveling point (negative values indicate volume gain). Time to shriveling measured from treatment initiation (DOY 108 for STS-G, DOY 157 for STS-R). Recovery time represents days required to return to ≥95% of initial volume after rewatering. Final recovery represents percentage of initial volume at experiment termination (DOY 123 for STS-G, DOY 169 for STS-R). Min/Max shows range across individual berries. N indicates number of berries tracked per genotype × treatment. STS-G treatments: NI (no irrigation). STS-R treatments: WD (water deficit).

3.1.2.3 Berry Growth Rate Dynamics

Relative growth rates (RGR, expressed as fractional change in volume per day) were calculated between consecutive measurement points to assess instantaneous growth responses (Table 6). RGR values were analyzed separately for stress phases (pre-shriveling and at shriveling) and recovery phases (post-rewatering).

During the green stage stress phase (from treatment initiation to shriveling), mean RGR values were -0.025 ± 0.13 day^{-1} for 3159, 0.012 ± 0.18 day^{-1} for G5, and -0.018 ± 0.20 day^{-1} for Luminan under NI conditions. These values indicate near-zero or slightly negative growth rates during progressive water deficit. Following recovery irrigation, mean RGR increased to 0.080 ± 0.16 day^{-1} (3159), 0.093 ± 0.18 day^{-1} (G5), and 0.061 ±

0.14 day^{-1} (Luminan), representing 4-8 fold increases in growth rate. Well-watered berries during green stage maintained mean RGR of 0.050 ± 0.13 day^{-1} (3159), 0.071 ± 0.07 day^{-1} (G5), and 0.038 ± 0.05 day^{-1} (Luminan) throughout the experimental period.

During the ripening stage stress phase, mean RGR values were -0.010 ± 0.07 day^{-1} for 3159, 0.025 ± 0.09 day^{-1} for G5, and 0.030 ± 0.09 day^{-1} for Luminan under WD conditions. Recovery phase RGR increased modestly to 0.012 ± 0.09 day^{-1} (3159), 0.013 ± 0.04 day^{-1} (G5), and 0.008 ± 0.04 day^{-1} (Luminan). Well-watered berries during ripening maintained mean RGR of 0.020 ± 0.04 day^{-1} (3159), 0.027 ± 0.08 day^{-1} (G5), and 0.027 ± 0.08 day^{-1} (Luminan). The approximately 5-10 fold reduction in RGR during ripening compared to green stage reflects the developmental transition from rapid cell expansion to slower biochemical accumulation processes.

The range of RGR values varied substantially between developmental stages and stress phases. During green stage stress, RGR ranged from -0.36 to +0.50 day^{-1} across all genotypes, while during recovery RGR ranged from -0.31 to +0.94 day^{-1}. During ripening stage stress, RGR ranged from -0.17 to +0.37 day^{-1}, and during recovery from -0.19 to +0.38 day^{-1}. The reduced range during ripening indicates more constrained growth responses regardless of water status.

3.1.2.4 Relationship Between Berry Growth and Water Status

The relationship between berry relative growth rate (RGR) and plant water status was analyzed using predawn water potential (Ψpd) at the end of each measurement interval. The analysis included NI treatment during the green stage (DOY 111-116) and WD treatment during the ripening stage (DOY 157-163), excluding post-rewatering recovery phases (Figure 24, Table 6).

During the green stage (STS-G, NI treatment), strong positive correlations between RGR and Ψpd were observed across all genotypes: G5 ($r = 0.88$, $p < 0.001$, $n = 33$), Luminan ($r = 0.83$, $p < 0.001$, $n = 29$), and 3159 ($r = 0.80$, $p < 0.001$, $n = 30$). Regression slopes ranged from 0.30 day^{-1} MPa^{-1} (Luminan) to 0.56 day^{-1} MPa^{-1} (G5). Mean RGR values during this period ranged from 0.053 ± 0.157 day^{-1} (3159) to 0.078 ± 0.171 day^{-1} (G5), with Ψpd values spanning -1.23 to -0.14 MPa.

During the ripening stage (STS-R, WD treatment), strong positive correlations between RGR and Ψpd were also observed: G5 ($r = 0.74$, $p < 0.001$, $n = 28$), 3159 ($r = 0.71$, $p < 0.001$, $n = 24$), and Luminan ($r = 0.70$, $p < 0.001$, $n = 24$). Regression slopes were substantially lower than during the green stage, ranging from 0.031 day^{-1} MPa^{-1} (G5) to 0.038 day^{-1} MPa^{-1} (Luminan), representing a 93-94% reduction relative to green stage slopes. Mean RGR values during ripening were close to zero, ranging from -0.003 ± 0.032 day^{-1} (3159) to 0.006 ± 0.034 day^{-1} (G5), with Ψpd values spanning -1.75 to -0.51 MPa.

Comparing developmental stages, correlation strength remained high in both green (r = 0.80-0.88) and ripening (r = 0.70-0.74) stages, while regression slopes decreased from 0.30-0.56 day^{-1} MPa^{-1} (green) to 0.031-0.038 day^{-1} MPa^{-1} (ripening). Mean RGR values were 8-13 fold lower during ripening compared to the green stage.

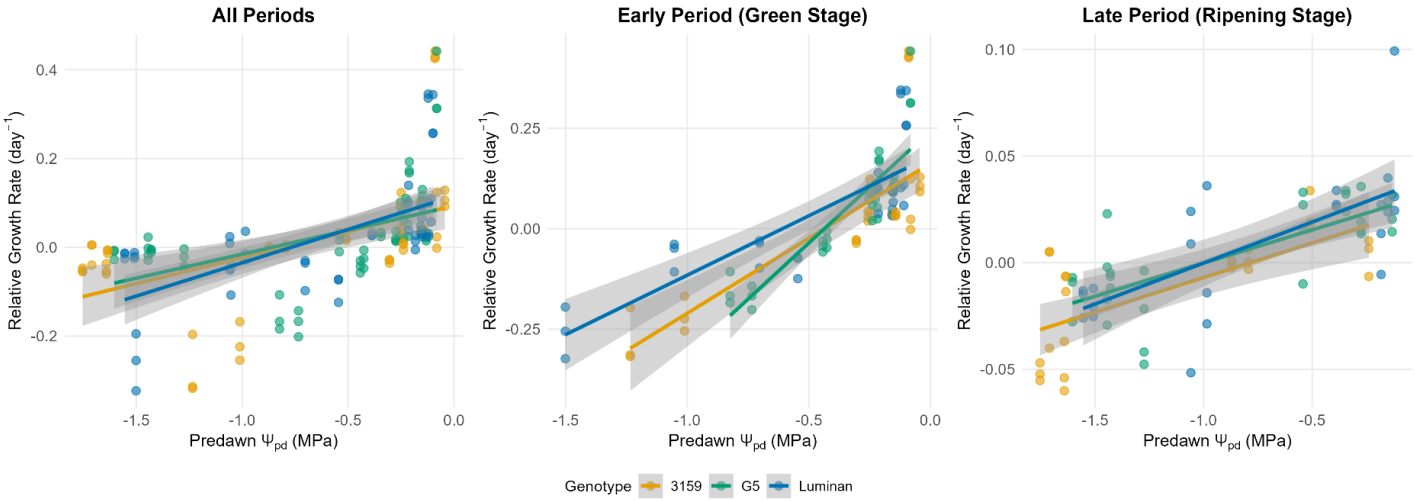

Figure 24. Relationship between berry relative growth rate and predawn water potential (Ψpd). Relationship between berry relative growth rate (RGR, day^{-1}) and predawn water potential (Ψpd, MPa) for three grapevine genotypes (3159 = orange, G5 = green, Luminan = blue). Left panel shows all periods combined, middle panel shows green stage (STS-G, NI treatment, DOY 111-116), and right panel shows ripening stage (STS-R, WD treatment, DOY 157-163). Each point represents a single berry measurement interval, with Ψpd measured at the end of each interval. Linear regression lines (solid) with 95% confidence intervals (shaded) are shown for each genotype. Green stage: r = 0.80-0.88, slopes = 0.30-0.56 day^{-1} MPa^{-1}. Ripening stage: r = 0.70-0.74, slopes = 0.031-0.038 day^{-1} MPa^{-1}. Data include only stressed treatments during active deficit periods.

Table 6. Berry growth rate dynamics and correlation with water status.

Genotype	Experiment	Treatment	N obs	Mean RGR ± SD (day^{-1})	Ψpd Range (MPa)	Correlation (r)	P-value	Slope (β, day^{-1} MPa^{-1})	Intercept
3159	STS-G	NI	30	0.053 ± 0.157	-1.23 to -0.26	0.797	<0.001	0.373	0.163
G5	STS-G	NI	33	0.078 ± 0.171	-1.23 to -0.14	0.880	<0.001	0.558	0.244
Luminan	STS-G	NI	29	0.047 ± 0.132	-1.23 to -0.18	0.828	<0.001	0.295	0.180
3159	STS-R	WD	24	-0.003 ± 0.032	-1.75 to -0.51	0.705	<0.001	0.032	0.026
G5	STS-R	WD	28	0.006 ± 0.034	-1.75 to -0.51	0.742	<0.001	0.031	0.031

Luminan	STS-R	WD	24	0.000 ± 0.034	-1.75 to -0.79	0.696	<0.001	0.038	0.038

RGR (relative growth rate) represents fractional change in berry volume per day. Ψpd range shows the span of predawn water potential values at the end of each measurement interval. Correlation (r) represents Pearson correlation coefficient between RGR and Ψpd. Slope (β) represents the linear regression slope (day^{-1} MPa^{-1}), indicating the change in RGR per unit change in Ψpd. Intercept represents the predicted RGR at Ψpd = 0 MPa. Analysis focused on stressed treatments during active water deficit periods: NI treatment during green stage (DOY 111-116) and WD treatment during ripening stage (DOY 157-163), excluding post-rewatering recovery phases. N obs indicates number of individual berry RGR observations per genotype × treatment.

3.1.3 Comparative Analysis Across Developmental Stages

Berry volume responses at the shriveling point showed quantitative differences between developmental stages. During green stage, mean volume loss ranged from -25.6% to +3.5% across genotypes (Table 5), with negative values indicating net volume gain despite stress. During ripening stage, mean volume loss ranged from -14.5% to +2.6% across genotypes, representing a 44-85% reduction in volume change amplitude compared to green stage. The coefficient of variation for volume loss was 87-189% during green stage compared to 64-144% during ripening stage, indicating reduced individual berry variability during ripening.

Relative growth rates during stress phases were 3-4 fold lower during ripening compared to green stage (Table 6). For stressed treatments, mean RGR was 0.053-0.078 day^{-1} during green stage (NI treatment) compared to -0.003 to 0.006 day^{-1} during ripening stage (WD treatment), representing a 92-95% reduction. The range of observed RGR values was also narrower during ripening compared to green stage, reflecting more constrained growth dynamics.

The strength of correlation between RGR and Ψpd remained high across both developmental stages (Table 6, Figure 24). During green stage under stress (NI treatment), correlation coefficients ranged from $r = 0.80$ to 0.88 (all $p < 0.001$) across genotypes. During ripening stage under stress (WD treatment), correlation coefficients ranged from $r = 0.70$ to 0.74 (all $p < 0.001$), representing only a 16-23% reduction in correlation strength. However, the regression slopes decreased markedly between stages, from 0.30-0.56 day^{-1} MPa^{-1} (green) to 0.031-0.038 day^{-1} MPa^{-1} (ripening), representing a 93-94% reduction in the rate of RGR change per unit change in water potential.

The ranking of genotypes by water stress tolerance, as indicated by predawn water potential at shriveling, reversed between developmental stages. During green stage, the order of increasing tolerance (lowest to highest Ψpd at shriveling) was G5 (-0.78 MPa) < 3159 (-1.12 MPa) < Luminan (-1.28 MPa), with a range of 0.50 MPa across genotypes. During ripening stage, the order reversed to Luminan (-1.31 MPa) < G5 (-1.52 MPa) <

3159 (-1.70 MPa), with a range of 0.39 MPa across genotypes. The change in shriveling threshold between stages was genotype-specific: Luminan showed minimal change (0.03 MPa), G5 showed a 0.74 MPa decrease (increased tolerance), and 3159 showed a 0.58 MPa decrease.

Time required to return to 95% of initial volume after rewatering was 1.0-1.38 days across genotypes during green stage (mean: 1.17 days) compared to 1.0-2.43 days during ripening stage (mean: 1.73 days), representing a 48% increase in recovery duration. The genotype showing fastest recovery also changed between stages: G5 was fastest during green stage (1.0 days) while 3159 was slowest during ripening stage (2.43 days).

Total volume accumulation from treatment initiation to experiment termination differed substantially between stages. Under water deficit treatments, final relative volumes during green stage were 1.68 ± 0.72 (3159), 2.22 ± 1.25 (G5), and 1.46 ± 0.50 (Luminan), representing 68-122% volume gains over 15 days. During ripening stage, final relative volumes were 1.02 ± 0.19 (3159), 1.21 ± 0.08 (G5), and 1.20 ± 0.18 (Luminan), representing 2-21% volume gains over 13 days. This represents an 84-97% reduction in growth capacity during ripening compared to green stage, despite similar durations of the experimental periods.

3.2 *Experiment 2: Long-term Water Deficit (LTS)* and Carbon Demand Interactions

3.2.1 Experimental Conditions

3.2.1.1 Climate Dynamics

Plants were maintained in the Phenodyn phenotyping platform under controlled environmental conditions from June 2 to July 15, 2025 (43 days) (Figure 25). Air temperature averaged 28.4 ± 0.7°C during the day (6:00-19:00h) and 23.3 ± 3.2°C at night (19:00-6:00h), with vapor pressure deficits of 1.59 ± 0.30 kPa and 0.93 ± 0.44 kPa during day and night periods, respectively. Daily cumulative photosynthetic photon flux density, measured by 6 sensors positioned above the canopy, averaged 25.1 ± 3.6 mol m^{-2} d^{-1}. These conditions were broadly consistent with those reported by Wilhelm de Almeida et al. (2024a) for the same platform, with slightly higher daytime temperatures and lower humidity, demonstrating stable controlled environment conditions through the experimetal period.

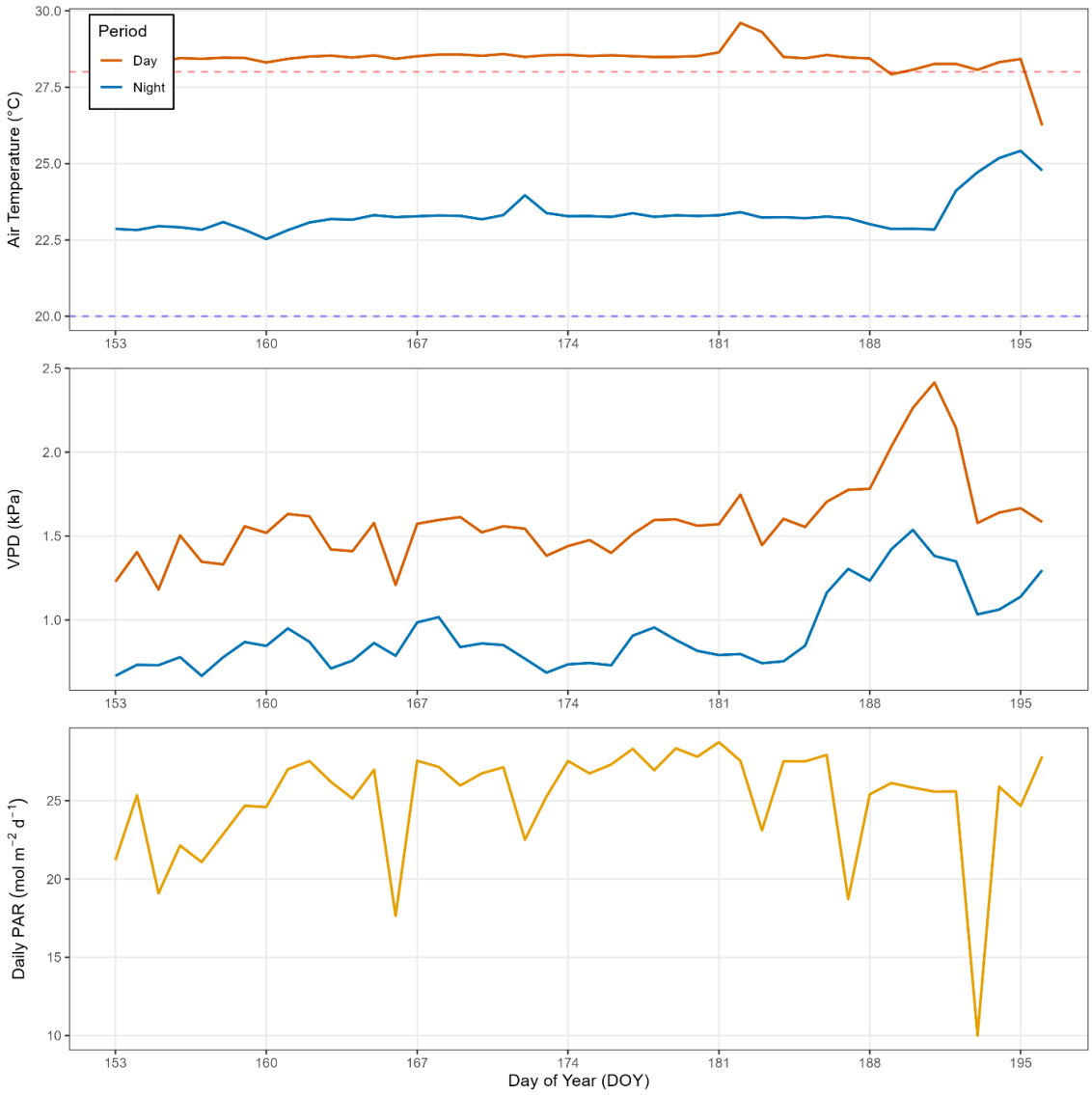

Figure 25. Climate dynamics during the experimental period from veraison to harvest. Environmental conditions in the Phenodyn phenotyping platform from DOY 153 to 196 (June 2 to July 15, 2025; 44 days). Top panel: Air temperature during day (6:00-19:00h, orange) and night (19:00-6:00h, blue) periods. Dashed lines indicate 20°C and 28°C reference temperatures. Middle panel: Vapor pressure deficit (VPD) during day and night periods. Bottom panel: Daily cumulative photosynthetic photon flux density (PAR) measured by 6 sensors positioned above the canopy. Air temperature averaged 28.4 ± 0.7°C (day) and 23.3 ± 3.2°C (night), with VPD of 1.59 ± 0.30 kPa (day) and 0.93 ± 0.44 kPa (night). Daily PAR averaged 25.1 ± 3.6 mol m^{-2} d^{-1}.

3.2.1.2 Soil Temperature

Soil temperature was continuously monitored at three depths (10, 20, and 30 cm) in six representative plants throughout the experimental period from DOY 153 to 196 (June 2 to July 15, 2025; 44 days). Three plants were maintained under well-watered conditions

(pots 2098, 2081, 2004) and three under water deficit conditions (pots 2099, 2089, 2075) (Figure 26).

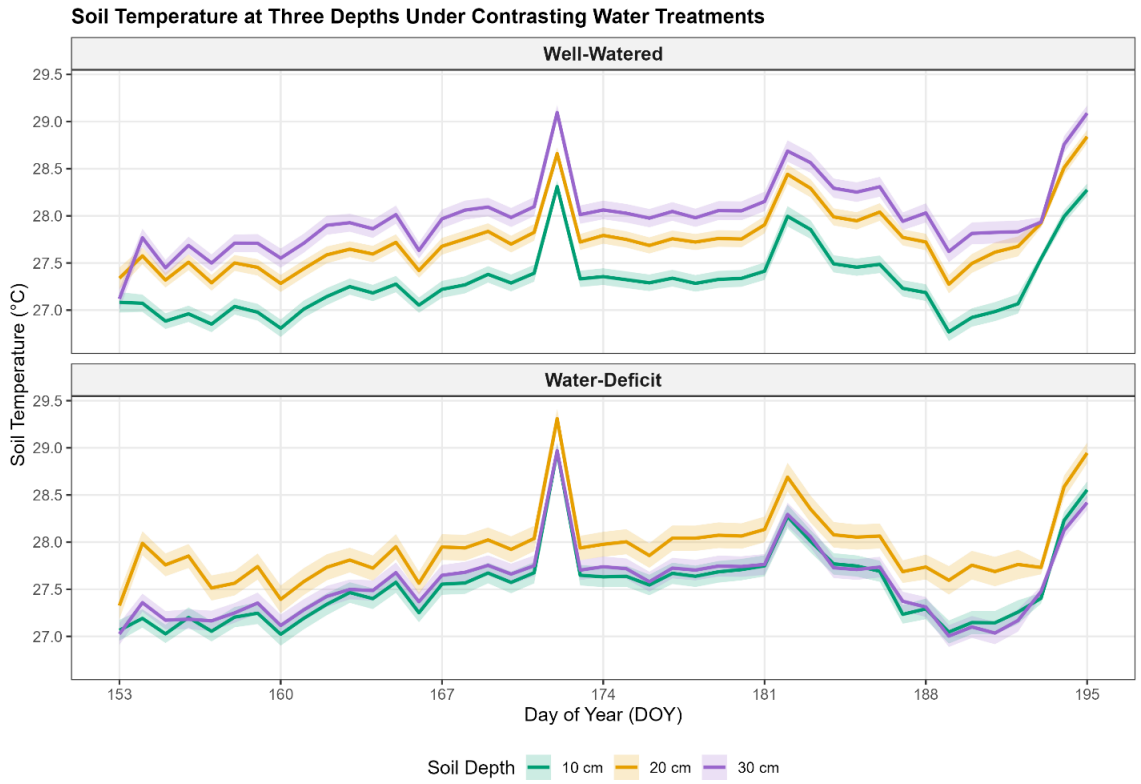

Figure 26. Soil temperature at three depths under contrasting water treatments. Solid lines represent mean temperature at each depth (10 cm = green, 20 cm = orange, 30 cm = purple) and shaded ribbons represent ± standard error of the mean (SE). Well-Watered: n = 3 plants (pots 2098, 2081, 2004); Water Deficit: n = 3 plants (pots 2099, 2089, 2075). Measurements recorded continuously throughout the experimental period (DOY 153 to 196; June 2 - July 15, 2025). Soil temperature showed minimal differences between treatments (mean difference < 0.5°C at all depths), with deeper layers exhibiting greater thermal stability and less daily fluctuation. Under well-watered conditions, soil temperature increased with depth (10 cm < 20 cm < 30 cm: 27.3 < 27.8 < 28.0°C), consistent with reduced heat exchange at greater soil depths. Under water deficit conditions, temperatures increased from 10 to 20 cm depth (27.5 to 27.9°C) but decreased at 30 cm (27.6°C).

At 10 cm depth, soil temperature averaged 27.3 ± 2.6°C under well-watered conditions and 27.5 ± 3.2°C under water deficit conditions (values reported as mean ± SD throughout). At 20 cm depth, temperatures averaged 27.8 ± 2.6°C (WW) and 27.9 ± 3.2°C (WD). At 30 cm depth, temperatures averaged 28.0 ± 2.9°C (WW) and 27.6 ± 3.1°C (WD). Two-way ANOVA (factors: water treatment and soil depth) revealed highly significant effects of water treatment ($p < 0.001$), depth ($p < 0.001$), and treatment × depth interaction ($p < 0.001$). Post-hoc pairwise comparisons (Tukey HSD test) showed that water deficit conditions resulted in slightly elevated temperatures at surface depths (10 cm: +0.24°C, $p < 0.001$; 20 cm: +0.18°C, $p < 0.001$) but reduced temperature at 30 cm depth (-0.43°C, $p < 0.001$) compared to well-watered conditions. However, the small

magnitude of these differences (< 0.5°C at all depths) indicates negligible physiological impact. (Figure 27).

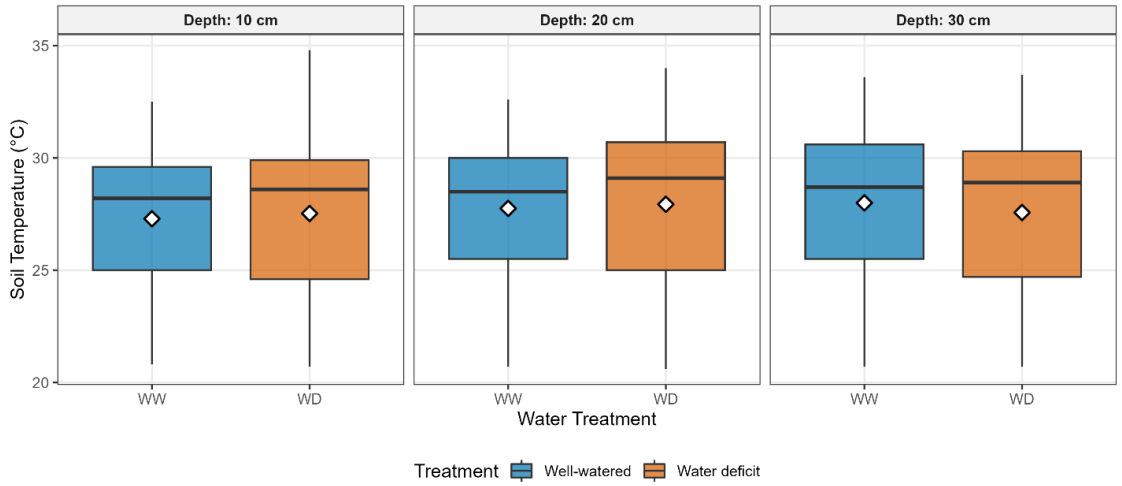

Figure 27. Soil temperature at three depths (10, 20, 30 cm) for given treatments. Boxplots show the distribution of soil temperature measurements at 10 cm (left), 20 cm (middle), and 30 cm (right) depth under well-watered (blue) and water deficit (orange) conditions. Box boundaries represent the 25th and 75th percentiles (interquartile range), horizontal lines show medians, white diamonds indicate means, and whiskers extend to 1.5× the interquartile range. Data collected continuously from DOY 153-196 (June 2 - July 15, 2025) across n = 3 plants per treatment (Well-watered: pots 2098, 2081, 2004; Water deficit: pots 2099, 2089, 2075). Two-way ANOVA revealed highly significant effects of water treatment ($F = 117.66$, $p < 0.001$), depth ($F = 547.57$, $p < 0.001$), and their interaction ($F = 282.25$, $p < 0.001$). Post-hoc comparisons showed treatment differences varied by depth: at 10 cm, WD was 0.24°C warmer ($p < 0.001$); at 20 cm, WD was 0.18°C warmer ($p < 0.001$); at 30 cm, WW was 0.43°C warmer ($p < 0.001$). Despite statistical significance, the small magnitude of differences (< 0.5°C) indicates minimal physiological impact on plant responses.

3.2.1.3 Treatment Duration and Phenological Timing

Plants were transferred to the Phenodyn platform on May 5, 2025 (DOY 125) and underwent a priming phase from May 8 at 0.6 FTSW to promote synchronized veraison across genotypes. Veraison, defined as 50% of berries showing softening, occurred between May 16 and May 30, 2025 (DOY 136-150), with genotype-specific timing reflecting genetic differences in phenology (Table 7, Supplementary Table S3). The earliest genotype to reach veraison was G14 (May 16, DOY 136), followed by 3176 and 3159 (both May 17, DOY 137), and G5 latest (May 20, DOY 140). Water treatments (WW at FTSW 0.8 and WD at FTSW 0.28) were imposed 1-2 days after each genotype reached veraison.

Table 7. Phenological timing and treatment duration by genotype.

Genotype	Veraison Date Range (DOY)	Treatment Start (DOY)	Harvest Date Range (DOY)	Treatment Duration (days)	Ripening Period (days)
3176	May 17-27 (137- 147)	May 18-28 (138-148)	July 3 (184)	44 ± 3	37-48
3159	May 17-22 (137-142)	May 18-23 (138-143)	July 8-9 (189-190)	49 ± 2	47-53
G5	May 20-30 (140-150)	May 21-31 (141-151)	July 9-10 (190-191)	47 ± 3	41-51
G14	May 16-27 (136-147)	May 17-28 (137-148)	July 2-3 (183-184)	41 ± 3	36-47

Values shown as mean ± SD. Veraison date defined as 50% softened berries within each genotype. Treatment start occurred 1-2 days after veraison. Harvest date determined when berries reached maximum volume and soluble solids content stabilized (physiological ripeness). Treatment duration calculated from veraison (treatment initiation) to harvest. Ripening period shows the range across individual plants within each genotype. DOY = Day of Year. See Supplementary Table S3 for individual plant data.

Bunch volume monitoring during ripening (Supplementary Figure S2, with representative examples in Figure 28) revealed genotype-specific maturation dynamics that determined harvest timing. Non-LSB genotype 3176 reached maximum bunch volume earliest, while 3159 showed more gradual bunch development with volumes reaching plateau by mid-July. LSB genotypes G5 and G14 exhibited intermediate patterns, with bunch volumes reaching maximum between early and mid-July. These differential developmental rates necessitated staggered harvest dates (DOY 183-191, July 2-10) to ensure all genotypes reached physiological ripeness, defined as maximum bunch volume indicating completion of berry expansion and solute accumulation. Water deficit did not substantially alter the timing of maximum volume achievement within genotypes, suggesting that maturation dynamics were primarily under genetic control. The 9-day range in harvest timing (Table 7, G14 and 3176 harvested DOY 183-184; 3159 and G5 harvested DOY 189-191) reflects genotype-specific ripening rates and ensured that berry composition measurements (Section 3.2.3) represent equivalent physiological maturity stages across genotypes.

Representative bunch area trajectories for non-LSB genotype 3176 and LSB genotype G5 illustrate the distinct developmental patterns observed across genotypes (Figure 28). Genotype 3176 under both well-watered and water deficit conditions exhibited relatively stable bunch areas throughout the monitoring period (DOY 162-176), with mean areas ranging from 60-70 cm^2, indicating early achievement of maximum cluster size. In contrast, under well-watered conditions, G5 individual bunches showed either continuous area increases or peak-then-decline patterns, with some reaching maximum areas around DOY 165 (115 cm^2) followed by decline. Water deficit conditions in G5

resulted in either early area peaks (DOY 155) followed by decline, or gradual increases throughout the period.

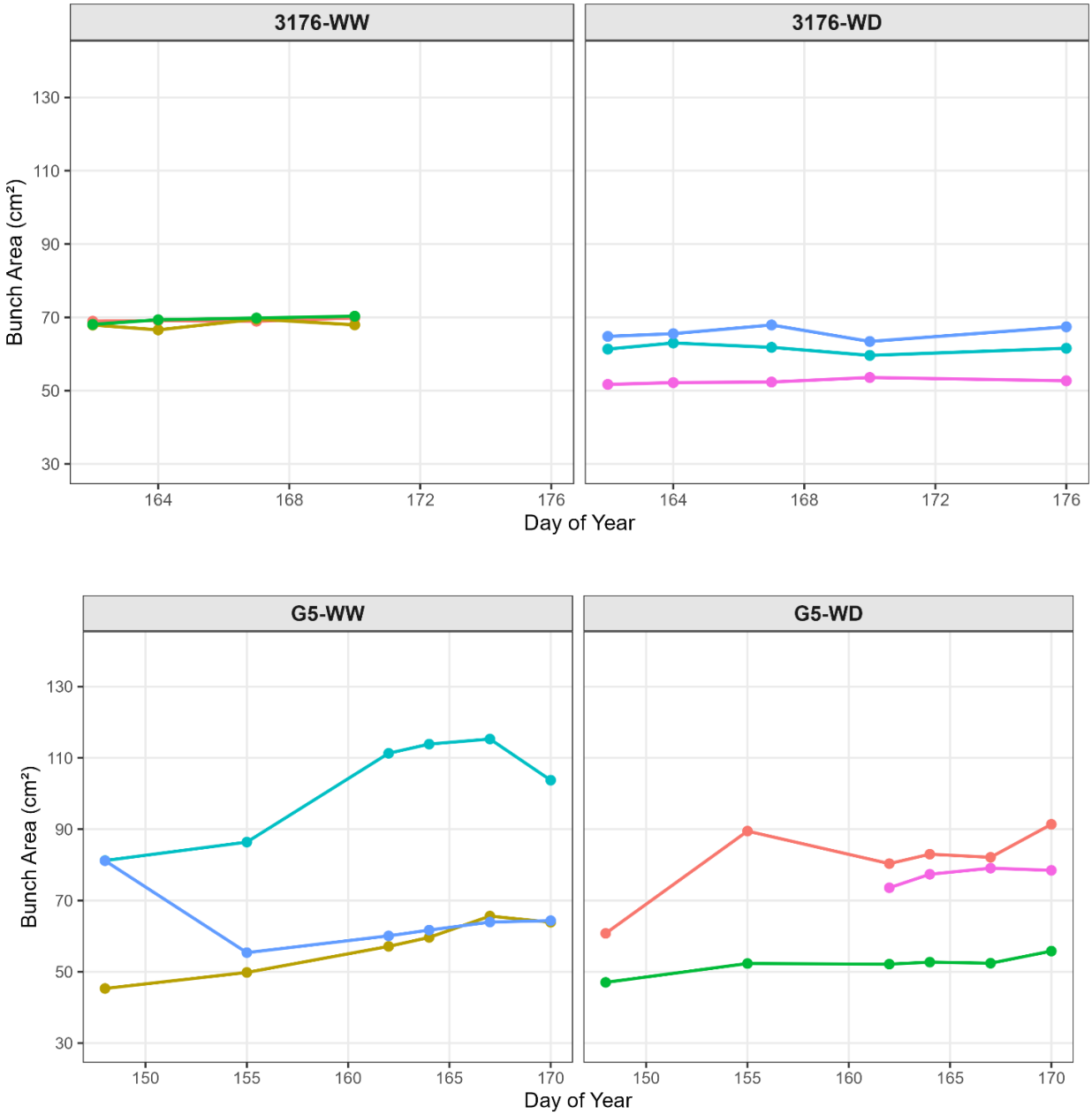

Figure 28. Representative bunch area dynamics from veraison to harvest. Individual plant trajectories (colored lines, each line = one bunch tracked on one plant) show weekly bunch area measurements for representative non-LSB genotype 3176 and LSB genotype G5 under well-watered (WW) and water deficit (WD) treatments. Measurements were determined through non-destructive imaging analysis of three representative clusters per plant tracked longitudinally throughout ripening. Bunch areas shown in cm². Y-axis scales are optimized per genotype for visual clarity. Harvest timing was determined when bunch area reached maximum size followed by stable or declining measurements over consecutive monitoring dates, indicating physiological ripeness and completion of berry cell expansion. Note the contrasting patterns between genotypes: 3176 showed stable bunch area development, while G5

exhibited more variable trajectories including peak-then-decline patterns in some individuals. See Supplementary Figure S2 for complete data including all genotypes and carbon-normalized treatments (WW-C, WD-C).

Across all genotypes and treatments (Supplementary Figure S2), LSB genotypes displayed more variable bunch area trajectories compared to non-LSB genotypes. Non-LSB genotype 3159 showed divergent patterns between treatments: well-watered plants displayed gradual bunch area increases throughout the monitoring period, with individual bunches reaching final areas ranging from 30-70 cm², while water deficit plants showed rapid area increases between DOY 162-167, reaching maximum bunch areas at approximately 75-80 cm² and maintaining stable areas thereafter. LSB genotype G14 under well-watered conditions showed continuous area increases throughout the monitoring period, while water deficit plants exhibited peak areas around DOY 155 (approximately 80 cm²) followed by gradual decline or stabilization. Carbon-normalized treatments showed distinct patterns, with detailed trajectories presented in Supplementary Figure S2.

Harvest decisions were triggered when bunch area monitoring (three representative clusters per plant tracked weekly through imaging analysis) indicated cessation of growth, defined as maximum area followed by stable or declining measurements in subsequent weeks. This criterion was met at genotype-specific intervals (Table 7), with harvest occurring between DOY 183 and 191 (July 2-10, 2025): G14 and 3176 were harvested earliest (DOY 183-184), followed by 3159 and G5 (DOY 189-191).

3.2.2 Water Relations Throughout the Experiment

3.2.2.1 Soil and Plant Water Status

3.2.2.1.1 FTSW Maintenance and Treatment Implementation

Water treatments were successfully established and maintained throughout the experimental period from veraison to physiological ripeness (Figure 29). The effectiveness of water treatment implementation was monitored through daily FTSW calculations, confirming maintenance of target FTSW levels and automated irrigation control (Supplementary Figure S3). Well-watered (WW) plants maintained an average FTSW of 0.64-0.71 across genotypes, approximating the target of 0.8, while water deficit (WD) plants were maintained at FTSW 0.18-0.25, approximating the target of 0.28 (Figure 30). Carbon-normalized treatments (WW-C and WD-C) maintained FTSW values within the same target ranges as their respective non-normalized counterparts.

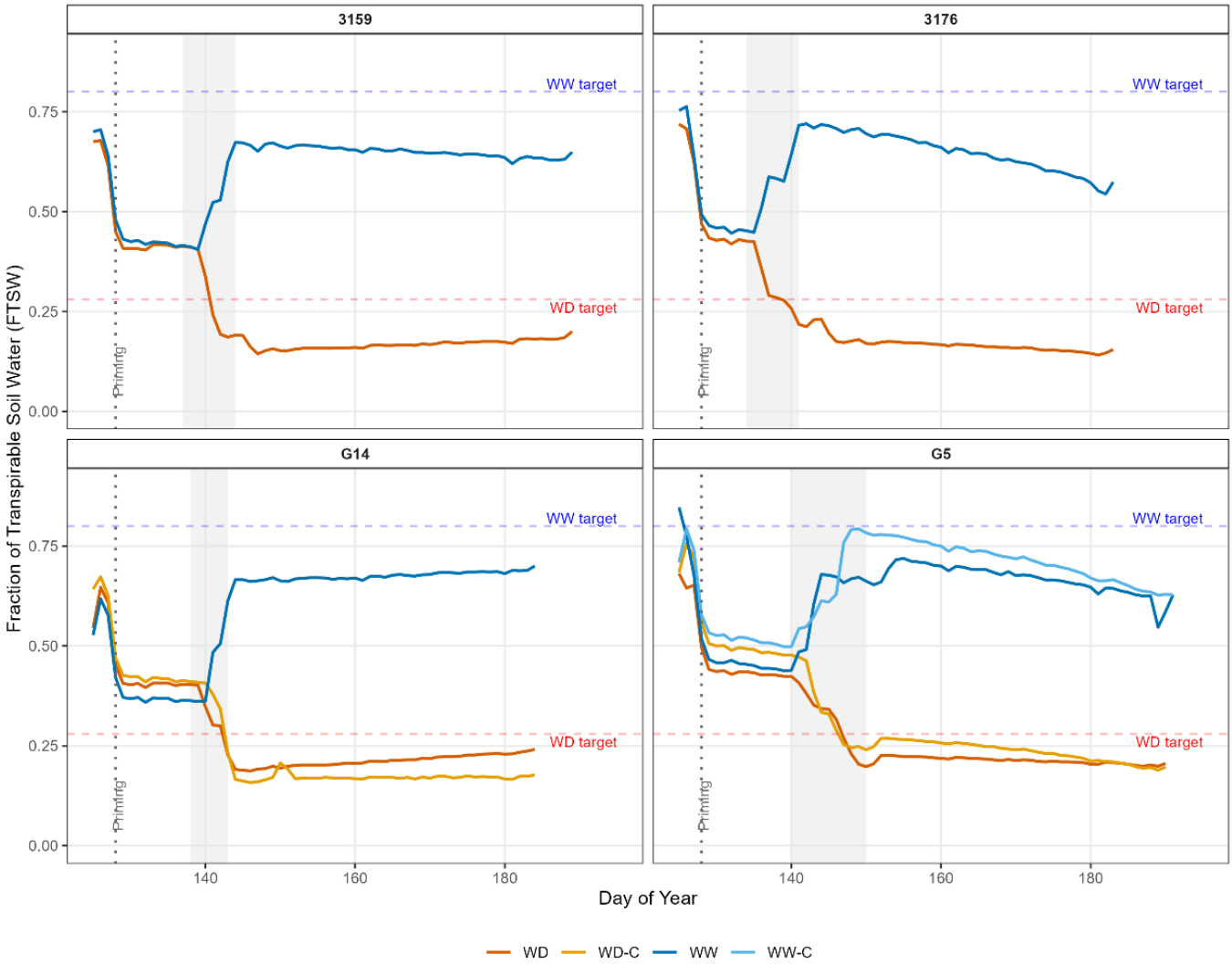

Figure 29. FTSW response by genotype and treatment. Lines represent mean FTSW trajectories for well-watered (blue and light blue, target 0.8) and water deficit (red and orange, target 0.28) treatments (n = 3-6 plants per treatment). Gray shaded area indicates the priming phase (FTSW 0.6) applied to all plants from DOY 128 until veraison to promote synchronized berry softening across genotypes. Vertical dashed line labeled "Priming" marks the transition from priming to differentiated water treatments for each genotype. Horizontal dashed lines show target FTSW levels for WW and WW-C (0.8, blue and light blue) and WD and WD-C (0.28, red and orange) treatments.

The priming phase initiated at DOY 128 (May 8) at FTSW 0.6 successfully synchronized veraison timing across genotypes, with all genotypes reaching 50% berry softening within a 15-day period (DOY 136-150, Table 7). Following veraison, differentiated water treatments were imposed based on individual plant phenology, with treatment initiation occurring 1-2 days after each plant reached the softening stage.

3.2.2.1.2 Whole-Plant Transpiration

Daily transpiration rates showed distinct temporal dynamics throughout the treatment period (Figure 30). Under well-watered conditions, transpiration rates remained

relatively stable varying between 0.8-1.2 L day^{-1} for most genotypes, with variation corresponding to environmental conditions. A notable exception was 3176, which exhibited a progressive increase in daily transpiration over the experimental period under well-watered conditions. Water deficit treatments showed consistently lower rates of 0.4-0.6 L day^{-1} throughout the experimental period, with no such progressive increase observed.

When normalized by leaf area to account for differences in canopy size, transpiration per unit leaf area showed similar treatment separation (Figure 31), with well-watered plants maintaining 0.8-1.3 L m^{-2} day^{-1} compared to 0.4-0.7 L m^{-2} day^{-1} under water deficit. This normalization showed similar treatment effects across the four genotypes. After leaf area normalization, 3176 no longer showed the progressive increase, indicating the temporal trend reflected canopy expansion. Well-watered plants showed a tendency toward decreased transpiration per unit leaf area during the final period of the treatment.

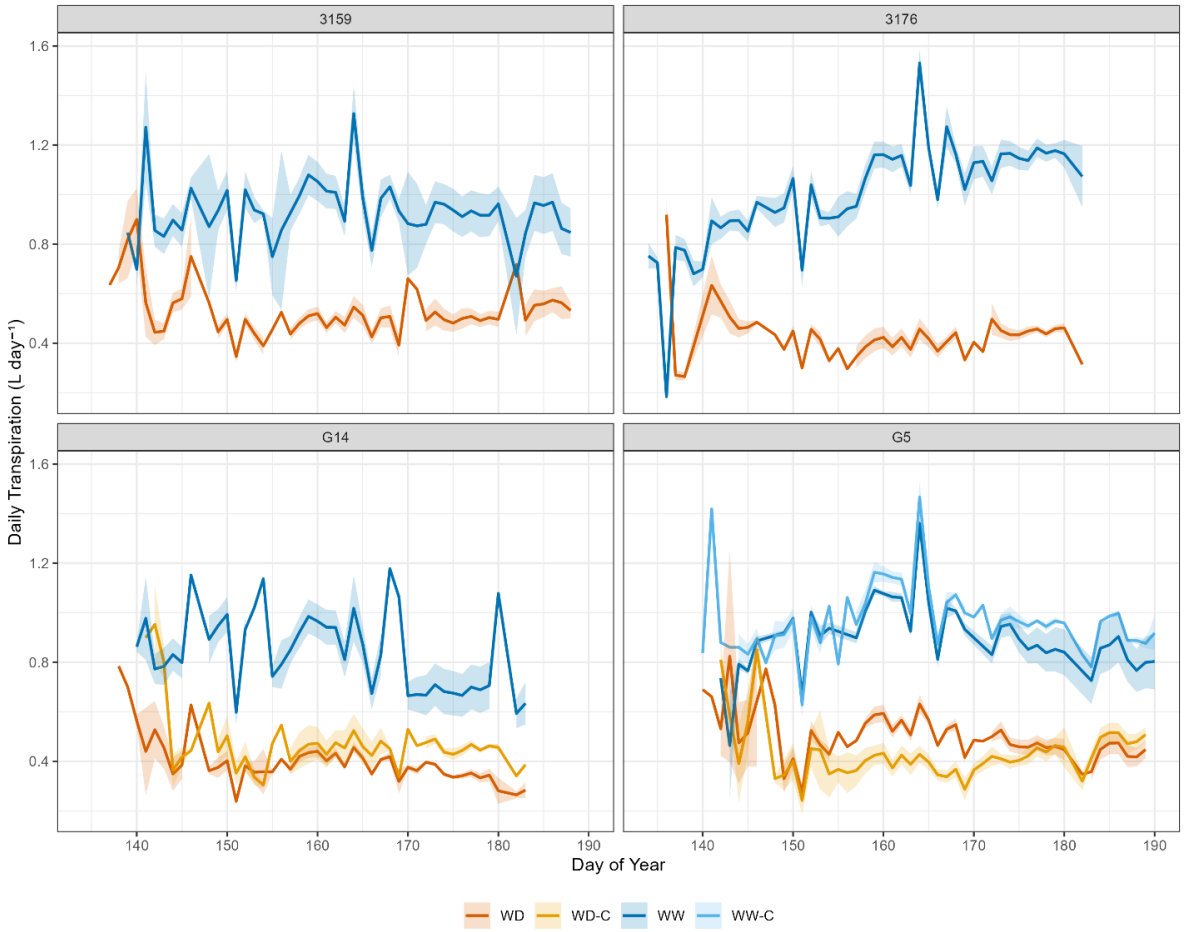

Figure 30. Daily transpiration from veraison to harvest by genotype and treatment. Daily transpiration from veraison to harvest by genotype and treatment. Lines represent mean daily transpiration (L day^{-1}) and shaded areas represent ± SE. Treatment abbreviations: WW = well-watered,

WW-C = well-watered carbon-normalized, WD = water deficit, WD-C = water deficit carbon-normalized. n = 3-6 plants per treatment.

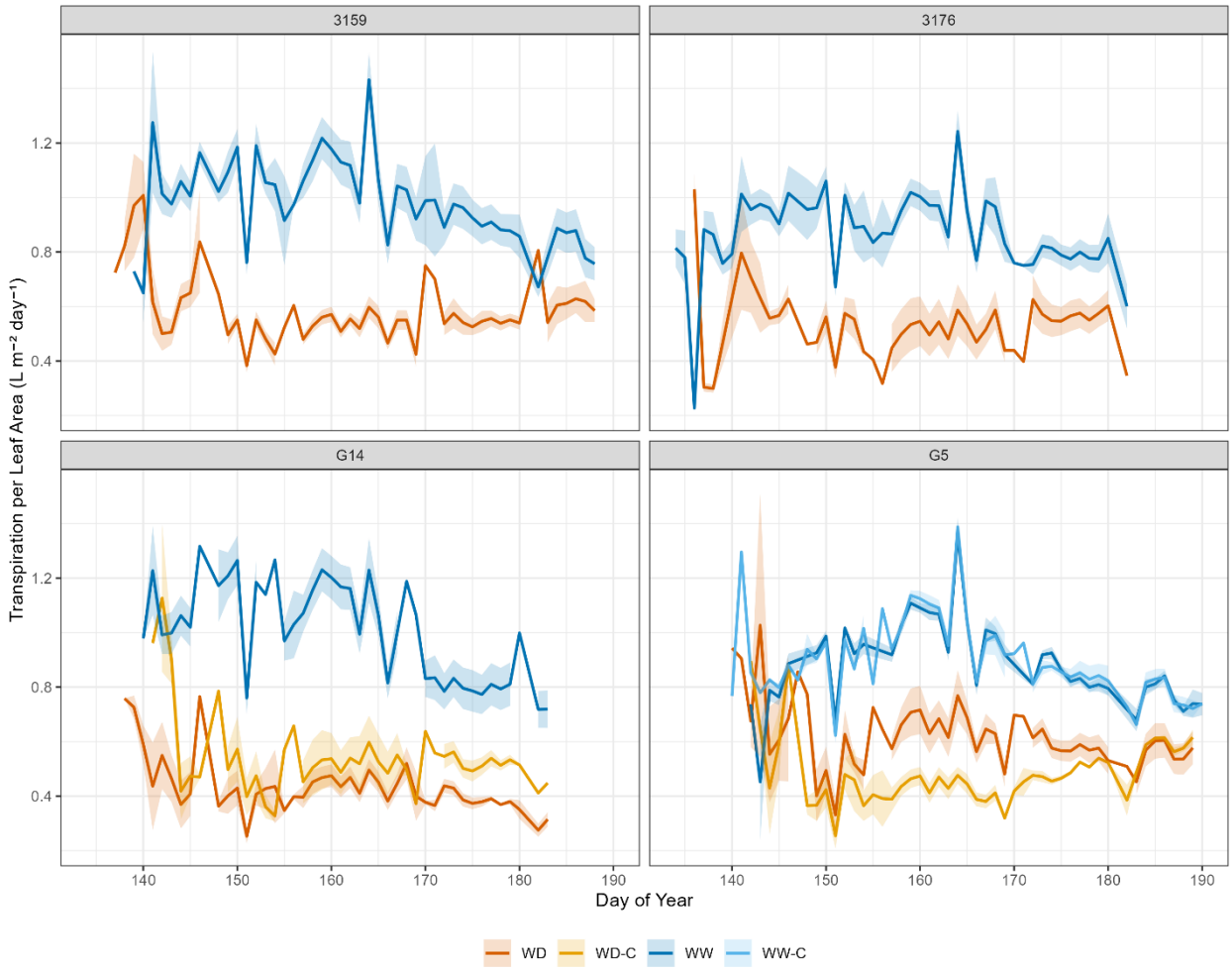

Figure 31. Daily transpiration per leaf area from veraison to harvest by genotype and treatment. Lines represent mean daily transpiration normalized by leaf area (L m^{-2} day^{-1}) and shaded areas represent ± SE. Normalization accounts for genotypic differences in canopy size. Treatment abbreviations as in Figure 30. n = 3-6 plants per treatment.

Total plant transpiration from veraison to harvest varied significantly by treatment and genotype (Table 8). Well-watered plants transpired 36.3-52.0 L over the treatment period (42-49 days), while water deficit plants showed substantially reduced transpiration of 15.7-21.4 L, representing a 43-59% reduction compared to WW controls ($p < 0.001$, two-way ANOVA). Among genotypes, total transpiration under well-watered conditions ranged from 36.3 L (G5) to 42.9 L (G14), while under water deficit conditions it ranged from 15.7 L (3176) to 21.4 L (3159). Carbon-normalized treatments showed comparable or slightly elevated transpiration relative to their non-normalized counterparts within the same water treatment, with G5 WW-C exhibiting the highest total transpiration (51.9 ± 19.6 L).

Table 8. Total transpiration and average daily transpiration per unit leaf area by genotype and treatment.

Genotype	Treatment	n	Total TR (L)	Average Daily TR per LA (L m^{-2} day^{-1})
3159	WW	5	37.6 ± 7.2	0.82 ± 0.11[a]
3159	WD	5	21.4 ± 3.9	0.48 ± 0.06[a]
3176	WW	6	38.5 ± 4.1	0.73 ± 0.11[a]
3176	WD	4	15.7 ± 0.9	0.45 ± 0.12[a]
G14	WW	4	42.9 ± 26.2	1.21 ± 0.90[b]
G14	WD	4	17.8 ± 8.3	0.43 ± 0.15[a]
G14	WD-C	3	15.8 ± 2.6	0.43 ± 0.10[a]
G5	WW	3	36.3 ± 2.6	0.74 ± 0.02[a]
G5	WW-C	3	51.9 ± 19.6	1.01 ± 0.51[a]
G5	WD	4	19.3 ± 1.8	0.50 ± 0.09[a]
G5	WD-C	4	16.5 ± 2.3	0.40 ± 0.02[a]

Values shown as mean ± SD. Total TR = cumulative transpiration from veraison to harvest. Average Daily TR per LA = mean daily transpiration normalized by total leaf area. Superscript letters indicate significant differences within each genotype based on Bonferroni post-hoc test ($p < 0.05$); treatments sharing a letter within a genotype are not significantly different. WD = water deficit; WW = well-watered; -C = carbon-normalized. Two-way ANOVA: Treatment effect ($F_{3,34} = 8.28$, $p < 0.001$), Genotype effect ($F_{3,34} = 0.20$, $p = 0.894$, ns), Genotype × Treatment interaction ($F_{4,34} = 1.05$, $p = 0.396$, ns). Treatment durations: 3176 (44 ± 3 days), 3159 (49 ± 2 days), G5 (47 ± 3 days), G14 (41 ± 3 days).

3.2.2.2 Leaf Area and Plant Balance

3.2.2.2.1 Crop Load (Berry number, Total Fruit Fresh Weight, Total Soluble Solids from °Brix)

Fresh fruit weight per plant (FFW) at harvest showed significant effects of both genotype ($p = 0.024$) and treatment ($p < 0.001$), with no significant genotype × treatment interaction ($p = 0.510$) (Table 9). FFW ranged from 0.35 kg (G14 WW) to 0.63 kg (G5 WD-C). Carbon-normalized LSB treatments achieved substantial crop load increases across both irrigation regimes. Under well-watered conditions, G5 WW-C reached 0.59 ± 0.16 kg compared to 0.57 ± 0.13 kg in G5 WW (+4% increase), while under water deficit conditions, G5 WD-C reached 0.63 ± 0.08 kg compared to 0.35 ± 0.02 kg in G5 WD (+80% increase), and G14 WD-C achieved 0.58 ± 0.01 kg compared to 0.38 ± 0.06 kg in G14 WD (+53% increase). These increases in fruit weight corresponded with elevated berry numbers (Supplementary Table S4).

Berry number per plant showed significant treatment effects ($p < 0.001$) but no significant genotype effect ($p = 0.532$, ns) or interaction ($p = 0.978$) (Table 9). Carbon-

normalized treatments for LSB genotypes successfully increased berry number by approximately 50-60%: G5 WD-C achieved 300 berries compared to 191 berries in G5 WD (+57%), while G14 WD-C reached 292 berries compared to 220 berries in G14 WD (+33%). Non-LSB genotypes 3159 and 3176 showed berry numbers of 224-247 berries across treatments, while LSB genotypes without carbon normalization ranged from 191-227 berries, reflecting variation in fruit set among genotypes and treatments. The actual berry numbers at harvest exceeded initial crop load targets (140 berries for standard treatments, 210 for carbon-normalized) due to the practical challenges of visual estimation during cluster thinning. Berry numbers varied among genotypes (non-LSB: 224-247 berries; LSB without C: 191-227 berries), with the actual numbers at harvest exceeding initial crop load targets (140 berries for standard treatments, 210 for carbon-normalized) due to practical challenges of visual estimation during cluster thinning. Carbon-normalized treatments increased berry numbers by approximately 40-50% under well-watered conditions (G5 WW-C vs G5 WW: 265 vs 261 berries, +1.5%; G14 treatment comparison not available due to missing G14 WW-C harvest data) and by 33-57% under water deficit conditions.

Despite this increased sink demand from elevated berry numbers, carbon-normalized LSB plants under water deficit achieved the highest absolute carbon accumulation in fruits (varC), reaching 67.9 g C for G5 WD-C and 58.4 g C for G14 WD-C. These values (G5 WD-C: 67.9 g C; G14 WD-C: 58.4 g C) exceeded those of standard LSB treatments (G5 WD: 45.4 g C; G14 WD: 40.7 g C) by approximately 50% and were comparable to or higher than non-LSB genotypes under water deficit (3159 WD: 54.3 g C; 3176 WD: 52.1 g C). Carbon-normalized LSB plants exhibited fruit-to-leaf ratios of 0.77 kg m^{-2} for G5 WD-C and 0.68 kg m^{-2} for G14 WD-C, levels comparable to or exceeding those of high-yielding non-LSB genotypes (Section 3.2.2.2.2).

Soluble solids concentration (°Brix) exhibited highly significant genotypic effects ($p < 0.001$) and a significant genotype × treatment interaction ($p = 0.027$), but no main treatment effect ($p = 0.219$) (Table 9). LSB genotypes showed lower °Brix values (19.9-23.2) compared to non-LSB genotypes (21.7-24.3), confirming the LSB phenotype. Carbon normalization resulted in slight reductions in °Brix concentrations in LSB genotypes (G5 WD-C: 20.9 vs G5 WD: 22.8; G14 WD-C: 20.0 vs G14 WD: 20.7), with LSB genotypes maintaining lower °Brix values overall (19.9-23.2) compared to non-LSB genotypes (21.7-24.3). However, water deficit reduced berry size across genotypes, meaning that despite similar °Brix concentrations between treatments, water-deficit berries accumulated less total sugar per berry due to their smaller size.

3.2.2.2.2 Fruit to Leaf Ratio (LA, Total FFW/LA and TSS/LA)

Leaf area at harvest showed highly significant effects of both genotype ($p < 0.001$) and water treatment ($p < 0.001$), with a significant genotype × treatment interaction ($p =$

0.001) (Table 9). Leaf area ranged from 0.82 m² (3176 WD) to 1.60 m² (3176 WW) per plant. Water deficit reduced final leaf area across genotypes compared to well-watered controls (3159: -23%, 3176: -49%, G14: -6%, G5: -26%), showing genotype-specific reductions in vegetative growth under water deficit. Genotype 3176 exhibited the largest canopy under well-watered conditions but showed the most pronounced reduction under water deficit. Carbon normalization through increased berry load in LSB genotypes did not substantially reduce leaf area within either water treatment (G5 WD-C: 0.84 ± 0.13 m² vs G5 WD: 0.82 ± 0.08 m²; G14 WD-C: 0.84 ± 0.05 m² vs G14 WD: 0.87 ± 0.12 m²), with leaf area remaining similar between carbon-normalized and standard treatments within each water treatment for LSB genotypes.

Table 9. Fresh fruit weight (FFW), berry number, sugar concentration (°Brix), leaf area (LA), and source-sink balance ratios at harvest by genotype and treatment.

Genotype	Treatment	n	FFW (kg)	Berry Number	°Brix	LA (m^2)	Fruit:Leaf (kg m^{-2})	Soluble Solids:LA (g m^{-2})
3159	WD	6	0.42 ± 0.10^{a}	250^{a}	24.3^{d}	0.87 ± 0.15^{ab}	0.50 ± 0.17^{abc}	119.8 ± 32.4^{abc}
3159	WW	6	0.43 ± 0.11^{ab}	244^{a}	23.1^{bcd}	1.13 ± 0.28^{ab}	0.39 ± 0.10^{ab}	89.2 ± 20.4^{ab}
3176	WD	5	0.47 ± 0.10^{abc}	233^{a}	22.0^{abcd}	0.82 ± 0.09^{ab}	0.57 ± 0.11^{bcd}	125.1 ± 20.2^{bc}
3176	WW	6	0.45 ± 0.10^{abc}	224^{a}	23.8^{cd}	1.60 ± 0.32^{c}	0.29 ± 0.10^{a}	69.1 ± 22.2^{a}
G14	WD	4	0.38 ± 0.06^{a}	220^{a}	20.7^{ab}	0.87 ± 0.12^{ab}	0.45 ± 0.11^{abc}	93.4 ± 22.8^{ab}
G14	WD-C	4	0.58 ± 0.01^{abc}	294^{a}	20.0^{a}	0.84 ± 0.05^{ab}	0.69 ± 0.05^{cd}	138.7 ± 11.6^{bc}
G14	WW	4	0.35 ± 0.11^{a}	203^{a}	20.7^{ab}	0.93 ± 0.14^{ab}	0.38 ± 0.09^{ab}	79.6 ± 21.9^{ab}
G5	WD	6	0.38 ± 0.06^{a}	217^{a}	22.8^{bcd}	0.82 ± 0.08^{a}	0.47 ± 0.06^{abc}	105.7 ± 9.8^{abc}
G5	WD-C	5	0.63 ± 0.07^{bc}	296^{a}	20.9^{ab}	0.84 ± 0.13^{ab}	0.76 ± 0.13^{d}	158.9 ± 24.3^{c}
G5	WW	5	0.50 ± 0.18^{abc}	227^{a}	21.4^{abc}	1.11 ± 0.17^{ab}	0.47 ± 0.22^{abc}	100.9 ± 46.9^{ab}
G5	WW-C	4	0.67 ± 0.13^{c}	282^{a}	21.7^{abcd}	1.21 ± 0.14^{bc}	0.56 ± 0.17^{abcd}	121.8 ± 36.4^{abc}

Values shown as mean ± SD. FFW = fresh fruit weight; Berry Number = total berries per plant; °Brix = soluble solids concentration; LA = leaf area at harvest; Fruit:Leaf = ratio of fresh fruit weight to leaf area; Soluble Solids:LA = total soluble solids per unit leaf area calculated as (°Brix × FFW × 10) / LA. Superscript letters indicate significant differences based on Tukey HSD test ($p < 0.05$); treatments sharing a letter are

not significantly different. WD = water deficit; WW = well-watered; WD-C/WW-C = carbon-normalized treatments with increased berry load (LSB genotypes only). Two-way ANOVA results: FFW (Genotype: $F_{3,44}$ = 3.47, p = 0.024; Treatment: $F_{3,44}$ = 11.00, p < 0.001; Interaction: $F_{4,44}$ = 0.51, p = 0.510, ns); Berry Number (Genotype: $F_{3,44}$ = 0.74, p = 0.532, ns; Treatment: $F_{3,44}$ = 6.62, p = 0.001; Interaction: $F_{4,44}$ = 0.11, p = 0.978, ns); °Brix (Genotype: $F_{3,44}$ = 15.63, p < 0.001; Treatment: $F_{3,44}$ = 1.53, p = 0.219, ns; Interaction: $F_{4,44}$ = 3.05, p = 0.027); LA (Genotype: $F_{3,44}$ = 8.79, p < 0.001; Treatment: $F_{3,44}$ = 17.81, p < 0.001; Interaction: $F_{4,44}$ = 6.55, p = 0.001); Fruit:Leaf (Genotype: $F_{3,44}$ = 3.84, p = 0.016; Treatment: $F_{3,44}$ = 13.36, p < 0.001; Interaction: $F_{4,44}$ = 1.90, p = 0.137, ns); Soluble Solids:LA (Genotype: $F_{3,44}$ = 2.76, p = 0.053, marginal; Treatment: $F_{3,44}$ = 12.31, p < 0.001; Interaction: $F_{4,44}$ = 1.46, p = 0.231, ns). n = 55 plants total (4-6 plants per treatment). See Supplementary Table S4 for individual plant data.

Fruit-to-leaf ratios, calculated as fresh fruit weight per unit leaf area (kg m^{-2}), showed significant effects of genotype (p = 0.016) and treatment (p < 0.001), with no significant interaction (p = 0.137) (Table 9). The elevated ratios in carbon-normalized LSB genotypes (G5 WD-C: 0.76 ± 0.13 kg m^{-2}, G14 WD-C: 0.69 ± 0.05 kg m^{-2}) corresponded with substantial increases in fruit weight (+53-66%). Standard water deficit treatments resulted in fruit-to-leaf ratios of 0.45-0.57 kg m^{-2}, while well-watered plants showed lower ratios of 0.29-0.55 kg m^{-2}. These patterns indicate that the variation in fruit-to-leaf ratios arose from both fruit weight responses (increased under carbon normalization) and leaf area responses (reduced under water deficit), with leaf area showing proportionally greater reduction than fruit production under water deficit.

To further characterize source-sink balance, soluble solids per unit leaf area (Soluble Solids:LA) was calculated as (°Brix × FFW × 10) / LA, providing a measure of total soluble solids normalized by photosynthetic surface area. Soluble Solids:LA showed a marginally significant genotype effect (p = 0.053) and a highly significant treatment effect (p < 0.001), with no significant interaction (p = 0.231, ns) (Table 9). Values ranged from 69.1 g m^{-2} (3176 WW) to 158.9 g m^{-2} (G5 WD-C), representing a 2.3-fold variation in sugar accumulation per unit leaf area across treatments. Water deficit consistently increased Soluble Solids:LA across all genotypes (mean increase: +38%), corresponding with reduced leaf area and maintained or increased sugar accumulation per plant. Carbon-normalized LSB genotypes exhibited the highest values (G5 WD-C: 158.9 ± 24.3 g m^{-2}; G14 WD-C: 138.7 ± 11.6 g m^{-2}), representing increases of +49% and +48% respectively compared to their standard treatments.

3.2.3 Berry Development and Primary Metabolism

3.2.3.1 Berry Growth Dynamics

Final berry fresh weight at harvest showed significant effects of both genotypes (p = 0.001) and water treatment (p = 0.011), with a significant genotype × treatment interaction (p = 0.027). Berry weight ranged from 1.42 g in G14 under well-watered conditions to 2.25 g in G5 under carbon-normalized well-watered treatment (G5 WW-C) (Figure 32). Berry volume showed no significant treatment effect while berry fresh

weight showed significant treatment effects. Carbon normalization in LSB genotypes (WD-C and WW-C treatments) resulted in larger individual berry weights compared to their standard treatments, corresponding with berry number adjustment in carbon-normalized treatments.

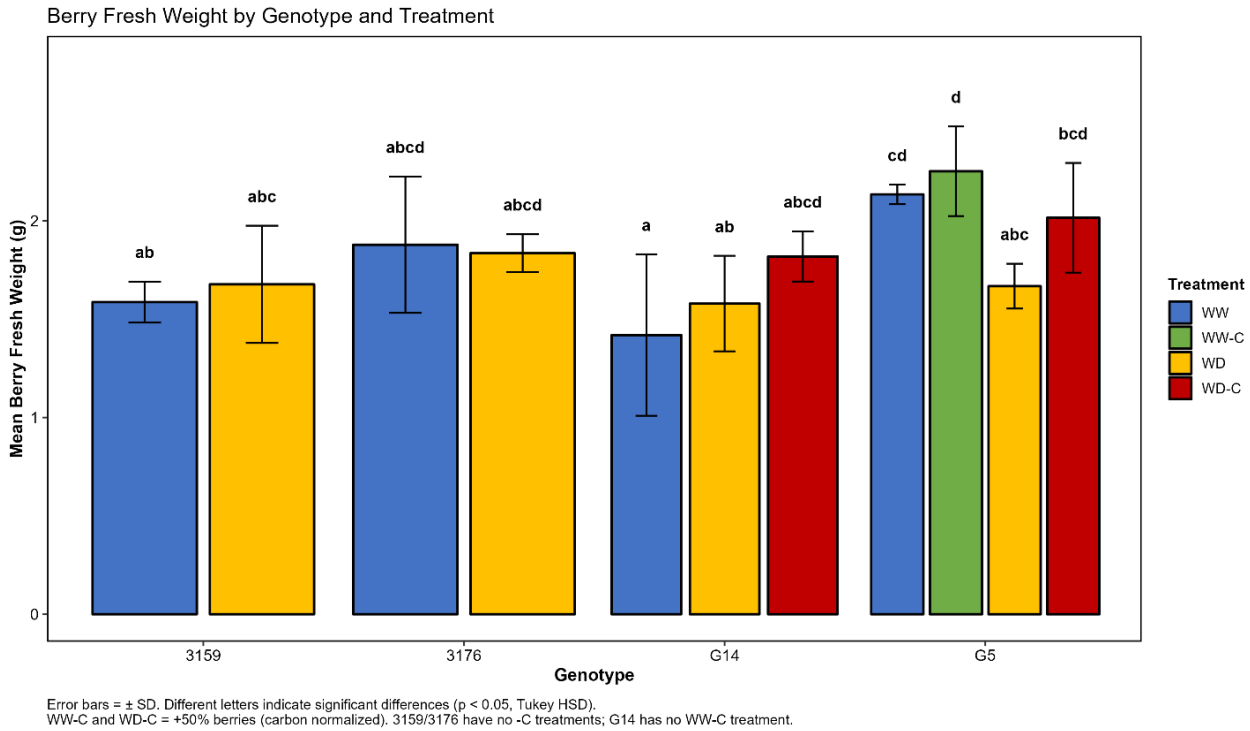

Figure 32. Berry fresh weight at harvest by genotype and treatment. Mean berry fresh weight (± SD) for each genotype × treatment combination. Bars represent treatments: WW = well-watered (blue), WW-C = well-watered carbon-normalized (green), WD = water deficit (yellow), WD-C = water deficit carbon-normalized (red). Different letters indicate significant differences among all genotype × treatment combinations ($p < 0.05$, Tukey HSD). Carbon-normalized treatments (+50% berry number) applied only to LSB genotypes (G14, G5); 3159 and 3176 have no -C treatments; G14 has no WW-C treatment. Two-way ANOVA: Genotype $F = 6.13$ ($p = 0.001$), Treatment $F = 4.21$ ($p = 0.011$), Genotype × Treatment $F = 3.05$ ($p = 0.027$). Values determined from 50-berry samples per plant at physiological ripeness. n = 4-6 plants per treatment.

Berry dry weight, representing total carbon investment per berry (including both structural components from pericarp and seed tissues and non-structural carbohydrates accumulated during ripening), showed marginally significant genotypic variation ($p = 0.058$), no significant treatment effect ($p = 0.643$), and a significant genotype × treatment interaction ($p = 0.041$) (Figure 33). Berry dry weight ranged from 0.422 g in G14 WW to 0.624 g in G5 WW across all treatments. Under well-watered conditions, substantial genotypic differences emerged: G5 (0.624 ± 0.056 g) and 3176 (0.594 ± 0.121 g) exhibited significantly higher berry dry weight compared to G14 (0.422 ± 0.132 g), while 3159 (0.499 ± 0.059 g) showed intermediate values. In contrast, water deficit conditions eliminated these genotypic differences, with all genotypes converging to similar berry

dry weights (0.502-0.515 g). Carbon-normalized treatments in LSB genotypes showed no significant differences from standard treatments within the same irrigation regime (G14 WD-C: 0.493 ± 0.059 g vs G14 WD: 0.509 ± 0.064 g; G5 WD-C: 0.518 ± 0.093 g vs G5 WD: 0.515 ± 0.032 g; G5 WW-C: 0.553 ± 0.025 g vs G5 WW: 0.624 ± 0.056 g), with berry dry weights showing no significant differences from standard treatments within the same irrigation regime. Berry dry weight remained relatively constant across genotypes under water deficit conditions (0.502-0.515 g), while berry fresh weight showed significant reductions under water deficit. The significant genotype × treatment interaction (p = 0.041) reflected the convergence of genotypic differences under water deficit compared to well-watered conditions.

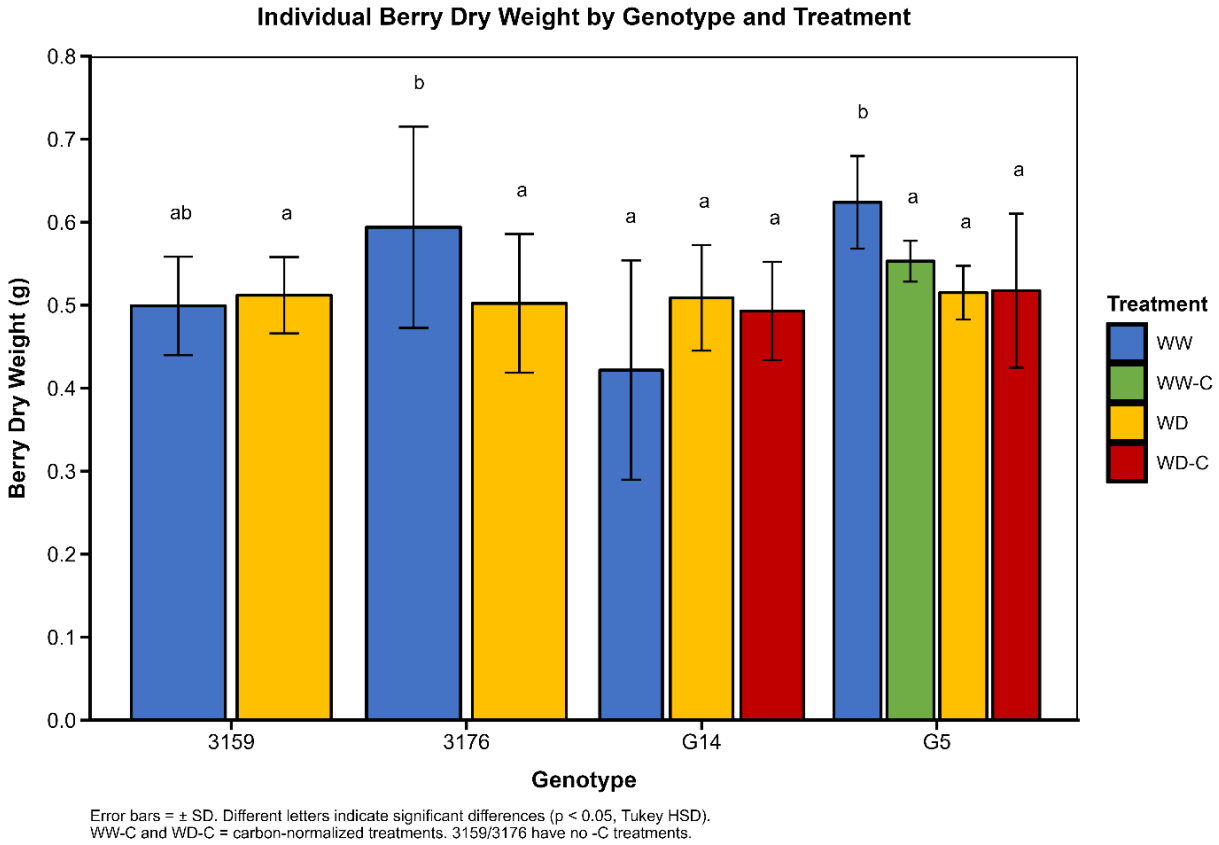

Figure 33. Individual berry dry weight by genotype and treatment. Mean berry dry weight (± SD) at harvest across genotypes and irrigation treatments. Bars represent well-watered (WW, blue), well-watered carbon-normalized (WW-C, green), water deficit (WD, yellow), and water deficit carbon-normalized (WD-C, red) treatments. Different letters indicate significant differences within each treatment ($p < 0.05$, Tukey HSD). Berry dry weight was calculated accounting for differential seed moisture content (20% at maturity, see Methods). Carbon-normalized treatments (WW-C, WD-C) represent increased berry numbers (+50%) and were only applied to LSB genotypes G5 and G14. Two-way ANOVA: Genotype $F_{3,43} = 2.68$ ($p = 0.058$), Treatment $F_{3,43} = 0.56$ ($p = 0.643$), Genotype × Treatment $F_{4,43} = 2.74$ ($p = 0.041$). n = 54 plants.

3.2.3.2 Sugar Accumulation

Final hexose concentration at harvest, measured as the sum of glucose and fructose by HPLC analysis, showed highly significant genotypic effects ($p < 0.001$) and a significant genotype × treatment interaction ($p = 0.002$), but no main effect of water treatment ($p = 0.130$). Total hexose concentrations ranged from 2152 mmol·L^{-1} in G14 WD-C to 2769 mmol·L^{-1} in 3159 WD, representing a 29% variation in sugar accumulation across genotypes and treatments (Figure 34). These concentrations were measured using the same HPLC methodology as Bigard et al. (2022), who reported ranges of approximately 2000-2250 mmol·L^{-1} total hexoses for physiologically ripe berries in traditional V. vinifera cultivars and 1600-1840 mmol·L^{-1} for LSB genotypes. The present study's LSB genotypes showed higher absolute hexose concentrations (G14: 2152-2274 mmol·L^{-1}; G5: 2291-2569 mmol·L^{-1}) than those reported by Bigard et al. (2022), though the LSB genotypes maintained 18-22% lower concentrations relative to non-LSB genotypes within this experiment.

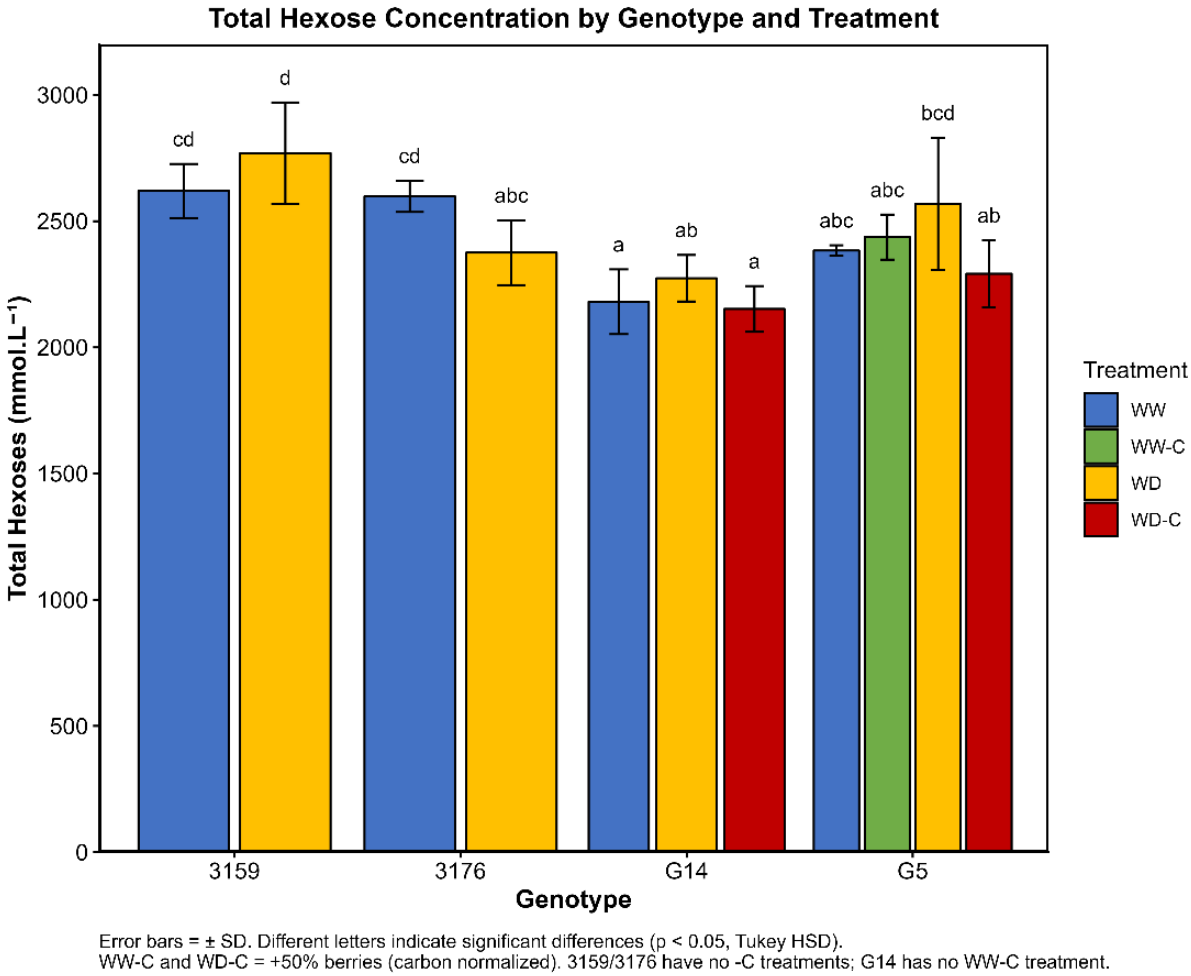

Figure 34. Total hexose concentration (glucose + fructose) at harvest by genotype and treatment. Mean total hexose concentration (± SD) for each genotype × treatment combination. Bars

represent treatments: WW = well-watered (blue), WW-C = well-watered carbon-normalized (green), WD = water deficit (yellow), WD-C = water deficit carbon-normalized (red). Different letters indicate significant differences ($p < 0.05$). Values determined by HPLC analysis. Hexoses (glucose and fructose) are the primary fermentable sugars in grape berries. Concentrations expressed in mmol·L^{-1}. Two-way ANOVA: Genotype $F_{3,46} = 16.51$ ($p < 0.001$), Treatment $F_{3,46} = 1.98$ ($p = 0.130$, ns), Genotype × Treatment $F_{4,46} = 4.98$ ($p = 0.002$). Carbon-normalized treatments applied only to LSB genotypes; 3159/3176 have no -C treatments; G14 has no WW-C treatment. n = 56 plants (4-6 per treatment). See Supplementary Table S5 for individual plant data.

LSB genotypes G14 and G5 exhibited significantly lower hexose concentrations compared to non-LSB genotypes. Genotype G14 showed the lowest total hexoses (2152-2274 mmol·L^{-1}) across all treatments, representing 18-22% lower sugar concentrations compared to 3159 (2620-2769 mmol·L^{-1}), which showed the highest accumulation. Genotype G5 displayed intermediate hexose levels (2291-2569 mmol·L^{-1}). Within LSB genotypes, carbon-normalized treatments showed reduced concentrations compared to standard treatments (G5 WD-C: 2291 mmol·L^{-1} vs G5 WD: 2569 mmol·L^{-1}, -11%; G5 WW-C: 2437 mmol·L^{-1} vs G5 WW: 2383 mmol·L^{-1}, +2%). Glucose:fructose ratios remained close to unity across all genotypes and treatments (0.98-1.02, Supplementary Table S5).

Water deficit showed no significant main effect on total hexose concentration ($p = 0.130$). However, the significant genotype × treatment interaction ($p = 0.002$) reflected differential responses among genotypes. Genotype 3159 showed 6% higher hexose concentration under water deficit (2769 mmol·L^{-1}) compared to well-watered conditions (2620 mmol·L^{-1}), while other genotypes showed minimal differences between irrigation treatments. Despite similar hexose concentrations between treatments, berry fresh weight decreased by 15-25% under water deficit (Section 3.2.3.1, Figure 32).

3.2.3.3 Organic Acids

Malic and tartaric acid concentrations at harvest showed highly significant genotypic effects ($p < 0.001$ for malic acid; $p < 0.001$ for tartaric acid), with no significant effects of water treatment ($p = 0.353$ for malic acid; $p = 0.220$ for tartaric acid) or genotype × treatment interactions ($p = 0.812$ for malic acid; $p = 0.525$ for tartaric acid).

Malic acid concentrations ranged from 20.0 mmol·L^{-1} in 3159 WD to 47.0 mmol·L^{-1} in 3176 WW, representing a 2.4-fold variation across genotypes (Figure 35). Genotype 3176 exhibited the highest malic acid concentrations across all treatments (43.8-47.0 mmol·L^{-1}), 2.2-fold higher than 3159 (20.0-24.5 mmol·L^{-1}), which showed the lowest values. LSB genotypes G5 and G14 displayed intermediate malic acid levels (29.2-36.4 mmol·L^{-1}). Water deficit had no significant effect on malic acid concentrations ($p = 0.353$), with values remaining stable within each genotype across irrigation treatments.

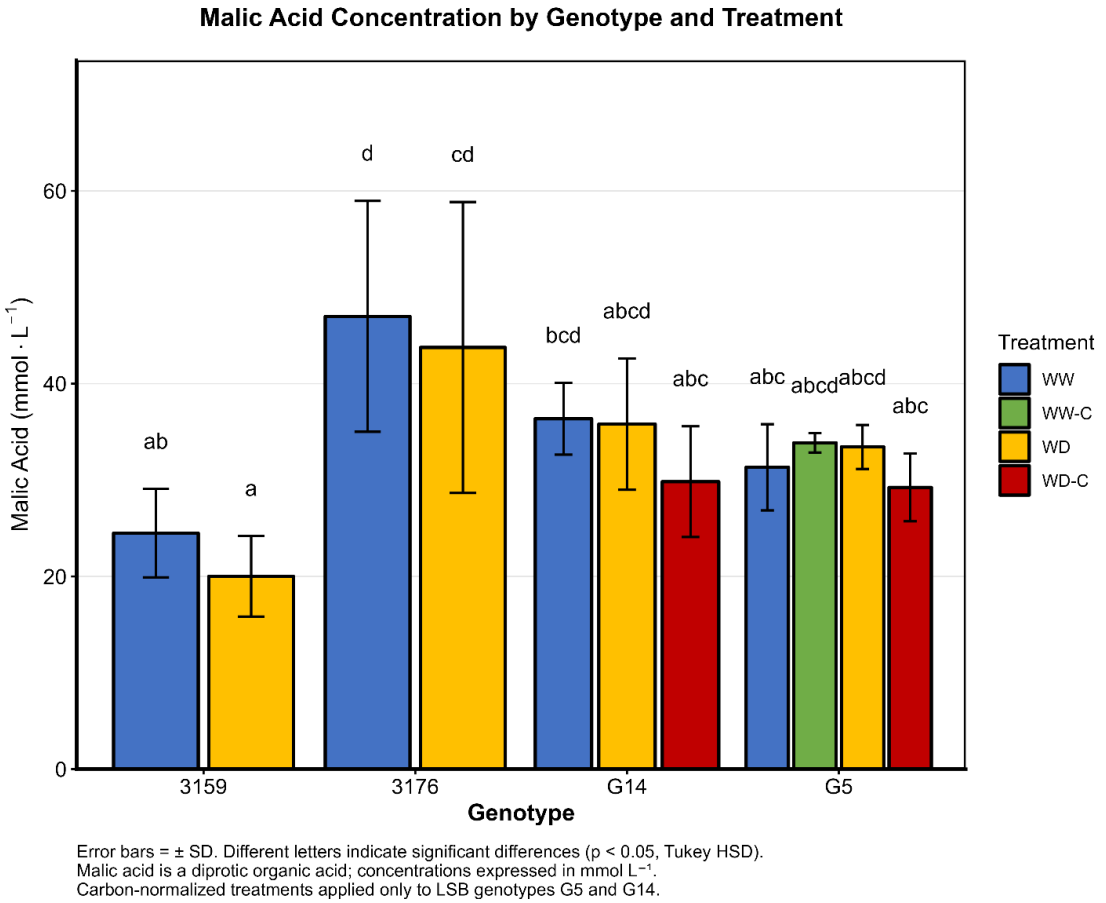

Figure 35. Malic acid concentration at harvest by genotype and treatment. Mean malic acid concentration (± SD) for each genotype × treatment combination. Bars represent treatments: WW = well-watered (blue), WW-C = well-watered carbon-normalized (green), WD = water deficit (yellow), WD-C = water deficit carbon-normalized (red). Different letters indicate significant differences ($p < 0.05$). Malic acid is a diprotic organic acid; concentrations expressed in mmol·L^{-1}. Two-way ANOVA: Genotype $F_{3,46} = 20.06$ ($p < 0.001$), Treatment $F_{3,46} = 1.11$ ($p = 0.353$, ns), Genotype × Treatment $F_{4,46} = 0.39$ ($p = 0.812$, ns). Carbon-normalized treatments applied only to LSB genotypes. n = 56 plants. See Supplementary Table S5.

Tartaric acid concentrations ranged from 29.3 mmol·L^{-1} in G5 to 43.4 mmol·L^{-1} in 3176 and G14, representing a 1.5-fold variation (Figure 36). Genotypes 3176 and G14 showed the highest tartaric acid levels (41.6-43.4 mmol·L^{-1}), forming a statistically homogeneous group significantly higher than G5 (29.3-34.0 mmol·L^{-1}), which exhibited the lowest concentrations. Genotype 3159 displayed intermediate tartaric acid values (35.9-36.0 mmol·L^{-1}). Water deficit did not significantly affect tartaric acid accumulation ($p = 0.220$), with concentrations remaining stable within genotypes across irrigation treatments.

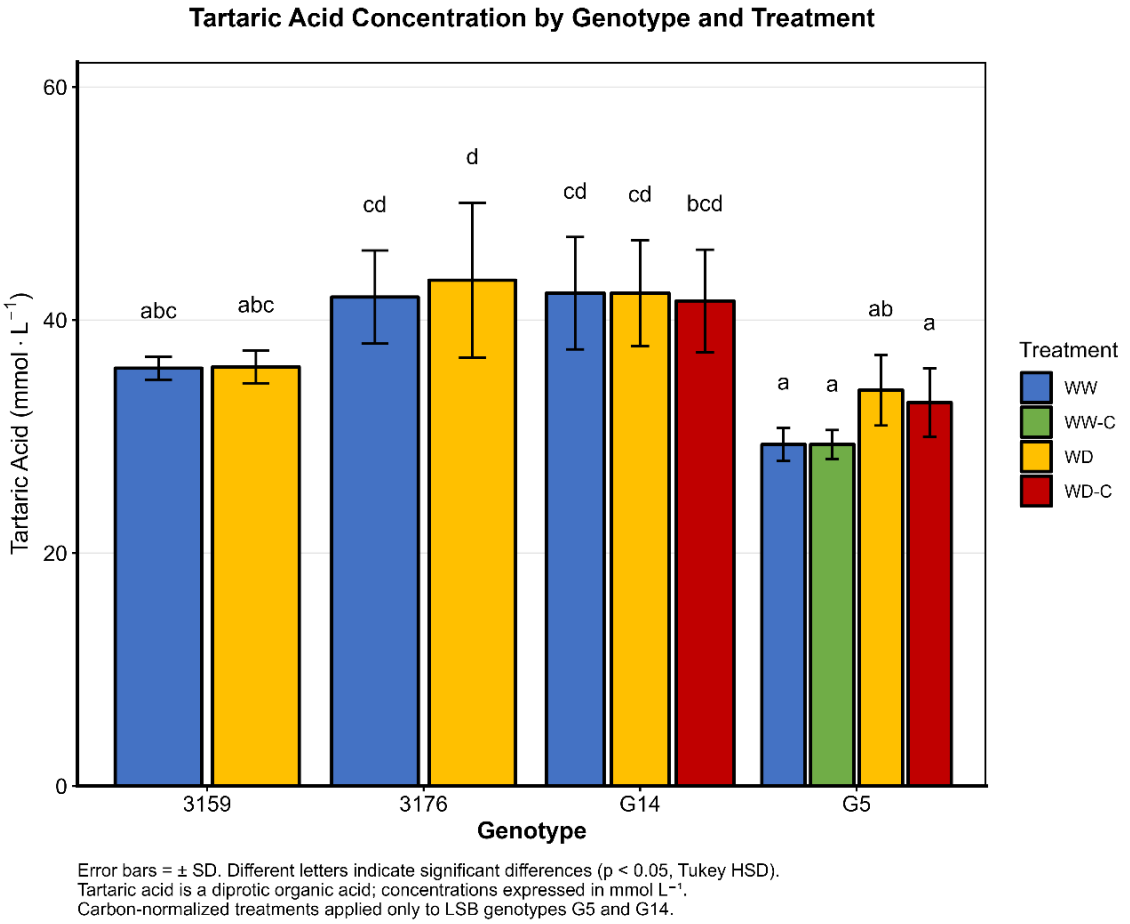

Figure 36. Tartaric acid concentration at harvest by genotype and treatment. Mean tartaric acid concentration (± SD) for each genotype × treatment combination. Bars represent treatments: WW = well-watered (blue), WW-C = well-watered carbon-normalized (green), WD = water deficit (yellow), WD-C = water deficit carbon-normalized (red). Different letters indicate significant differences ($p < 0.05$). Tartaric acid is a diprotic organic acid; concentrations expressed in mmol·L^{-1}. Two-way ANOVA: Genotype $F_{3,46} = 26.91$ ($p < 0.001$), Treatment $F_{3,46} = 1.53$ ($p = 0.220$, ns), Genotype × Treatment $F_{4,46} = 0.81$ ($p = 0.525$, ns). Carbon-normalized treatments applied only to LSB genotypes. n = 56 plants. See Supplementary Table S5.

The malic:tartaric acid ratio showed highly significant genotypic effects ($p < 0.001$) and a significant treatment effect ($p = 0.018$), with no significant interaction ($p = 0.958$). Ratios ranged from 0.50 in 3159 WD to 1.19 in G5 WW, representing a 2.4-fold variation in organic acid balance (Figure 37). Genotype means across all treatments showed distinct patterns: 3176 displayed the highest ratio (1.09 ± 0.20), followed by LSB genotype G5 (0.99 ± 0.13), LSB genotype G14 (0.82 ± 0.11), and non-LSB genotype 3159 with the lowest ratio (0.62 ± 0.09). The elevated malic:tartaric ratio in G5 is consistent with the LSB metabolic phenotype described by Bigard et al. (2022), who reported higher malic:tartaric ratios in LSB genotypes compared to traditional cultivars. Water deficit slightly increased the malic:tartaric ratio across genotypes ($p = 0.018$), though this effect (5-8% average increase) was modest compared to genotypic differences.

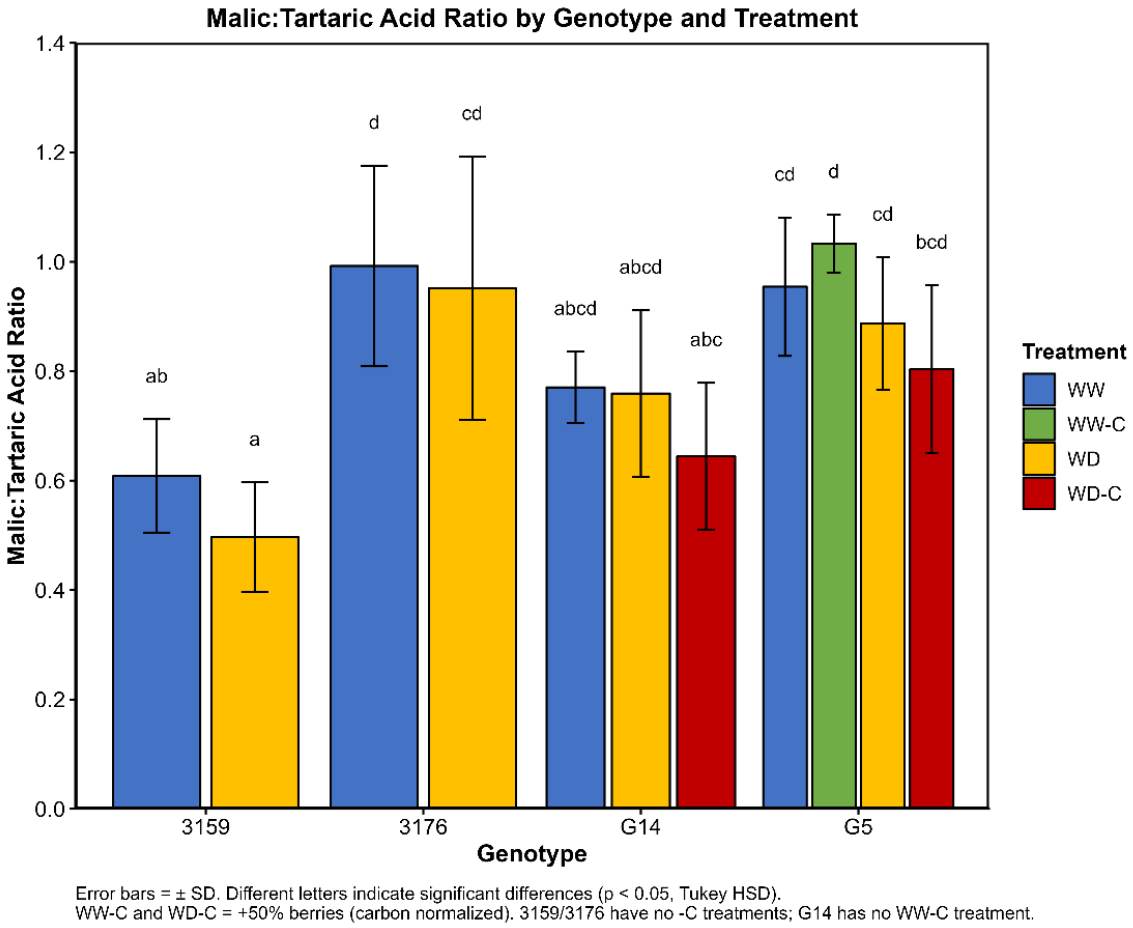

Figure 37. Malic:tartaric acid ratio at harvest by genotype and treatment. Mean malic:tartaric acid ratio (± SD) for each genotype × treatment combination. Bars represent treatments: WW = well-watered (blue), WW-C = well-watered carbon-normalized (green), WD = water deficit (yellow), WD-C = water deficit carbon-normalized (red). Different letters indicate significant differences ($p < 0.05$). The malic:tartaric ratio is a diagnostic metabolic trait for LSB genotypes (Bigard et al., 2022). Ratio is dimensionless ($mmol \cdot L^{-1}/mmol \cdot L^{-1}$). Two-way ANOVA: Genotype $F_{3,46} = 19.42$ ($p < 0.001$), Treatment $F_{3,46} = 3.71$ ($p = 0.018$), Genotype × Treatment $F_{4,46} = 0.16$ ($p = 0.958$, ns). Carbon-normalized treatments applied only to LSB genotypes. n = 56 plants. See Supplementary Table S5.

Total organic acids (malic + tartaric) ranged from 60.4 to 89.0 $mmol \cdot L^{-1}$ across all genotype × treatment combinations. Genotype 3176 showed the highest total acidity (87.2-89.0 $mmol \cdot L^{-1}$), 1.4-1.5-fold higher than 3159 (56.0-60.4 $mmol \cdot L^{-1}$), which showed the lowest values. LSB genotypes G14 and G5 displayed intermediate total acidity (62.1-78.7 $mmol \cdot L^{-1}$). Organic acid concentrations remained stable across water treatments, contrasting with the variable responses observed in berry growth and hexose accumulation.

The malic acid:hexoses ratio, reflecting the balance between metabolically active malic acid and hexose sugars, showed highly significant genotypic effects ($p < 0.001$) but no treatment effect ($p = 0.557$) or genotype × treatment interaction ($p = 0.653$). Ratios

ranged from 0.0072 in 3159 WD to 0.0187 in 3176 WD, representing a 2.6-fold variation (Figure 38). Genotype means showed distinct patterns: 3176 exhibited the highest ratio (0.0184 ± 0.0036), followed by G14 (0.0154 ± 0.0019), G5 (0.0132 ± 0.0011), and 3159 with the lowest ratio (0.0083 ± 0.0015). The higher malic:hexoses ratio in 3176 reflects its combination of high malic acid (45.4 mmol·L^{-1}) and moderate hexoses (2455 mmol·L^{-1}), while the lower ratio in 3159 results from low malic acid (22.2 mmol·L^{-1}) and high hexoses (2694 mmol·L^{-1}). LSB genotypes showed intermediate ratios, with greater differences in hexose accumulation than in malic acid concentrations between LSB and non-LSB genotypes. This ratio remained stable across irrigation treatments (p = 0.557).

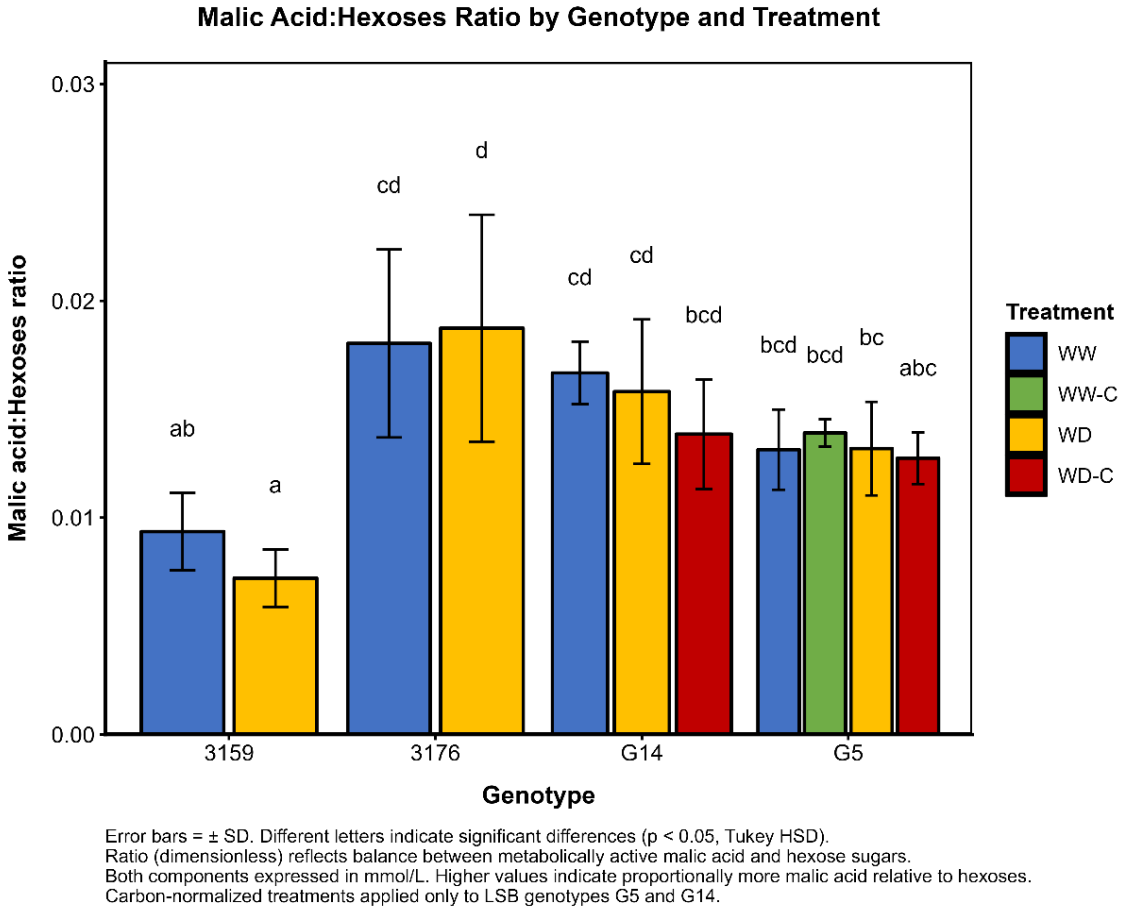

Figure 38. Malic acid:hexoses ratio at harvest by genotype and treatment. Mean malic acid:hexoses ratio (± SD) for each genotype × treatment combination. Bars represent treatments: WW = well-watered (blue), WW-C = well-watered carbon-normalized (green), WD = water deficit (yellow), WD-C = water deficit carbon-normalized (red). Different letters indicate significant differences (p < 0.05). Ratio (dimensionless) reflects balance between metabolically active malic acid and hexose sugars. Both components expressed in mmol·L^{-1}. Higher values indicate proportionally more malic acid relative to hexoses. Two-way ANOVA: Genotype $F_{3,46}$ = 28.51 (p < 0.001), Treatment $F_{3,46}$ = 0.70 (p = 0.557, ns), Genotype × Treatment $F_{4,46}$ = 0.62 (p = 0.653, ns). Carbon-normalized treatments applied only to LSB genotypes G5 and G14. n = 56 plants. See Supplementary Table S5.

Organic acid composition showed significant genotypic effects ($p < 0.001$ for both malic and tartaric acids) with no significant treatment effects (malic: $p = 0.353$; tartaric: $p = 0.220$), with concentrations remaining stable under moderate water deficit during ripening. The substantial genotypic variation observed in individual organic acids (2.4-fold for malic acid, 1.5-fold for tartaric acid), the malic:tartaric ratio (2.4-fold), and the malic:hexoses ratio (2.6-fold) reflecting the diversity in berry composition across the genotype panel. The elevated malic:tartaric ratio in LSB genotype G5 (0.99) compared to non-LSB genotype 3159 (0.62) was consistent with the metabolic phenotype described by Bigard et al. (2022). The malic:hexoses ratio showed genotypic differences, with 3176 showing the highest ratio and 3159 the lowest.

3.2.4 Vegetative Biomass and Carbon Partitioning

3.2.4.1 Fresh Weight Analysis

Total vegetative fresh biomass at harvest showed highly significant effects of genotype ($p < 0.001$), treatment ($p < 0.001$), and their interaction ($p = 0.001$). Total vegetative biomass ranged from 408 g in 3159 WD to 954 g in 3176 WW, representing a 2.3-fold variation across genotypes and treatments (Figure 39). Genotype means across all treatments revealed distinct patterns: 3176 showed the highest mean biomass (677 ± 132 g), followed by G5 (590 ± 82 g), 3159 (587 ± 130 g), and G14 with the lowest (538 ± 56 g).

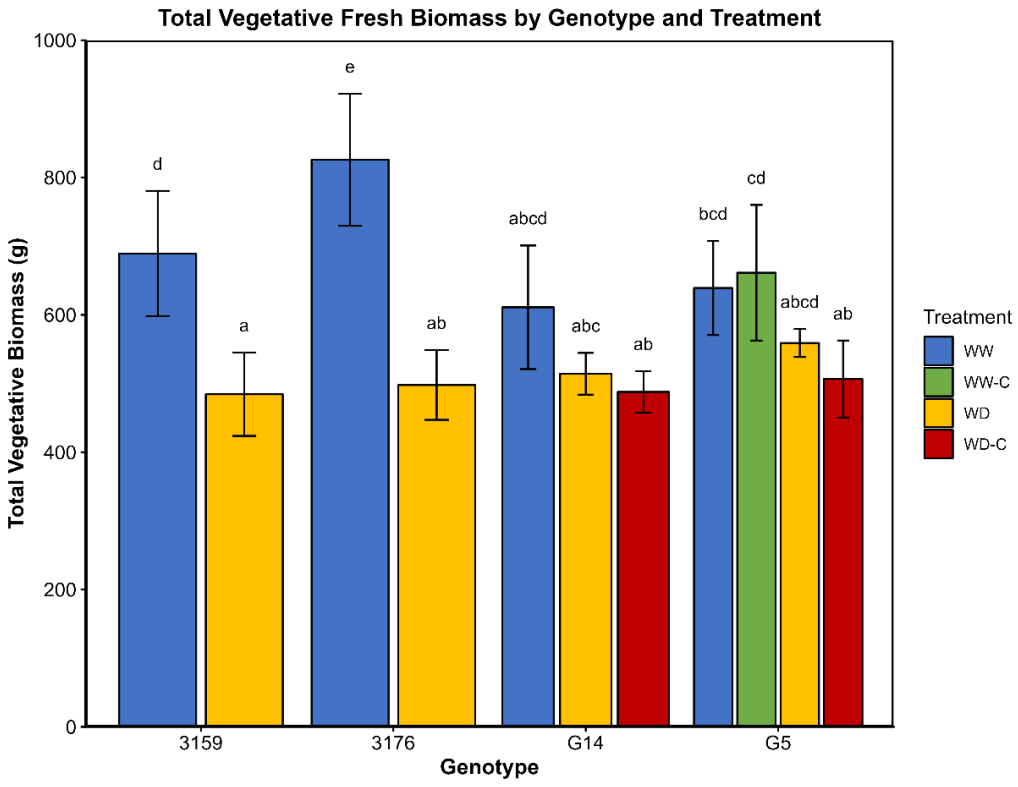

Error bars = ± SD. Different letters indicate significant differences ($p < 0.05$, Tukey HSD).
WW-C and WD-C = +50% berries (carbon normalized). 3159/3176 have no -C treatments; G14 has no WW-C treatment.

Figure 39. Total vegetative fresh biomass by genotype and treatment. Mean total vegetative biomass (± SD) at harvest. Bars represent treatments: WW = well-watered (blue), WW-C = well-watered carbon-normalized (green), WD = water deficit (yellow), WD-C = water deficit carbon-normalized (red). Different letters indicate significant differences ($p < 0.05$, Tukey HSD). Total vegetative biomass = shoots + leaves + trunk + canes + roots. Two-way ANOVA: Genotype $F_{3,45} = 7.83$ ($p < 0.001$), Treatment $F_{3,45} = 29.34$ ($p < 0.001$), Genotype × Treatment $F_{4,45} = 5.31$ ($p = 0.001$). Carbon-normalized treatments applied only to LSB genotypes. n = 56 plants.

Water deficit significantly reduced total vegetative biomass across all genotypes. Well-watered plants showed 14-66% higher biomass compared to water deficit plants within each genotype (3159: 689 vs 484 g, +42%; 3176: 826 vs 498 g, +66%; G14: 611 vs 514 g, +19%; G5: 639 vs 559 g, +14%). The significant genotype × treatment interaction reflects differential sensitivity to water availability, with 3176 showing the largest absolute reduction under water deficit (328 g reduction) and G14 the smallest (97 g reduction). Carbon-normalized treatments in LSB genotypes showed reduced total vegetative biomass compared to standard treatments within the same irrigation regime (G5 WW-C: 661 g vs G5 WW: 639 g; G5 WD-C: 507 g vs G5 WD: 559 g; G14 WD-C: 488 g vs G14 WD: 514 g), corresponding with increased berry numbers (+34-36%) in carbon-normalized treatments.

Individual biomass components showed highly significant genotypic and treatment effects with varying magnitudes (detailed measurements provided in Supplementary Table S6). Total shoots (main + lateral) showed significant effects of genotype ($p < 0.001$), treatment ($p < 0.001$), and their interaction ($p < 0.001$), ranging from 107 g in G5 WD-C to 288 g in 3176 WW. Total leaves (main + lateral) showed similar patterns with significant effects of genotype ($p < 0.001$), treatment ($p < 0.001$), and interaction ($p < 0.001$), ranging from 113 g in G14 WD-C to 275 g in 3176 WW. Cane biomass showed significant genotypic effects ($p < 0.001$) but no treatment effects ($p = 0.449$), with genotype means of 96 g for 3159, 123 g for 3176, 95 g for G14, and 100 g for G5. Root biomass showed significant genotypic effects ($p < 0.001$) but no treatment effects ($p = 0.228$), ranging from 111 g in 3176 3120 to 280 g in G5 2075, with genotype means of 163 g for 3159, 133 g for 3176, 174 g for G14, and 194 g for G5. Trunk biomass showed no significant effects of genotype ($p = 0.153$) or treatment ($p = 0.264$), remaining stable at 15-31 g across all genotypes and treatments.

Biomass partitioning patterns revealed distinct allocation strategies among genotypes (Figure 40). Genotype 3176 allocated the highest proportion to leaves and shoots, particularly under well-watered conditions, while LSB genotypes G5 and G14 showed more balanced distributions. Water deficit reduced allocation to photosynthetic tissues (shoots and leaves) while maintaining relatively stable allocation to structural components (trunk and canes) and roots. Carbon-normalized treatments in LSB

genotypes showed similar partitioning patterns to standard treatments despite lower absolute biomass.

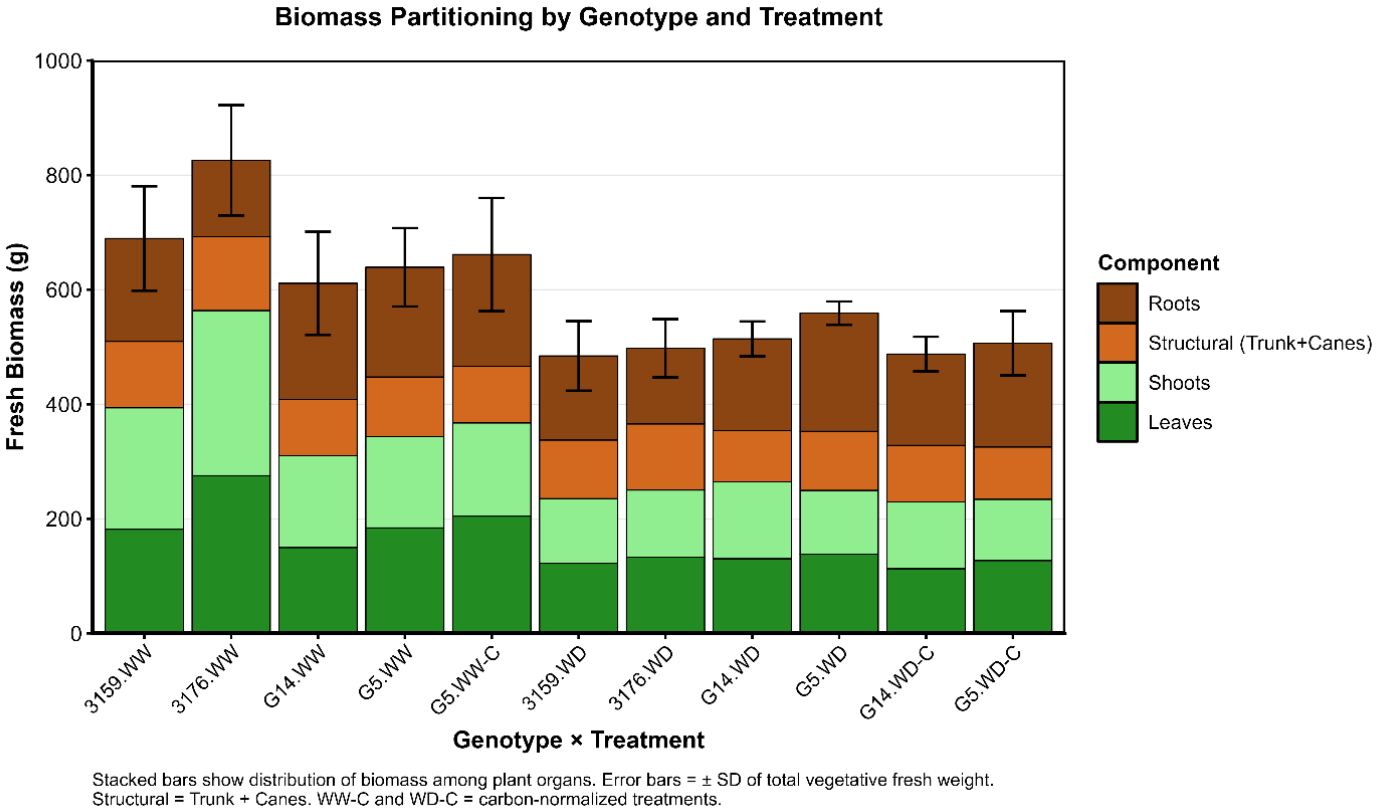

Figure 40. Biomass partitioning among plant organs by genotype and treatment. Stacked bars showing distribution of fresh biomass among roots (brown), structural tissues including trunk and canes (tan), shoots (light green), and leaves (dark green). Each bar represents mean biomass allocation for a genotype × treatment combination. Error bars = ± SD of total vegetative fresh weight. Biomass values in grams. Carbon-normalized treatments applied only to LSB genotypes. n = 56 plants.

The shoot:root ratio showed highly significant effects of genotype ($p < 0.001$), treatment ($p < 0.001$), and their interaction ($p < 0.001$), ranging from 1.27 to 7.34 across individual plants (Figure 41). Genotype 3176 under well-watered conditions exhibited a dramatically higher shoot:root ratio (5.49 ± 1.52) compared to all other genotype × treatment combinations (1.72-2.87), representing a 1.9-2.3-fold increase. This single treatment combination was significantly different from all others (Tukey HSD, $p < 0.05$), while the remaining treatments formed a homogeneous group with ratios between 1.7 and 2.9. Genotype means across treatments showed 3176 with the highest ratio (4.26 ± 1.79), followed by 3159 (2.60 ± 0.53), G14 (2.16 ± 0.40), and G5 with the lowest (2.08 ± 0.45). Water deficit tended to reduce shoot:root ratios within genotypes (treatment means: WW = 3.35 ± 1.65; WD = 2.25 ± 0.47), though this effect was primarily driven by the extreme value in 3176 WW. LSB genotypes G5 and G14 maintained consistently low shoot:root ratios (2.0-2.4) across all treatments.

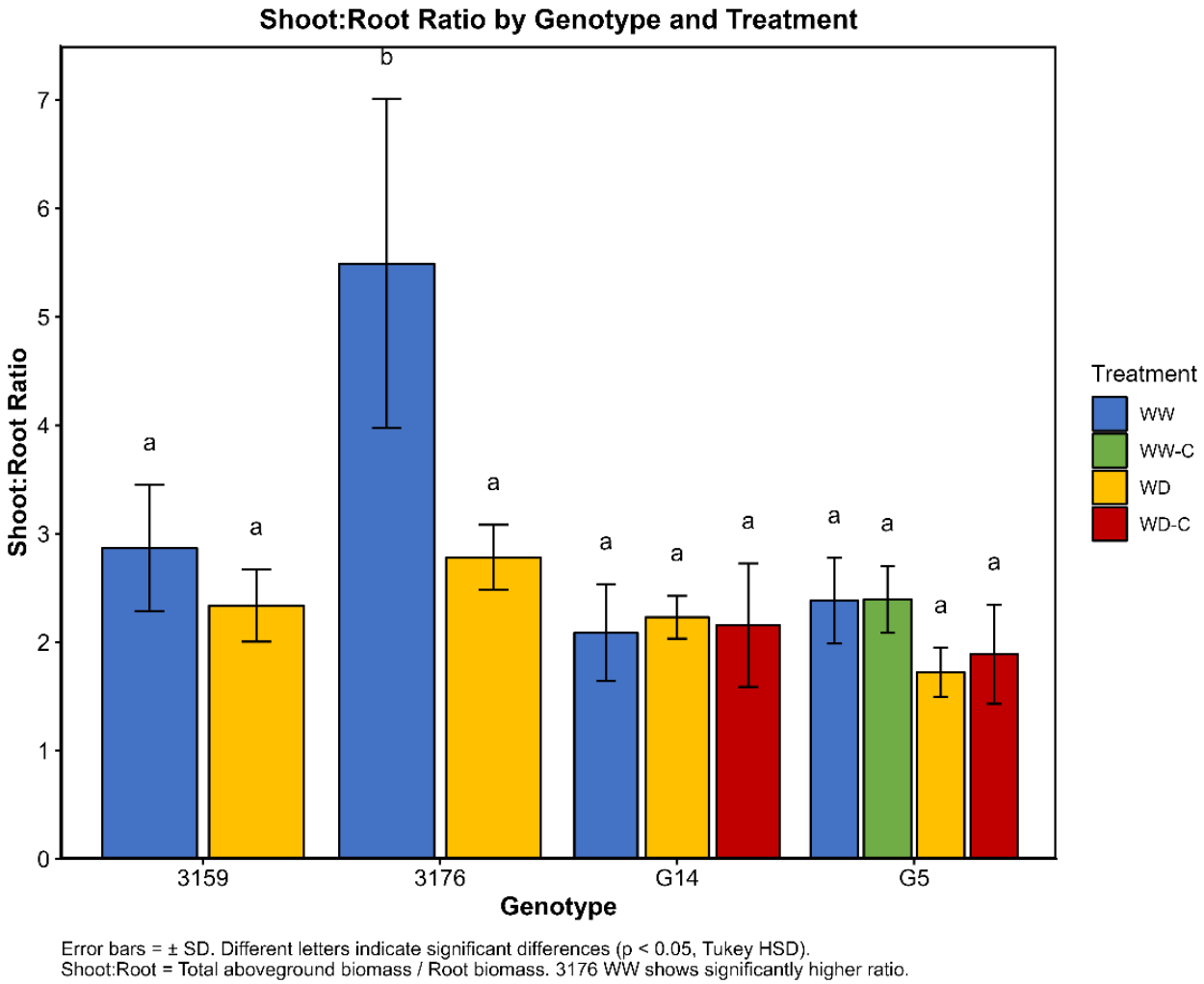

Figure 41. Shoot:root ratio by genotype and treatment (fresh weight). Mean shoot:root ratio (± SD) calculated as total aboveground biomass / root biomass. Bars represent treatments: WW = well-watered (blue), WW-C = well-watered carbon-normalized (green), WD = water deficit (yellow), WD-C = water deficit carbon-normalized (red). Different letters indicate significant differences ($p < 0.05$, Tukey HSD). Higher ratios indicate greater allocation to above-ground organs. Two-way ANOVA: Genotype $F_{3,45} = 32.05$ ($p < 0.001$), Treatment $F_{3,45} = 9.37$ ($p < 0.001$), Genotype × Treatment $F_{4,45} = 7.29$ ($p < 0.001$). Genotype 3176 under well-watered conditions shows significantly higher ratio compared to all other combinations. Carbon-normalized treatments applied only to LSB genotypes. n = 56 plants.

3.2.4.2 Dry Weight Analysis

Total vegetative dry weight at harvest showed a highly significant treatment effect ($p < 0.001$) but no significant genotype effect ($p = 0.372$) or genotype × treatment interaction ($p = 0.147$). Total vegetative dry weight ranged from 198 g in 3176 WD to 282 g in 3159 WW (Figure 42). Treatment means revealed that well-watered conditions supported significantly higher dry biomass accumulation (WW: 258-282 g) compared to water deficit conditions (WD: 198-243 g), representing a 15-25% reduction in total carbon investment depending on genotype. Under well-watered conditions, all genotypes

showed similar total dry weight (258-282 g, all group "a"), with no significant differences among genotypes. However, under water deficit, genotypic differences emerged: 3176 exhibited the lowest dry weight (198 ± 27 g, group "a"), while G5 showed the highest (243 ± 10 g, group "b"), with 3159 and G14 intermediate (216-238 g, groups "ab"). Carbon-normalized treatments in LSB genotypes did not significantly alter total vegetative dry weight compared to standard treatments within the same irrigation regime (G5 WW-C: 257 g vs G5 WW: 261 g; G5 WD-C: 221 g vs G5 WD: 243 g; G14 WD-C: 217 g vs G14 WD: 238 g), with modest increases in berry number (+34-36%) showing no significant effect on whole-plant carbon accumulation.

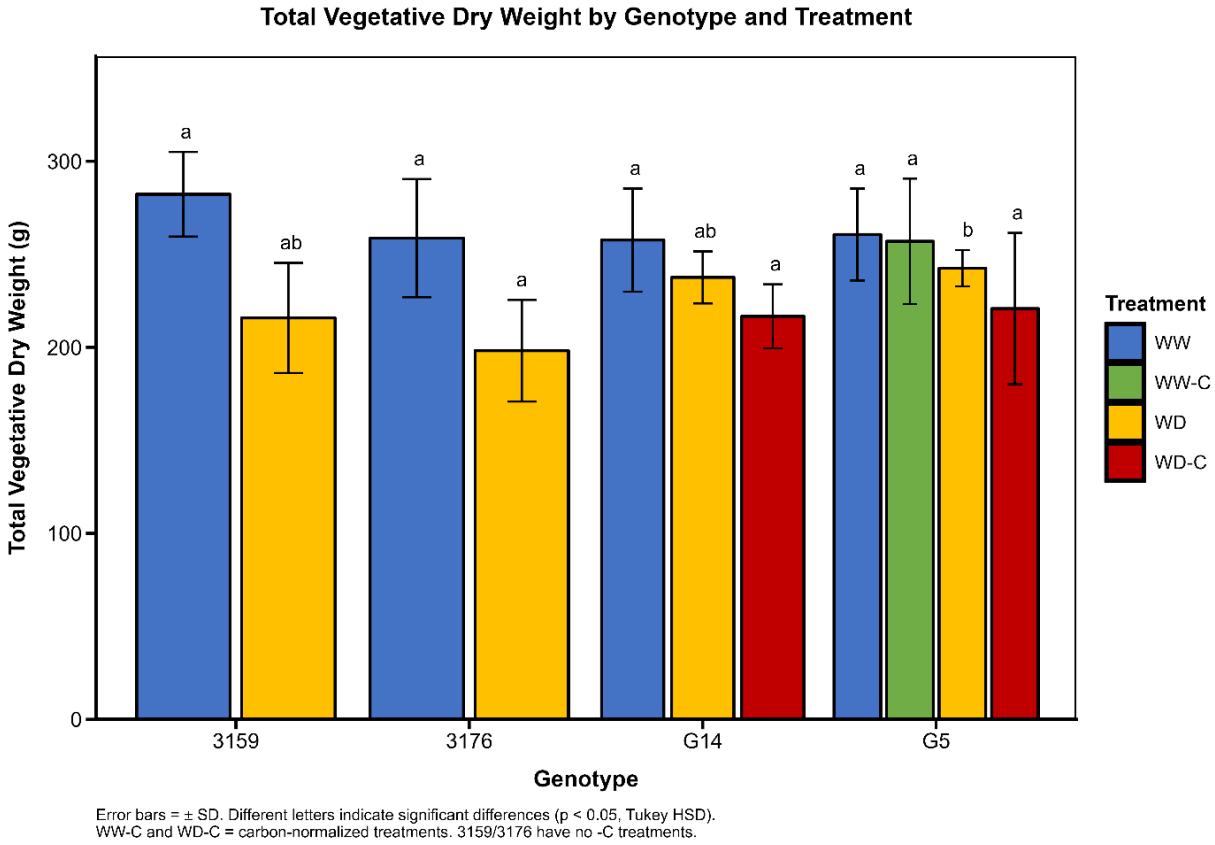

Figure 42. Total vegetative dry weight by genotype and treatment. Mean total vegetative dry biomass (± SD) at harvest. Bars represent treatments: WW = well-watered (blue), WW-C = well-watered carbon-normalized (green), WD = water deficit (yellow), WD-C = water deficit carbon-normalized (red). Different letters indicate significant differences ($p < 0.05$, Tukey HSD). Total vegetative dry weight = shoots + leaves + trunk + canes + roots. Two-way ANOVA: Genotype $F_{3,45} = 1.068$ ($p = 0.372$), Treatment $F_{3,45} = 11.998$ ($p < 0.001$), Genotype × Treatment $F_{4,45} = 1.791$ ($p = 0.147$). Carbon-normalized treatments applied only to LSB genotypes. n = 56 plants.

Individual dry weight components showed distinct patterns of genotypic and treatment responses (detailed measurements provided in Supplementary Table S7). Total shoots showed significant effects of genotype ($p < 0.001$), treatment ($p < 0.001$), and their interaction ($p = 0.024$), with water deficit reducing shoot dry weight by 25-50% across

genotypes. Total leaves exhibited similar patterns with significant genotype ($p = 0.289$), treatment ($p < 0.001$), and interaction effects $p = 0.028$). In contrast, structural organs showed no significant treatment effects: trunk dry weight showed a marginally significant genotype effect $p = 0.053$) but no treatment effect ($p = 0.305$), while cane dry weight showed significant genotypic variation ($p < 0.001$) but no treatment effect ($p = 0.579$). Root dry weight exhibited strong genotypic differences ($p < 0.001$) but no treatment effect ($p = 0.607$). Notably, LSB genotype G5 maintained the highest root dry weight across all treatments (103-112 g), 40-75% greater than genotype 3176 (64-71 g), showing substantial genotypic variation in belowground carbon allocation with no significant treatment effect.

Dry weight partitioning patterns were consistent with those observed in fresh weight analysis (Figure 43). LSB genotype G5 allocated proportionally more carbon to roots compared to non-LSB genotypes, maintaining root dry weight above 100 g across all treatments while aboveground organs showed greater plasticity in response to water availability. Genotype 3176 allocated proportionally more carbon to photosynthetic tissues (shoots and leaves) under well-watered conditions, with structural organs (trunk and canes) representing a smaller proportion of total dry biomass. Water deficit reduced the proportion of carbon allocated to photosynthetic tissues across all genotypes while proportional allocation to structural organs and roots remained stable across water treatments. Carbon-normalized and standard treatments within LSB genotypes showed similar partitioning patterns, though absolute carbon accumulation was modestly reduced in carbon-normalized treatments.

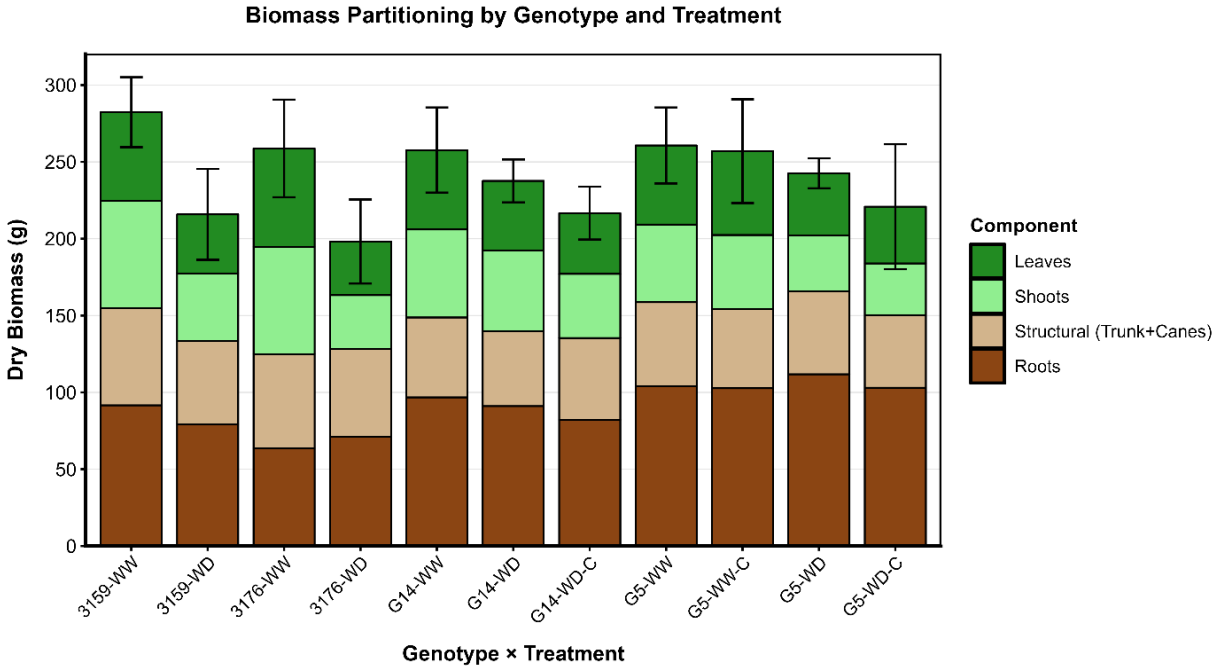

Stacked bars show distribution of dry biomass among plant organs. Error bars = ± SD of total vegetative dry weight. Structural = Trunk + Canes. WW-C and WD-C = carbon-normalized treatments.

Figure 43. Biomass partitioning among plant organs by genotype and treatment (dry weight). Stacked bars showing distribution of dry biomass among roots (brown), structural tissues including trunk and canes (tan), shoots (light green), and leaves (dark green). Each bar represents mean biomass allocation for a genotype × treatment combination. Error bars = ± SD of total vegetative dry weight. Biomass values in grams. Carbon-normalized treatments applied only to LSB genotypes. n = 56 plants.

The shoot:root ratio based on dry weight showed highly significant effects of genotype ($p < 0.001$), treatment ($p < 0.001$), and their interaction ($p < 0.001$), ranging from 0.84 to 4.05 across individual plants (Figure 44). Genotype 3176 under well-watered conditions exhibited the highest shoot:root ratio based on dry weight (3.16 ± 0.71, group "c"), with the elevated ratio observed in fresh weight analysis (5.49 ± 1.52) also evident in dry weight (3.16 ± 0.71). LSB genotype G5 consistently showed the lowest shoot:root ratios across all treatments (1.17-1.53, predominantly group "a"), with genotype means of 1.35 for G5, 1.68 for G14, 1.92 for 3159, and 2.54 for 3176. Water deficit reduced shoot:root ratios across genotypes (treatment means: WW = 2.20; WD = 1.57; WD-C = 1.43), though the magnitude of this effect varied among genotypes. The dry weight shoot:root ratios were consistently lower than fresh weight ratios (e.g., 3176 WW: 3.16 DW vs 5.49 FW; G5 WD: 1.17 DW vs 2.08 FW), with shoot tissues showing higher water content relative to roots. Carbon-normalized treatments showed no significant difference in shoot:root ratio compared to standard treatments within LSB genotypes (G5 WD-C: 1.21 vs G5 WD: 1.17; G5 WW-C: 1.51 vs G5 WW: 1.53).

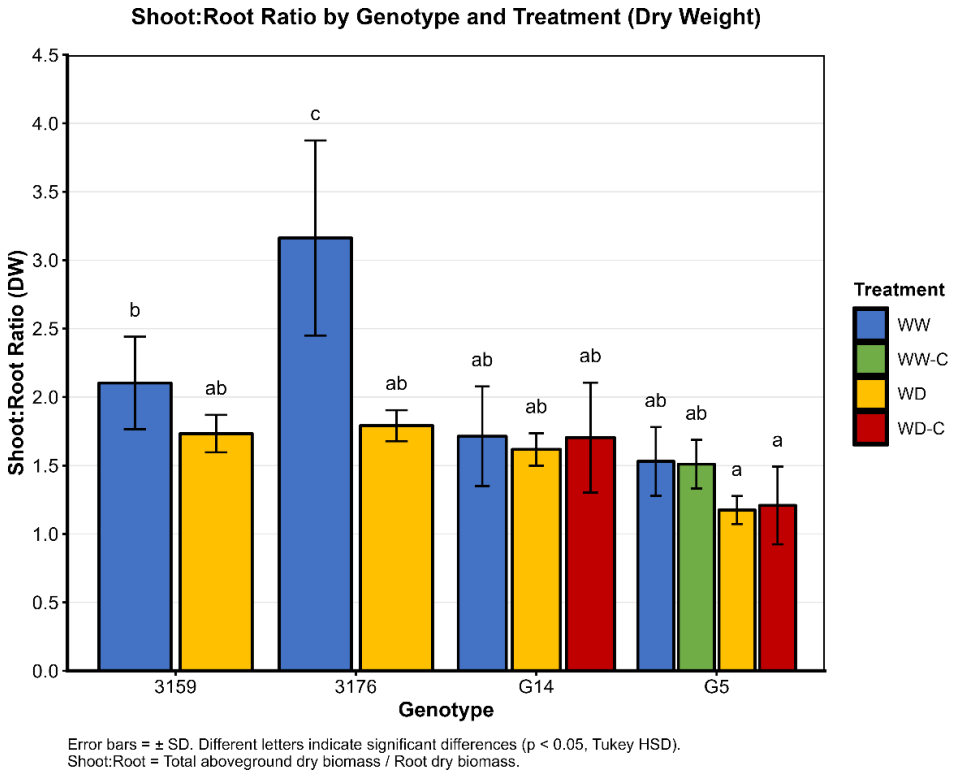

Figure 44. Shoot:root ratio by genotype and treatment (dry weight). Mean shoot:root ratio (± SD) calculated as total aboveground dry biomass / root dry biomass. Bars represent treatments: WW = well-watered (blue), WW-C = well-watered carbon-normalized (green), WD = water deficit (yellow), WD-C = water deficit carbon-normalized (red). Different letters indicate significant differences ($p < 0.05$, Tukey HSD). Higher ratios indicate greater allocation to aboveground organs. Two-way ANOVA: Genotype $F_{3,45} = 32.335$ ($p < 0.001$), Treatment $F_{3,45} = 11.053$ ($p < 0.001$), Genotype × Treatment $F_{4,45} = 5.707$ ($p < 0.001$). Dry weight ratios were consistent with patterns observed in fresh weight. Carbon-normalized treatments applied only to LSB genotypes. n = 56 plants.

3.2.5 Whole-Plant Carbon Balance

3.2.5.1 Plant Carbon Gain

3.2.5.1.1 Variation in Fruit Carbon Content (varC)

The variation in fruit carbon content from veraison to harvest (varC), calculated as the difference in carbon equivalents of major soluble metabolites (sugars, tartaric acid, and malic acid) between the two developmental stages, ranged from 35.64 g C per plant (G14 WW) to 76.75 g C per plant (G5 WW-C) across all treatments (Table 10). ANOVA revealed no significant effects of genotype ($p = 0.235$) or treatment ($p = 0.421$) on varC, showing stable carbon accumulation in fruits across water availability conditions despite differences in water consumption (Section 3.2.2).

Table 10. Carbon accumulation in fruits from veraison to harvest (varC).

Genotype	Treatment	n	Mean_varC	SD_varC	SE_varC	Min_varC	Max_varC
3159	WD	6	54,28	9,23	3,77	45,53	70,19
3159	WW	6	53,23	17,34	7,08	37,56	80,65
3176	WD	6	52,95	8,77	3,58	39,13	60,08
3176	WW	6	55,04	12,09	4,94	40,20	70,40
G14	WD	4	40,68	6,02	3,01	32,07	45,60
G14	WD-C	4	58,38	3,94	1,97	53,53	63,04
G14	WW	4	35,64	11,76	5,88	19,38	44,77
G5	WD	6	45,38	5,00	2,04	39,41	53,37
G5	WD-C	5	67,91	10,67	4,77	51,50	79,56
G5	WW	5	56,54	21,94	9,81	23,22	77,16
G5	WW-C	4	76,75	17,91	8,95	53,18	96,20

Variation in fruit carbon content (varC) from veraison to physiological ripeness by genotype and water treatment. Values calculated as the change in carbon equivalents of major soluble metabolites (glucose, fructose, tartaric acid, and malic acid) measured by HPLC at both developmental stages. Carbon content derived from molecular weights and carbon stoichiometry of each metabolite. Values represent mean ± SD with sample size (n), standard error (SE), minimum, and maximum values per treatment group. ANOVA results: Genotype $p = 0.235$ (ns), Treatment $p = 0.421$ (ns), Genotype × Treatment $p > 0.05$ (ns). WW = well-watered (FTSW ~0.6-0.7), WD = water deficit (FTSW ~0.18-0.25), WW-C and WD-C = carbon-normalized treatments with +50% berry number for LSB genotypes G5 and G14. No significant differences

were detected among treatments, indicating stable fruit carbon accumulation despite contrasting water availability.

Under well-watered conditions, varC averaged 35.64-56.54 g C per plant across genotypes, with no significant differences among varieties. The highest carbon accumulation under WW was observed in G5 WW (56.54 ± 21.94 g C, n=5), followed by 3176 WW (55.04 ± 12.09 g C, n=6) and 3159 WW (53.23 ± 17.34 g C, n=6), while the lowest was recorded in G14 WW (35.64 ± 11.76 g C, n=4). Water deficit did not consistently reduce fruit carbon accumulation compared to well-watered conditions. Three of four genotypes (3159, 3176, G14) showed similar or slightly higher varC under water deficit (40.68-54.28 g C per plant) compared to well-watered conditions, with only G5 exhibiting a modest 20% reduction (G5 WD: 45.38 ± 5.00 g C vs G5 WW: 56.54 ± 21.94 g C, difference not statistically significant due to high variability in G5 WW).

Carbon-normalized LSB genotypes, which received increased berry numbers (+50%) to match the carbon demand of conventional varieties, achieved the highest absolute varC values across all treatments. G5 WD-C accumulated 67.91 ± 10.67 g C per plant (n=5) and G14 WD-C reached 58.38 ± 3.94 g C per plant (n=4), both operating under water deficit conditions (FTSW 0.18-0.25). G5 WW-C achieved the highest varC of all treatments (76.75 ± 17.91 g C, n=4).

The maintained or increased varC under water deficit in most genotypes, despite 43-59% reductions in total plant transpiration (Section 3.2.2.1.2, Table 8), resulted in the substantially elevated whole-plant water use efficiency (WUEpl) observed under water deficit conditions (Section 3.2.5.2.1). Carbon accumulation in fruits remained stable across water treatments despite reductions in total plant transpiration and photosynthesis (Sections 3.2.2.1.2 and 3.2.5.3.3).

3.2.5.1.2 Total Plant Biomass and Fruit Allocation

Total plant dry biomass at harvest, comprising all vegetative organs (shoots, leaves, trunk, canes, roots) plus fruits, ranged from 326 g per plant (3176 WD) to 434 g per plant (G5 WW-C) across genotypes and treatments (Supplementary Table S8). Two-way ANOVA revealed a highly significant effect of water treatment on total plant biomass ($p < 0.001$), but no significant genotype effect ($p = 0.095$) or genotype × treatment interaction ($p = 0.232$). Water deficit reduced mean total plant biomass by approximately 12% compared to well-watered conditions (340 ± 25 g vs 387 ± 39 g per plant across non-carbon-normalized treatments), primarily through reductions in vegetative growth (Figure 42, Section 3.2.4.2) rather than fruit biomass (Section 3.2.3.1).

The proportion of total plant biomass allocated to fruits showed significant treatment ($p < 0.001$) and genotype effects ($p = 0.041$), with no interaction ($p = 0.738$). Fruit allocation ranged from 26.6% (G14 WW) to 42.7% (G5 WD-C) of total plant dry biomass

(Supplementary Table S8). Water deficit significantly increased the proportion of biomass allocated to reproductive organs compared to well-watered conditions: mean fruit allocation under water deficit was 35.5 ± 6.5% compared to 30.4 ± 6.7% under well-watered conditions (excluding carbon-normalized treatments), representing a 17% relative increase in reproductive allocation. This increased proportional fruit allocation under water deficit occurred despite absolute reductions in both fruit and vegetative biomass, with vegetative biomass showing proportionally greater reductions than fruit biomass.

Carbon-normalized LSB genotypes (G5-C and G14-C), which received 50% more berries per plant to equalize carbon demand with non-LSB genotypes, showed the highest fruit allocation percentages across all treatments. G5 WD-C allocated 42.7 ± 7.6% to fruits and G14 WD-C allocated 40.6 ± 3.4% to fruits, both under severe water deficit conditions (FTSW 0.18-0.25). These elevated fruit allocations were achieved while maintaining vegetative biomass of 217-221 g per plant under water deficit conditions. The carbon-normalized treatments under well-watered conditions (G5 WW-C: 39.3 ± 9.3%) also showed elevated fruit allocation compared to standard treatments.

Genotypic differences in fruit allocation were primarily driven by variation in vegetative biomass rather than fruit biomass, as fruit carbon accumulation (varC, Section 3.2.5.1.1) showed no significant genotypic differences. Genotype G5 showed significantly higher root:shoot ratios (0.371-0.464) compared to genotypes 3159 and 3176 (0.197-0.298), with greater proportional allocation to root systems (Supplementary Table S8). Water deficit significantly increased root:shoot ratios across genotypes ($p = 0.004$), from a mean of 0.283 ± 0.075 under well-watered conditions to 0.353 ± 0.098 under water deficit, showing enhanced belowground allocation under water limitation.

3.2.5.2 Whole-Plant Water Use Efficiency

3.2.5.2.1 Observed Whole-Plant Water Use Efficiency (WUEpl)

Whole-plant water use efficiency, calculated as the ratio of carbon accumulated in fruits (varC) to total plant transpiration from veraison to harvest (WUEpl = varC/TR), varied significantly among treatments but not among genotypes (Figure 45). Water deficit substantially increased WUEpl across all genotypes, with plants under water-limited conditions (WD and WD-C treatments) achieving 2.86-4.59 g C L^{-1} compared to 1.44-2.10 g C L^{-1} in well-watered plants (WW and WW-C treatments), representing an average increase of 115-170% (Treatment $p < 0.001$, Genotype $p = 0.079$, Genotype × Treatment $p = 0.109$).

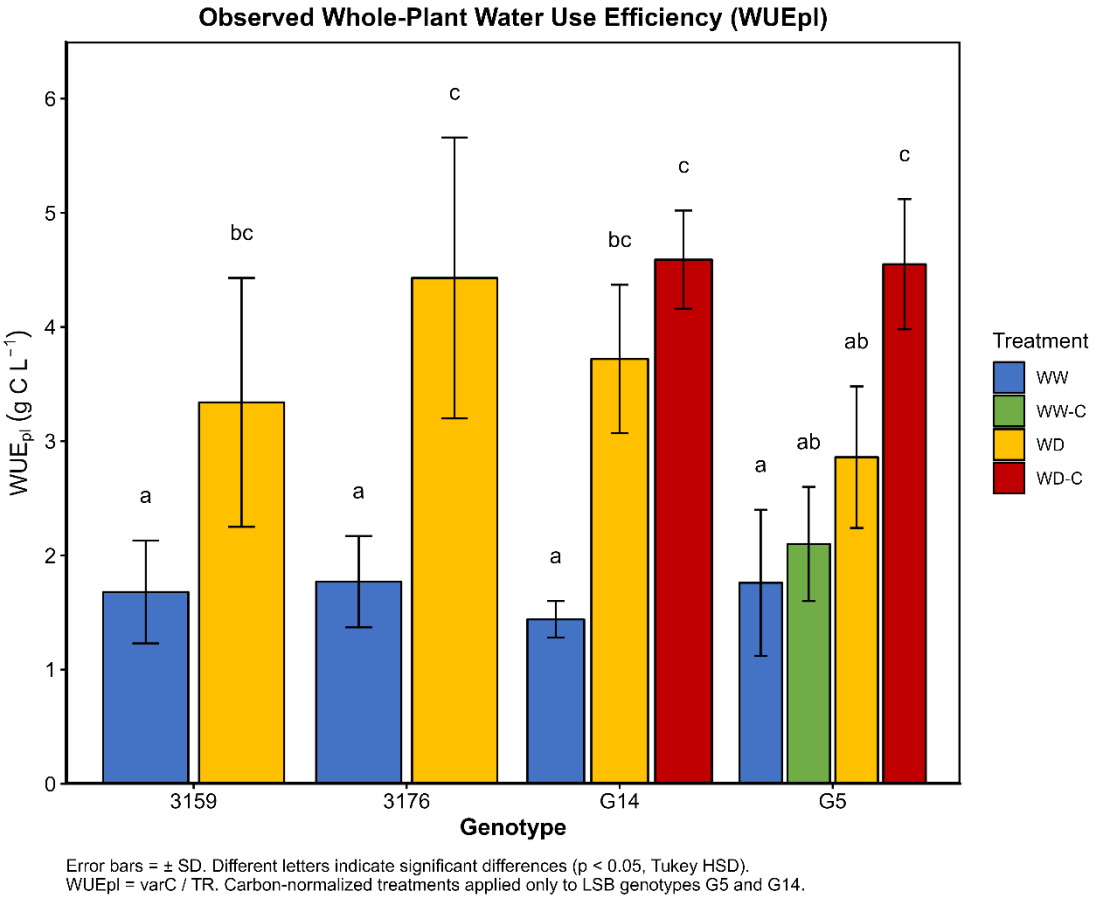

Figure 45. Observed whole-plant water use efficiency from veraison to harvest. Observed whole-plant water use efficiency (WUEpl) calculated as the ratio of carbon accumulated in fruits (varC) to total plant transpiration from veraison to harvest (TR). Values represent mean ± SD for each genotype × treatment combination. WUEpl = varC / TR, where varC includes carbon in sugars (glucose + fructose), tartaric acid, and malic acid. Bars represent different genotypes (3159 = orange, 3176 = blue, G14 = green, G5 = yellow) within each water treatment. Error bars indicate ± 1 SD. Different letters above bars indicate significant differences among all genotype × treatment combinations ($p < 0.05$, Tukey HSD). ANOVA results: Treatment $p < 0.001$ (***), Genotype $p = 0.079$ (ns), Genotype × Treatment $p = 0.109$ (ns). WW = well-watered, WD = water deficit, WW-C and WD-C = carbon-normalized treatments with +50% berry number for LSB genotypes G5 and G14. n = 2-6 plants per treatment. Plant 2104 (G5 WW-C), excluded from analysis, resulting in n = 55 plants total.

Among water deficit treatments, carbon-normalized LSB genotypes exhibited the highest observed WUEpl values. G14 WD-C achieved 4.59 ± 0.43 g C L^{-1} (mean ± SD), followed closely by G5 WD-C (4.55 ± 0.57 g C L^{-1}) and 3176 WD (4.43 ± 1.23 g C L^{-1}), all significantly higher than well-watered treatments (Figure 45). Non-LSB genotypes under standard water deficit showed intermediate values, with G14 WD and 3159 WD averaging 3.72 ± 0.65 and 3.34 ± 1.09 g C L^{-1} respectively, while G5 WD reached 2.86 ± 0.62 g C L^{-1}. Well-watered plants displayed the lowest WUEpl values, ranging from 1.44 ± 0.16 g C L^{-1} in G14 WW to 1.77 ± 0.40 g C L^{-1} in 3176 WW, with no significant differences among well-watered genotypes.

Carbon-normalized LSB genotypes under water deficit (G5 WD-C and G14 WD-C) showed elevated WUEpl values while accumulating substantial fruit carbon despite restricted water availability. However, interpretation of these absolute WUEpl values is complicated by inherent differences in plant architecture among genotypes, particularly variations in vegetative vigor (total leaf area) and fruit load (berry number and weight), which together determine the fruit-to-leaf ratio. These structural differences can substantially influence WUEpl independently of physiological water use efficiency, as plants with naturally low leaf area or high fruit load will exhibit elevated WUEpl values even if their underlying physiological efficiency is similar to other genotypes.

3.2.5.2.2 Normalized Whole-Plant Water Use Efficiency (WUEpl_n)

To account for genotypic variations in plant architecture and enable fair physiological comparisons, WUEpl was normalized by the fruit-to-leaf ratio, effectively standardizing all plants to a theoretical configuration of 1 kg fresh fruit per 1 m² leaf area (WUEpl_n = WUEpl × [Fruit fresh weight / Leaf area]). This normalization revealed more nuanced patterns in water use efficiency that were partially obscured in the observed WUEpl values (Figure 46).

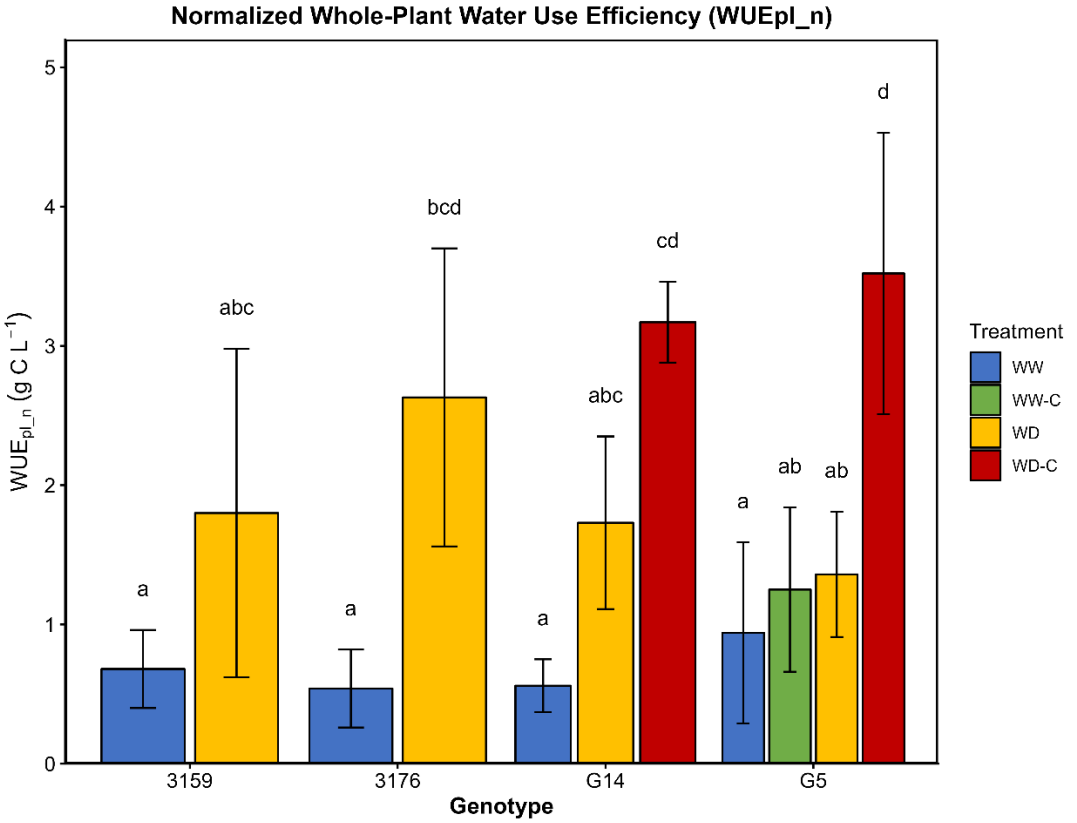

Error bars = ± SD. Different letters indicate significant differences ($p < 0.05$, Tukey HSD).
WUEpl_n = WUEpl × (Fruit/Leaf ratio). Normalized to 1 kg fruit per 1 m² leaf area.

Figure 46. Normalized whole-plant water use efficiency accounting for plant architecture. Normalized whole-plant water use efficiency (WUEpl_n) calculated as WUEpl × (Fresh fruit weight / Leaf area), standardizing all plants to 1 kg fruit per 1 m² leaf area. This normalization removes the confounding effect of genotypic differences in plant architecture (vegetative vigor and crop load) on water use efficiency, enabling comparison of physiological efficiency independent of plant size. Values represent mean ± SD. Bars represent different genotypes (3159 = orange, 3176 = blue, G14 = green, G5 = yellow) within each water treatment. Error bars indicate ± 1 SD. Different letters above bars indicate significant differences among all genotype × treatment combinations ($p < 0.05$, Tukey HSD). ANOVA results: Treatment $p < 0.001$ (***), Genotype $p = 0.464$ (ns), Genotype × Treatment $p = 0.105$ (ns). WW = well-watered, WD = water deficit, WW-C and WD-C = carbon-normalized treatments for LSB genotypes. Carbon-normalized LSB genotypes under water deficit (G5 WD-C, G14 WD-C) achieved the highest WUEpl_n values, showing differences in physiological water use efficiency when accounting for plant architecture. n = 55 plants.

After normalization, water deficit continued to exert a dominant effect, significantly increasing WUEpl_n across all genotypes (ANOVA: Treatment $p < 0.001$). The genotype × treatment interaction was not significant ($p = 0.105$), though carbon-normalized LSB genotypes under water deficit achieved the highest normalized water use efficiency, with G5 WD-C reaching 3.52 ± 1.01 g C L^{-1} and G14 WD-C attaining 3.17 ± 0.29 g C L^{-1} (Figure 47). These values significantly exceeded those of well-watered plants, which ranged from 0.54 ± 0.28 g C L^{-1} (3176 WW) to 1.25 ± 0.59 g C L^{-1} (G5 WW-C).

Non-LSB genotypes under water deficit showed intermediate normalized efficiency values. 3176 WD achieved 2.63 ± 1.07 g C L^{-1}, while 3159 WD and standard LSB treatments (G14 WD, G5 WD) ranged from 1.36 to 1.80 g C L^{-1}. After normalization, standard (non-carbon- normalized) LSB genotypes under water deficit showed WUEpl_n values comparable to or slightly lower than non-LSB genotypes under the same water treatment.

The normalization procedure substantially altered the relative ranking of genotypes. 3176 WD exhibited high observed WUEpl (4.43 g C L^{-1}, Figure 45) but moderate WUEpl_n (2.63 g C L^{-1}, Figure 46), with a fruit-to-leaf ratio of 0.61 kg m^{-2}. Conversely, G14 WW showed relatively low observed WUEpl (1.44 g C L^{-1}) but maintained a normalized value of 0.56 g C L^{-1} despite low fruit load.

3.2.5.2.3 Integration of Plant Architecture and Carbon Demand

Fruit-to-leaf ratios at harvest varied considerably among genotype × treatment combinations, ranging from 0.28 kg m^{-2} (3176 WW) to 0.77 kg m^{-2} (G5 WD-C) (Table 9). Water deficit generally increased fruit-to-leaf ratios by 15-75% compared to well-watered conditions within the same genotype, with proportionally greater reduction in vegetative growth (leaf area) than reproductive development (fruit mass) under water limitation. As described in Section 3.2.2.2, carbon-normalized treatments in LSB genotypes showed elevated fruit-to-leaf ratios exceeding those of non-LSB genotypes

through substantial increases in berry number combined with maintained fruit carbon accumulation despite water limitation.

3.2.5.2.4 Carbon Isotope Composition (δ13C)

Carbon isotope discrimination (δ13C) in leaf tissue sampled at harvest ranged from -30.1‰ to -23.7‰ across all genotype × treatment combinations (Figure 47), with highly significant effects of water treatment (ANOVA, $p < 0.001$) but no significant effects of genotype ($p = 0.374$) or genotype × treatment interaction ($p = 0.215$). Well-watered plants exhibited more negative δ13C values, ranging from -29.8‰ (G5 WW-C) to -27.3‰ (3159 WW). Water deficit plants showed consistently less negative δ13C values, ranging from -27.8‰ (G5 WD) to -24.2‰ (G14 WD and 3176 WD).

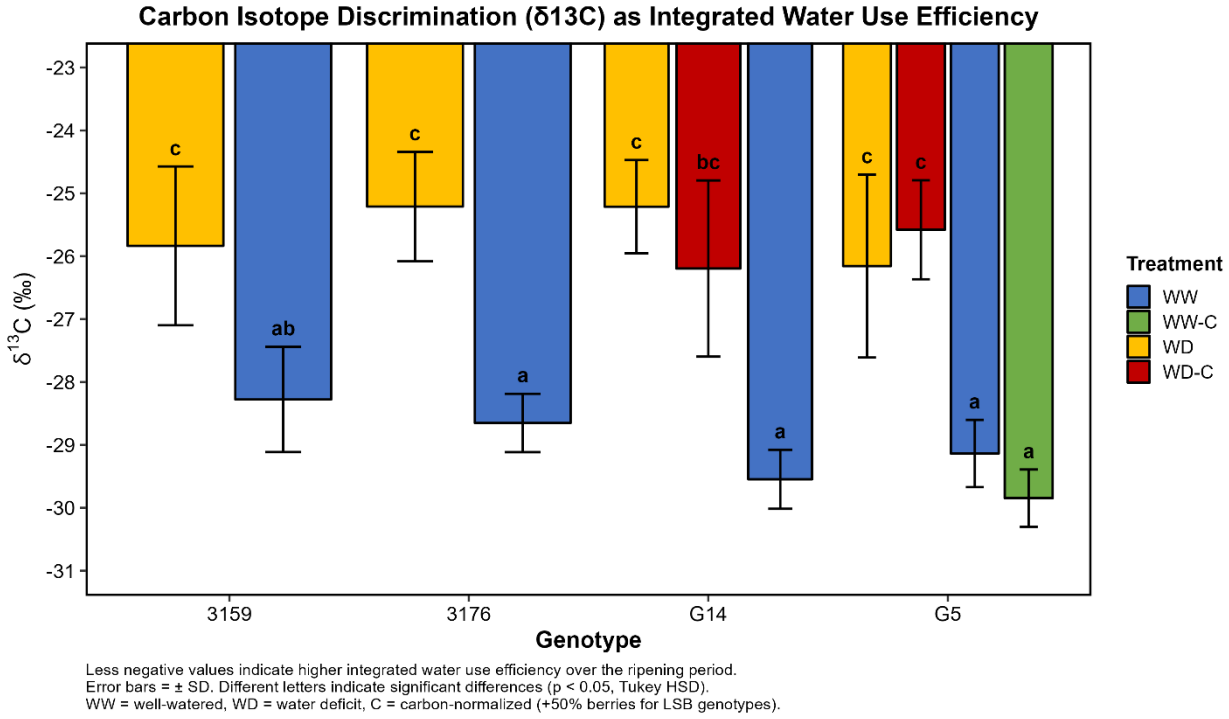

Figure 47. Carbon isotope discrimination (δ13C) in leaf tissue at harvest. Carbon isotope composition (δ13C) measured in fully expanded leaves sampled at harvest for all genotypes and treatments. Bars represent mean ± SD. Different letters indicate significant differences among genotype × treatment combinations ($p < 0.05$, Tukey HSD). ANOVA results: Treatment $p < 0.001$ (***), Genotype $p = 0.374$ (ns), Genotype × Treatment $p = 0.215$ (ns). WW = well-watered (FTSW ≥0.6), WD = water deficit (FTSW ≈0.25), WW-C and WD-C = carbon-normalized treatments with +50% berries for LSB genotypes G5 and G14. n = 5-6 plants per treatment.

Water deficit treatments exhibited δ13C values approximately 2.5-3.5% less negative than their well-watered counterparts within each genotype (Figure 47). Carbon-normalized LSB genotypes under well-watered conditions showed δ13C values of -29.8‰ (G5 WW-C), while carbon-normalized treatments under water deficit showed values of -25.6‰ (G5 WD-C) and -26.2‰ (G14 WD-C), comparable to standard water

deficit treatments. The lack of significant genotype effects on δ13C (p = 0.374) paralleled the lack of genotypic differentiation in instantaneous leaf-level water use efficiency (Section 3.2.5.3.3, WUE and iWUE: genotype p > 0.05).

Less negative δ13C values showed a positive correlation with higher normalized whole-plant water use efficiency (WUEpl_n) across all plants (Pearson r = 0.635, p < 0.001, R^2 = 0.40; Figure 48). Water deficit plants (less negative δ13C, higher WUEpl_n) clustered in the upper right quadrant, while well-watered plants (more negative δ13C, lower WUEpl_n) clustered in the lower left quadrant. Within-treatment correlations showed: well-watered plants r = 0.232 (p = 0.37), water deficit plants r = 0.423 (p = 0.091), and carbon-normalized water deficit LSB genotypes r = 0.632 (p = 0.18).

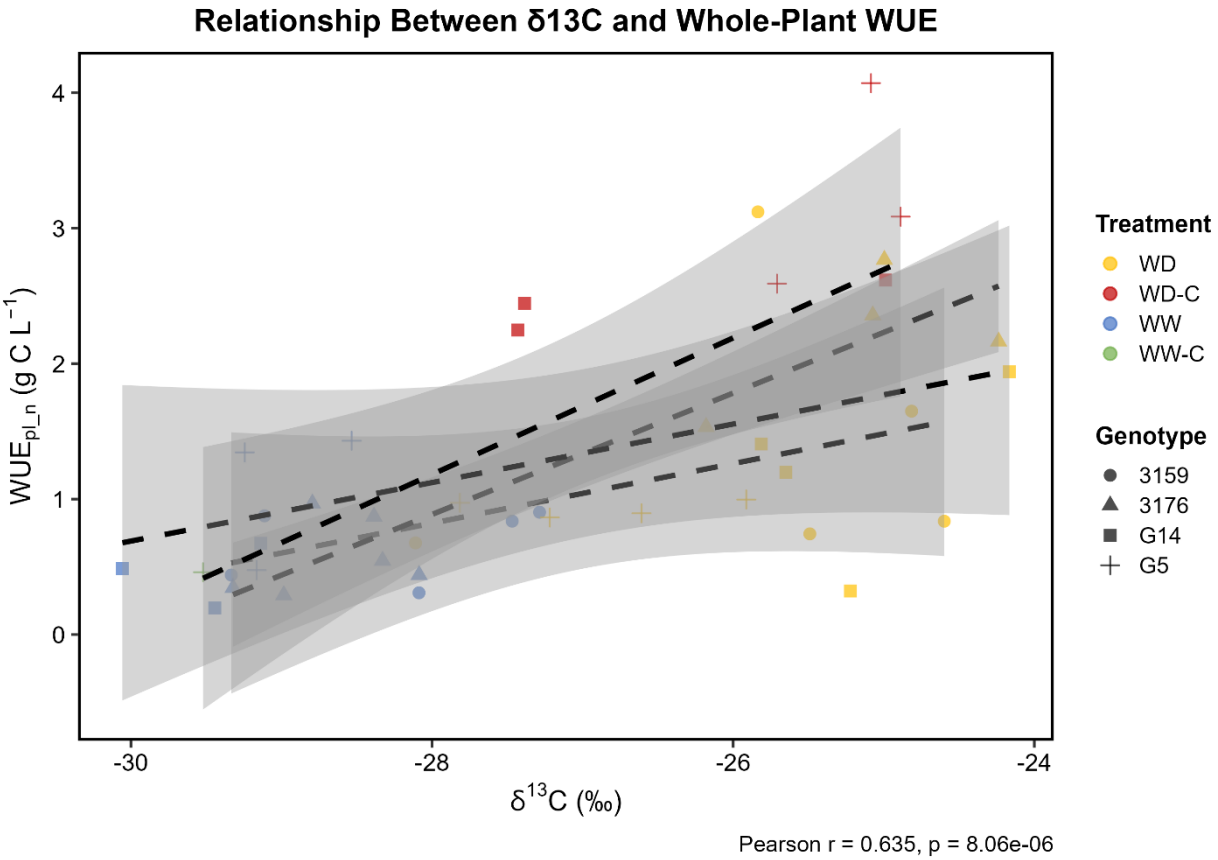

Figure 48. Relationship between δ13C and normalized whole-plant water use efficiency. Correlation between carbon isotope discrimination (δ13C) and normalized whole-plant water use efficiency (WUEpl_n). Each point represents one plant, colored by water treatment (WD = red/orange, WW = blue/green) and shaped by genotype. The dashed line shows linear regression across all treatments with 95% confidence interval (shaded area). Pearson r = 0.635, p = 8.06e-06, R^2 = 0.40, n = 41 plants. Treatment groups showed distinct clustering, with well-watered plants in the lower left quadrant (more negative δ13C, lower WUEpl_n) and water deficit plants in the upper right (less negative δ13C, higher WUEpl_n).

3.2.5.3 Leaf-Level Chlorophyll Content, Gas Exchange and Water Use Efficiency

3.2.5.3.1 Leaf Chlorophyll Content (SPAD)

Leaf chlorophyll content, estimated using SPAD readings, remained stable throughout the experimental period across all genotypes and treatments (Figure 49). SPAD values were monitored weekly from veraison (DOY 147) through harvest (DOY 181-196, depending on genotype) to assess potential stress-induced chlorophyll degradation or nitrogen remobilization patterns.

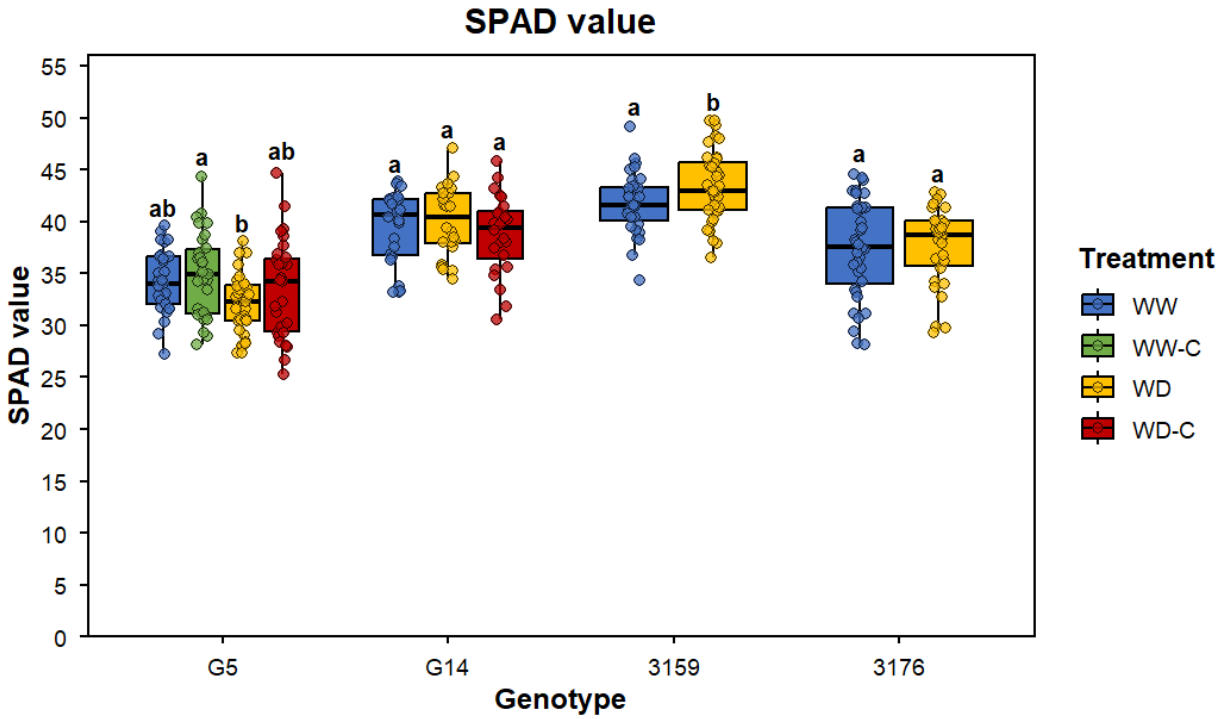

Boxes show the interquartile range, the line is the median, and whiskers extend to 1.5 × IQR.
Different letters indicate significant differences ($p < 0.05$, Tukey HSD).

Figure 49. Leaf chlorophyll content (SPAD) throughout the experimental period by genotype and treatment. Weekly SPAD readings measured on fully expanded leaves for genotypes G5, G14, 3159, and 3176 under different water and carbon treatments from veraison through physiological ripeness. Each panel shows one genotype with boxplots displaying median (horizontal line), interquartile range (box), range (whiskers), and outliers (points) for each measurement date (Day of Year, DOY). Treatments: WW-W = well-watered standard crop load (blue), WW-C = well-watered carbon-normalized (green), WD-W = water deficit standard crop load (yellow), WD-C = water deficit carbon-normalized (red). Different letters within each timepoint indicate significant differences ($p < 0.05$, Tukey HSD). Statistical results shown in each panel: DOY = day-of-year (time) effect, T = treatment effect, DOY×T = interaction effect. *, **, *** indicate significance at $p < 0.05$, 0.01, and 0.001, respectively; ns = not significant. Carbon-normalized treatments (WW-C, WD-C) with +50% berry number applied only to LSB genotypes G5 and G14; genotypes 3159 and 3176 have only two treatments (WW-W and WD-W). Measurements: n = 4-6 plants per treatment per timepoint..

SPAD readings ranged from approximately 30 units in genotype G5 to 48 units in genotype 3159, showing substantial genotypic variation in leaf chlorophyll content. Water deficit treatment had no significant effect on SPAD readings in any genotype (G5: $p = 0.515$, G14: $p = 0.352$, 3159: $p = 0.621$, 3176: $p = 0.168$). Genotype 3159 exhibited the highest chlorophyll content (SPAD 38-48), while G5 showed the lowest values (SPAD 30-40), with G14 and 3176 displaying intermediate levels (SPAD 35-45). SPAD values remained stable throughout the 34-49 day treatment period.

Day-of-year effects on SPAD readings were variable among genotypes. Genotypes G5 and G14 showed significant temporal changes ($p < 0.05$), though the magnitude remained small (typically < 5 SPAD units) and did not indicate progressive chlorophyll loss. Genotypes 3159 and 3176 displayed stable SPAD values throughout the measurement period ($p > 0.05$), consistent with maintained leaf function during fruit ripening. The day × treatment interactions were not significant for any genotype (all $p > 0.05$), with temporal patterns of chlorophyll content independent of water availability.

3.2.5.3.2 Gas Exchange Parameters During Ripening

Leaf gas exchange parameters were measured at three timepoints during berry ripening (DOY 154, 169, and 181) under dark-adapted conditions following a 12-hour dark adaptation period. Statistical analysis revealed no significant temporal effects (DOY $p > 0.05$ for all parameters), indicating that gas exchange parameters remained stable throughout the ripening period. Consequently, measurements were pooled across all three timepoints for analysis of treatment and genotype effects.

Dark respiration rates ranged from -0.15 to -0.95 µmol CO_2 m^{-2} s^{-1} across all genotype × treatment combinations (Figure 50). Statistical analysis revealed significant treatment effects for genotype G5 ($p < 0.001$) but not for other genotypes (G14: $p = 0.091$, 3159: $p = 0.168$, 3176: $p = 0.312$), indicating that water deficit effects on dark respiration were most pronounced in LSB genotype G5.

Under well-watered conditions, dark respiration rates were similar across genotypes, ranging from -0.50 to -0.65 µmol CO_2 m^{-2} s^{-1}. Water deficit significantly reduced dark respiration in G5 and G14, with WD treatments showing rates of approximately -0.45 to -0.50 µmol CO_2 m^{-2} s^{-1} compared to WW conditions. Carbon-normalized treatments in LSB genotypes showed intermediate respiration rates, with G5 WD-C exhibiting significantly lower respiration (-0.45 ± 0.09 µmol CO_2 m^{-2} s^{-1}) compared to G5 WW ($p < 0.001$). Genotypes 3159 and 3176 maintained stable dark respiration rates across water treatments, with no significant differences between WW and WD conditions.

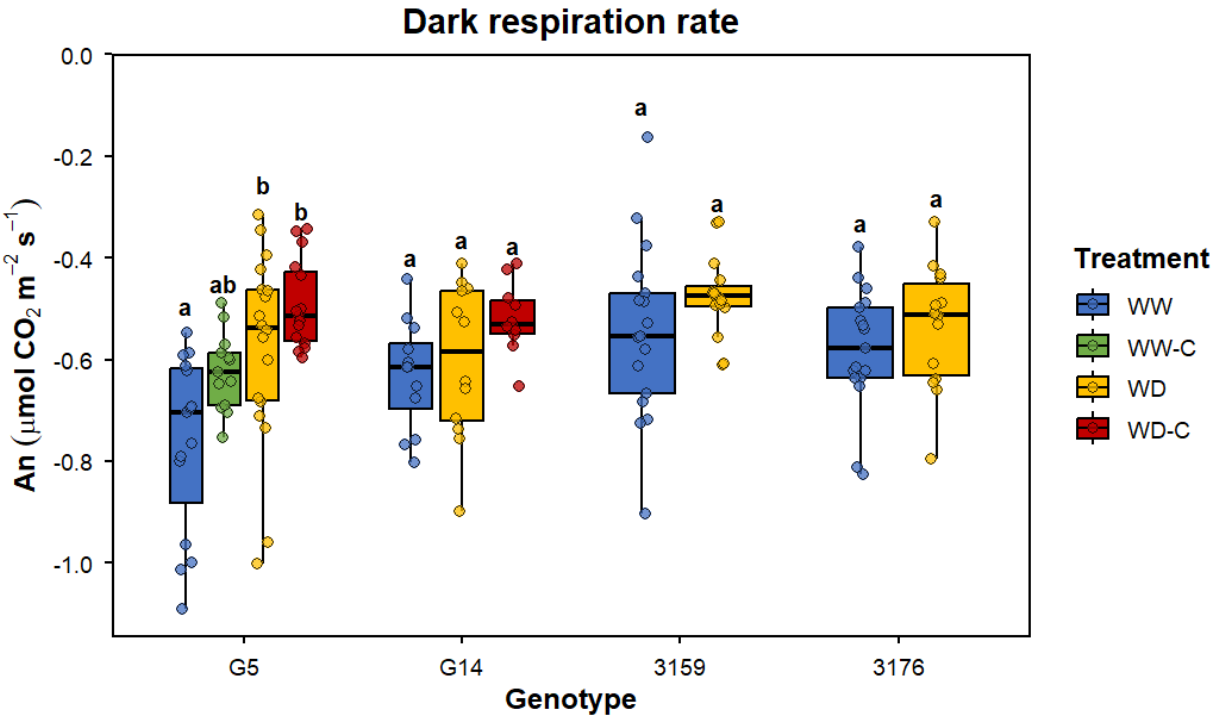

Figure 50. Dark respiration rate by genotype and treatment. Dark respiration measured after 12-hour dark adaptation period. Measurements pooled across three sampling dates (DOY 154, 169, 181). Boxes show the interquartile range, the line is the median, and whiskers extend to 1.5 × IQR. Individual data points overlaid. Different letters indicate significant differences ($p < 0.05$, Tukey HSD). WW = well-watered (blue), WW-C = well-watered carbon-normalized (green), WD = water deficit (yellow), WD-C = water deficit carbon-normalized (red). Carbon-normalized treatments applied only to LSB genotypes G5 and G14. n = 30-36 measurements per genotype × treatment (3 timepoints × 10-12 plants).

Stomatal conductance under dark-adapted conditions ranged from 0.001 to 0.070 mol H_2O m^{-2} s^{-1} across all treatments (Figure 51). Treatment effects were highly significant for genotype G5 ($p < 0.001$) but not significant for other genotypes (G14: $p = 0.202$, 3159: $p = 0.091$, 3176: $p = 0.102$). Genotype G5 showed the highest dark stomatal conductance under both well-watered conditions (0.028 ± 0.009 mol H_2O m^{-2} s^{-1}) and carbon-normalized well-watered treatment (0.037 ± 0.016 mol H_2O m^{-2} s^{-1}).

Water deficit substantially reduced dark stomatal conductance in G5, with WD treatments showing 52% lower gs compared to WW (0.0135 ± 0.006 vs 0.028 ± 0.009 mol H_2O m^{-2} s^{-1}, $p = 0.001$). The carbon-normalized treatment under well-watered conditions (G5 WW-C) exhibited elevated gs (0.037 ± 0.016 mol H_2O m^{-2} s^{-1}), significantly higher than WD treatments ($p < 0.001$). Other genotypes (G14, 3159, 3176) maintained lower dark stomatal conductance values (0.010-0.025 mol H_2O m^{-2} s^{-1}) with no significant treatment effects.

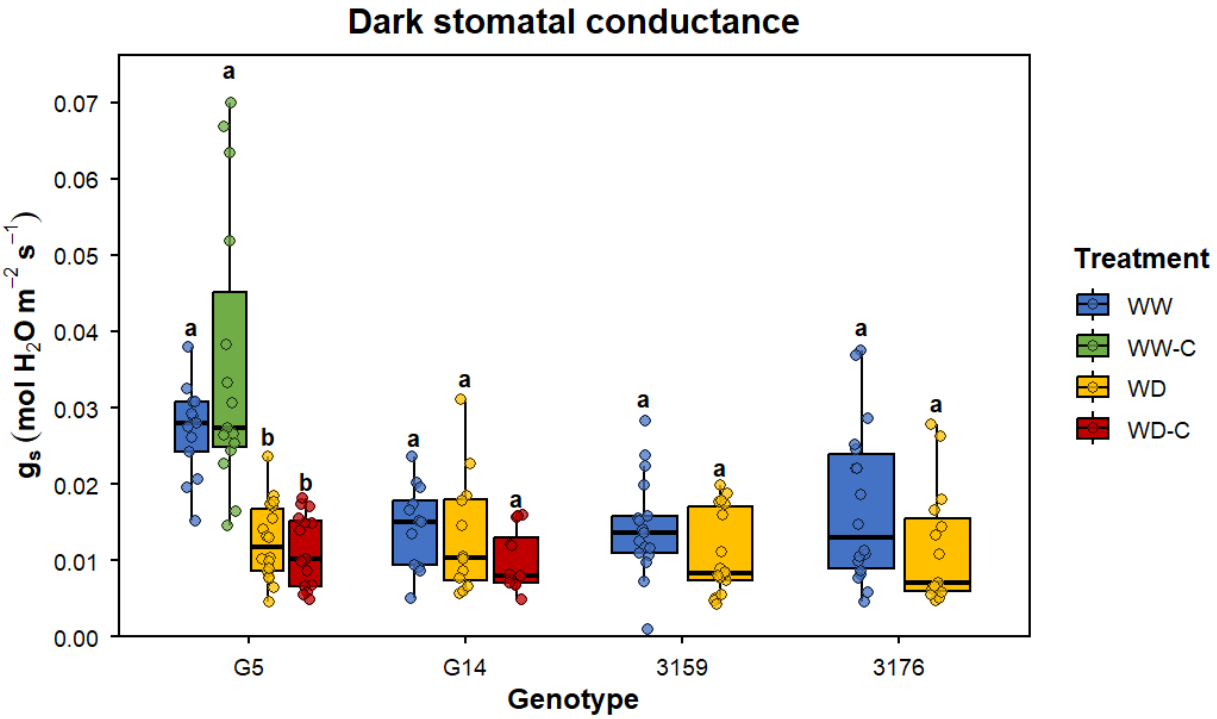

Figure 51. Dark stomatal conductance by genotype and treatment. Stomatal conductance measured under dark-adapted conditions. Format as Figure 50. Carbon-normalized treatments applied only to LSB genotypes G5 and G14.

Dark transpiration rates followed patterns similar to dark stomatal conductance, ranging from 0.0001 to 0.0012 mmol H_2O m^{-2} s^{-1} across treatments (Figure 52). Significant treatment effects were observed for genotypes G5 ($p < 0.001$) and 3159 ($p = 0.049$), but not for G14 ($p = 0.206$) or 3176 ($p = 0.101$). Genotype G5 under well-watered conditions showed the highest dark transpiration rates (0.00048 ± 0.00018 mmol H_2O m^{-2} s^{-1}), with the carbon-normalized treatment (G5 WW-C) reaching even higher values (0.00065 ± 0.00029 mmol H_2O m^{-2} s^{-1}).

Water deficit reduced dark transpiration by approximately 54% in G5 (0.000219 ± 0.000088 mmol H_2O m^{-2} s^{-1} in WD vs 0.00048 ± 0.00018 mmol H_2O m^{-2} s^{-1} in WW, $p = 0.001$). Carbon-normalized treatments under water deficit (G5 WD-C, G14 WD-C) showed transpiration rates comparable to standard water deficit treatments, indicating that the increased berry load did not significantly alter dark transpiration under water-limited conditions. Genotype 3159 also showed a significant reduction in dark transpiration under water deficit ($p = 0.049$), though the absolute difference was smaller than observed in G5.

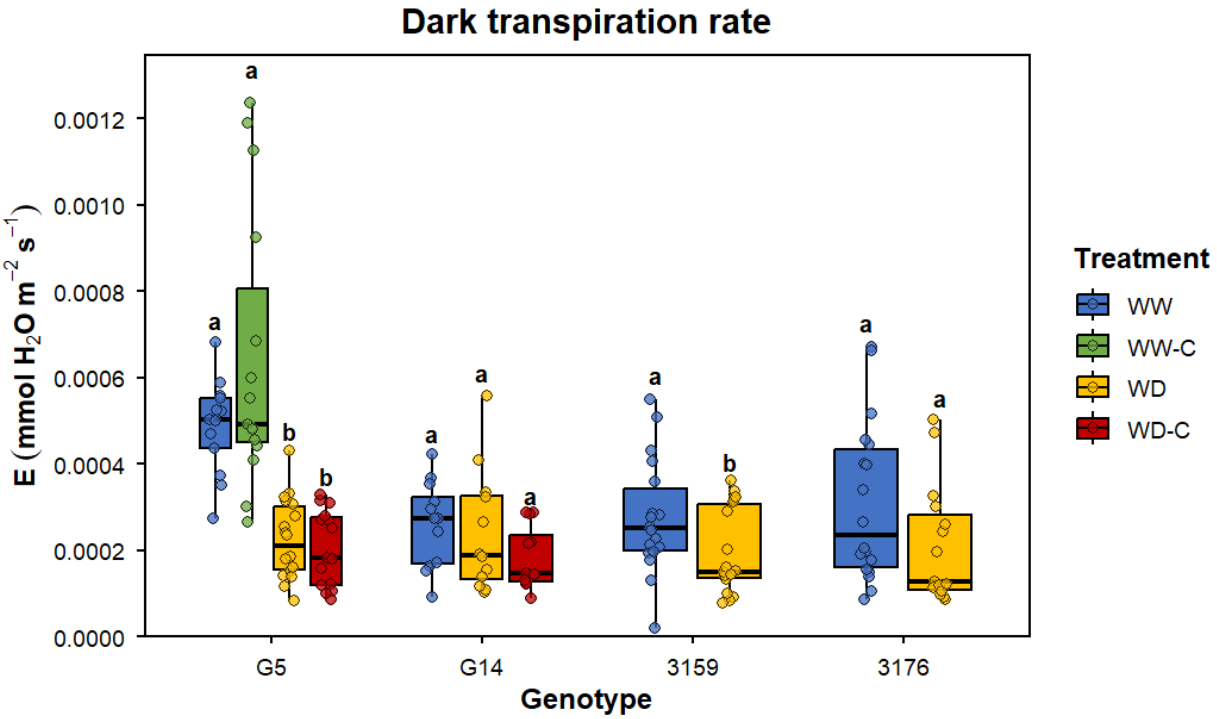

Figure 52. Dark transpiration rate by genotype and treatment. Transpiration measured under dark-adapted conditions. Format as Figure 50. Carbon-normalized treatments applied only to LSB genotypes G5 and G14.

The dark-adapted measurements revealed the base physiological activity and stomatal regulation in the absence of active photosynthesis. Water deficit primarily affected LSB genotype G5, which showed significant reductions in all three dark-adapted parameters. The elevated dark stomatal conductance and transpiration in G5 WW-C (carbon-normalized well-watered treatment) suggests increased leaf activity in response to enhanced sink demand from the additional berry load, even in the absence of light-driven photosynthesis.

Gas exchange measurements under saturating light conditions (PAR 1500 µmol photons m^{-2} s^{-1}) showed similar treatment patterns to those observed under dark adaptation. Water deficit reduced net photosynthesis by 43-57% across genotypes under saturating light, with proportionally greater reductions in stomatal conductance (72-81%) and transpiration (72-79%) (Supplementary Table S9). Relative changes under dark-adapted conditions showed comparable patterns, with water deficit reducing dark respiration to 65-96% of well-watered controls while gs and E were reduced to 42-69% (Supplementary Table S10). These patterns were consistent across all genotypes regardless of LSB trait, indicating that treatment effects on gas exchange were similar under both light and dark conditions.

3.2.5.3.3 Leaf-Level Water Use Efficiency Under Water Deficit

Water deficit significantly increased leaf-level water use efficiency across all genotypes (Figure 53). Instantaneous water use efficiency (WUE = An/E) under well-watered conditions ranged from 3000-4500 µmol CO_2 $mmol^{-1}$ H_2O across genotypes, increasing to 7000-9500 µmol CO_2 $mmol^{-1}$ H_2O under water deficit conditions, representing a 2.0-2.6 fold increase. Treatment effects were highly significant for all genotypes (G5: $p < 0.001$, G14: $p < 0.001$, 3159: $p < 0.001$, 3176: $p < 0.001$), with no significant genotype effect ($p > 0.05$), indicating similar water use efficiency responses across LSB and non-LSB varieties.

Similarly, intrinsic water use efficiency (iWUE = An/gs) increased substantially under water deficit. Well-watered plants showed iWUE values of 50-80 µmol CO_2 mol^{-1} H_2O, which increased to 120-160 µmol CO_2 mol^{-1} H_2O under deficit conditions, representing increases of 69-93 µmol CO_2 mol^{-1} H_2O depending on genotype. Treatment effects were highly significant for all genotypes (all $p < 0.001$), reflecting the proportionally greater stomatal closure relative to photosynthetic rate decline under water deficit.

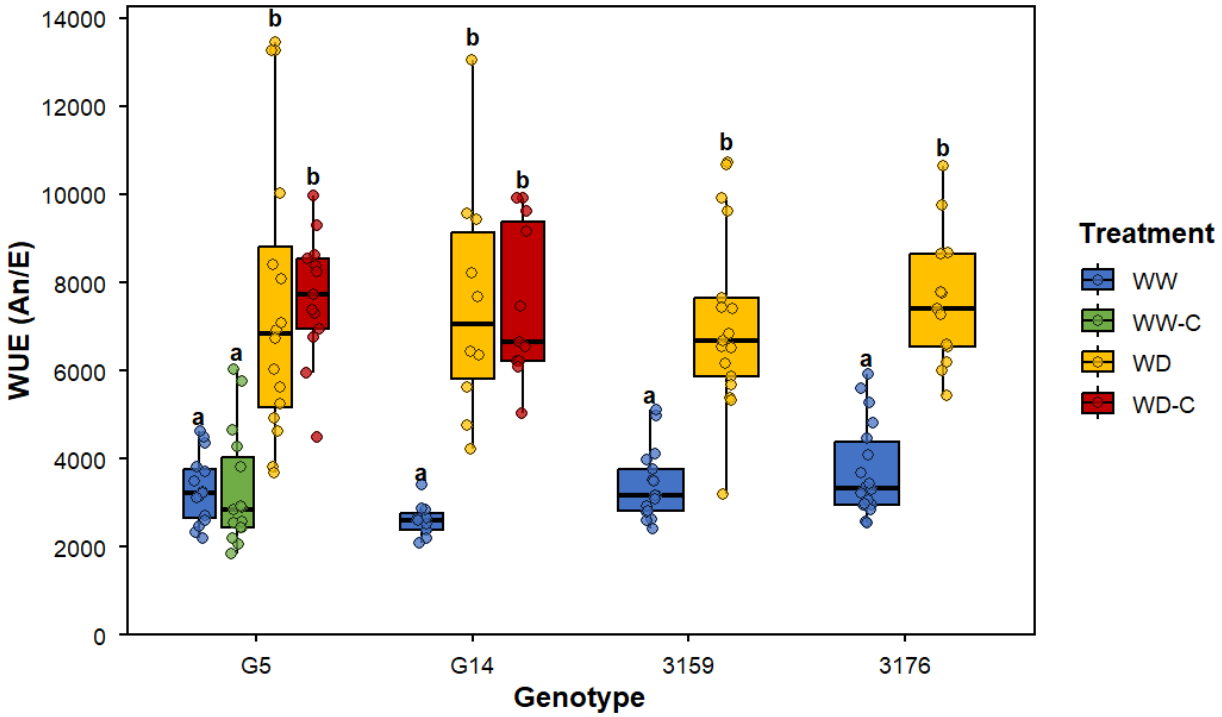

Boxes show the interquartile range, the line is the median, and whiskers extend to 1.5 × IQR. Different letters indicate significant differences ($p < 0.05$, Tukey HSD).

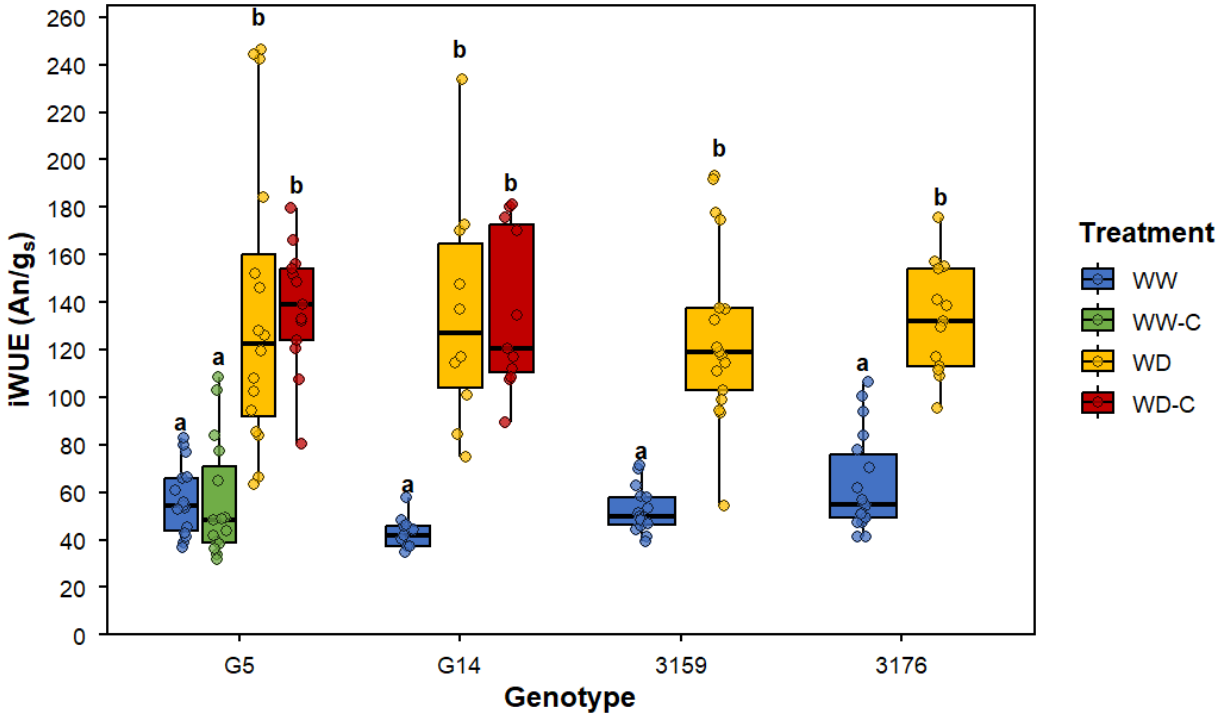

Boxes show the interquartile range, the line is the median, and whiskers extend to 1.5 × IQR.
Different letters indicate significant differences ($p < 0.05$, Tukey HSD).

Figure 53. Leaf-level water use efficiency across genotypes. Instantaneous water use efficiency (WUE = An/E, top panel) and intrinsic water use efficiency (iWUE = An/gs, bottom panel) measured under saturating light conditions (PAR 1500 µmol photons m^{-2} s^{-1}, CO_2 400 ppm) for all genotypes. Values averaged across three measurement dates (DOY 154, 169, 181). Boxes represent interquartile range, horizontal lines show medians, and whiskers extend to 1.5× IQR. Different letters indicate significant differences among treatments within each genotype ($p < 0.05$, Tukey HSD). Statistical results: T = treatment effect, G = genotype effect, T×G = interaction effect. Treatment effect highly significant ($p < 0.001$ for all genotypes), genotype effect not significant ($p > 0.05$).

No significant genotype effects were detected for either WUE or iWUE ($p > 0.05$), indicating that LSB varieties and conventional genotypes exhibited similar water use efficiency at the leaf level under both well-watered and water-limited conditions. This contrasts with whole-plant water use efficiency results (Section 3.2.5.2), where LSB genotypes showed superior normalized WUEpl_n values, particularly under carbon-normalized water deficit conditions (G5 WD-C, G14 WD-C).

Carbon-normalized LSB plants (G5 WW-C, G14 WD-C) showed WUE and iWUE values comparable to their non-normalized counterparts within the same water treatment, despite exhibiting higher gs and E in some cases. Treatment effects remained dominant, with water deficit consistently increasing both WUE and iWUE across all genotypes and crop load configurations, reflecting the proportionally greater reduction in transpiration compared to photosynthesis under water-limited conditions.

4 Discussion

This study investigated the hypothesis that at equivalent fruit water budget, the lower berry sugar demand characteristic of LSB genotypes favors a more comfortable carbon status of the vine under water deficit, which represents the main limiting factor of carbon assimilation during summer in Mediterranean viticulture. Two complementary experiments (*Experiment 1 (Short-Term Stress, STS & Experiment 2 (Long-Term Stress, LTS)* were designed to test this hypothesis across different temporal scales and developmental stages.

The following discussion is organized around three interconnected themes that address different aspects of the central hypothesis: *(1) Berry Development and the LSB Phenotype* establishes how the trait manifests under short water deficit at the fruit level; *(2) Carbon Gain, Allocation, and Source-Sink Relationships* examines whether reduced fruit sugar demand translates to improved whole-plant carbon balance, directly testing the core hypothesis; and (3) Water Requirements and Water Use Efficiency evaluates whether any carbon status advantages are linked to water-saving properties or altered water use patterns. Together, these sections integrate findings across scales (berry to whole-plant) and timeframes (short-term to seasonal) to evaluate the adaptive potential of the LSB trait under drought conditions.

4.1 Berry Development and the LSB Phenotype

The short-term water deficit experiments (STS-G and STS-R) directly addressed whether individual berries of LSB and non-LSB genotypes display similar growth and primary responses to acute water deficit and recovery applied at contrasting developmental stages. These experiments revealed that developmental stage, rather than genotype per se, emerged as the dominant factor governing berry hydraulic sensitivity and growth dynamics under water stress. The findings fundamentally reshape our understanding of how berry-level responses relate to whole-plant drought adaptation strategies.

4.1.1 Developmental Stage Dependency of Berry Hydraulic Sensitivity

Berry responses to acute water deficit exhibited profound developmental stage dependency that overshadowed genotypic differences. During the green stage (STS-G), berries displayed high hydraulic sensitivity to declining plant water status, with strong positive correlations between berry relative growth rate and predawn water potential across all genotypes ($r=0.80$-0.88, $p < 0.001$; Section 3.1.2.4, Table 6). This tight coupling indicates that green-stage berry expansion responds rapidly to short-term fluctuations in whole-plant water availability, consistent with cell expansion being a turgor-driven process highly sensitive to water potential gradients (Castellarin et al., 2011). During the ripening stage (STS-R), while correlations between berry growth rate and water status

remained statistically significant ($r = 0.70$-0.74, $p < 0.001$; Section 3.1.2.4, Table 6), the sensitivity of berry growth to water potential changes decreased dramatically. This developmental transition reflects the shift from cell expansion dominated growth to accumulation-dominated ripening, where berry growth rate becomes increasingly governed by metabolic programming rather than immediate hydraulic conditions, accompanied by a shift in the dominant water import pathway from xylem to phloem (Keller et al., 2015; Lecourieux et al., 2017). This transition fundamentally alters the carbon demand profile: green berries require both structural carbon for cell wall synthesis and osmotic solutes for expansion, while ripening berries primarily accumulate storage compounds without substantial volume increase, suggesting that any LSB advantages related to reduced carbon demand should be most pronounced during active hexose accumulation rather than expansion (Sections 3.1.2.1-3.1.2.2).

The magnitude of berry growth reduction under water stress quantitatively demonstrated this developmental shift. Green-stage berries exhibited mean relative growth rates of 0.047-0.078 day^{-1} under no irrigation conditions, with Ψpd values spanning -1.23 to -0.14 MPa (Section 3.1.2.4, Table 6). In contrast, ripening-stage berries under water deficit maintained mean RGR values close to zero (ranging from -0.003 to 0.006 day^{-1}), with Ψpd values spanning -1.75 to -0.51 MPa. The approximately 8-13 fold reduction in mean RGR between green and ripening stages reflects the fundamental transition from rapid cell expansion to slower biochemical accumulation processes characteristic of berry maturation.

The differential sensitivity to water potential across developmental stages is most clearly revealed by regression slopes relating RGR to Ψpd. During the green stage, slopes ranged from 0.30 day^{-1} MPa^{-1} (Luminan) to 0.56 day^{-1} MPa^{-1} (G5), indicating that each 1 MPa decrease in water potential corresponded to a 0.30-0.56 day^{-1} reduction in growth rate. During the ripening stage, regression slopes decreased to 0.031-0.038 day^{-1} MPa^{-1}, representing a 93-94% reduction relative to green stage slopes (Section 3.1.2.4, Table 6). This dramatic reduction in hydraulic coupling means that ripening berries can maintain near-stable growth rates across a wide range of plant water potentials that would severely constrain green-stage expansion.

Shriveling thresholds, defined as the predawn water potential at which 10% of berries displayed wrinkled skin surface, provided an independent measure of developmental stage effects on berry hydraulic tolerance. Across all genotypes, berries withstood substantially lower water potentials before shriveling during ripening (mean: -1.51 MPa) compared to green stage (mean: -1.06 MPa), representing a 42% increase in stress tolerance (Section 3.1.1). This enhanced hydraulic buffering during ripening likely reflects multiple coordinated changes including increased osmotic adjustment through apoplastic solute accumulation (Wada et al., 2008), cell wall polysaccharide

modifications (Nunan et al., 1998), and reduced xylem conductance that collectively protect ripening berries from hydraulic dysfunction (Tilbrook & Tyerman, 2008). The biological significance of this developmental shift is substantial: it enables continued berry development and sugar accumulation even when whole-plant water status reaches levels that would arrest green-stage berry expansion.

4.1.2 Individual Berry Variability and Population-Level Responses

During the green stage, individual berry volume responses at the shriveling point exhibited substantial heterogeneity within genotypes, with standard deviations approaching or exceeding mean values (Section 3.1.2.1, Table 5). This extreme variability reflects the asynchronous development characteristic of grape clusters, where individual berries within the same cluster can differ substantially in cell number, expansion rate, hydraulic conductance (Rogiers et al., 2004), and particularly in the timing of ripening initiation (Shahood et al., 2020). While population means suggest minimal volume loss or even slight gains for some genotypes, individual berries experienced responses ranging from substantial shrinkage to continued modest expansion.

During the ripening stage, individual berry variability was substantially reduced compared to green stage, indicating more constrained and synchronized responses during the accumulation phase (Section 3.1.2.1, Table 5). This reduced variability likely reflects the developmental transition whereby ripening berries have completed most cell expansion and entered a more uniform metabolic phase focused on solute accumulation. The generally modest volume changes at the individual berry level indicate that ripening berries possess substantial hydraulic buffering capacity that maintains organ integrity despite severe whole-plant water deficit.

The absence of LSB-specific advantages in berry-level hydraulic tolerance has important implications for understanding LSB drought adaptation mechanisms. The similar berry shriveling thresholds across LSB and non-LSB genotypes during ripening (Section 3.1.1) indicate that the LSB trait does not confer superior intrinsic tissue-level drought tolerance. Rather, any drought advantages associated with LSB genotypes must emerge from system-level properties such as resource allocation patterns or architectural characteristics, rather than from enhanced hydraulic resilience at the organ scale. This distinction is critical for understanding breeding objectives: selecting for LSB phenotype does not necessarily select for berry-level stress tolerance, but may nonetheless influence whole-plant drought performance through altered source-sink dynamics.

The ranking of genotypes by shriveling tolerance shifted between developmental stages, with G5 being most sensitive during green stage but more tolerant during ripening (Section 3.1.3). This developmental instability in stress tolerance rankings indicates that simple classification of genotypes as "drought tolerant" or "drought sensitive" based on

single-timepoint assessment is inadequate. Rather, genotypic drought response must be evaluated across developmental stages and stress durations, recognizing that mechanisms conferring advantages during one phase may be irrelevant or even disadvantageous during other phases.

4.1.3 Recovery Capacity and Resilience to Acute Stress

All genotypes exhibited rapid recovery of plant water status following rewatering (return to Ψpd >-0.15 MPa within 3-6 days; Section 3.1.1), regardless of preceding stress severity. This rapid hydraulic recovery indicates that young potted vines maintain substantial capacity for water uptake and restoration of favorable water relations following acute stress episodes, consistent with the relatively high root:shoot ratios characteristic of juvenile vines and the absence of severe xylem embolism under the moderate stress levels imposed.

Berry-level recovery was similarly rapid and complete. Following rewatering, berries rapidly reached ≥95% of initial volume within 1-2 days (Section 3.1.2.1-3.1.2.2, Table 5), with final volumes exceeding initial values, indicating not only complete recovery but compensatory growth that partially or fully offset stress-induced growth suppression. The capacity for rapid recovery and compensatory growth demonstrates that temporary severe water deficit, while constraining instantaneous growth rate, does not permanently impair berry developmental potential when water availability is restored during the same developmental phase.

The strong correlations between berry relative growth rate and predawn water potential during both green stage (r = 0.80-0.88) and ripening stage (r = 0.70-0.74; Section 3.1.2.4, Table 6) indicate tight hydraulic coupling across development. However, the dramatically reduced regression slopes during ripening (93-94% reduction relative to green stage; Section 3.1.2.4) indicate that ripening berries integrate water availability over longer timescales—days to weeks rather than hours to days. This developmental shift in integration timescale suggests that sustained moderate stress might be more effective than acute severe stress for revealing genotypic differences during the ripening phase, when berries possess hydraulic buffering that protects against temporary limitation but remain sensitive to prolonged resource availability patterns.

The maintenance of sink activity following stress-recovery cycles has important implications for understanding whole-plant responses under fluctuating drought conditions. The observation that berries rapidly resume growth after rewatering (Section 3.1.2.3, Table 6) indicates that berry sink activity remains latent during water deficit and can be rapidly reactivated when conditions improve. This organ-level resilience suggests that berries can maintain sink competence despite temporary water limitation, which may enable plants to allocate resources flexibly when facing sustained stress conditions.

The ranking of genotypes by recovery rate shifted between developmental stages (Section 3.1.2.1-3.1.2.2, Table 5). However, the small absolute differences in recovery time and the rapid restoration of water status across all genotypes (Section 3.1.1) indicate that recovery capacity per se is not a major source of genotypic differentiation in drought response. These findings suggest that genotypic differences may be more pronounced under sustained stress conditions, where the ability to maintain coordinated resource allocation over extended periods becomes critical.

Berry hydraulic sensitivity and growth dynamics are primarily governed by developmental stage, with genotypic differences being relatively minor and context-dependent at the berry scale. LSB genotypes do not possess inherently superior berry-level drought tolerance, suggesting that any whole-plant performance differences must emerge from system-level properties rather than organ-level advantages.

4.2 Carbon Gain, Allocation, and Source-Sink Relationships

4.2.1 Testing the Carbon Demand Hypothesis Through Carbon-Normalized Treatments

The LSB trait, characterized by 20-30% lower hexose accumulation in berries compared to traditional varieties (Bigard et al., 2022), presents a physiological paradox relevant to drought adaptation. While conventional Vitis vinifera cultivars exhibit tight coupling between sugar accumulation and water uptake during ripening, LSB genotypes demonstrate a decoupling of these processes, maintaining comparable berry size with significantly reduced sugar levels (Bigard et al., 2022). This decoupling led to the hypothesis that lower per-berry carbon demand in LSB genotypes could confer advantages under water deficit by reducing the competitive pressure for photoassimilates between reproductive and vegetative sinks (Wilhelm de Almeida et al., 2024a). Previous phenotyping platform studies by Wilhelm de Almeida et al. (2024a) provided initial support for this hypothesis, demonstrating superior carbon accumulation performance in LSB genotype G14 under drought conditions in controlled environment. However, their comparison of controlled platform versus field responses (Wilhelm de Almeida et al., 2023) revealed important genotype × environment interactions, highlighting the need for mechanistic understanding of how reduced sugar demand translates to drought advantages under different experimental conditions.

To directly test whether drought advantages stem from reduced carbon demand per se, our experiment employed a carbon-normalized treatment where LSB genotypes received approximately 50% increase in berry number, effectively matching the total fruit carbon demand of non-LSB genotypes at the whole-plant level. This experimental design allows decoupling of carbon demand effects from other physiological traits associated with the LSB phenotype. If the carbon demand hypothesis is correct, two predictions follow: (1) standard LSB genotypes under water deficit should demonstrate

superior carbon status compared to non-LSB genotypes due to lower sink pressure, and (2) carbon-normalized LSB genotypes should lose this advantage, performing similarly to non-LSB genotypes when total carbon demand is equalized. The carbon-normalized treatment represents a critical manipulation for understanding source-sink relationships under stress, as previous grapevine studies have shown that fruit load directly influences photosynthetic capacity and carbon partitioning patterns (Edson et al., 1993), with sink strength playing a regulatory role in source activity particularly under resource-limited conditions (Pagay, 2016). Grapevine carbon allocation models have established that sink strength—defined by potential growth rate, respiration costs, and storage demand—is the primary determinant of carbon partitioning, with maintenance respiration prioritized when demand exceeds supply (Vivin et al., 2002).

Contrary to expectations, fruit carbon content per plant (varC) remained remarkably stable across well-watered and water-deficit treatments (Section 3.2.5.1.1). We anticipated that prolonged moderate water deficit would reduce varC through decreased photosynthesis (Section 3.2.5.3.2) and impaired phloem transport. Instead, both LSB and non-LSB genotypes maintained similar varC under water deficit compared to well-watered conditions, indicating the operation of powerful compensatory mechanisms. This maintenance of fruit carbon accumulation despite substantial source limitation aligns with the reproductive prioritization strategy commonly observed in grapevines, where fruit growth is less sensitive to water stress than vegetative growth (Holzapfel et al., 2012; Greer & Sicard, 2009). Our results suggest that grapevines reallocate resources from vegetative to reproductive sinks under water deficit, as evidenced by increased fruit allocation percentage (Section 3.2.5.1.2) despite overall plant biomass reduction. The lack of treatment effect on varC indicates that water deficit affects where carbon is allocated more than how much carbon reaches fruits.

The most striking finding emerged from carbon-normalized LSB genotypes under water deficit, which achieved the highest absolute varC values (Section 3.2.5.1.1), maintaining substantial fruit carbon accumulation despite facing both high sink demand and restricted water availability. This performance reveals a latent carbon allocation capacity in LSB genotypes that becomes apparent only when challenged by combined stresses. Standard LSB genotypes under water deficit did not show advantages over non-LSB genotypes, indicating that simply having lower per-berry sugar demand is insufficient for improved drought performance. Instead, LSB genotypes appear to possess greater carbon allocation flexibility—the ability to maintain fruit carbon supply when sink demand is high and source activity is constrained. This flexibility may involve multiple mechanisms: (1) more efficient carbon transport from leaves to fruits under limiting conditions, (2) greater capacity for remobilizing stored carbohydrates from vegetative organs, or (3) maintained photosynthetic capacity despite drought (Section 3.2.5.3.1). Similar patterns of increased carbon allocation to reproductive sinks under combined

stress have been reported in other fruit crops, where drought combined with high sink demand enhanced sugar metabolism enzyme activity and promoted assimilate transport (Ruan et al., 2013; Walker, 2021).

These results require refinement of the original carbon demand hypothesis. The hypothesis that lower sugar accumulation per berry directly confers drought advantages by "freeing up" carbon for vegetative growth or reducing photosynthetic pressure is not supported—standard LSB genotypes showed no vegetative growth advantages and similar carbon allocation patterns to non-LSB under water deficit. Instead, our findings suggest an alternative framework: the LSB trait creates carbon allocation flexibility rather than carbon abundance. This flexibility remains unexpressed under standard conditions but provides advantage when vines face high combined demand—simultaneous pressure from large fruit loads and restricted source activity. The mechanism likely involves source-sink coordination rather than simple supply-demand balance. Grapevine source-sink relationships are highly plastic under stress (Douthe et al., 2018; Gambetta et al., 2020), with sink signals influencing source activity and carbon partitioning patterns. LSB genotypes may respond more effectively to sink signals, upregulating transport and allocation pathways to maintain fruit carbon supply under challenging conditions. This interpretation aligns with observations in drought-rehydrated grapevines, where approximately double the proportion of newly fixed carbon was allocated to berries compared to well-watered controls, demonstrating the plant's capacity to prioritize reproductive sinks when source availability improves following stress (Castellarin et al., 2007).

4.2.2 Whole-Plant Carbon Balance Under Prolonged Drought

The observed pattern of maintained fruit carbon accumulation under water deficit, despite substantial reductions in total plant biomass, reveals a fundamental reproductive prioritization strategy common to perennial fruit crops under stress. Water deficit reduced total plant biomass, yet this reduction occurred almost entirely through vegetative organs rather than fruits (Section 3.2.5.1.2). The proportion of total plant biomass allocated to fruits increased significantly under water deficit, representing substantial relative increase in reproductive allocation despite absolute biomass reductions in both compartments. This differential sensitivity between vegetative and reproductive growth under water limitation has been extensively documented in grapevine, where fruit growth during ripening is considerably less sensitive to water stress than shoot or leaf expansion (Lovisolo et al., 2010; Chaves et al., 2010). The mechanisms underlying this prioritization involve both hydraulic and metabolic regulation, with moderate water deficit inducing changes in source-sink relationships through reduced competition for carbon resources as vegetative meristems become progressively more sensitive to water limitation while fruit demand remains strong

(Castellarin et al., 2007). From an evolutionary perspective, this strategy ensures reproductive success even under resource scarcity, though the extent of prioritization can vary among genotypes depending on their native ecological conditions and breeding history.

The components of vegetative biomass exhibited contrasting responses to water deficit, with actively growing organs showing high sensitivity while structural components remained stable. Water deficit significantly reduced photosynthetic tissues across all genotypes (Section 3.2.4.2, Supplementary Table S7), with significant genotype × treatment interactions indicating genotypic variation in the extent to which vegetative growth is suppressed under drought. In striking contrast, structural components showed remarkable stability: trunk and cane biomass exhibited no significant water deficit response. Root biomass also maintained stability across treatments, though genotypic effects were highly significant, with G5 consistently allocating more biomass belowground compared to other genotypes. This pattern of response reflects fundamental differences in tissue construction costs and functional priorities. Structural organs represent long-term carbon investments essential for perennial survival, and their maintenance ensures capacity for recovery following stress release. The selective inhibition of leaf and shoot growth while preserving structural components allows the plant to reduce water demand through decreased transpiring surface area without sacrificing future productive capacity.

Water deficit induced systematic shifts in biomass partitioning toward belowground organs, with increased root:shoot ratios across all genotypes (Section 3.2.5.1.2, $p = 0.004$). This reflects the general plant strategy of allocating resources preferentially to organs acquiring the most limiting resource (Poorter et al., 2012). Under water limitation, enhanced root allocation potentially improves water access through exploration of deeper or previously untapped soil volumes, though the effectiveness depends on soil characteristics and the severity and duration of deficit. Importantly, genotypic differences in root allocation strategies were substantial. LSB genotype G5 maintained consistently higher root:shoot ratios compared to non-LSB genotypes, representing approximately doubled relative root investment independent of water treatment. This constitutive difference suggests that G5 possesses an inherently more extensive root system relative to its canopy size, potentially contributing to drought resilience through improved soil water capture capacity. The preferential allocation of recently assimilated carbon to roots under drought, as demonstrated through isotope tracing studies in perennial species (Bahn et al., 2013), likely underlies the enhanced root dry matter accumulation observed in LSB genotypes under combined carbon-normalized and water deficit conditions.

Carbon-normalized LSB genotypes achieved the highest fruit allocation percentages despite facing combined challenges of elevated sink demand and restricted water availability (Section 3.2.5.1.2). These elevated fruit allocations exceeded those of any standard treatment, demonstrating that LSB genotypes can sustain high reproductive investment even when simultaneously challenged by large crop loads and drought stress. Critically, these high fruit allocations were achieved while maintaining vegetative biomass comparable to standard LSB treatments under the same water regime. This finding refutes the hypothesis that carbon-normalized LSB plants achieve high fruit allocation by sacrificing vegetative tissues beyond what water stress alone would impose. Instead, the elevated fruit allocation arose primarily from absolute increases in fruit biomass rather than disproportionate vegetative reduction. The capacity to maintain both adequate vegetative structure and enhanced reproductive output under combined stress distinguishes LSB genotypes from traditional varieties and provides mechanistic insight into allocation flexibility. This pattern aligns with emerging evidence that fruit load can influence whole-plant carbon partitioning through sink signaling mechanisms, though the effects vary considerably among crop species and environmental conditions (Gambetta et al., 2020).

The altered source-sink balance under water deficit is quantitatively captured by fruit-to-leaf area ratios and soluble solids per unit leaf area (Section 3.2.2.2.2, Table 9). Water deficit increased fruit-to-leaf ratios substantially, while carbon-normalized LSB genotypes reached the highest values. These elevated ratios arose from both increased fruit fresh weight and reduced leaf area under deficit. The compound effect created source-sink imbalances where each unit of photosynthetic tissue supported substantially greater reproductive demand. These quantitative shifts in source-sink relationships occurred despite substantial reductions in net photosynthesis (Section 3.2.5.3.2). The maintenance of high fruit carbon accumulation under these constrained conditions suggests compensatory mechanisms beyond current assimilation, including remobilization of stored carbohydrates from vegetative organs and temporal integration of carbon acquisition over the full ripening period rather than instantaneous source-sink matching.

The biomass partitioning patterns observed across treatments reveal that whole-plant carbon balance under water deficit is not a static equilibrium but a dynamic resource allocation process shaped by hierarchical priorities. Grapevines under drought maintain reproductive allocation by suppressing the most responsive vegetative tissues while preserving structural components essential for perennial survival and post-stress recovery. The stability of perennial structures despite significant overall biomass reductions represents a strategic "bet-hedging" approach where short-term growth reductions preserve long-term productive capacity. LSB genotypes, particularly under carbon-normalized conditions, push this allocation hierarchy further by sustaining both

elevated fruit production and adequate vegetative structure simultaneously. This capacity suggests more efficient carbon use or enhanced mobilization of previously stored reserves during periods of high demand. The observation that carbon-normalized LSB plants maintained similar vegetative biomass to standard LSB plants while producing substantially more fruit (Section 3.2.4.2) indicates that the "cost" of additional fruit production was distributed across multiple carbon pools and temporal scales rather than extracted exclusively from concurrent photosynthesis. This interpretation is consistent with recent work emphasizing the importance of stored non-structural carbohydrates in grapevine stress responses and the complex temporal dynamics of carbon allocation in perennial crops (Holzapfel et al., 2012). The differential capacity of genotypes to manage these allocation tradeoffs under combined resource limitations represents a key target for breeding climate-resilient varieties.

4.3 Water Use Strategies and Requirements

4.3.1 Leaf-Level Physiology and the Absence of Genotypic Differentiation

The absence of genotypic differentiation in leaf-level gas exchange parameters presents an apparent paradox when contrasted with the substantial whole-plant performance differences observed between LSB and non-LSB genotypes under water deficit. Water deficit significantly reduced gas exchange parameters across all genotypes (Section 3.2.5.3.2, Supplementary Table S8), yet these responses showed no significant genotypic variation ($p > 0.05$). Similarly, instantaneous and intrinsic water use efficiency increased 2-2.6 fold under water deficit across all genotypes, but again with no genotypic differences (Section 3.2.5.3.3, Figure 53). This uniformity extended to integrated water use efficiency assessed through carbon isotope discrimination ($\delta^{13}C$), where water deficit produced consistent shifts toward less negative values across genotypes, but no significant genotype effect emerged ($p = 0.374$, Section 3.2.5.2.4, Figure 47). The disconnect between uniform leaf-level responses and differentiated whole-plant performance (as will be discussed in Section 4.3.2) indicates that the LSB trait confers drought advantages through mechanisms operating at scales beyond individual leaf physiology.

The proportionally greater reduction in stomatal conductance relative to net photosynthesis represents a fundamental drought adaptation response conserved across both LSB and non-LSB genotypes. This disproportionate stomatal closure resulted in the observed 2-3 fold increases in instantaneous water use efficiency across all genotypes, representing a coordinated physiological response where reduced water loss per unit carbon fixed provides immediate adaptive value under drought (Section 3.2.5.3.2). The consistency of this response pattern indicates that all genotypes share similar stomatal sensitivity thresholds and photosynthetic resilience to moderate water stress. This uniformity aligns with broader patterns in grapevine drought physiology,

where genetic variation in drought tolerance often manifests through differences in hydraulic architecture, root depth, or whole-plant carbon allocation rather than through leaf-level biochemical or stomatal properties (Schultz, 2003; Lovisolo et al., 2010).

Carbon-normalized LSB genotypes under well-watered conditions exhibited a distinctive leaf-level response pattern. These plants showed elevated stomatal conductance and transpiration throughout the ripening period, yet net photosynthesis remained comparable to standard treatments (Section 3.2.5.3.2, Figure 50). This apparent paradox suggests that elevated sink demand from additional berries triggered stomatal opening as an anticipatory response, potentially to improve leaf microclimate or to facilitate transpiration-driven nutrient transport to developing fruits. However, under water deficit conditions, this sink-driven stomatal response was completely overridden by drought-induced stomatal closure, with both standard and carbon-normalized treatments showing similar reductions in gas exchange parameters. The observation that sink signals influence stomatal behavior under favorable conditions but are subordinated to water conservation imperatives under drought demonstrates a hierarchical control system where hydraulic safety takes precedence over carbon acquisition optimization.

The uniform leaf-level responses across genotypes contrast with previous findings. Wilhelm de Almeida et al. (2024a) reported that LSB genotype G14 achieved substantially higher photosynthesis and stomatal conductance under severe progressive drought in the same Phenodyn platform. Our study under moderate sustained deficit reveals no such leaf-level advantages, suggesting these differences may reflect stress severity rather than intrinsic LSB properties. The critical insight from our carbon-normalized treatments is that LSB genotypes possess allocation flexibility rather than photosynthetic superiority. Under standard crop loads, this flexibility remains unexpressed and LSB genotypes perform similarly to conventional varieties. When challenged by high sink demand under water limitation, LSB genotypes demonstrate capacity to maintain fruit carbon supply through more efficient allocation of fixed carbon. This allocation-based mechanism, operating downstream of primary photosynthesis, explains why leaf-level measurements fail to differentiate genotypes despite clear whole-plant performance differences under specific stress combinations.

4.3.2 Whole-Plant Water Use Efficiency and the Role of Plant Architecture

The assessment of water use efficiency at the whole-plant scale revealed patterns fundamentally different from those observed at the leaf level, highlighting the critical importance of scale in evaluating genotypic drought performance. While leaf-level gas exchange showed no genotypic differentiation (Section 4.3.1), whole-plant water use efficiency (WUEpl = varC/TR) varied substantially among treatments and, following normalization for plant architecture, revealed significant differences in how genotypes allocate carbon under combined resource limitations. This disconnect between leaf-level

uniformity and whole-plant variation emphasizes that drought advantages in LSB genotypes emerge not from superior photosynthetic machinery but from differences in carbon allocation strategies that operate downstream of primary assimilation.

Observed whole-plant water use efficiency exhibited a strong treatment effect, with water deficit substantially increasing WUEpl across all genotypes compared to well-watered conditions (Section 3.2.5.2.1, Figure 45). These dramatic increases in WUEpl under water deficit arise primarily from the asymmetric responses of the numerator and denominator: fruit carbon accumulation (varC) remained stable despite substantial reductions in photosynthesis (Section 4.2.1), while total transpiration decreased substantially (Section 3.2.2.1.2, Table 8). This disproportionate response reflects the reproductive prioritization strategy discussed in Section 4.2.2, where grapevines under stress maintain fruit carbon supply by reallocating resources from vegetative to reproductive sinks. The consistency of elevated WUEpl under water deficit across all genotypes demonstrates that this is a universal drought adaptation response in grapevine rather than a trait specific to LSB varieties.

However, interpretation of absolute WUEpl values is complicated by inherent architectural differences among genotypes that influence this metric independently of physiological water use efficiency. Plant architecture—particularly the fruit-to-leaf ratio determined by berry number, berry weight, and total leaf area—can substantially inflate or deflate WUEpl without reflecting genuine differences in the efficiency of converting water into harvestable carbon. The challenge of separating architectural from physiological contributions to WUE has been recognized in grapevine research, with studies emphasizing that fruit load effects on apparent efficiency must be accounted for when comparing genotypes with different growth habits or when crop load manipulations are imposed experimentally (Medrano et al., 2015; Wilhelm de Almeida et al., 2024a).

To remove architectural confounds and enable fair physiological comparisons, WUEpl was normalized by the fruit-to-leaf ratio, effectively standardizing all plants to a theoretical configuration of 1 kg fresh fruit per 1 m^2 leaf area (WUEpl_n = WUEpl × [Fruit/Leaf]; Section 3.2.5.2.2). This normalization procedure substantially altered the relative ranking of genotypes. After normalization, treatment effects remained dominant ($p < 0.001$), but carbon-normalized LSB genotypes under water deficit achieved the highest normalized efficiency values (Figure 46). These values significantly exceeded all other treatments, including well-watered plants and other water deficit combinations. Critically, standard (non-carbon-normalized) LSB genotypes under water deficit showed WUEpl_n values comparable to or slightly lower than non-LSB genotypes under the same water treatment, indicating that the LSB trait per se does not confer water use efficiency advantages under standard crop loads. This finding directly supports the refined carbon

demand hypothesis presented in Section 4.2.1: LSB advantages emerge only under combined stress conditions where both sink demand is elevated and source activity is constrained.

The superior normalized WUE of carbon-normalized LSB genotypes under water deficit provides critical insight into the mechanism underlying LSB drought advantages. These plants achieved high WUEpl_n not through reduced water consumption—transpiration rates were similar across genotypes when normalized by leaf area (Section 3.2.2.1.2, Table 8)—but through enhanced carbon allocation to fruits despite severe constraints. This performance occurred despite these plants experiencing the most challenging conditions in the experiment: high sink demand from increased berry numbers, prolonged moderate water stress, and associated reductions in photosynthesis comparable to all other water deficit treatments (Section 3.2.5.1.1, Table 10). The capacity to maintain this carbon allocation efficiency under combined stress distinguishes carbon-normalized LSB genotypes from both standard LSB and non-LSB varieties, revealing a latent allocation flexibility that becomes apparent only when the carbon supply-demand balance is severely tested.

Integration of the WUEpl patterns with leaf-level responses (Section 4.3.1) and carbon allocation dynamics (Sections 4.2.1-4.2.2) reveals a coherent mechanistic framework for understanding LSB genotype behavior under water deficit. At the leaf scale, all genotypes exhibited uniform stomatal closure and photosynthetic downregulation under stress, with no genotypic differentiation in gas exchange parameters or instantaneous water use efficiency. However, at the whole-plant scale, genotypic differences emerged in how the limited carbon fixed by this constrained photosynthetic apparatus was partitioned among competing sinks. Carbon-normalized LSB genotypes directed carbon more effectively toward fruits, achieving higher fruit allocation percentages while maintaining adequate vegetative structure (Section 4.2.2). This preferential allocation to reproductive over vegetative sinks, combined with stable transpiration rates typical of all water deficit treatments, manifests as superior normalized WUEpl. The mechanism operates not through enhanced carbon acquisition but through enhanced carbon distribution efficiency—getting more fixed carbon to harvestable products rather than to transient vegetative tissues or respiration losses.

The contrast between our findings and those of Wilhelm de Almeida et al. (2024a) warrants consideration. In the same Phenodyn phenotyping platform, Wilhelm de Almeida et al. (2024a) reported that LSB genotype G14 achieved superior WUEpl_n with this advantage accompanied by superior leaf-level physiology. Our study found no such leaf-level advantages for LSB genotypes, with uniform gas exchange responses across genotypes (Section 4.3.1), yet observed even higher WUEpl_n values in carbon-normalized LSB treatments. This difference likely reflects the specific treatments

compared: Wilhelm de Almeida et al. (2024a) compared standard crop loads across genotypes with naturally varying fruit-to-leaf ratios, while our study experimentally manipulated LSB berry numbers, directly testing responses to extreme source-sink imbalances. The absence of leaf-level advantages in our study, combined with superior whole-plant performance under carbon-normalized conditions, more definitively isolates allocation efficiency as the key mechanism.

The implications for breeding and phenotyping strategies are significant. Whole-plant WUE measurements in grapevine must account for architectural confounds to avoid selecting genotypes with favorable fruit-to-leaf ratios rather than genuine physiological efficiency. Breeding programs targeting improved WUE should therefore employ normalized metrics that remove fruit load and canopy size effects, enabling comparison of inherent physiological capacity across genotypes with diverse growth habits. Moreover, our findings suggest that screening under standard conditions may fail to identify allocation flexibility advantages that only manifest under combined stress. Carbon-normalized or high crop load treatments imposed under water deficit could provide more discriminating test conditions for revealing latent drought adaptation traits related to source-sink coordination.

The observation that standard LSB genotypes showed no WUE advantages compared to non-LSB genotypes under standard crop loads has practical implications for viticulture. Simply planting LSB varieties will not automatically improve vineyard water use efficiency unless those varieties are grown under conditions that challenge their allocation capacity—specifically, elevated crop loads combined with water limitation during ripening. Under favorable irrigation or naturally low fruit set, LSB allocation flexibility remains unexpressed and these varieties perform similarly to conventional cultivars. This suggests that the deployment of LSB varieties should be targeted toward water-limited environments where crop load can be actively managed, rather than as a universal solution to drought challenges.

4.3.3 Carbon Isotope Discrimination ($\delta^{13}C$) as Integrated Water Use Efficiency

Carbon isotope discrimination analysis provided an independent validation of the water use efficiency responses observed at both leaf and whole-plant scales. The $\delta^{13}C$ measurements in leaf tissue at harvest integrated the physiological responses throughout the ripening period, offering a time-integrated assessment of water use efficiency that complemented the instantaneous gas exchange measurements and cumulative whole-plant WUE calculations.

Water deficit treatments exhibited $\delta^{13}C$ values approximately 2.5-3.5‰ less negative than their well-watered counterparts across all genotypes (Figure 47), reflecting the cumulative effect of reduced stomatal conductance under water deficit conditions. The

magnitude of this isotopic shift was consistent with previous observations in grapevine cultivars subjected to water deficit (Bchir et al., 2016; Tomás et al., 2014). The absence of significant genotype effects on $\delta^{13}C$ ($p = 0.374$) paralleled the lack of genotypic differentiation observed in instantaneous leaf-level water use efficiency (Section 4.3.1), indicating that all genotypes employed similar stomatal regulation strategies in response to water deficit throughout the ripening period.

The positive correlation between $\delta^{13}C$ and normalized whole-plant water use efficiency (WUEpl_n) across all treatments (Pearson $r = 0.635$, $p < 0.001$, $R^2 = 0.40$; Figure 48) demonstrated that leaf-level physiological responses captured by carbon isotope discrimination scaled to whole-plant carbon-water relationships. However, the moderate correlation coefficient ($R^2 = 0.40$) indicated that 60% of the variation in WUEpl_n remained unexplained by $\delta^{13}C$ values alone. This residual variation likely reflected the complex relationship between instantaneous leaf-level processes captured by $\delta^{13}C$ and the integrated whole-plant carbon balance captured by WUEpl_n, including post-photosynthetic processes such as respiration, carbon allocation to different organs, and berry sugar accumulation, none of which were directly reflected in the leaf isotopic signal.

Carbon-normalized LSB genotypes under water deficit showed $\delta^{13}C$ values comparable to their standard water deficit counterparts, indicating that increased berry number did not substantially alter the leaf-level integrated WUE response captured by carbon isotope discrimination. This similarity in $\delta^{13}C$ values despite vastly different fruit loads suggested that leaf-level stomatal regulation responded primarily to soil water availability rather than to downstream sink demand during the ripening period. However, these similar $\delta^{13}C$ values occurred alongside substantially elevated WUEpl_n values in the carbon-normalized treatments, demonstrating that increased sink strength enhanced whole-plant carbon accumulation efficiency without proportionally increasing water consumption or altering the time-integrated stomatal response captured by $\delta^{13}C$.

The methodological approach employed in this study, measuring $\delta^{13}C$ in the same leaves used for instantaneous gas exchange assessments, enabled direct comparison between integrated and instantaneous measures of leaf-level WUE. The consistency between the $\delta^{13}C$ results (no genotype effect, strong treatment effect) and the instantaneous WUE measurements (Section 4.3.1) validated the use of carbon isotope discrimination as a reliable proxy for time-integrated leaf-level water use efficiency in grapevine. However, the moderate correlation between $\delta^{13}C$ and WUEpl_n ($R^2 = 0.40$) indicated that leaf-level isotopic measurements alone were insufficient to predict whole-plant carbon-water relationships, highlighting the importance of measuring WUE at multiple scales to capture the full complexity of plant responses to water deficit.

From a breeding perspective, the strong treatment effect on $\delta^{13}C$ ($p < 0.001$) combined with the absence of genotype effects ($p = 0.374$) suggested that $\delta^{13}C$ analysis would be most effective as a tool for assessing the intensity and duration of water deficit experienced by vineyard blocks rather than for discriminating among genotypes for superior water use efficiency under drought. The lack of genotypic variation indicated that carbon isotope discrimination alone would not effectively identify LSB or non-LSB genotypes with superior drought adaptation potential, and that such screening efforts would need to incorporate additional metrics such as carbon accumulation capacity, fruit load response, or whole-plant water use efficiency under standardized conditions.

4.3.4 Stress Timing and Duration Effects on Water Use Efficiency

The integration of findings from short-term acute water deficit (STS) and long-term moderate water deficit (LTS) reveals that stress timing, duration, and severity fundamentally shape plant water use strategies and the expression of genotypic differences in drought response. While both experiments imposed water limitation, the contrasting temporal dynamics and physiological contexts generated qualitatively different response patterns at both berry and whole-plant scales.

Short-term water deficit in STS imposed rapid, severe stress, with plants reaching critical water status within days of treatment initiation (Section 3.1.1). This acute stress protocol tested the hydraulic tolerance limits of berries and the minimum water potential thresholds triggering visible berry damage. Under these conditions, berry volume responses reflected primarily passive hydraulic adjustments to rapidly declining water availability, with minimal opportunity for acclimation or coordinated resource allocation adjustments at the whole-plant level. In contrast, long-term water deficit in LTS maintained moderate, sustained stress over the 6-7 week ripening period (Section 2.1), allowing plants to implement coordinated acclimation responses including stomatal regulation, osmotic adjustment, and resource allocation modifications that operate over timescales of days to weeks.

The fundamental difference between these stress protocols lies in the opportunity for physiological integration and adjustment. Acute stress in STS revealed the intrinsic hydraulic tolerance of organs operating near constitutional limits, while chronic stress in LTS engaged regulatory systems governing resource allocation, growth coordination, and acclimation responses. This distinction proves critical for understanding why genotypic differences emerged strongly in LTS but remained subtle or context-dependent in STS.

Berry responses differed markedly between experiments. During short-term stress in STS, berry volume at the shriveling point exhibited high variability and developmental stage dependency (Section 3.1.2, Table 5), followed by rapid compensatory growth after recovery irrigation. Under long-term moderate water deficit in LTS, berry development

proceeded with sustained carbon accumulation despite reduced water availability, with harvest measurements revealing that water deficit treatments maintained fruit carbon accumulation comparable to well-watered controls within most genotypes (Section 3.2.5.1.1). The critical difference from STS lies in the absence of acute hydraulic crisis: berries in LTS never experienced the severe water potential declines or visible shriveling that defined stress severity in STS. This contrast underscores a fundamental principle: moderate, sustained water limitation during ripening permits continued metabolic activity and sugar accumulation through regulated adjustments, while acute severe stress forces berries into survival mode characterized by growth arrest and passive volume loss.

Water use efficiency at the whole-plant scale exhibited strong treatment effects in LTS, with water deficit substantially increasing WUEpl across genotypes (Section 3.2.5.2.1), consistent with proportionally greater reduction in transpiration relative to carbon assimilation. The emergence of genotypic differences in normalized whole-plant WUE under combined carbon-normalized and water deficit conditions (Section 3.2.5.2.2, Figure 46) represents a critical finding absent in STS. Short-term stress provided insufficient duration for whole-plant water use efficiency patterns to differentiate among genotypes, as the rapid stress imposition precluded the integration of carbon gain over extended periods. The significance of stress duration for expressing genotypic WUE differences likely relates to the time required for architectural and allocation adjustments to develop through sustained acclimation processes (Chaves et al., 2010; Vincent et al., 2019).

The developmental stage at which water stress was imposed fundamentally shaped both the mechanisms of stress response and the relevant timescales for physiological adjustment. Green-stage stress targeted berries during rapid cell expansion, when growth is turgor-dependent and hydraulically sensitive (Section 4.1.1), with berry expansion responding nearly immediately to fluctuations in plant water status. Ripening-stage stress applications targeted berries during the sugar accumulation phase, when berry growth has transitioned from cell expansion to metabolic ripening. The dramatically reduced regression slopes during ripening (93-94% reduction; Section 3.1.2.4) indicate that ripening berries integrate water availability over longer timescales—days to weeks rather than hours to days. This developmental shift in integration timescale explains why chronic moderate stress (LTS) proved more effective than acute severe stress (STS) for revealing genotypic differences in ripening-phase drought response.

Leaf-level gas exchange responses showed no significant genotypic differentiation in either instantaneous measurements (LTS) or integrated responses assessed through $\delta^{13}C$ analysis (Sections 4.3.1, 4.3.3). The emergence of genotypic differences at the whole-

plant scale despite uniform leaf-level responses indicates that water use efficiency advantages of LSB genotypes arise from plant architecture and resource allocation patterns rather than from superior leaf-level physiology. This scale-dependent pattern only becomes apparent under conditions permitting extended carbon accumulation and resource allocation adjustments—specifically, the chronic moderate stress of LTS rather than the acute severe stress of STS.

The shriveling thresholds observed in STS represent critical lower limits for berry water status that were deliberately avoided in LTS's moderate stress protocol (Section 3.1.1). This distinction in stress severity fundamentally alters the physiological state of the plant: berries approaching shriveling thresholds experience incipient hydraulic dysfunction, while berries under moderate sustained stress maintain cellular function and continue developmental programming (Gambetta et al., 2020). Recovery dynamics also differed fundamentally between experiments. In STS, recovery irrigation produced rapid restoration of plant water status and compensatory berry growth, demonstrating resilience to temporary severe stress. In LTS, plants remained under sustained moderate stress without recovery irrigation until harvest, better simulating field drought conditions where water limitation typically persists for extended periods.

The contrasting findings between STS and LTS clarify the nature of LSB drought adaptation, demonstrating that advantages emerge under specific drought scenarios rather than representing generalized stress tolerance (Tardieu et al., 2018). Under acute severe stress (STS), LSB genotypes showed no consistent advantages (Section 4.1.2). Under chronic moderate stress combined with normalized carbon sink demand (LTS), LSB genotypes demonstrated clear advantages in maintaining fruit carbon accumulation while investing in root systems and achieving high normalized whole-plant WUE (Sections 4.2.1, 4.2.2, 4.3.2).

The timing-dependent expression of LSB advantages has practical implications for viticulture management and breeding selection. Field drought conditions in Mediterranean viticulture typically manifest as sustained moderate water limitation during ripening rather than acute severe stress (Costa et al., 2016). The LTS protocol therefore better represents agronomically relevant drought scenarios than the STS protocol. LSB genotypes appear adapted specifically to the chronic stress scenario, where their reduced per-berry carbon demand enables allocation flexibility that manifests as simultaneous fruit carbon accumulation and root investment. Selection for LSB-type drought adaptation should therefore focus on whole-plant architectural traits and allocation patterns observable under sustained moderate stress rather than on leaf-level physiological measurements or responses to acute stress.

4.4 Synthesis and Broader Implications

4.4.1 The LSB Phenotype in Fruit Crop Breeding Context

The Low Sugar Berry trait represents a departure from conventional fruit breeding paradigms, which have historically prioritized increased sugar concentration as a primary quality objective. The LSB phenotype achieves 20-30% lower hexose accumulation while maintaining or exceeding berry size and total yield performance (Bigard et al., 2022), fundamentally reorienting the carbon economy of the plant and creating opportunities for resource allocation flexibility.

The present findings demonstrate that the LSB trait operates as a system-level characteristic rather than merely a fruit composition attribute. LSB genotypes without crop load adjustment showed no clear advantages over non-LSB genotypes (Sections 4.2.1, 4.3.2). However, when sink demand was normalized through berry number adjustment, LSB genotypes revealed allocation flexibility not accessible to non-LSB genotypes, simultaneously maintaining fruit carbon accumulation while investing substantially more in root systems (Sections 4.2.1-4.2.2). The mechanistic basis lies not in superior photosynthetic capacity or enhanced stomatal regulation—leaf-level parameters showed no genotypic differentiation (Sections 4.3.1, 4.3.3)—but rather in architectural and partitioning responses to combined stress. The reduced per-berry carbon requirement provides decision-making flexibility in resource partitioning rather than simply creating a carbon surplus.

This interpretation has implications beyond viticulture for understanding source-sink relationships in perennial fruit crops generally. Under combined carbon and water stress, excessive sink strength may constrain allocation flexibility, forcing plants into sub-optimal resource distribution patterns that compromise long-term resilience. The LSB phenotype demonstrates that moderating sink demand per reproductive unit, while maintaining total reproductive output through increased unit numbers, can enable more adaptive allocation strategies under stress. Similar patterns appear in apple, citrus, and stone fruit crops where excessive fruit sink strength can compromise vegetative growth and stress resilience, with drought-tolerant genotypes often exhibiting enhanced carbon allocation to roots and sustained carbohydrate reserves during stress periods (Reyes et al., 2016; Falchi et al., 2020).

4.4.2 Breeding Strategies and Selection Approaches

The developmental and environmental context-dependency of LSB advantages documented here provides specific guidance for breeding program design and selection methodology. First, screening for allocation flexibility requires appropriate stress application protocols. Sustained moderate stress during the ripening period provides the appropriate selective environment for revealing allocation flexibility traits, while acute

stress screening may identify hydraulic tolerance traits that prove developmentally unstable and unassociated with superior whole-plant drought performance (Section 4.1.2).

First, screening for allocation flexibility requires appropriate stress application protocols. The absence of clear genotypic differentiation in STS (acute severe stress to berry shriveling) contrasted sharply with the emergence of strong LSB advantages in LTS (sustained moderate stress during ripening), demonstrating that selection environments must match target deployment conditions. Acute stress screening may identify hydraulic tolerance traits, but these appear developmentally unstable (genotype rankings reversed between green and ripening stages; Section 4.1.2) and were not associated with superior whole-plant drought performance. Instead, sustained moderate stress during the ripening period, when carbon demand for sugar accumulation peaks and water deficit typically occurs in Mediterranean viticultural regions, provides the appropriate selective environment for revealing allocation flexibility traits, consistent with breeding principles emphasizing that selection environments should match target deployment conditions to effectively manage genotype × environment interactions (Cooper & DeLacy, 1994).

Second, carbon-normalized treatment protocols offer powerful tools for exposing allocation constraints versus flexibility in germplasm screening. This approach could be systematically applied to breeding populations to identify individuals capable of maintaining balanced resource allocation under combined stress. The challenge for practical implementation is that these normalized metrics and stress combination treatments require substantially more labor and experimental control than simple yield measurements, creating tension between breeding program throughput and phenotyping accuracy. Development of early-predictive markers—potentially including transcriptomic signatures of allocation flexibility or molecular markers linked to partitioning traits—could accelerate selection without sacrificing predictive accuracy.

4.4.3 Viticulture Management Implications

The practical deployment of LSB genotypes in commercial viticulture requires management practices that enable expression of their allocation advantages while addressing their distinctive physiological characteristics. The experimental finding that LSB genotypes without crop load adjustment showed no water use efficiency advantages indicates that simply planting LSB varieties under standard management will not automatically improve drought performance. Rather, deployment requires deliberate crop load manipulation (approximately +35-50% berry numbers above natural set), sustained moderate deficit irrigation during ripening (Ψpd: -0.8 to -1.0 MPa), and potentially optimized rootstock selection to complement scion allocation patterns. This systems approach to LSB cultivation aligns with broader recommendations for climate

adaptation in viticulture, emphasizing that no single intervention provides sufficient adaptation alone (Naulleau et al., 2021).

4.4.4 Climate Change Adaptation Potential

The LSB phenotype addresses both primary constraints imposed by climate change on viticulture: increasing temperatures and decreasing water availability. Warming trends drive excessive potential alcohol levels that compromise wine quality, which LSB genotypes directly address by enabling harvest at physiological maturity with moderate potential alcohol levels (Baltazar et al., 2025; van Leeuwen et al., 2019). The water deficit adaptation component operates through allocation flexibility enabling simultaneous fruit production and stress mitigation investment under sustained moderate drought. Climate projections indicate that up to 90% of traditional Mediterranean wine regions may experience unsuitable conditions by century's end without significant adaptation measures (Hannah et al., 2013). LSB genotypes appear adapted for "drought coexistence"—continued productive function under sustained moderate water limitation through optimized resource allocation rather than through accessing additional water or enduring severe dehydration.

However, several caveats temper this assessment. First, allocation flexibility advantages emerged only under specific conditions (normalized high crop load plus sustained moderate deficit), suggesting limited manifestation across all scenarios. Second, the experiments employed young potted vines over single growing seasons, leaving open questions about mature field-grown vines over multiple years. Third, the genetic basis of allocation flexibility remains unknown, creating uncertainty about trait transmission in breeding programs or specificity to particular interspecific genetic backgrounds.

4.4.5 Integration Across Scales and Perspectives

The synthesis of findings across experimental scales—from daily berry volume dynamics to seasonal whole-plant carbon accumulation patterns—reveals that comprehensive characterization of drought adaptation requires integration of multiple temporal and organizational scales. Berry-level responses provided essential information about hydraulic tolerance limits but proved insufficient for predicting whole-plant performance under chronic stress. Leaf-level gas exchange measurements revealed universal stomatal responses but failed to differentiate genotypes. Only at the whole-plant scale, integrating carbon gain and water consumption over the full ripening period, did genotypic differences manifest clearly (Sections 4.2, 4.3.2).

This scale-dependency has methodological implications for phenotyping approaches. High-throughput platforms employing leaf-level or berry-level sensors may have limited power for identifying genotypic variation in allocation flexibility that determines whole-plant drought performance. The temporal integration requirement similarly challenges

rapid screening approaches, as allocation advantages developed progressively over 6-7 weeks under sustained moderate stress. Development of early-predictive markers could accelerate selection without sacrificing predictive accuracy.

4.5 Experimental Limitations and Interpretation Constraints

The present study provides novel insights into LSB genotype responses to water deficit through controlled experimentation enabling precise physiological measurements. However, several experimental and methodological limitations constrain the generalizability of findings and warrant careful consideration when extrapolating results to field viticulture conditions or broader germplasm contexts.

The controlled greenhouse environment (Phenodyn platform) provided essential control for isolating treatment effects but may not fully represent field drought stress complexity where Mediterranean vineyards experience higher light intensities, greater temperature fluctuations, and dynamic environmental changes (Section 4.5.1). Plants grown in 7-liter pots faced physical constraints absent in field soils, including limited rooting volume that restricted root development and eliminated deep water extraction capacity. The study spanned a single growing season, precluding evaluation of multi-year cumulative effects, carryover impacts, or carbohydrate reserve dynamics across years—critical for perennial woody crops.

The study examined four genotypes from a single interspecific breeding program, limiting generalization. The confounding of LSB phenotype with interspecific genetic background prevents definitive attribution of drought advantages specifically to reduced sugar accumulation versus other genetic components (Section 4.5.2). The physiological responses operate as integrated phenotypes without resolution of underlying molecular mechanisms, gene expression patterns, or genetic architecture essential for breeding applications.

Methodological constraints include indirect carbon accumulation calculations rather than direct $^{13}CO_2$ labeling, standardized substrate evaporation corrections, and absence of detailed root architecture characterization (Section 4.5.3). The study employed single rootstock (SO4) and moderate water deficit protocol (Ψpd -0.8 to -1.0 MPa), limiting assessment of scion × rootstock interactions and responses across the full drought severity spectrum (Section 4.5.4). Berry composition analysis focused on primary metabolites, excluding secondary metabolites critical for wine quality. These limitations collectively emphasize that while controlled experiments provide mechanistic insights, field validation across multiple environments remains essential for practical breeding and viticulture applications.

5 Conclusion

5.1 Synthesis of Main Findings

This thesis investigated how Low Sugar Berry (LSB) grapevine genotypes respond to water deficit compared to traditional varieties, addressing the central hypothesis that lower berry sugar demand favors a more comfortable carbon status under water deficit through reduced sink competition and enhanced allocation flexibility. Two complementary experiments examined short-term acute stress responses (STS) and long-term moderate water deficit effects (LTS), providing multi-scale physiological characterization from individual berry dynamics to whole-plant resource allocation patterns.

At the individual berry scale, water deficit responses showed strong developmental stage dependency but limited genotypic differentiation. During the green expansion phase, berries exhibited tight hydraulic coupling to plant water status, with all genotypes showing similar sensitivity to acute water limitation regardless of sugar accumulation phenotype. Genotype rankings for shriveling tolerance reversed between developmental stages, and the absence of LSB-specific advantages in berry hydraulic resilience indicated that the LSB trait does not confer superior intrinsic tissue-level drought tolerance. Following acute stress relief through recovery irrigation, all genotypes demonstrated rapid water status restoration and compensatory berry growth, confirming young vine resilience to temporary severe stress.

The long-term moderate water deficit experiment revealed that carbon accumulation in fruits (varC) remained stable across water treatments for most genotypes, with LSB and non-LSB varieties showing no significant differences when compared at their natural crop loads. The critical experimental manipulation—increasing berry numbers in LSB genotypes by approximately 35% to normalize total plant carbon demand—successfully revealed allocation flexibility not accessible at natural crop loads. Carbon-normalized LSB plants under water deficit simultaneously maintained fruit carbon accumulation while investing substantially more in root systems compared to non-LSB genotypes. This allocation pattern enabled carbon-normalized LSB genotypes to achieve the highest normalized whole-plant water use efficiency across all treatments, significantly exceeding both well-watered plants and standard water deficit treatments.

Importantly, LSB genotypes without crop load adjustment showed no WUE advantages over non-LSB genotypes, demonstrating that allocation flexibility benefits emerge specifically when LSB varieties carry fruit loads comparable to the carbon sink strength that non-LSB varieties achieve naturally. Gas exchange measurements at the leaf level revealed universal physiological responses to water deficit but no genotypic differentiation in photosynthetic capacity or stomatal regulation. Carbon isotope

discrimination analysis paralleled the instantaneous gas exchange patterns, with strong treatment effects but no genotype effects. The correlation between integrated leaf-level efficiency ($\delta^{13}C$) and normalized whole-plant efficiency (WUEpl_n) explained only 40% of variance, with the substantial unexplained variance attributable to architectural factors that operate independently of instantaneous leaf physiological capacity.

This scale-dependent response pattern—uniform leaf-level physiology coexisting with differentiated whole-plant performance—demonstrates that LSB drought adaptation operates through system-level resource allocation rather than through enhanced photosynthetic efficiency or superior stomatal control. The mechanistic basis lies in the architectural flexibility enabled by reduced per-berry carbon demand, manifesting as coordinated adjustments in biomass partitioning, source-sink relationships, and belowground investment that collectively determine whole-plant drought response.

5.2 Evaluation of the Central Hypothesis

The central hypothesis—that lower berry sugar demand in LSB genotypes favors a more comfortable carbon status under water deficit through reduced sink competition—receives *conditional support* with important contextual dependencies that refine our understanding of when and how the LSB trait confers drought advantages.

The hypothesis is not supported when evaluating LSB genotypes at their natural crop loads. Standard LSB plants showed no advantages in carbon balance, water use efficiency, or stress tolerance compared to non-LSB varieties under either acute or sustained water deficit. The absence of advantages at natural crop loads suggests that merely having lower per-berry sugar requirements provides insufficient selective pressure to drive allocation adjustments when overall plant carbon demand remains modest.

The hypothesis is supported when LSB genotypes carry normalized high fruit loads equalizing whole-plant carbon sink strength with non-LSB varieties. Under these conditions, LSB genotypes demonstrated superior allocation flexibility manifesting as simultaneous maintenance of fruit carbon accumulation and enhanced root investment under water deficit—a combination not achieved by non-LSB varieties under equivalent total carbon demand. This allocation flexibility operated specifically under sustained moderate water deficit maintained over 6-7 weeks rather than under acute severe stress, indicating that LSB advantages emerge through progressive resource partitioning adjustments requiring extended stress duration for full expression.

The refined interpretation is that the LSB trait provides potential allocation flexibility rather than constitutive drought advantage. This flexibility manifests only when specific conditions align: (1) high total plant carbon sink demand requiring strategic resource allocation decisions, (2) sustained moderate water deficit providing selective pressure

for allocation optimization while maintaining metabolic activity, and (3) sufficient stress duration for architectural adjustments to develop. The mechanism operates not through reduced carbon acquisition burden but through enhanced allocation autonomy—the capacity to invest in belowground resilience without compromising reproductive success when faced with simultaneous high carbon demand and water limitation.

5.3 Future Research Perspectives

The controlled pot experiments provided essential mechanistic insights but require field validation to assess whether observed advantages translate to commercial viticulture conditions. Multi-year field trials should evaluate whether root investment advantages enable improved deep water extraction in vineyard soils, whether allocation flexibility advantages accumulate progressively as root systems develop, and whether carryover effects influence subsequent growing seasons. Field trials must incorporate comprehensive harvest composition analysis and wine fermentation with sensory evaluation to confirm that allocation adjustments do not compromise wine quality.

The physiological and architectural responses documented here operate as integrated phenotypes without resolution of underlying molecular mechanisms or genetic architecture. Priority research directions include transcriptomic analysis of allocation regulation pathways, hormonal signaling characterization, sugar transporter expression profiling, and genetic dissection through controlled crosses segregating for LSB phenotype. Development of molecular markers for allocation flexibility traits would enable marker-assisted selection without requiring labor-intensive whole-plant phenotyping under controlled stress conditions.

The fundamental mechanism enabling LSB genotypes to maintain comparable berry size with 20-30% reduced sugar accumulation—the defining characteristic of the phenotype—remains mechanistically unresolved. Priority research should quantify pericarp cell wall composition throughout berry development and investigate alternative osmoregulatory mechanisms through comprehensive metabolomic profiling coupled with direct osmotic potential measurements. Understanding whether enhanced extensibility derives from few major loci or complex polygenic architecture will determine optimal breeding strategies.

Root system characterization requires advancement beyond total biomass quantification to assess specific root length, fine root density, branching patterns, and rhizosphere interactions. Practical deployment of LSB advantages in breeding programs requires development of high-throughput phenotyping protocols targeting allocation flexibility under sustained moderate stress rather than acute stress screening. Broader germplasm screening should evaluate LSB phenotype expression across diverse genetic backgrounds beyond the interspecific crosses examined here.

The dual climate adaptation potential of LSB genotypes—reducing alcohol levels under warming while enabling drought coexistence through allocation flexibility—positions this germplasm as valuable for regions experiencing both temperature increase and water scarcity. However, deployment requires integrated management approaches deliberately adjusting crop load upward, maintaining sustained moderate deficit irrigation, and potentially optimizing rootstock selection. Research should evaluate LSB × rootstock interactions and canopy management practices that optimize expression of LSB allocation advantages. Modeling approaches integrating the physiological response functions documented here with climate projections would identify regions and production systems where LSB advantages provide greatest value.

5.4 Final Statement

This thesis demonstrates that the Low Sugar Berry trait operates as a system-level characteristic enabling allocation flexibility under specific combinations of carbon demand and water availability rather than conferring constitutive drought tolerance through superior tissue-level hydraulic resistance or enhanced leaf-level physiological efficiency. The LSB advantage emerges not from reduced photosynthetic burden or intrinsic stress tolerance but from architectural autonomy—the capacity to simultaneously meet reproductive demands and invest in belowground resilience infrastructure when faced with high total plant carbon requirements under sustained moderate water deficit.

The findings challenge simplistic interpretations of source-sink relationships in perennial crops under stress, demonstrating that excessive sink strength may constrain allocation flexibility and force plants into suboptimal resource distribution patterns compromising long-term resilience. Moderating per-unit sink demand while maintaining total reproductive output through increased unit numbers enables more adaptive allocation strategies balancing immediate reproduction against stress mitigation investments.

For viticulture confronting climate change, the LSB phenotype offers a climate adaptation tool addressing both warming-driven alcohol increases and water scarcity-driven production constraints. However, realizing these advantages requires moving beyond simple varietal substitution to integrated management systems that deliberately manipulate crop load, maintain sustained moderate deficit irrigation, and potentially optimize rootstock selection. The context-dependency of LSB benefits means that deployment must target appropriate production environments and management scenarios rather than representing a universal solution.

The mechanistic insights developed here provide foundation for breeding programs targeting allocation flexibility as a selection objective, though practical implementation requires high-throughput phenotyping protocols, molecular marker development, and

field validation across diverse environments. Ultimately, this work contributes to fundamental understanding of how perennial crops navigate competing resource demands under environmental stress, demonstrating that architectural flexibility enabling dynamic resource reallocation may represent a more robust adaptation strategy than constitutive stress tolerance mechanisms. For grapevine specifically, the LSB trait exemplifies how breeding objectives targeting wine composition can generate unexpected collateral benefits when the physiological consequences of trait expression interact with whole-plant resource economy. This systems perspective on crop adaptation should inform future breeding efforts targeting resilience in an increasingly variable climate.

6 List of References

Alatzas, A., Theocharis, S., Miliordos, D., Leontaridou, K., Kanellis, A. K., Kotseridis, Y., Hatzopoulos, P., & Koundouras, S. (2021). The Effect of Water Deficit on Two Greek *Vitis vinifera* L. Cultivars: Physiology, Grape Composition and Gene Expression during Berry Development. *Plants, 10(9)*, 1947. https://doi.org/10.3390/plants10091947

Alston, J.M., Sambucci, O. (2019). Grapes in the World Economy. In: Cantu, D., Walker, M. (eds) *The Grape Genome. Compendium of Plant Genomes*. Springer, Cham. https://doi.org/10.1007/978-3-030-18601-2_1

Baeza, P., Junquera, P., Peiro, E., Lissarrague, J. R., Uriarte, D., & Vilanova, M. (2019). Effects of vine water status on yield components, vegetative response and must and wine composition. In *IntechOpen eBooks*. https://doi.org/10.5772/intechopen.87042

Bahn, M., Lattanzi, F. A., Hasibeder, R., Wild, B., Koranda, M., Danese, V., Brüggemann, N., Schmitt, M., Siegwolf, R., & Richter, A. (2013). Responses of belowground carbon allocation dynamics to extended shading in mountain grassland. *New Phytologist, 198(1)*, 116-126. https://doi.org/10.1111/nph.12138

Baltazar, M., Castro, I., & Gonçalves, B. (2025). Adaptation to Climate Change in Viticulture: The Role of Varietal Selection - A Review. *Plants, 14(1)*, 104. https://doi.org/10.3390/plants14010104

Bauerle, T. L., Smart, D. R., Bauerle, W. L., Stockert, C., & Eissenstat, D. M. (2008). Root foraging in response to heterogeneous soil moisture in two grapevines that differ in potential growth rate. *New Phytologist*, 179(3), 857-866. https://doi.org/10.1111/j.1469-8137.2008.02489.x

Bchir, A., Escalona, J. M., Gallé, A., Hernández-Montes, E., Tortosa, I., Brahm, A., & Medrano, H. (2016). Carbon isotope discrimination ($\delta^{13}C$) as an indicator of vine water status and water use efficiency (WUE): Looking for the most representative sample and sampling time. *Agricultural Water Management, 167*, 11-20. https://doi.org/10.1016/j.agwat.2015.12.018

Bennett, J., Jarvis, P., Creasy, G. L., & Trought, M. C. (2005). Influence of defoliation on overwintering carbohydrate reserves, return bloom, and yield of mature chardonnay grapevines. *American Journal of Enology and Viticulture, 56(4)*, 386-393. https://doi.org/10.5344/ajev.2005.56.4.386

Berhe, D. T. (2022). Post-Veraison Water Stress and Pruning Level on Merlot Grapevine (*Vitis vinifera* L.): Effects on Berry Development and Composition. *International Journal of Agronomy, 2022*, 1-11. https://doi.org/10.1155/2022/7307078

Bigard, A., Berhe, D. T., Maoddi, E., Sire, Y., Boursiquot, J., Ojeda, H., Péros, J., Doligez, A., Romieu, C., & Torregrosa, L. (2018). *Vitis vinifera* L. Fruit Diversity to Breed

Varieties Anticipating Climate Changes. *Frontiers in Plant Science, 9*. https://doi.org/10.3389/fpls.2018.00455

Bigard, A., Romieu, C., Sire, Y., & Torregrosa, L. (2020). *Vitis vinifera* L. Diversity for Cations and Acidity Is Suitable for Breeding Fruits Coping With Climate Warming. *Frontiers in Plant Science, 11*. https://doi.org/10.3389/fpls.2020.01175

Bigard, A., Romieu, C., Ojeda, H., & Torregrosa, L. J. (2022). The sugarless grape trait characterised by single berry phenotyping. *OENO One, 56(3)*, 89-102. https://doi.org/10.20870/oeno-one.2022.56.3.5495

Bigard, A., Wilhelm de Almeida, L., Pellegrino, A., Ojeda, H., Romieu, C., Torregrosa, L. (2025). *LSB Data Paper*. Not Published. https://doi.org/10.6084/m9.figshare.28308986.v1

Bonada, M., Sadras, V., Moran, M., & Fuentes, S. (2013). Elevated temperature and water stress accelerate mesocarp cell death and shrivelling, and decouple sensory traits in Shiraz berries. *Irrigation Science, 31(6)*, 1317-1331. https://doi.org/10.1007/s00271-013-0407-z

Bonarota, M., Toups, H. S., Bristow, S. T., Santos, P., Jackson, L. E., Cramer, G. R., & Barrios-Masias, F. H. (2024). Drought response and recovery mechanisms of grapevine rootstocks grafted to a common *Vitis vinifera* scion. *Plant Stress, 11*, 100346. https://doi.org/10.1016/j.stress.2024.100346

Brault, C., Segura, V., Roques, M., Lamblin, P., Bouckenooghe, V., Pouzalgues, N., Cunty, C., Breil, M., Frouin, M., Garcin, L., Camps, L., Ducasse, M., Romieu, C., Masson, G., Julliard, S., Flutre, T., & Cunff, L. L. (2024). Enhancing grapevine breeding efficiency through genomic prediction and selection index. *G3 Genes Genomes Genetics, 14(4)*. https://doi.org/10.1093/g3journal/jkae038

Brichet, N., Fournier, C., Turc, O., Strauss, O., Artzet, S., Pradal, C., et al. (2017). A robot-assisted imaging pipeline for tracking the growths of maize ear and silks in a high-throughput phenotyping platform. *Plant Methods 13*(1). https://doi.org/10.1186/s13007-017-0246-7

Brillante, L., Mathieu, O., Lévêque, J., & Bois, B. (2020). Carbon isotope discrimination ($\delta^{13}C$) of grape musts is a reliable tool for zoning and the physiological ground-truthing of sensor-based maps in precision viticulture. *Frontiers in Environmental Science, 8*, 561477. https://doi.org/10.3389/fenvs.2020.561477

Buesa, I., Pérez, D., Castel, J., Intrigliolo, D. S., & Castel, J. R. (2020). Effects of leaning grapevine canopy to the West on water use efficiency and yield under Mediterranean conditions. *Agricultural and Forest Meteorology, 295*, 108175. https://doi.org/10.1016/j.agrformet.2020.108166

Buesa, I., Hernández-Montes, E., Tortosa, I., Baraldi, G., Rosselló, M., Medrano, H., Escalona, J. M., & Mir, A. (2022). Unraveling the physiological mechanisms

underlying the intracultivar variability of water use efficiency in *Vitis vinifera* 'Grenache'. *Plants, 11(21)*, 3008. https://doi.org/10.3390/plants11213008

Cabrera-Bosquet, L., Fournier, C., Brichet, N., Welcker, C., Suard, B., and Tardieu, F. (2016). High-throughput estimation of incident light, light interception and radiationuse efficiency of thousands of plants in a phenotyping platform. *New Phytologist*, *212*(1), 269–281. https://doi.org/10.1111/nph.14027

Castellarin, S. D., Matthews, M. A., Di Gaspero, G., & Gambetta, G. A. (2007). Water deficits accelerate ripening and induce changes in gene expression regulating flavonoid biosynthesis in grape berries. *Planta*, *227*(1), 101–112. https://doi.org/10.1007/s00425-007-0598-8

Castellarin, S. D., Gambetta, G. A., Wada, H., Shackel, K. A., & Matthews, M. A. (2011). Fruit ripening in *Vitis vinifera*: Spatiotemporal relationships among turgor, sugar accumulation, and anthocyanin biosynthesis. *Journal of Experimental Botany, 62(12)*, 4345-4354. https://doi.org/10.1093/jxb/err150

Chaves, M. M., Zarrouk, O., Francisco, R., Costa, J. M., Santos, T., Regalado, A. P., Rodrigues, M. L., & Lopes, C. M. (2010). Grapevine under deficit irrigation: hints from physiological and molecular data. *Annals of Botany, 105(5)*, 661-676. https://doi.org/10.1093/aob/mcq030

Clemens, M., Faralli, M., Lagreze, J., Bontempo, L., Piazza, S., Varotto, S., Malnoy, M., Oechel, W., Rizzoli, A., & Dalla Costa, L. (2022). VvEPFL9-1 knock-out via CRISPR/Cas9 reduces stomatal density in grapevine. *Frontiers in Plant Science*, *13*. https://doi.org/10.3389/fpls.2022.878001

Comas, L. H., Bauerle, T. L., & Eissenstat, D. M. (2010). Biological and environmental factors controlling root dynamics and function: effects of root ageing and soil moisture. *Australian Journal of Grape and Wine Research*, *16*, 131–137. https://doi.org/10.1111/j.1755-0238.2009.00078.x

Cooper, M., & DeLacy, I. H. (1994). Relationships among analytical methods used to study genotypic variation and genotype-by-environment interaction in plant breeding multi-environment experiments. *Theoretical and Applied Genetics, 88(5)*, 561-572. https://doi.org/10.1007/BF01240919

Cosme, F., Gonçalves, B., Ines, A., Jordão, A. M., & Vilela, A. (2016). Grape and Wine Metabolites: Biotechnological Approaches to Improve Wine Quality. In *InTech eBooks*. https://doi.org/10.5772/64822

Costa, J. M., Vaz, M., Escalona, J., Egipto, R., Lopes, C., Medrano, H., & Chaves, M. M. (2016). Modern viticulture in southern Europe: Vulnerabilities and strategies for adaptation to water scarcity. *Agricultural Water Management, 164*, 5-18. https://doi.org/10.1016/j.agwat.2015.08.021

Cramer, G. R., Van Sluyter, S. C., Hopper, D. W., Pascovici, D., Keighley, T., & Haynes, P. A. (2013). Proteomic analysis indicates massive changes in metabolism prior to the inhibition of growth and photosynthesis of grapevine (*Vitis vinifera* L.) in

response to water deficit. *BMC Plant Biology, 13*(1), 49. https://doi.org/10.1186/1471-2229-13-49

Davies, C., & Robinson, S. P. (1996). Sugar accumulation in grape berries: Cloning of two putative vacuolar invertase cDNAs and their expression in grapevine tissues. *Plant Physiology, 111*(1), 275–283. https://doi.org/10.1104/pp.111.1.275

Delrot, S., Grimplet, J., Carbonell-Bejerano, P., Schwandner, A., Bert, P., Bavaresco, L., Costa, L. D., Di Gaspero, G., Duchêne, E., Hausmann, L., Malnoy, M., Morgante, M., Ollat, N., Pecile, M., & Vezzulli, S. (2020). Genetic and genomic approaches for adaptation of grapevine to climate change. In *Springer eBooks* (pp. 157-270). https://doi.org/10.1007/978-3-319-97946-5_7

Douthe, C., Medrano, H., Tortosa, I., Escalona, J. M., Hernández-Montes, E., & Pou, A. (2018). Whole-Plant water use in field grown grapevine: Seasonal and environmental effects on water and carbon balance. *Frontiers in Plant Science, 9*. https://doi.org/10.3389/fpls.2018.01540

Droulia, F., & Charalampopoulos, I. (2021). Future climate change impacts on European Viticulture: A review on recent scientific advances. *Atmosphere, 12*(4), 495. https://doi.org/10.3390/atmos12040495

Duursma, R. A. (2015). Plantecophys - an R package for analysing and modelling leaf gas exchange data. *PLoS ONE*, *10*(11), e0143346. https://doi.org/10.1371/journal.pone.0143346

Edson, C. E., Howell, G. S., & Flore, J. A. (1993). Influence of crop load on photosynthesis and dry matter partitioning of Seyval grapevines. I. Single leaf and whole vine response pre- and post-harvest. *American Journal of Enology and Viticulture*, *44*(2), 139–147. https://doi.org/10.5344/ajev.1993.44.2.139

Escalona, J. M., Flexas, J., Bota, J., & Medrano, H. (2003). Distribution of leaf photosynthesis and transpiration within grapevine canopies under different drought conditions. *Vitis*, *42*(2), 57–64. https://doi.org/10.5073/vitis.2003.42.57-64

Falchi, R., Bonghi, C., Drincovich, M. F., Famiani, F., Lara, M. V., Walker, R. P., & Vizzotto, G. (2020). Sugar metabolism in stone fruit: Source-sink relationships and environmental and agronomical effects. *Frontiers in Plant Science, 11*, 573982. https://doi.org/10.3389/fpls.2020.573982

Flexas, J., Bota, J., Escalona, J. M., Sampol, B., & Medrano, H. (2002). Effects of drought on photosynthesis in grapevines under field conditions: an evaluation of stomatal and mesophyll limitations. *Functional Plant Biology, 29*(4), 461. https://doi.org/10.1071/pp01119

Flexas, J., Bota, J., Cifre, J., Escalona, J. M., Galmés, J., Gulías, J., Lefi, E., Martínez-cañellas, S. F., Moreno, M. T., Ribas-carbó, M., Riera, D., Sampol, B., & Medrano, H. (2004). Understanding down-regulation of photosynthesis under

water stress: future prospects and searching for physiological tools for irrigation management. *Annals of Applied Biology, 144*(3), 273-283. https://doi.org/10.1111/j.1744-7348.2004.tb00343.x

Fraga, H., De Cortázar Atauri, I. G., & Santos, J. (2018). Viticultural irrigation demands under climate change scenarios in Portugal. *Agricultural Water Management, 196*, 66-74. https://doi.org/10.1016/j.agwat.2017.10.023

Gambetta, G. A., Herrera, J. C., Dayer, S., Feng, Q., Hochberg, U., & Castellarin, S. D. (2020). The physiology of drought stress in grapevine: Towards an integrative definition of drought tolerance. *Journal of Experimental Botany*, *71*(16), 4658–4676. https://doi.org/10.1093/jxb/eraa245

Girona, J., Mata, M., del Campo, J., Arbonés, A., Bartra, E., & Marsal, J. (2006). The use of midday leaf water potential for scheduling deficit irrigation in vineyards. *Irrigation Science*, *24*(2), 115–127. https://doi.org/10.1007/s00271-005-0015-7

Greer, D. H., & Sicard, S. M. (2009). The net carbon balance in relation to growth and biomass accumulation of grapevines (*Vitis vinifera* cv. Semillon) grown in a controlled environment. *Functional Plant Biology, 36*(7), 645-654. https://doi.org/10.1071/fp09037

Greer, D. H., & Weedon, M. M. (2012). Modelling photosynthetic responses to temperature of grapevine (*Vitis vinifera* cv. Semillon) leaves on vines grown in a hot climate. *Plant Cell & Environment*, *35*(6), 1050–1064. https://doi.org/10.1111/j.1365-3040.2011.02471.x

Guilpart, N., Metay, A., & Gary, C. (2014). Grapevine bud fertility and number of berries per bunch are determined by water and nitrogen stress around flowering in the previous year. *European Journal of Agronomy, 54*, 9-20. https://doi.org/10.1016/j.eja.2013.11.002

Hannah, L., Roehrdanz, P. R., Ikegami, M., et al. (2013). Climate change, wine, and conservation. *Proceedings of the National Academy of Sciences*, *110*(17), 6907–6912. https://doi.org/10.1073/pnas.1210127110

Harding, J. MW, Robinson, J. OBE MW, & Thomas, T. Q. (Eds.). (2023). *The Oxford companion to wine (5th ed.)*. Oxford University Press

Hochberg, U., Rockwell, F. E., Holbrook, N. M., & Cochard, H. (2018). Iso/Anisohydry: a Plant-Environment interaction rather than a simple hydraulic trait. *Trends in Plant Science, 23*(2), 112-120. https://doi.org/10.1016/j.tplants.2017.11.002

Holzapfel, B. P., & Smith, J. P. (2012). Developmental stage and climatic factors impact more on carbohydrate reserve dynamics of Shiraz than cultural practice. *American Journal of Enology and Viticulture, 63*(3), 333-342. https://doi.org/10.5344/ajev.2012.11071

Iglesias, D. J., Lliso, I., Tadeo, F. R., & Talon, M. (2002). Regulation of photosynthesis through source: sink imbalance in citrus is mediated by carbohydrate content in

leaves. *Physiologia Plantarum*, *116*(4), 563–572. https://doi.org/10.1034/j.1399-3054.2002.1160416.x

Intrigliolo, D. S., & Castel, J. R. (2010). Response of grapevine cv. 'Tempranillo' to timing and amount of irrigation: water relations, vine growth, yield and berry and wine composition. *Irrigation Science*, *28*(2), 113–125. https://doi.org/10.1007/s00271-009-0164-1

Jackson, R. S. (2008). *Wine science: Principles and Applications*. Academic Press.

Keller, M. (2005). Deficit irrigation and vine mineral nutrition. *American Journal of Enology and Viticulture*, *56*(3), 267–283. https://doi.org/10.5344/ajev.2005.56.3.267

Keller, M., Zhang, Y., Shrestha, P. M., Biondi, M., & Bondada, B. R. (2015). Sugar demand of ripening grape berries leads to recycling of surplus phloem water via the xylem. *Plant Cell & Environment, 38*(6), 1048-1059. https://doi.org/10.1111/pce.12465

Keller, M. (2020). *The science of grapevines*. Academic Press.

Khadatkar, A., Sawant, C. P., Thorat, D., Gupta, A., Jadhav, S., Gawande, D., & Magar, A. P. (2025). A comprehensive review on grapes (*Vitis* spp.) cultivation and its crop management. *Discover Agriculture, 3*(1). https://doi.org/10.1007/s44279-025-00162-2

Kliewer, W. M. (1965). Changes in concentration of glucose, fructose, and total soluble solids in flowers and berries of *Vitis vinifera*. *American Journal of Enology and Viticulture*, *16*(2), 101–110. https://doi.org/10.5344/ajev.1965.16.2.101

Kliewer, W. M., & Dokoozlian, N. K. (2005). Leaf Area/Crop Weight Ratios of grapevines: Influence on fruit composition and wine quality. *American Journal of Enology and Viticulture, 56*(2), 170-181. https://doi.org/10.5344/ajev.2005.56.2.170

Lebon, E., Pellegrino, A., Louarn, G., & Lecoeur, J. (2006). Branch development controls leaf area dynamics in grapevine (*Vitis vinifera*) growing in drying soil. *Annals of Botany*, *98*(1), 175–185. https://doi.org/10.1093/aob/mcl085

Lecourieux, F., Kappel, C., Lecourieux, D., Serrano, A., Torres, E., Arce-Johnson, P., & Delrot, S. (2013). An update on sugar transport and signalling in grapevine. *Journal of Experimental Botany, 65*(3), 821-832. https://doi.org/10.1093/jxb/ert394

Lecourieux, F., Kappel, C., Pieri, P., et al. (2017). Dissecting the biochemical and transcriptomic effects of a locally applied heat treatment on developing Cabernet Sauvignon grape berries. *Frontiers in Plant Science*, *8*. https://doi.org/10.3389/fpls.2017.00053

van Leeuwen, C., & Destrac-Irvine, A. (2017). Modified grape composition under climate change conditions requires adaptations in the vineyard. *OENO One, 51*(2), 147-154. https://doi.org/10.20870/oeno-one.2017.51.2.1647

van Leeuwen, C., Destrac-Irvine, A., Dubernet, M., Duchêne, E., Gowdy, M., Marguerit, E., Pieri, P., Parker, A., De Rességuier, L., & Ollat, N. (2019). An update on the impact of climate change in viticulture and potential adaptations. *Agronomy, 9*(9), 514. https://doi.org/10.3390/agronomy9090514

Li, Y., Tang, X., Sun, M., Zhang, H., & Xie, Z. (2024). Expression and function identification of senescence-associated genes under continuous drought treatment in grapevine (*Vitis vinifera* L.) leaves. *Physiology and Molecular Biology of Plants, 30*(6), 877-891. https://doi.org/10.1007/s12298-024-01465-2

Lovisolo, C., Perrone, I., Carra, A., Ferrandino, A., Flexas, J., Medrano, H., & Schubert, A. (2010). Drought-induced changes in development and function of grapevine (*Vitis* spp.) organs and in their hydraulic and non-hydraulic interactions at the whole-plant level: a physiological and molecular update. *Functional Plant Biology*, *37*(2), 98. https://doi.org/10.1071/fp09191

Marguerit, E., Brendel, O., Lebon, E., van Leeuwen, C., & Ollat, N. (2012). Rootstock control of scion transpiration and its acclimation to water deficit are controlled by different genes. *New Phytologist*, *194*(2), 416–429. https://doi.org/10.1111/j.1469-8137.2012.04059.x

Matthews, M. A., Cheng, G., & Weinbaum, S. A. (1987). Changes in water potential and dermal extensibility during grape berry development. *Journal of the American Society for Horticultural Science*, *112*(2), 314–319. https://doi.org/10.21273/jashs.112.2.314

Matthews, M. A., & Anderson, M. M. (1989). Reproductive development in grape (*Vitis vinifera* L.): responses to seasonal water deficits. *American Journal of Enology and Viticulture, 40*(1), 52-60. https://doi.org/10.5344/ajev.1989.40.1.52

Medrano, H., Escalona, J. M., Cifre, J., Bota, J., & Flexas, J. (2003). A ten-year study on the physiology of two Spanish grapevine cultivars under field conditions: effects of water availability from leaf photosynthesis to grape yield and quality. *Functional Plant Biology*, *30*(6), 607. https://doi.org/10.1071/fp02110

Medrano, H., Tomás, M., Martorell, S., Escalona, J. M., Pou, A., Fuentes, S., Flexas, J., & Bota, J. (2015). Improving water use efficiency of vineyards in semi-arid regions. A review. *Agronomy for Sustainable Development, 35*(2), 499-517. https://doi.org/10.1007/s13593-014-0280-z

Morales-Castilla, I., García de Cortázar-Atauri, I., Cook, B. I., et al. (2020). Diversity buffers winegrowing regions from climate change losses. *Proceedings of the National Academy of Sciences*, *117*(6), 2864–2869. https://doi.org/10.1073/pnas.1906731117

Moreno, D., Berli, F. J., Piccoli, P. N., & Bottini, R. (2011). Gibberellins and abscisic acid promote carbon allocation in roots and berries of grapevines. *Journal of Plant Growth Regulation, 30*(2), 220-228. https://doi.org/10.1007/s00344-010-9186-4

Mori, K., Goto-Yamamoto, N., Kitayama, M., & Hashizume, K. (2007). Loss of anthocyanins in red-wine grape under high temperature. *Journal of Experimental Botany*, *58*(8), 1935–1945. https://doi.org/10.1093/jxb/erm055

Muller, B., Pantin, F., Génard, M., Turc, O., Freixes, S., Piques, M., & Gibon, Y. (2011). Water deficits uncouple growth from photosynthesis, increase C content, and modify the relationships between C and growth in sink organs. *Journal of Experimental Botany, 62*(6), 1715-1729. https://doi.org/10.1093/jxb/erq438

Naor, A., Gal, Y., & Bravdo, B. (2002). Shoot and cluster thinning influence vegetative growth, fruit yield, and wine quality of 'Sauvignon blanc' grapevines *Journal of the American Society for Horticultural Science*, *127*(4), 628–634. https://doi.org/10.21273/jashs.127.4.628

Naulleau, A., Gary, C., Prévot, L., & Hossard, L. (2021). Evaluating strategies for adaptation to climate change in grapevine production- A systematic review. *Frontiers in Plant Science*, *11*. https://doi.org/10.3389/fpls.2020.607859

Nunan, K. J., Sims, I. M., Bacic, A., Robinson, S. P., & Fincher, G. B. (1998). Changes in cell wall composition during ripening of grape berries. *Plant Physiology, 118*(3), 783-792. https://doi.org/10.1104/pp.118.3.783

Ojeda, H., Deloire, A., Carbonneau, A., Ageorges, A., & Romieu, C. (1999). Berry development of grapevines: Relations between the growth of berries and their DNA content indicate cell multiplication and enlargement. *Vitis, 38*, 145-150. https://doi.org/10.5073/vitis.1999.38.145-150

Ojeda, H., Deloire, A., & Carbonneau, A. (2001). Influence of water deficits on grape berry growth. *HAL (Le Centre Pour La Communication Scientifique Directe)*. https://doi.org/10.5073/vitis.2001.40.141-145

Ojeda, H., Andary, C., Kraeva, E., Carbonneau, A., & Deloire, A. (2002). Influence of Pre- and Postveraison Water Deficit on Synthesis and Concentration of Skin Phenolic Compounds during Berry Growth of *Vitis vinifera* cv. Shiraz. *American Journal of Enology and Viticulture*. https://www.ajevonline.org/content/53/4/261.1

Ollat, N., Gaudillère, J.-P., & Marguerit, E. (2002). Grape berry development: A review. *OENO One, 36*(3), 111-119. https://oeno-one.eu/article/view/970

Ollat, N., Peccoux, A., Papura, D., Esmenjaud, D., Marguerit, E., Tandonnet, J., Bordenave, L., Cookson, S., Barrieu, F., Rossdeutsch, L., Lecourt, J., Lauvergeat, V., Vivin, P., Bert, P., & Delrot, S. (2015). Rootstocks as a component of adaptation to environment. *Wiley*, 68-108. https://doi.org/10.1002/9781118735985.ch4

Pagay, V. (2016). Environmental control of carbon and water relations in grapevine: Applications in irrigation scheduling and climate change scenarios [Doctoral dissertation, University of California]. *ProQuest Dissertations Publishing*.

Pastore, C., Frioni, T., & Diago, M. P. (2022). Editorial: Resilience of grapevine to climate change: From plant physiology to adaptation strategies *Frontiers in Plant Science*, *13*. https://doi.org/10.3389/fpls.2022.994267

Paul, M. J., & Foyer, C. H. (2001). Sink regulation of photosynthesis. *Journal of Experimental Botany*, *52*(360), 1383–1400. https://doi.org/10.1093/jexbot/52.360.1383

Paul, M. J., & Pellny, T. K. (2003). Carbon metabolite feedback regulation of leaf photosynthesis and development. *Journal of Experimental Botany*, *54*(382), 539–547. https://doi.org/10.1093/jxb/erg052

Pellegrino, A., Lebon, E., Simonneau, T. T., & Wery, J. (2005). Towards a simple indicator of water stress in grapevine (*Vitis vinifera* L.) based on the differential sensitivities of vegetative growth components. *Australian Journal of Grape and Wine Research, 11*(3), 306-315. https://doi.org/10.1111/j.1755-0238.2005.tb00030.x

Pellegrino, A., Gozé, E., Lebon, E., & Wery, J. (2006). A model-based diagnosis tool to evaluate the water stress experienced by grapevine in field sites. *European Journal of Agronomy, 25*(1), 49-59. https://doi.org/10.1016/j.eja.2006.03.003

Pellegrino, A., Clingeleffer, P., Cooley, N., & Walker, R. (2014). Management practices impact vine carbohydrate status to a greater extent than vine productivity. *Frontiers in Plant Science, 5*. https://doi.org/10.3389/fpls.2014.00283

Pirrello, C., Magon, G., Palumbo, F., Farinati, S., Lucchin, M., Barcaccia, G., & Vannozzi, A. (2023). Past, present, and future of genetic strategies to control tolerance to the main fungal and oomycete pathogens of grapevine. *Journal of Experimental Botany*, *74*(5), 1309–1330. https://doi.org/10.1093/jxb/erac487

Poorter, H., Niklas, K. J., Reich, P. B., Oleksyn, J., Poot, P., & Mommer, L. (2012). Biomass allocation to leaves, stems and roots: Meta-analyses of interspecific variation and environmental control. *New Phytologist, 193*(1), 30-50. https://doi.org/10.1111/j.1469-8137.2011.03952.x

Prieto, J. A., Lebon, É., & Ojeda, H. (2010). Stomatal behavior of different grapevine cultivars in response to soil water status and air water vapor pressure deficit. *OENO One, 44*(1), 9. https://doi.org/10.20870/oeno-one.2010.44.1.1459

Quereix, A., Dewar, R. C., Gaudillère, J. P., Dayau, S., & Valancogne, C. (2001). Sink feedback regulation of photosynthesis in vines: measurements and a model. *Journal of Experimental Botany*, *52*(365), 2313–2322. https://doi.org/10.1093/jexbot/52.365.2313

Reyes, F., DeJong, T., Franceschi, P., Tagliavini, M., & Gianelle, D. (2016). Maximum growth potential and periods of resource limitation in apple tree. *Frontiers in Plant Science, 7*, 233. https://doi.org/10.3389/fpls.2016.00233

Reynolds, A. G. (2021). Viticultural and vineyard management practices and their effects on grape and wine quality. In *Elsevier eBooks* (pp. 443-539). https://doi.org/10.1016/b978-0-08-102067-8.00012-9

Rienth, M., Torregrosa, L., Sarah, G., et al. (2016). Temperature desynchronizes sugar and organic acid metabolism in ripening grapevine fruits and remodels their transcriptome. *BMC Plant Biology*, *16*(1). https://doi.org/10.1186/s12870-016-0850-0

Rienth, M., Vigneron, N., Darriet, P., Sweetman, C., Burbidge, C., Bonghi, C., Walker, R. P., Famiani, F., & Castellarin, S. D. (2021). Grape Berry Secondary Metabolites and their Modulation by Abiotic Factors in a Climate Change Scenario- A Review. *Frontiers in Plant Science, 12*. https://doi.org/10.3389/fpls.2021.643258

Rogiers, S. Y., Hatfield, J. M., Gunta, S., & Keller, M. (2004). Solute transport into Shiraz berries during development and late-ripening shrinkage. *American Journal of Enology and Viticulture*, *57*(1), 73–80. https://doi.org/10.5344/ajev.2006.57.1.73

Rogiers, S. Y., Greer, D. H., Hatfield, J. M., et al. (2012). Stomatal response of an anisohydric grapevine cultivar to evaporative demand, available soil moisture and abscisic acid. *Tree Physiology*, *32*(3), 249–261. https://doi.org/10.1093/treephys/tpr131

Rogiers, S. Y., Greer, D. H., Liu, Y., Baby, T., & Xiao, Z. (2022). Impact of climate change on grape berry ripening: An assessment of adaptation strategies for the Australian vineyard. *Frontiers in Plant Science, 13*. https://doi.org/10.3389/fpls.2022.1094633

Romero, P., & García-García, J. (2020). The productive, economic, and social efficiency of vineyards using combined drought-tolerant rootstocks and efficient low water volume deficit irrigation techniques under Mediterranean semiarid conditions. *Sustainability*, *12*(5), 1930. https://doi.org/10.3390/su12051930

Romero, P., Navarro, J. M., & Ordaz, P. B. (2022). Towards a sustainable viticulture: The combination of deficit irrigation strategies and agroecological practices in Mediterranean vineyards. A review and update. *Agricultural Water Management*, *259*, 107216. https://doi.org/10.1016/j.agwat.2021.107216

Romero, P., Navarro, J. M., García, F., & Ordaz, P. B. (2025). The rootstock imparts different drought tolerance strategies in long-term field-grown deficit irrigated grapevines. *Scientia Horticulturae*, *346*, 114167. https://doi.org/10.1016/j.scienta.2025.114167

Rossdeutsch, L., Edwards, E., Cookson, S. J., Barrieu, F., Gambetta, G. A., Delrot, S., & Ollat, N. (2016). ABA-mediated responses to water deficit separate grapevine genotypes by their genetic background. *BMC Plant Biology, 16*(1). https://doi.org/10.1186/s12870-016-0778-4

Ruan, Y.-L., Patrick, J. W., Bouzayen, M., Osorio, S., & Fernie, A. R. (2013). Molecular regulation of seed and fruit set. *Trends in Plant Science, 17*(11), 656-665. https://doi.org/10.1016/j.tplants.2012.06.005

Rubel, F., & Kottek, M. (2010). Observed and projected climate shifts 1901-2100 depicted by world maps of the Köppen-Geiger climate classification. *Meteorologische Zeitschrift, 19*(2), 135-141. https://doi.org/10.1127/0941-2948/2010/0430

Sadras, V. O., & Moran, M. A. (2012). Elevated temperature decouples anthocyanins and sugars in berries of Shiraz and Cabernet Franc. *Australian Journal of Grape and Wine Research*, *18*(2), 115–122. https://doi.org/10.1111/j.1755-0238.2012.00180.x

Salazar-Parra, C., Aranjuelo, I., Pascual, I., Erice, G., Sanz-Sáez, Á., Aguirreolea, J., Sánchez-Díaz, M., Irigoyen, J. J., Araus, J. L., & Morales, F. (2015). Carbon balance, partitioning and photosynthetic acclimation in fruit-bearing grapevine (*Vitis vinifera* L. cv. Tempranillo) grown under simulated climate change (elevated CO2, elevated temperature and moderate drought) scenarios in temperature gradient greenhouses. *Journal of Plant Physiology, 174*, 97-109. https://doi.org/10.1016/j.jplph.2014.10.009

Santos, J. A., Fraga, H., Malheiro, A. C., Moutinho-Pereira, J., Dinis, L., Correia, C., Moriondo, M., Leolini, L., Dibari, C., Costafreda-Aumedes, S., Kartschall, T., Menz, C., Molitor, D., Junk, J., Beyer, M., & Schultz, H. R. (2020). A review of the potential climate change impacts and adaptation options for European viticulture. *Applied Sciences, 10*(9), 3092. https://doi.org/10.3390/app10093092

Savoi, S., Torregrosa, L., & Romieu, C. (2021). Transcripts switched off at the stop of phloem unloading highlight the energy efficiency of sugar import in the ripening *V. vinifera* fruit. *Horticulture Research, 8*(1). https://doi.org/10.1038/s41438-021-00628-6

Schmidt, M., Strack, T., Andrews, H. et al. A new climate for genomic and epigenomic innovation in grapevine. *Molecular Horticulture*, *5*(1). https://doi.org/10.1186/s43897-025-00171-1

Schultz, H. R. (2003). Differences in hydraulic architecture account for near-isohydric and anisohydric behaviour of two field-grown *Vitis vinifera* L. cultivars during drought. *Plant Cell & Environment*, *26*(8), 1393–1405. https://doi.org/10.1046/j.1365-3040.2003.01064.x

Shahbaz, U., Videau, P., Coulonnier, E., Papon, C., Navarro-Payá, D., Vidal Valenzuela, A., Matus, J. T., Malnoy, M., Zekri, O., Fiorani, F., Faralli, M., & Dalla Costa, L. (2025). Reduced stomatal density improves water-use efficiency in grapevine under climate scenarios of decreased water availability. *Plant Cell Reports, 44*, Article 236. https://doi.org/10.1007/s00299-025-03577-9

Shahood, R., Torregrosa, L., Savoi, S., & Romieu, C. (2020). First quantitative assessment of growth, sugar accumulation and malate breakdown in a single ripening berry. *OENO One, 54*(4), 1077-1092. https://doi.org/10.20870/oeno-one.2020.54.4.3787

Sheppard, D. (2025). Global vineyard values tumble as falling wine consumption hits industry. *Financial Times*. https://www.ft.com/content/8cb9d573-c449-48f9-97c1-e8d89fc7d112

Stoll, M., Loveys, B., & Dry, P. (2000). Hormonal changes induced by partial rootzone drying of irrigated grapevine. *Journal of Experimental Botany, 51*(350), 1627-1634. https://doi.org/10.1093/jexbot/51.350.1627

Stratonovitch, P., & Semenov, M. A. (2015). Heat tolerance around flowering in wheat identified as a key trait for increased yield potential in Europe under climate change. *Journal of Experimental Botany, 66*(12), 3599-3609. https://doi.org/10.1093/jxb/erv070

Sweetman, C., Sadras, V. O., Hancock, R. D., Soole, K. L., & Ford, C. M. (2014). Metabolic effects of elevated temperature on organic acid degradation in ripening *Vitis vinifera* fruit. *Journal of Experimental Botany, 65*(20), 5975-5988. https://doi.org/10.1093/jxb/eru343

Tardieu, F., Granier, C., & Muller, B. (2011). Water deficit and growth. Co-ordinating processes without an orchestrator? *Current Opinion in Plant Biology*, *14*(3), 283–289. https://doi.org/10.1016/j.pbi.2011.02.002

Tardieu, F., Simonneau, T., & Muller, B. (2018). The physiological basis of drought tolerance in crop plants: A scenario-dependent probabilistic approach. *Annual Review of Plant Biology, 69*, 733-759. https://doi.org/10.1146/annurev-arplant-042817-040218

Terrier, N., & Romieu, C. (2001). Grape berry acidity. In K. A. Roubelakis-Angelakis (Ed.), Molecular biology and biotechnology of the grapevine (pp. 35-57). In *Springer eBooks* (pp. 35–57). https://doi.org/10.1007/978-94-017-2308-4_2

Tilbrook, J., & Tyerman, S. D. (2008). Cell death in grape berries: Varietal differences linked to xylem pressure and berry weight loss. *Functional Plant Biology, 35*(3), 173-184. https://doi.org/10.1071/FP07278

De Toda F, M., & Balda, P. (2017). *Delaying berry ripening through manipulating leaf area to fruit ratio*. DIGITAL.CSIC. http://hdl.handle.net/10261/144000

Tonietto, J., & Carbonneau, A. (2004). A multicriteria climatic classification system for grape-growing regions worldwide. *Agricultural and Forest Meteorology, 124*(1-2), 81-97. https://doi.org/10.1016/j.agrformet.2003.06.001

Tyerman, S., Vandeleur, R., Shelden, M., Tilbrook, J., Mayo, G., Gilliham, M., & Kaiser, B. (2009). Water Transport & Aquaporins in Grapevine. In *Springer eBooks* (pp. 73-104). https://doi.org/10.1007/978-90-481-2305-6_4

Urban, L., Aarrouf, J., & Bidel, L. P. R. (2017). Assessing the Effects of Water Deficit on Photosynthesis Using Parameters Derived from Measurements of Leaf Gas Exchange and of Chlorophyll a Fluorescence. *Frontiers in Plant Science, 8*. https://doi.org/10.3389/fpls.2017.02068

Veley, K. M., Okwuonu, I., Jensen, G., Yoder, M., Taylor, N. J., Meyers, B. C., & Bart, R. S. (2021). Gene tagging via CRISPR-mediated homology-directed repair in cassava. *G3 Genes Genomes Genetics*, *11*(4). https://doi.org/10.1093/g3journal/jkab028

Verdenal, T., Dienes-Nagy, Á., Spangenberg, J. E., Zufferey, V., Spring, J., Viret, O., Marin-Carbonne, J., & van Leeuwen, C. (2021). Understanding and managing nitrogen nutrition in grapevine: a review. *OENO One, 55*(1), 1-43. https://doi.org/10.20870/oeno-one.2021.55.1.3866

Villalobos-González, L., Alarcón, N., Bastías, R., Pérez, C., Sanz, R., Peña-Neira, Á., et al. (2022). Photoprotection is achieved by photorespiration and modification of the leaf incident light, and their extent is modulated by the stomatal sensitivity to water deficit in grapevines. *Plants, 11*, 1050. https://doi.org/10.3390/plants11081050

Vincent, C., Rowland, D., Na, C., & Schaffer, B. (2019). Primed acclimation: A physiological process offers a strategy for more resilient and irrigation-efficient crop production. *Plant Science, 295*, 110240. https://doi.org/10.1016/j.plantsci.2019.110240

Vivin, P., Castelan, M., & Gaudillère, J. (2002). A source/sink model to simulate seasonal allocation of carbon in grapevine. *Acta Horticulturae, 584*, 43-56. https://doi.org/10.17660/actahortic.2002.584.4

Wada, H., Shackel, K. A., & Matthews, M. A. (2008). Fruit ripening in *Vitis vinifera*: Apoplastic solute accumulation accounts for pre-veraison turgor loss in berries. *Planta, 227*(6), 1351-1361. https://doi.org/10.1007/s00425-008-0707-3

Walker, R. P., Bonghi, C., Varotto, S., Battistelli, A., Burbidge, C. A., Castellarin, S. D., Chen, Z., Darriet, P., Moscatello, S., Rienth, M., Sweetman, C., & Famiani, F. (2021). Sucrose Metabolism and Transport in Grapevines, with Emphasis on Berries and Leaves, and Insights Gained from a Cross-Species Comparison. *International Journal of Molecular Sciences, 22*(15), 7794. https://doi.org/10.3390/ijms22157794

Wilhelm De Almeida, L., Pellegrino, A., Fontez, B., Torregrosa, L., & Ojeda, H. (2023). Short and long-term acclimation to water status at leaf and plant level of fungus-tolerant genotypes. *OENO One, 57*(2), 203-218. https://doi.org/10.20870/oeno-one.2023.57.2.7431

Wilhelm De Almeida, L., Pastenes, C., Ojeda, H., Torregrosa, L., & Pellegrino, A. (2024a). Water deficit differentially modulates leaf photosynthesis and

transpiration of fungus-tolerant *Muscadinia* x *Vitis* hybrids. *Frontiers in Plant Science, 15*. https://doi.org/10.3389/fpls.2024.1405343

Wilhelm de Almeida, L., Ojeda, H., Pellegrino, A., & Torregrosa, L. (2024b). Carbon trade-offs in the fruits of fungus-tolerant *Muscadinia* x *Vitis* hybrids exposed to water deficit. *Plant Physiology and Biochemistry*, *212*, 108774. https://doi.org/10.1016/j.plaphy.2024.108774

Yang, C., Ceglar, A., Menz, C., Martins, J., Fraga, H., & Santos, J. A. (2023). Performance of seasonal forecasts for the flowering and veraison of two major Portuguese grapevine varieties. *Agricultural and Forest Meteorology, 331*, 109342. https://doi.org/10.1016/j.agrformet.2023.109342

Yildirim, K., Yagci, A., Sucu, S., & Tunç, S. (2018). Responses of grapevine rootstocks to drought through altered root system architecture and root transcriptomic regulations. *Plant Physiology and Biochemistry*, *127*, 256–268. https://doi.org/10.1016/j.plaphy.2018.03.034

Zapata, C., Deléens, E., Chaillou, S., & Magné, C. (2004). Partitioning and mobilization of starch and N reserves in grapevine (*Vitis vinifera* L.). *Journal of Plant Physiology, 161*(9), 1031-1040. https://doi.org/10.1016/j.jplph.2003.11.009

Zhang, X., Wang, X., Wang, X., Xia, G., Pan, Q., Fan, R., Wu, F., Yu, X., & Zhang, D. (2006). A Shift of Phloem Unloading from Symplasmic to Apoplasmic Pathway Is Involved in Developmental Onset of Ripening in Grape Berry. *PLANT PHYSIOLOGY, 142(1), 220–232. https://doi.org/10.1104/pp.106.081430*

Zhang, Y., & Keller, M. (2017). Discharge of surplus phloem water may be required for normal grape ripening. *Journal of Experimental Botany*, erw476. https://doi.org/10.1093/jxb/erw476

Zhu, J., Fraysse, R., Trought, M. C., Raw, V., Yang, L., Greven, M., Martin, D., & Agnew, R. (2020). Quantifying the seasonal variations in grapevine yield components based on pre- and post-flowering weather conditions. *OENO One, 54*(2). https://doi.org/10.20870/oeno-one.2020.54.2.2926

Zufferey, V., Cochard, H., Ameglio, T., Spring, J. L., & Viret, O. (2011). Diurnal cycles of embolism formation and repair in petioles of grapevine (*Vitis vinifera* cv. Chasselas). *Journal of Experimental Botany*, *62*(11), 3885–3894. https://doi.org/10.1093/jxb/err081

Zufferey, V., Murisier, F., Vivin, P., Belcher, S., Lorenzini, F., Spring, J.L., & Viret, O. (2012). Carbohydrate reserves in grapevine (*Vitis vinifera* L. "Chasselas"): The influence of the leaffruit ratio. *VITIS - Journal of Grapevine Research, 51*(3), 103-110. https://doi.org/10.5073/vitis.2012.51.103-110

7 Annex

7.1 Supplementary Tables

Supplementary Table S1. Individual plant biomass at green stage.

Genotype	Plant ID	Shoot FW (g)	Leaf FW (g)	Trunk FW (g)	Root FW (g)	Leaf Area (cm^2)	Total Veg FW (g)
G14	2036	153.17	135.05	49.41	219.55	12862.0	337.63
G14	2038	129.34	125.47	41.29	196.31	9708.7	296.10
G5	2002	143.29	125.30	29.68	163.67	9164.1	298.27
G5	2003	135.18	127.92	32.72	159.28	9358.9	295.82
G5	2108	138.67	118.24	31.58	153.51	12143.1	288.49
G5	2017	87.39	86.32	38.72	71.18	6394.4	212.43
3159	2042	258.54	145.84	33.50	115.71	13070.4	437.88
3159	2040	244.49	127.20	40.03	158.72	11579.3	411.72
3159	2054	264.13	135.83	45.25	173.27	12567.9	445.21
3159	2043	173.49	114.34	44.43	158.08	9017.3	332.26
3176	2065	64.62	81.75	57.19	119.11	7147.2	203.56
3176	2073	64.57	93.77	64.75	126.91	9785.6	223.09
3176	2069	131.16	134.33	70.47	122.53	11138.0	335.96
Luminan	2082	165.11	105.11	56.83	120.21	8654.0	327.05

Destructive sampling measurements from 14 plants at the end of STS-G, including shoot fresh weight (FW), leaf FW, trunk FW, root FW, leaf area, and total vegetative FW. Five genotypes were assessed: G14, G04, G5 (LSB); 3159, 3176 (non-LSB); and Luminan (control). These data established initial biomass estimates for FTSW calculations and provided allometric relationships for subsequent experiments (STS-R and LTS).

Supplementary Table S2. Mean biomass by genotype at green stage.

Genotype	n	Shoot_FW	Leaf_FW	Trunk_FW	Root_FW	Leaf_Area	Total_Veg
3159	4	235.16 ± 41.94	130.80 ± 13.36	40.80 ± 5.38	151.44 ± 24.83	11558.7 ± 1804.0	406.77 ± 51.71
3176	3	86.78 ± 38.43	103.28 ± 27.55	64.14 ± 6.66	122.85 ± 3.91	9356.9 ± 2029.6	254.20 ± 71.47
G14	2	141.25 ± 16.85	130.26 ± 6.77	45.35 ± 5.74	207.93 ± 16.43	11285.4 ± 2229.7	316.87 ± 29.37
G5	4	126.13 ± 26.04	114.45 ± 19.19	33.17 ± 3.90	136.91 ± 44.02	9265.1 ± 2348.2	273.75 ± 41.09
Luminan	1	165.11 ± NA	105.11 ± NA	56.83 ± NA	120.21 ± NA	8654.0 ± NA	327.05 ± NA

Mean values (± standard error) of shoot fresh weight (FW), leaf FW, trunk FW, root FW, leaf area, and total vegetative FW calculated from destructive sampling of 14 plants at the end of STS-G. Sample sizes varied by genotype: 3159 (n = 4), 3176 (n = 3), G14 (n = 2), G5 (n = 4), and Luminan (n = 1, no variance calculated). These mean genotype values were used to estimate initial vegetative biomass at the start of

subsequent experiments (STS-R and LTS), providing the baseline plant weight required for accurate FTSW calculations during the priming phase and treatment periods. Shoot weight showed substantial genotypic variation, ranging from 141.25 g (G14) to 235.16 g (3159), reflecting differences in vegetative vigor among genotypes under well-watered conditions during the vegetative growth phase.

Supplementary Table S3. Individual plant phenological timing and treatment duration.

Plant ID	Treatment	Genotype	Veraison Date (DOY)	Harvest Date (DOY)	Treatment Duration (days)
2071	WW	3176	May 20, 2025 (140)	July 3, 2025 (184)	44
2011	WW	G5	May 22, 2025 (142)	July 9, 2025 (190)	48
2006	WD	G5	May 20, 2025 (140)	July 9, 2025 (190)	50
2052	WD	3159	May 22, 2025 (142)	July 8, 2025 (189)	47
2077	WD	3176	May 21, 2025 (141)	July 3, 2025 (184)	43
2046	WW	3159	May 20, 2025 (140)	July 8, 2025 (189)	49
2064	WW	3176	May 19, 2025 (139)	July 3, 2025 (184)	45
3121	WD	3176	May 19, 2025 (139)	July 3, 2025 (184)	45
2004	WW	G5	May 20, 2025 (140)	July 9, 2025 (190)	50
2018	WW-C	G5	May 22, 2025 (142)	July 10, 2025 (191)	49
2016	WD-C	G5	May 20, 2025 (140)	July 9, 2025 (190)	50
2058	WW	3159	May 19, 2025 (139)	July 8, 2025 (189)	50
2026	WD-C	G14	May 27, 2025 (147)	July 2, 2025 (183)	36
2053	WD	3159	May 17, 2025 (137)	July 8, 2025 (189)	52
2005	WD	G5	May 20, 2025 (140)	July 9, 2025 (190)	50
2007	WW	G5	May 20, 2025 (140)	July 10, 2025 (191)	51
2101B	WD-C	G5	May 22, 2025 (142)	July 9, 2025 (190)	48
2050	WD	3159	May 19, 2025 (139)	July 8, 2025 (189)	50
2020	WD-C	G14	May 21, 2025 (141)	July 2, 2025 (183)	42
2051	WW	3159	May 21, 2025 (141)	July 8, 2025 (189)	48
2009	WW	G5	May 30, 2025 (150)	July 10, 2025 (191)	41
2060	WW	3176	May 19, 2025 (139)	July 3, 2025 (184)	45
2029	WW	G14	May 22, 2025 (142)	July 2, 2025 (183)	41
2100A	WD	G5	May 22, 2025 (142)	July 9, 2025 (190)	48
3120	WD	3176	May 27, 2025 (147)	July 3, 2025 (184)	37
2104	WW-C	G5	May 26, 2025 (146)	July 10, 2025 (191)	45
2037	WW	G14	May 21, 2025 (141)	July 2, 2025 (183)	42

2019	WD	3159	May 17, 2025 (137)	July 8, 2025 (189)	52
2012	WW	G5	May 26, 2025 (146)	July 10, 2025 (191)	45
2021	WD	G14	May 22, 2025 (142)	July 2, 2025 (183)	41
2103	WD-C	G5	May 25, 2025 (145)	July 9, 2025 (190)	45
2062	WD	3176	May 16, 2025 (136)	July 3, 2025 (184)	48
2032	WW	G14	May 21, 2025 (141)	July 2, 2025 (183)	42
2057	WW	3159	May 22, 2025 (142)	July 8, 2025 (189)	47
2073	WD	3176	May 19, 2025 (139)	July 3, 2025 (184)	45
2024	WD-C	G14	May 22, 2025 (142)	July 2, 2025 (183)	41
2028	WW	G14	May 21, 2025 (141)	July 2, 2025 (183)	42
2063	WW	3176	May 16, 2025 (136)	July 3, 2025 (184)	48
2035	WD	G14	May 16, 2025 (136)	July 2, 2025 (183)	47
2028	WD-C	G5	May 26, 2025 (146)	July 9, 2025 (190)	44
2000	WD	G5	May 22, 2025 (142)	July 9, 2025 (190)	48
2045	WW	3159	May 22, 2025 (142)	July 8, 2025 (189)	47
2023	WD-C	G14	May 21, 2025 (141)	July 2, 2025 (183)	42
2055	WD	G5	May 23, 2025 (143)	July 9, 2025 (190)	47
2008	WD-C	G5	May 22, 2025 (142)	July 9, 2025 (190)	48
2076	WW	3176	May 17, 2025 (137)	July 3, 2025 (184)	47
2081	WW	3159	May 17, 2025 (137)	July 8, 2025 (189)	52
2044	WW	3159	May 18, 2025 (138)	July 8, 2025 (189)	51
2028	WW	G14	May 22, 2025 (142)	July 2, 2025 (183)	41
2083	WW	3176	May 20, 2025 (140)	July 3, 2025 (184)	44
2035	WW	G14	May 20, 2025 (140)	July 2, 2025 (183)	43
2019	WD	G5	May 27, 2025 (147)	July 9, 2025 (190)	43
2014	WW-C	G5	May 20, 2025 (140)	July 10, 2025 (191)	51
2025	WW	3159	May 16, 2025 (136)	July 8, 2025 (189)	53
2104	WD-C	G5	May 25, 2025 (145)	July 9, 2025 (190)	45
2070	WW	3176	May 19, 2025 (139)	July 3, 2025 (184)	45

Veraison date defined as the day when 50% of berries on the plant showed softening. Harvest date determined when berries reached physiological ripeness (maximum volume and stable soluble solids content). Treatment duration calculated from veraison (treatment initiation) to harvest. DOY = Day of Year. Plants sorted by Plant ID.

Supplementary Table S4. Individual plant measurements at harvest for all genotype and treatment combinations.

Plant ID	Genotype	Treatment	Berry Number	Mean Berry Weight (g)	Fresh Fruit Weight (kg)	°Brix	Leaf Area (m^2)	Fruit:Leaf (kg m^{-2})	Soluble Solids:LA (g m^{-2})
2049	3159	WD	237	1,44	0,34	26,3	0,97	0,35	92,6
2050	3159	WD	202	1,71	0,34	25	1,08	0,32	79,8
2052	3159	WD	300	2,03	0,61	21,1	0,81	0,75	158,7
2053	3159	WD	277	1,61	0,45	24,6	0,83	0,53	131,4
2055	3159	WD	220	1,74	0,38	24,4	0,9	0,43	104,4
2056	3159	WD	262	1,52	0,4	24,7	0,65	0,61	151,7
2041	3159	WW	247	1,64	0,4	22,8	1,08	0,38	85,4
2045	3159	WW	300	2	0,6	24,6	1,48	0,41	100
2046	3159	WW	244	1,56	0,38	23	1,21	0,32	72,9
2051	3159	WW	170	1,81	0,31	23,2	1,18	0,26	60,4
2057	3159	WW	205	1,66	0,34	21,5	0,63	0,54	116,1
2058	3159	WW	300	1,77	0,53	23,3	1,23	0,43	100,6
2076	3176	WD	200	2,66	0,53	21	0,91	0,59	123,4
2077	3176	WD	300	1,8	0,54	21,3	0,83	0,65	138,6
2079	3176	WD	175	1,91	0,33	23,6	0,87	0,38	90,7
3120	3176	WD	295	1,87	0,55	21,1	0,84	0,66	139,3
3121	3176	WD	194	1,97	0,38	23,1	0,66	0,58	133,4
2060	3176	WW	212	1,9	0,4	23,5	1,26	0,32	75,3
2062	3176	WW	200	2,42	0,48	23,9	1,86	0,26	62,1
2063	3176	WW	231	1,41	0,33	24,8	1,74	0,19	46,4
2064	3176	WW	226	2,28	0,51	23,6	1,14	0,45	106,4
2070	3176	WW	300	1,94	0,58	23,4	1,79	0,33	76,1
2071	3176	WW	173	2,16	0,37	23,9	1,83	0,2	48,6
2021	G14	WD	200	2,18	0,44	22,2	0,86	0,51	112,4
2024	G14	WD	278	1,44	0,4	18,4	0,9	0,44	81,9
2035	G14	WD	200	1,53	0,31	21,8	0,99	0,31	66,9
2037	G14	WD	200	1,96	0,39	20,5	0,71	0,55	112,5
2020	G14	WD-C	260	2,19	0,57	19,3	0,85	0,67	129,4
2023	G14	WD-C	300	1,99	0,6	20,4	0,83	0,72	147,2
2026	G14	WD-C	315	1,84	0,58	20,1	0,91	0,64	128,1
2039	G14	WD-C	300	1,95	0,59	20,2	0,79	0,74	150,1
2025	G14	WW	242	1,89	0,46	21,4	0,97	0,47	100,3
2028	G14	WW	170	1,96	0,33	20,7	0,78	0,43	88,9
2029	G14	WW	200	2,06	0,41	21,4	1,1	0,37	79,9
2032	G14	WW	200	1,08	0,22	19,4	0,85	0,25	49,2
2000	G5	WD	186	1,84	0,34	22,6	0,67	0,51	114,6
2005	G5	WD	203	1,7	0,34	24,4	0,84	0,41	99,3
2006	G5	WD	200	1,89	0,38	22,4	0,87	0,44	97,4
2010	G5	WD	295	1,69	0,5	18,9	0,88	0,57	107,3
2100A	G5	WD	175	1,87	0,33	23,5	0,8	0,41	96,1

2100B	G5	WD	245	1,64	0,4	25,3	0,85	0,47	119,6
2008	G5	WD-C	300	2,2	0,66	20,4	0,84	0,78	160
2016	G5	WD-C	300	1,78	0,53	19,8	0,69	0,77	153,6
2019	G5	WD-C	300	2,44	0,73	20,4	0,78	0,94	191,4
2101B	G5	WD-C	300	2,01	0,6	21,4	1,04	0,58	123,9
2107	G5	WD-C	282	2,26	0,64	22,5	0,87	0,74	165,5
2001	G5	WW	100	2,28	0,23	21,5	1,24	0,18	39,6
2007	G5	WW	300	2,22	0,67	21,4	1,14	0,59	125,9
2009	G5	WW	288	2,18	0,63	21,6	0,85	0,74	159,9
2012	G5	WW	194	2,18	0,42	21,4	1,27	0,33	71,2
2013	G5	WW	251	2,18	0,55	21,1	1,07	0,51	108
2014	G5	WW-C	300	2,32	0,7	21,7	1,18	0,59	127,7
2018	G5	WW-C	230	2,07	0,48	22,1	1,41	0,34	74,5
2102A	G5	WW-C	300	2,33	0,7	20,8	1,19	0,59	122,1
2102B	G5	WW-C	300	2,63	0,79	22	1,07	0,74	163

Individual plant values for fresh fruit weight, berry composition, leaf area, and source-sink balance ratios. Plant ID = unique plant identifier; Berry Number = total berries counted per plant at harvest; Mean Berry Weight = fresh weight per individual berry calculated as (Fresh Fruit Weight × 1000) / Berry Number; Fresh Fruit Weight = total fruit fresh weight per plant (kg); °Brix = soluble solids concentration measured by digital refractometry on fresh juice; Leaf Area = total leaf area per plant (m^2) measured at harvest from daily transpiration data via the Phenodyn automated weighing system; Fruit:Leaf = ratio of fresh fruit weight to leaf area (kg m^{-2}); Soluble Solids:LA = total soluble solids per unit leaf area (g m^{-2}) calculated as (°Brix × Fresh Fruit Weight × 10) / Leaf Area, representing sink demand normalized by source capacity. Treatments: WD = water deficit (FTSW ~0.20), WW = well-watered (FTSW ~0.65); WD-C and WW-C = carbon-normalized treatments with increased berry load (+50% berry number target, actual +34-36%) applied only to LSB genotypes G5 and G14 to equalize carbon sink strength with non-LSB genotypes. Non-LSB genotypes (3159, 3176) and standard LSB treatments maintained ~140 berries per plant; carbon-normalized LSB treatments maintained ~210 berries per plant (actual harvest values: 203-300 berries per plant, see Berry Number column). Plant 2068 (genotype 3176 WD, 438 berries) was excluded as statistical outlier. Data represent physiological ripeness at harvest (DOY 183-191, July 2-10, 2025). n = 55 plants total. These data support the summary statistics presented in Table 9.

Supplementary Table S5. Individual berry composition data at harvest by plant, genotype, and treatment.

Plant ID	Genotype	Treatment	Glucose (mmol/L)	Fructose (mmol/L)	Total Hexoses (mmol/L)	Malic Acid (meq/L)	Tartaric Acid (meq/L)	Total Organic Acids (meq/L)	Malic:Tartaric Ratio	Sugar:Acid Ratio
2049	3159	WD	1489,2	1503,3	2992,5	37,3	74,6	111,9	0,446	66,6
2050	3159	WD	1414,3	1418,8	2833,1	40,3	74,6	114,9	0,482	61,5
2052	3159	WD	1187,8	1201,8	2389,6	29,8	72	101,8	0,37	58,2
2053	3159	WD	1404,9	1407,3	2812,2	40,3	69,3	109,6	0,519	64,1
2055	3159	WD	1382,7	1386,3	2769	37,3	68	105,2	0,49	65,6
2056	3159	WD	1429,8	1388,5	2818,3	55,2	73,3	128,5	0,673	55,2
2041	3159	WW	1263,3	1300,9	2564,2	37,3	72	109,2	0,463	58,5
2045	3159	WW	1382,1	1385	2767,1	61,2	73,3	134,4	0,745	51,9
2046	3159	WW	1295,5	1293,8	2589,3	49,2	73,3	122,5	0,6	53
2051	3159	WW	1322,2	1352,8	2674,9	43,3	69,3	112,5	0,558	59,5
2057	3159	WW	1238,9	1218	2456,9	58,2	73,3	131,5	0,709	47,1
2058	3159	WW	1342,1	1322,8	2664,9	44,7	69,3	114	0,577	58,6
2076	3176	WD	1205	1075,3	2280,4	65,6	90,6	156,2	0,647	36,7
2077	3176	WD	1202,8	1076,9	2279,7	77,6	69,3	146,9	1	39,5
2079	3176	WD	1359,3	1166,9	2526,2	144,7	99,9	244,6	1,293	26,5
3120	3176	WD	1189,5	1094,7	2284,2	67,1	73,3	140,4	0,818	41,2
3121	3176	WD	1327,7	1176,3	2504	96,9	86,6	183,6	1	34,7
2060	3176	WW	1349,4	1187,4	2536,7	67,1	85,3	152,4	0,703	41,9
2062	3176	WW	1418,7	1216,8	2635,5	95,5	85,3	180,7	1	37,1
2063	3176	WW	1425,4	1236,7	2662,1	126,8	94,6	221,4	1,197	30,7
2064	3176	WW	1407,6	1230	2637,7	76,1	74,6	150,7	0,911	44,4
2070	3176	WW	1338,3	1168,7	2506,9	80,5	74,6	155,2	0,964	41,1
2071	3176	WW	1405,4	1205,2	2610,6	117,8	89,3	207,1	1,179	32,2
2021	G14	WD	1133,4	1079,6	2213	65,6	83,9	149,6	0,698	37,3
2024	G14	WD	1154	1036	2189,9	82	76	158	0,965	35,2
2035	G14	WD	1187,8	1112,2	2300	83,5	97,3	180,8	0,767	32,1
2037	G14	WD	1235	1157	2392	55,2	81,3	136,5	0,607	44
2020	G14	WD-C	1045,2	996,7	2041,9	52,2	77,3	129,5	0,603	39,6
2023	G14	WD-C	1171,7	1087,5	2259,3	67,1	74,6	141,7	0,804	40,3
2026	G14	WD-C	1099	1031,2	2130,2	71,6	93,3	164,9	0,686	32,5
2039	G14	WD-C	1092,4	1084,3	2176,7	47,7	87,9	135,7	0,485	40
2025	G14	WW	1054,1	972,2	2026,2	73,1	95,9	169	0,681	30,2
2028	G14	WW	1178,4	1084,3	2262,7	74,6	81,3	155,9	0,82	36,7
2029	G14	WW	1206,7	1100,3	2307	80,5	87,9	168,5	0,818	34,6
2032	G14	WW	1107,3	1019,2	2126,6	62,6	73,3	135,9	0,764	39,5
2000	G5	WD	1423,2	1277,1	2700,3	70,1	68	138,1	0,922	49,6
2005	G5	WD	1407,1	1309,1	2716,2	70,1	73,3	143,4	0,855	48
2006	G5	WD	1290	1198,9	2488,9	64,1	68	132,1	0,843	47,7
2010	G5	WD	1040,2	1042,9	2083,1	71,6	60	131,6	1,067	40,4
2100A	G5	WD	1358,2	1255,7	2614	65,6	62,6	128,3	0,936	51,8
2100B	G5	WD	1446,5	1365,1	2811,6	59,7	76	135,6	0,702	52,2
2008	G5	WD-C	1120,7	1110,7	2231,4	47,7	70,6	118,4	0,604	47,3
2016	G5	WD-C	1050,7	1069,3	2120,1	55,2	73,3	128,5	0,673	41,5
2019	G5	WD-C	1155,1	1137,3	2292,4	61,2	60	121,1	0,911	48
2101B	G5	WD-C	1185,1	1144,5	2329,5	64,1	61,3	125,4	0,935	47,2
2107	G5	WD-C	1267,8	1215,2	2482,9	64,1	64	128,1	0,896	49,2
2001	G5	WW	1238,9	1128,8	2367,7	67,1	61,3	128,4	0,978	46,9
2007	G5	WW	1238,9	1147,7	2386,6	59,7	57,3	117	0,93	51,8
2009	G5	WW	1239,5	1148	2387,5	49,2	58,6	107,9	0,75	55,9
2012	G5	WW	1232,2	1128,7	2361	64,1	54,6	118,8	1,049	50,6

2013	G5	WW	1247,8	1166,8	2414,6	73,1	61,3	134,4	1,065	45,8
2014	G5	WW-C	1290,5	1190,2	2480,7	65,6	57,3	122,9	1,023	51,4
2018	G5	WW-C	1285	1168,2	2453,2	68,6	57,3	125,9	1,07	49,7
2102A	G5	WW-C	1198,4	1102,3	2300,7	68,6	56	124,6	1,095	47,1
2102B	G5	WW-C	1327,7	1211,5	2539,2	70,1	61,3	131,4	1,022	49,2
2104	G5	WW-C	1257,2	1153,2	2410,4	65,6	61,3	126,9	0,957	48,3

Individual plant measurements of berry composition determined by HPLC analysis at harvest. Hexoses (glucose and fructose) and organic acids (malic and tartaric) expressed in mmol·L^{-1}. Both malic and tartaric acids are diprotic organic acids. Glucose:Fructose ratio (range 0.97-1.17, mean 1.07) shows equimolar balance consistent with invertase-mediated sucrose hydrolysis during berry ripening. Malic:Tartaric ratio is a diagnostic metabolic trait for LSB genotypes, with higher values characteristic of the LSB phenotype (Bigard et al., 2022). Malic:Hexoses ratio (dimensionless) reflects the balance between metabolically active malic acid and hexose sugars in berry juice, with higher values indicating proportionally more malic acid relative to storage carbohydrates. All ratios are dimensionless (mmol·L^{-1}/mmol·L^{-1}). Carbon-normalized treatments (WW-C, WD-C) applied only to LSB genotypes G5 and G14 through 50% increase in berry number per plant; genotypes 3159 and 3176 have no carbon-normalized treatments; G14 has no WW-C treatment due to experimental design. Plant 2068 (3176 WD) excluded due to technical issues during experiment. n = 56 plants total: 3159 WD (n=6), 3159 WW (n=6), 3176 WD (n=5), 3176 WW (n=6), G14 WD (n=4), G14 WD-C (n=4), G14 WW (n=4), G5 WD (n=6), G5 WD-C (n=5), G5 WW (n=5), G5 WW-C (n=5). Statistical analyses reported in Section 3.2.3.2 (hexoses, Figure 34) and Section 3.2.3.3 (organic acids and ratios, Figures 35-38).

Supplementary Table S6. Vegetative fresh weight by organ, genotype, and treatment.

Genotype	Treatment	n	Main Shoots (g)	Lateral Shoots (g)	Total Shoots (g)	Main Leaves (g)	Lateral Leaves (g)	Total Leaves (g)	Trunk (g)	Canes (g)	Roots (g)	Total Vegetative (g)
3159	WD	6	100.7 ± 38.1	12.6 ± 5.6	113.3 ± 36.3	88.8 ± 9.9	33.3 ± 15.4	122.0 ± 23.5	21.7 ± 8.3	80.5 ± 7.7	146.9 ± 27.2	484.4 ± 60.8
3159	WW	6	147.9 ± 24.1	64.2 ± 43.1	212.1 ± 53.7	94.5 ± 11.9	87.2 ± 41.3	181.7 ± 41.1	22.6 ± 5.2	93.3 ± 3.4	179.6 ± 20.2	689.4 ± 91.2
3176	WD	5	110.3 ± 16.7	7.0 ± 1.9	117.3 ± 18.5	109.3 ± 14.9	23.6 ± 2.7	132.9 ± 16.5	16.2 ± 2.7	99.2 ± 13.2	132.2 ± 16.6	497.8 ± 50.7
3176	WW	6	183.9 ± 38.3	104.4 ± 69.7	288.3 ± 49.5	151.8 ± 46.5	123.5 ± 64.9	275.3 ± 32.3	20.7 ± 4.7	108.4 ± 13.1	133.1 ± 34.3	825.9 ± 96.3
G14	WD	4	123.0 ± 16.2	11.2 ± 3.5	134.2 ± 18.6	99.1 ± 17.8	31.3 ± 13.8	130.4 ± 5.1	19.3 ± 7.5	70.2 ± 23.1	160.1 ± 19.2	514.2 ± 30.4
G14	WD-C	4	98.1 ± 1.6	18.5 ± 10.1	116.6 ± 8.7	88.1 ± 4.7	24.8 ± 8.7	112.9 ± 12.5	25.0 ± 14.6	73.6 ± 10.5	159.6 ± 37.6	487.7 ± 30.1
G14	WW	4	121.9 ± 19.4	38.5 ± 25.9	160.4 ± 25.7	94.5 ± 4.4	55.4 ± 22.0	149.8 ± 18.2	25.7 ± 7.1	72.1 ± 6.4	203.0 ± 55.0	611.0 ± 90.0
G5	WD	6	100.7 ± 14.0	10.8 ± 7.9	111.5 ± 16.3	109.9 ± 14.8	28.1 ± 14.6	138.1 ± 21.6	19.2 ± 1.9	84.0 ± 14.5	206.3 ± 15.5	559.0 ± 20.4
G5	WD-C	5	96.7 ± 14.6	10.2 ± 6.2	106.9 ± 9.4	100.7 ± 19.0	26.4 ± 16.5	127.1 ± 18.5	16.9 ± 5.3	74.5 ± 16.1	181.2 ± 49.6	506.6 ± 56.1
G5	WW	5	130.5 ± 31.3	28.7 ± 19.5	159.2 ± 33.8	130.7 ± 18.5	53.5 ± 28.4	184.2 ± 30.8	22.6 ± 3.9	81.7 ± 13.2	191.5 ± 32.6	639.2 ± 68.5
G5	WW-C	5	113.0 ± 16.3	49.8 ± 27.0	162.8 ± 33.3	120.0 ± 11.6	84.6 ± 38.7	204.6 ± 45.5	16.8 ± 2.8	82.0 ± 11.7	195.1 ± 24.7	661.4 ± 98.7

Values represent mean ± standard deviation (g) for each organ compartment at harvest. Total Shoots = Main Shoots + Lateral Shoots; Total Leaves = Main Leaves + Lateral Leaves; Total Vegetative = sum of all organs. Two-way ANOVA results for each component are reported in Section 3.2.2.3. Carbon-normalized treatments (WW-C, WD-C) applied only to LSB genotypes G5 and G14. n = number of plants per genotype

× treatment combination.

Supplementary Table S7. Vegetative dry weight by organ, genotype, and treatment.

Genotype	Treatment	n	Main Shoots (g)	Lateral Shoots (g)	Total Shoots (g)	Main Leaves (g)	Lateral Leaves (g)	Total Leaves (g)	Trunk (g)	Canes (g)	Roots (g)	Total Vegetative (g)
3159	WD	6	40.9 ± 8.9	3.0 ± 1.4	43.9 ± 9.5	27.9 ± 3.9	10.6 ± 4.8	38.4 ± 7.6	11.3 ± 5.4	42.9 ± 4.2	79.2 ± 11.8	215.8 ± 29.6
3159	WW	6	54.0 ± 8.4	15.9 ± 10.9	70.0 ± 15.4	30.8 ± 4.4	26.7 ± 11.6	57.5 ± 10.6	12.5 ± 3.0	50.7 ± 1.3	91.6 ± 9.5	282.3 ± 22.8
3176	WD	5	33.6 ± 6.8	1.4 ± 0.5	35.0 ± 7.3	28.7 ± 4.7	6.2 ± 1.0	34.9 ± 5.6	7.3 ± 1.4	49.8 ± 7.5	71.1 ± 10.5	198.2 ± 27.3
3176	WW	6	47.4 ± 9.6	22.3 ± 15.5	69.7 ± 16.5	36.3 ± 10.3	27.7 ± 14.8	64.0 ± 8.8	9.8 ± 2.8	51.6 ± 5.6	63.6 ± 12.6	258.7 ± 31.8
G14	WD	4	49.5 ± 6.0	3.3 ± 1.3	52.7 ± 6.9	34.1 ± 4.7	11.1 ± 5.2	45.2 ± 1.5	9.9 ± 5.1	38.7 ± 13.1	91.1 ± 9.4	237.6 ± 14.0
G14	WD-C	4	37.9 ± 2.0	3.8 ± 2.3	41.7 ± 2.4	29.4 ± 1.8	10.1 ± 1.6	39.6 ± 2.9	13.4 ± 9.0	39.9 ± 6.9	82.1 ± 18.0	216.7 ± 17.2
G14	WW	4	46.8 ± 4.7	10.4 ± 7.3	57.3 ± 6.9	32.8 ± 2.9	18.8 ± 7.3	51.6 ± 7.0	13.3 ± 4.4	38.6 ± 3.9	96.8 ± 20.9	257.7 ± 27.7
G5	WD	6	33.9 ± 4.9	2.4 ± 1.9	36.4 ± 4.7	32.2 ± 4.8	8.3 ± 4.2	40.5 ± 6.2	9.3 ± 1.3	44.6 ± 7.2	111.8 ± 8.0	242.6 ± 9.7
G5	WD-C	5	31.4 ± 5.6	2.2 ± 1.4	33.6 ± 4.3	29.1 ± 6.3	7.9 ± 4.6	36.9 ± 5.8	8.4 ± 2.8	38.9 ± 9.0	103.0 ± 32.6	220.8 ± 40.7
G5	WW	5	44.0 ± 11.1	6.5 ± 4.8	50.5 ± 11.4	37.1 ± 5.3	14.4 ± 7.2	51.5 ± 8.8	11.3 ± 2.0	43.4 ± 7.0	103.9 ± 15.2	260.7 ± 24.7
G5	WW-C	5	36.5 ± 6.5	11.6 ± 7.3	48.2 ± 10.1	31.8 ± 3.8	22.8 ± 10.8	54.6 ± 11.9	8.2 ± 1.8	43.4 ± 6.6	102.7 ± 14.3	257.0 ± 33.7

Values represent mean ± standard deviation (g) for each organ compartment at harvest. Dry weight determined after oven-drying at 60°C to constant weight. Total Shoots = Main Shoots + Lateral Shoots; Total Leaves = Main Leaves + Lateral Leaves; Total Vegetative = sum of all organs. Two-way ANOVA results for each component are reported in Section 2.2.3. Carbon-normalized treatments (WW-C, WD-C) applied only to LSB genotypes G5 and G14. n = number of plants per genotype × treatment combination.

Supplementary Table S8. Total plant biomass and carbon partitioning among organs at harvest by genotype and treatment.

Genotype	Treatment	n	Total Plant DW	Fruit DW	Vegetative DW	Roots DW	Fruit %	Vegetative %	Root:Shoot
3159	WD	6	347.1 ± 22.7	131.3 ± 21.4	215.8 ± 29.6	79.2 ± 11.8	37.9 ± 6.3	62.1 ± 6.3	0.297 ± 0.046
3159	WW	6	408.3 ± 44.6	126.0 ± 41.3	282.3 ± 22.8	91.6 ± 9.5	30.4 ± 7.1	69.6 ± 7.1	0.298 ± 0.069
3176	WD	5	326.4 ± 13.9	128.2 ± 24.7	198.2 ± 27.3	71.1 ± 10.5	39.3 ± 7.8	60.7 ± 7.8	0.280 ± 0.051
3176	WW	6	389.3 ± 44.5	130.6 ± 28.1	258.7 ± 31.8	63.6 ± 12.6	33.4 ± 5.2	66.6 ± 5.2	0.197 ± 0.042
G14	WD	4	338.2 ± 7.6	100.6 ± 18.5	237.6 ± 14.0	91.1 ± 9.4	29.7 ± 5.0	70.3 ± 5.0	0.371 ± 0.058
G14	WD-C	4	364.6 ± 15.5	147.9 ± 11.9	216.7 ± 17.2	82.1 ± 18.0	40.6 ± 3.4	59.4 ± 3.4	0.291 ± 0.069
G14	WW	4	353.3 ± 44.7	95.6 ± 33.5	257.7 ± 27.7	96.8 ± 20.9	26.6 ± 7.9	73.4 ± 7.9	0.375 ± 0.052

G5	WD	6	353.1 ± 21.4	110.5 ± 13.5	242.6 ± 9.7	111.8 ± 8.0	31.2 ± 2.1	68.8 ± 2.1	0.464 ± 0.024
G5	WD-C	5	384.2 ± 25.0	163.4 ± 26.2	220.8 ± 40.7	103.0 ± 32.6	42.7 ± 7.6	57.3 ± 7.6	0.371 ± 0.138
G5	WW	5	370.4 ± 16.1	116.2 ± 35.4	260.7 ± 24.7	103.9 ± 15.2	31.1 ± 8.7	68.9 ± 8.7	0.362 ± 0.046
G5	WW-C	5	433.7 ± 30.1	170.1 ± 38.2	257.0 ± 33.7	102.7 ± 14.3	39.3 ± 9.3	60.7 ± 9.3	0.313 ± 0.054

Mean total plant dry biomass and allocation among major organ systems. Total Plant DW = sum of all vegetative organs (shoots, leaves, trunk, canes, roots) plus fruits. Fruit Allocation = percentage of total plant dry biomass allocated to reproductive organs. Vegetative Allocation = percentage allocated to all vegetative structures. Root:Shoot Ratio calculated as root biomass divided by aboveground biomass (vegetative + fruits). Values represent mean ± SD with sample size (n). Carbon-normalized treatments (WW-C, WD-C) applied only to LSB genotypes G5 and G14 through +50% berry number; genotypes 3159 and 3176 have no carbon-normalized treatments; G14 has no WW-C treatment. Two-way ANOVA results: Total Plant DW showed significant treatment effect ($F_{3,42} = 11.83$, $p < 0.001$) but no genotype effect ($F_{3,42} = 2.26$, $p = 0.095$); Fruit Allocation showed significant treatment ($F_{3,42} = 8.69$, $p < 0.001$) and genotype effects ($F_{3,42} = 3.00$, $p = 0.041$); Root:Shoot Ratio showed significant genotype ($F_{3,42} = 16.58$, $p < 0.001$) and treatment effects ($F_{3,42} = 5.28$, $p = 0.004$). n = 56 plants total.

Supplementary Table S9. Relative changes in leaf gas exchange parameters under saturating light conditions (Asat) compared to well-watered control (WW = 1.0).

Parameter	Genotype	WW-C	WD-C	WD
Asat-An	G5	1.046b	0.507aA	0.514aA
	G14	NA	0.572aA	0.428aA
	3159	NA	NA	0.459A
	3176	NA	NA	0.464A
Asat-gs	G5	1.142b	0.197aA	0.267aA
	G14	NA	0.206aA	0.139aA
	3159	NA	NA	0.224A
	3176	NA	NA	0.188A
Asat-E	G5	1.126b	0.208aA	0.277aA
	G14	NA	0.226aA	0.152aA
	3159	NA	NA	0.238A
	3176	NA	NA	0.201A

Parameters measured at PAR 1500 µmol photons m^{-2} s^{-1}. Values represent mean ratios averaged across three measurement dates (DOY 154, 169, 181). An = net photosynthesis, gs = stomatal conductance, E = transpiration rate. Different letters within rows indicate significant differences among treatments (Bonferroni adjustment, $p < 0.05$). WW-C and WD-C represent carbon-normalized treatments available only for LSB genotypes G5 and G14.

Supplementary Table S10. Relative changes in leaf gas exchange parameters under dark-adapted conditions (Adark) compared to well-watered control (WW = 1.0).

Parameter	Genotype	WW-C	WD-C	WD
Adark-An	G5	0.823b	0.650aA	0.694abA
	G14	NA	0.887aB	0.956aB
	3159	NA	NA	0.951B
	3176	NA	NA	0.866AB
Adark-gs	G5	1.089b	0.418aA	0.452aA
	G14	NA	0.687aB	0.804aB
	3159	NA	NA	0.618AB
	3176	NA	NA	0.561AB
Adark-E	G5	1.091b	0.420aA	0.455aA
	G14	NA	0.690aB	0.807aB
	3159	NA	NA	0.620AB
	3176	NA	NA	0.562AB

Leaves were dark-adapted for 12 hours prior to measurements. Values represent mean ratios averaged across three measurement dates. An = net photosynthesis after dark adaptation, gs = stomatal conductance, E = transpiration rate. Different letters within rows indicate significant differences among treatments (Bonferroni adjustment, $p < 0.05$).

7.2 Supplementary Figures

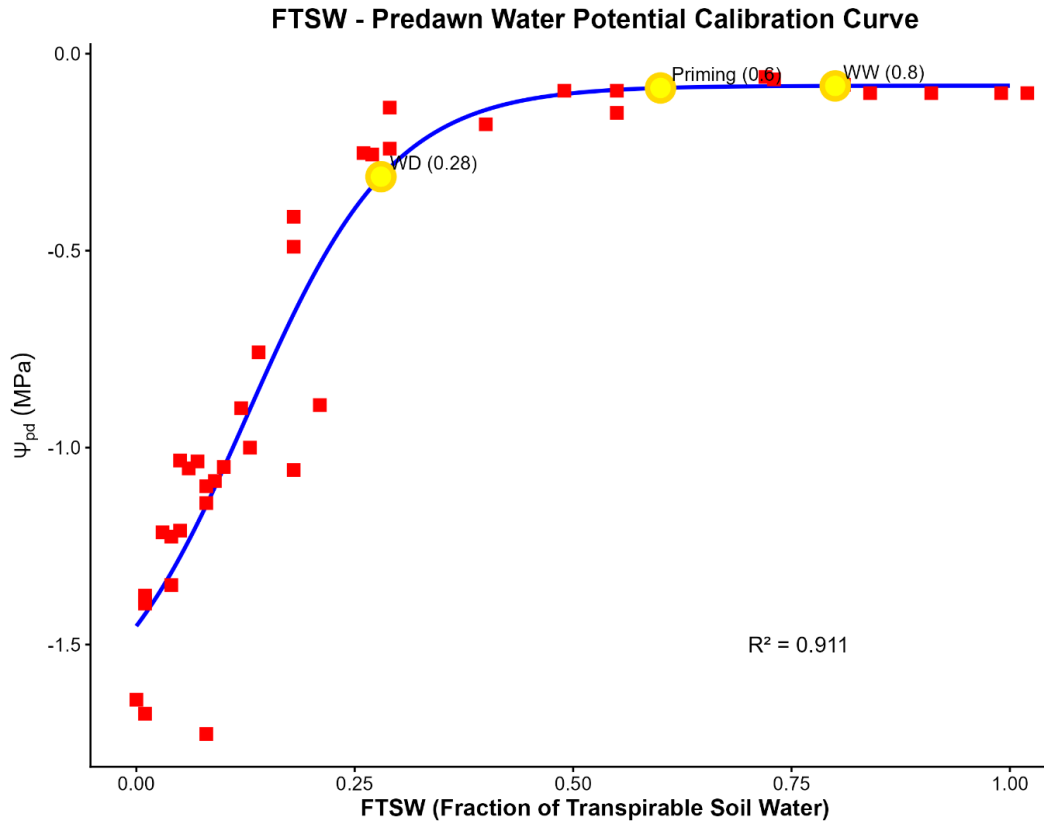

Supplementary Figure S1. Relationship between fraction of transpirable soil water (FTSW) and predawn leaf water potential (Ψpd).The calibration curve was established by combining FTSW reference values from previous experiments conducted in the Phenodyn platform with Ψpd measurements from the green stage water deficit treatment (STS-G). Red squares represent measured data points (n = 39), and the blue line shows the fitted four-parameter logistic curve (R^2 = 0.911). Yellow circles indicate the target FTSW values selected for well-watered (0.8), priming (0.6), and water deficit (0.28) treatments in STS-R and LTS, corresponding to Ψpd thresholds of approximately -0.08, -0.09, and -0.31 MPa, respectively. The plateau in Ψpd values at high FTSW reflects the well-watered physiological state where further increases in soil water availability do not substantially improve plant water status.

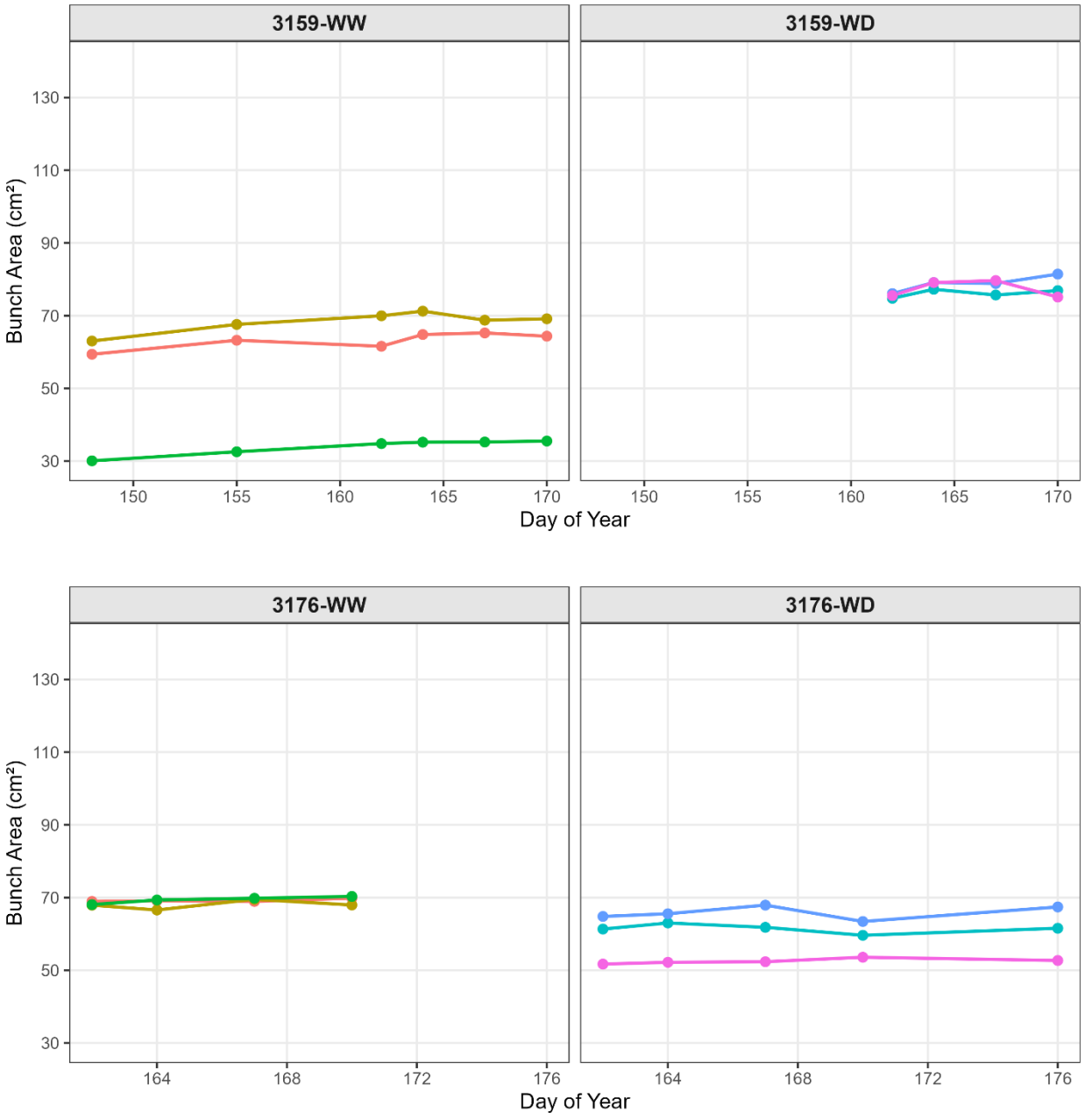

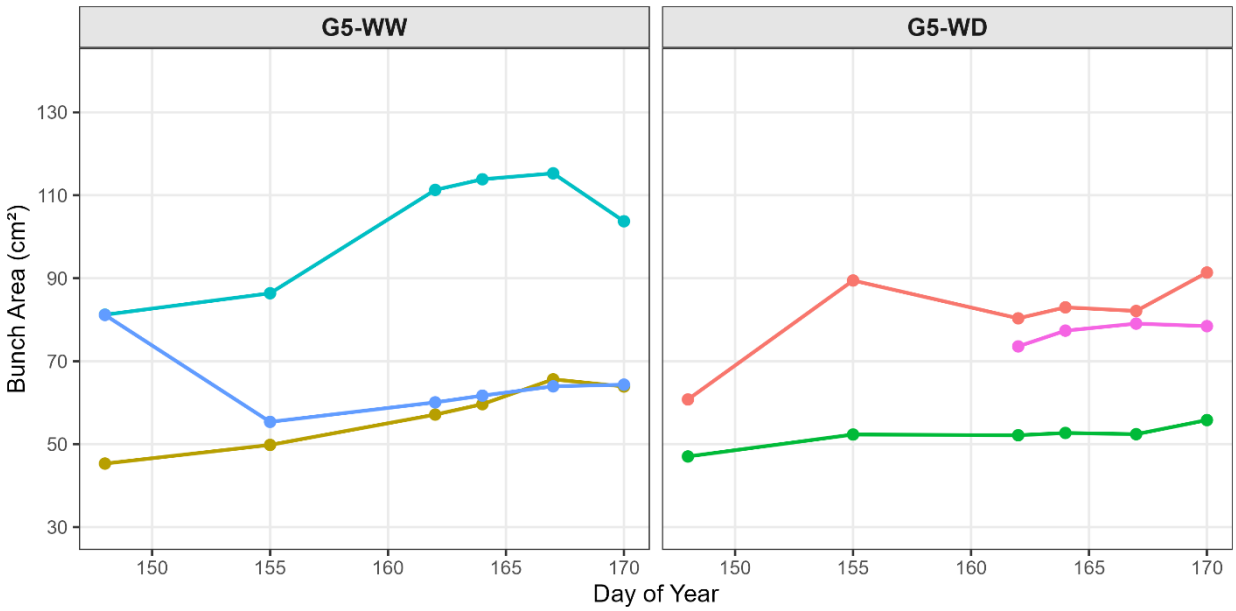
G5-WW
G5-WD
Bunch Area (cm²)
130
110
90
70
50
30
150
155
160
165
170
Day of Year

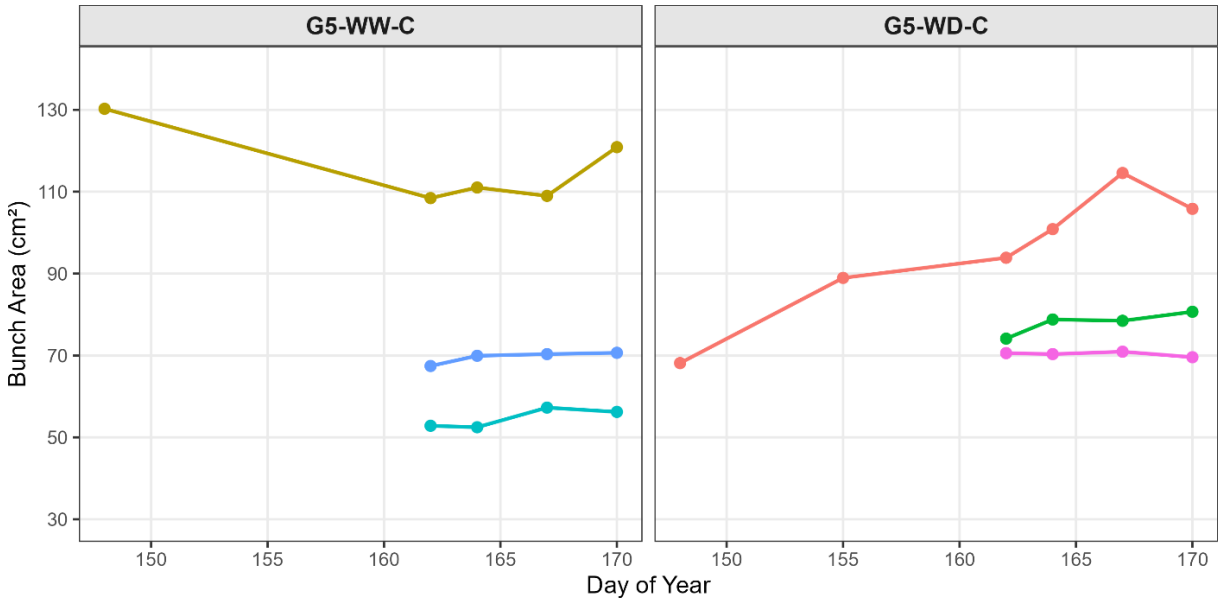
G5-WW-C
G5-WD-C
Bunch Area (cm²)
130
110
90
70
50
30
150
155
160
165
170
Day of Year

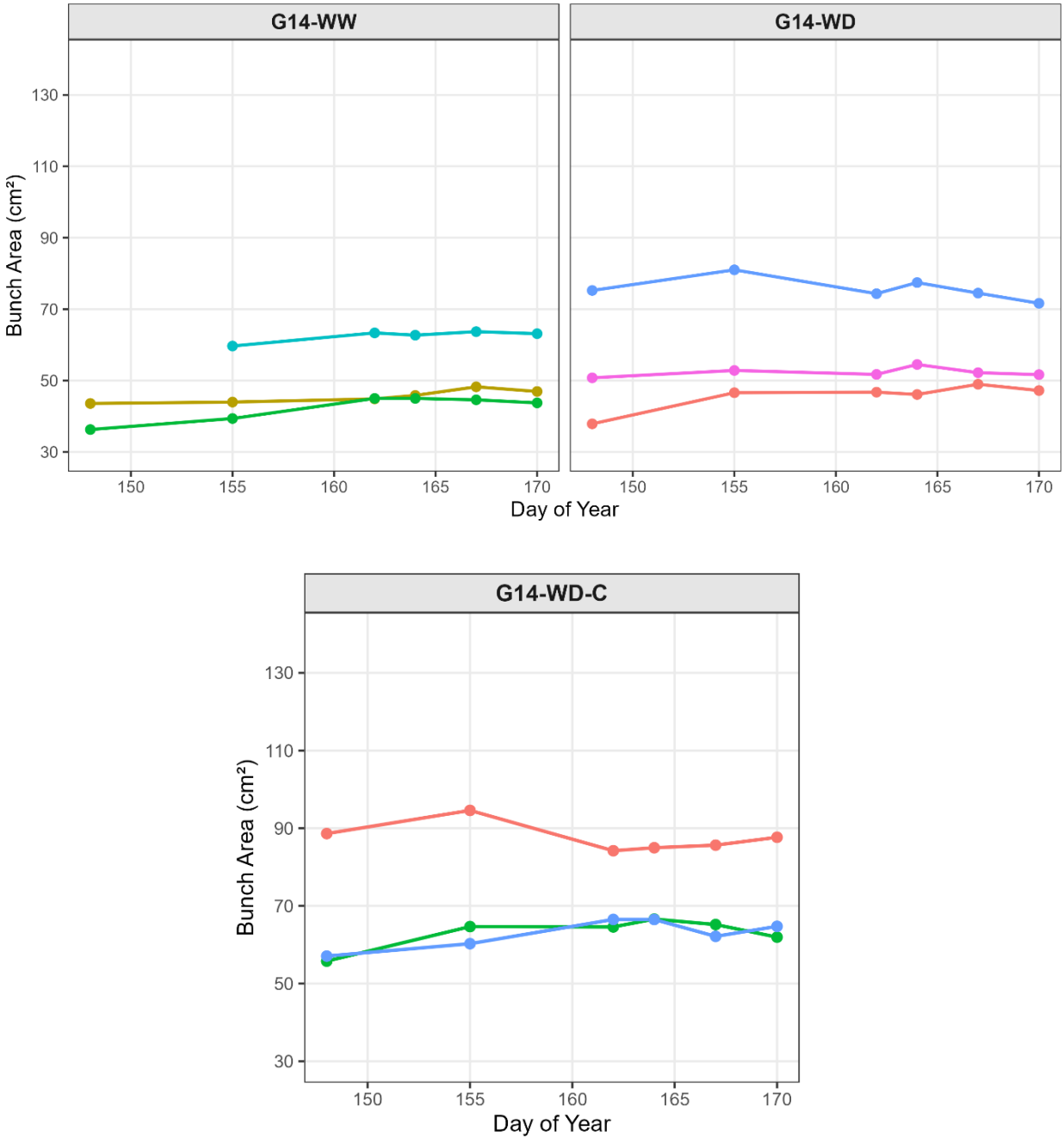

Supplementary Figure S2. Complete bunch area dynamics from veraison to harvest by genotype and treatment. Individual plant trajectories (colored lines, each line = one bunch tracked on one plant) show weekly bunch area measurements determined through non-destructive imaging analysis of three representative clusters per plant. Each panel represents a genotype-treatment combination: WW = well-watered, WD = water deficit, WW-C and WD-C = carbon-normalized LSB

treatments with increased berry load (+50% berry number for LSB genotypes G5 and G14). Bunch areas shown in cm². Harvest timing (Table 7) was determined when bunch area reached maximum size followed by stable or declining measurements over consecutive monitoring dates, indicating physiological ripeness and completion of berry cell expansion across all berries within each cluster. Final bunch areas ranged from 51.3 cm² (G14 WW) to 85.4 cm² (G5 WD-C). This figure complements Figure 28, which shows representative trajectories for genotypes 3176 and G5 under standard treatments.

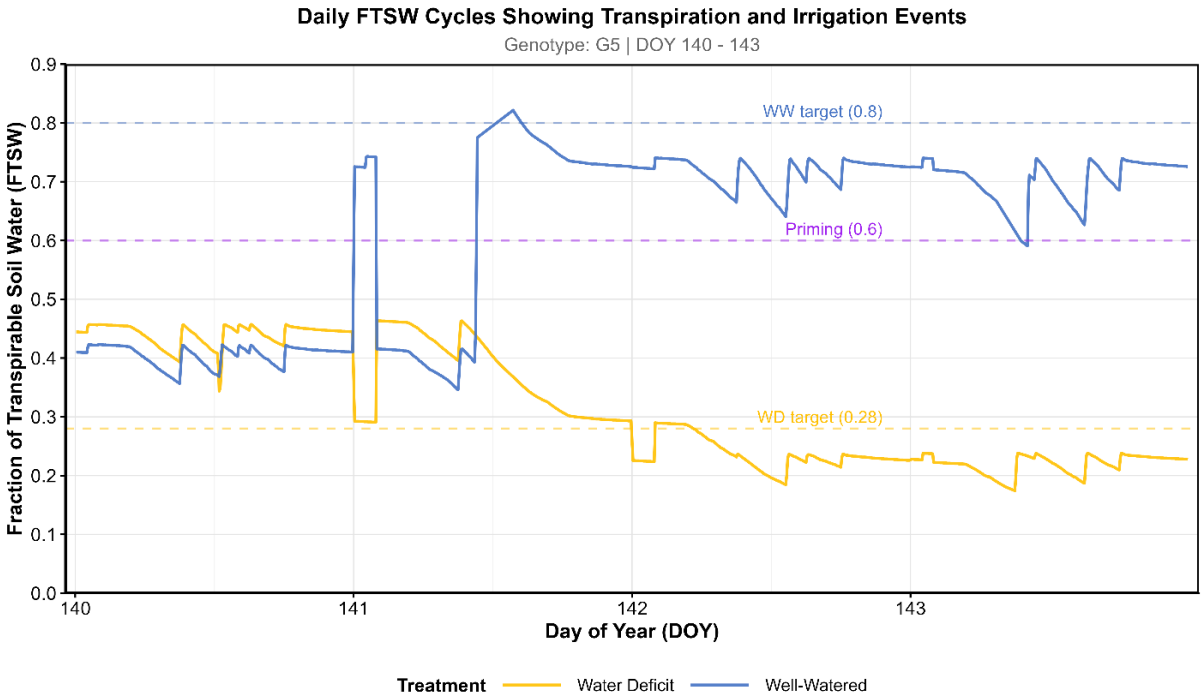

Supplementary Figure S3. Daily FTSW cycles showing transpiration and irrigation events of G5 WD and WW plants. High-resolution FTSW trajectories for one well-watered (blue) and one water deficit (yellow) plant during the early treatment period (DOY 140-143) demonstrate the precision of the automated irrigation system. Downward slopes indicate transpiration-driven water loss, while sharp upward spikes represent automated irrigation events triggered when plants reached their target FTSW thresholds. Horizontal dashed lines indicate target FTSW levels: WW target (0.8, blue), priming level (0.6, purple), and WD target (0.28, yellow). The WW plant maintained FTSW near 0.8 through frequent small irrigation events, while the WD plant was maintained near 0.28 with less frequent irrigation. Daily FTSW fluctuations reflect the diurnal cycle of plant transpiration under controlled environmental conditions in the Phenodyn platform.